NATIONAL ACADEMIES OF SCIENCE AND ENGINEERING

NATIONAL RESEARCH COUNCIL

of the

UNITED STATES OF AMERICA

UNITED STATES NATIONAL COMMITTEE

International Union of Radio Science

National Radio Science Meeting

5-8 January 1994

Sponsored by USNC/URSI

University of Colorado
Boulder, Colorado
U.S.A.

National Radio Science Meeting
5-8 January 1994
Condensed Technical Program

Tuesday, 4 January
2000-2400
USNC-URSI Meeting   Broker Inn

Wednesday, 5 January
0855-1200
B-1   ANTENNAS AND RADIATION   CR1-40
B-2   INTEGRAL EQUATION METHODS   CR2-28
D/J   MICROWAVE, MM AND SUB-MM INSTRUMENTATION   CR0-30
F-1   ACTS AND OLYMPUS PROPAGATION EXPERIMENTS   CR2-26
G-1   IONOSPHERIC VARIABILITY/PERTURBATION   CR2-6
H-1   INHOMOGENEOUS FLOWS AND THEIR STABILITY IN   CR1-46
      LABORATORY AND SPACE PLASMAS

1335-1700
G-2   RADIO PROPAGATION AND CHANNEL MODELING   CR2-6

1355-1700
A-1   EM FIELD AND ANTENNA MEASUREMENTS   CR1-42
B-3   SCATTERING I   CR2-28
D-1   ELECTROMAGNETIC DEVICE MODELING   CR1-9
E-1   NOISE MEASUREMENTS, MODELING, AND PREDICTION   CR1-40
F-2   POLARIMETRIC OBSERVATIONS AND SCATTERING   CR2-26
      CHARACTERISTICS OF THE OCEAN SURFACE
H-2   INHOMOGENEOUS FLOWS AND THEIR STABILITY IN   CR1-46
      LABORATORY AND SPACE PLASMAS
H-3   PLANETARY RADIO SOUNDING AND EMISSIONS   CR0-36
J-1   RADIO ASTRONOMY FROM SPACE   CR0-30

1700-1800
Commission A Business Meeting   CR1-42
Commission C Business Meeting   CR0-36
Commission E Business Meeting   CR1-40
Commission F Business Meeting   CR2-26
Commission H Business Meeting   CR1-46

Thursday, 6 January
0815-1200
PLENARY SESSION   CR2-28

1335-1700
G-3   IONOSPHERIC EFFECTS ON SYSTEMS/RADAR STUDIES   CR2-6

1355-1700
E/A   HPE GENERATION, MEASUREMENT AND SHIELDING   CR1-40
F-3   REMOTE SENSING AND PROPAGATION MEASUREMENTS   CR2-26
H-4   ACTIVE EXPERIMENTS IN SPACE   CR1-46
J-2   DIGITAL TECHNIQUES   CR0-30

United States National Committee

INTERNATIONAL UNION OF RADIO SCIENCE

PROGRAM AND ABSTRACTS

National Radio Science Meeting
5-8 January 1994

Sponsored by USNC/URSI

25
182

NOTE:

Programs and Abstracts of the USNC/URSI Meetings are available from:

USNC/URSI
National Academy of Sciences
2101 Constitution Avenue, N.W.
Washington, DC 20418

at $5 for 1983-1994 meetings.

The full papers are not published in any collected format; requests for them should be addressed to the authors who may have them published on their own initiative. Please note that these meetings are national. They are not organized by the International Union, nor are the programs available from the International Secretariat.

MEMBERSHIP
United States National Committee
INTERNATIONAL UNION OF RADIO SCIENCE

Chairman: Dr. David C. Chang*
Vice Chairman: Dr. Charles M. Rush*
Secretary: Dr. Susan K. Avery*
Immediate Past Chairman: Dr. Chalmers M. Butler*

Members Representing Societies, Groups, and Institutes:

American Geophysical Union   Dr. George W. Reid
American Astronomical Society   Dr. William J. Welch
IEEE Antennas & Propagation
    Society   Dr. Gary S. Brown
IEEE Microwave Theory and
    Techniques Society   Dr. A. A. Oliner
IEEE Geosciences and Remote
    Sensing Society   Dr. Robert E. McIntosh
American Meterological Society   Dr. Richard Hallgren

Members-at-Large: Dr. Ming-Chen Lee
                                    Dr. Robert J. Mattauch
                                    Dr. Yahya Rahmat-Samii
                                    Dr. Roland Tsunoda
                                    Dr. Donald Wilton
                                    Dr. Edgeworth R. Westwater

Liaison Representatives from Government Agencies:

National Telecommunications &
    Information Administration   Dr. Hans Liebe
National Science Foundation   Dr. Hugh Van Horn
Federal Communications
    Commission   Mr. William A. Daniel
Department of the Navy   Mr. William J. Cook
Department of the Army   Mr. Earl J. Holliman
Department of the Air Force   Dr. Allen C. Schell
NASA   Dr. Erwin R. Schmerling

Chairmen of the USNC/URSI Commissions:

Commission A   Dr. Sedki Riad
Commission B   Dr. Donald G. Dudley
Commission C   Dr. David J. Thomson
Commission D   Dr. Michael Shur
Commission E   Dr. Robert L. Gardner
Commission F   Dr. Julius Goldhirsh
Commission G   Dr. Sunanda Basu
Commission H   Dr. Paul A. Bernhardt
Commission J   Dr. Michael M. Davis
Commission K   Dr. James C. Lin

* Member of USNC/URSI Executive Committee

Officers, Chairmen and Vice
   Chairmen of Commissions of URSI
   resident in the United States:

   Honorary President   Dr. William E. Gordon
   Vice Chairman, Commission A   Dr. Motohisa Kanda
   Vice Chairman, Commission B   Dr. Chalmers M. Butler
   Chairman, Commission D   Dr. Tatsuo Itoh
   Chairman, Commission F   Dr. Richard K. Moore
   Vice Chairman, Commission G   Dr. Bodo W. Reinisch
   Vice Chairman, Commission K   Dr. James C. Lin

Foreign Secretary of the U.S.
   National Academy of Sciences   Dr. James B. Wyngaarden

Chair, Commission on
   Physical Sciences, Mathematics,
   and Applications, National
   Research Council   Dr. Richard N. Zare

Chair, Board on Physics and
   Astronomy, Commission on
   Physical Sciences, Mathematics,
   and Applications, National
   Research Council   Dr. David Schramm

Honorary Members   Dr. Harold H. Beverage
                                                Dr. Ernst Weber

Director, Board on Physics and
   Astronomy, National
   Research Council   Dr. Donald C. Shapero

Program Officer, U.S. National
   Committee for URSI, National
   Research Council   Dr. Robert L. Riemer

DESCRIPTION OF THE
INTERNATIONAL UNION OF RADIO SCIENCE

The International Union of Radio Science is one of the world scientific unions organized under the International Council of Scientific Unions (ICSU). It is commonly designated as URSI (from its French name, Union Radio Scientifique Internationale). Its aims are (1) to promote the scientific study of radio communications, (2) to aid and organize radio research requiring cooperation on an international scale and to encourage the discussion and publication of the results, (3) to facilitate agreement upon common methods of measurement and the standardization of measuring instruments, and (4) to stimulate and to coordinate studies of the scientific aspects of telecommunications using electromagnetic waves, guided and unguided. The International Union itself is an organizational framework to aid in promoting these objectives. The actual technical work is largely done by the National Committee in the various countries.

The new officers of the International Union are:

President:	Dr. P. Bauer (France)
Past President:	Prof. E.V. Jull (Canada)
Vice Presidents:	Prof. J. Bach Anderson (Denmark)
	Prof. P.J.B. Clarricoats (U.K.)
	Prof T. Okoshi (Japan)
	Prof. T.B.A. Senior (U.S.A.)
Secretary-General	Prof. P. Lagasse (Belgium)
Honorary Presidents:	Sir G. Beynon (U.K.)
	Dr. W. Dieminger (West Germany)
	Prof. W. Christiansen (Australia)
	Prof. W.E. Gordon (U.S.A.)
	Dr. F.L.H.M. Stumpers (Netherlands)

The Secretary-General's office and the headquarters of the organization are located at Avenue Albert Lancaster, 32, B-1180 Brussels, Belgium. The Union is supported by contributions (dues) from 38 member countries. Additional funds for symposia and other scientific activities of the Union are provided by ICSU from contributions received for this purpose from UNESCO.

The International Union, as of the XXIVth General Assembly held in Kyoto, Japan, August 25-September 3, 1993, has ten bodies called Commissions for centralizing studies in the principal technical fields.

Every three years the International Union holds a meeting called the General Assembly. The next is the XXVth, to be held in 1996, in Lille, France. The Secretariat prepares and distributes the Proceedings of the General Assemblies. The International Union arranges international symposia on specific subjects pertaining to the work of one or several Commissions and also cooperates with other Unions in international symposia on subjects of joint interest.

Radio is unique among the fields of scientific work in having a specific adaptability to large-scale international research programs, since many of the phenomena that must be studied are worldwide in extent and yet are in a measure subject to control by experimenters. Exploration of space and the extension of scientific observations to the space environment are dependent on radio for their research. One branch, radio astronomy, involves cosmic phenomena. URSI thus has a distinct field of usefulness in furnishing a meeting ground for the numerous workers in the manifold aspects of radio research; its meetings and committee activities furnish valuable means of promoting research through exchange of ideas.

Steering Committee:

E. K. Smith, Chairman (303) 492-7123
D. Cook   S. K. Avery
P. L. Jensen   M. J. Ruehlman

Technical Program Committee:

C. M. Rush, Chairman   S. Riad
S. Avery   J. Richter
P. Bernhardt   E. K. Smith
M. Davis   E. Soderberg
D. Dudley   H. Soicher
J. Lin   D. Thomson
A. Mickelson

Session B-1 0855-Wed. CR1-40
ANTENNAS AND RADIATION
Chairman: Steven L. Dvorak, Dept. of Electrical and Computer Engineering, Univ. of Arizona,
Tucson, AZ 85721

B1-1   **FOURIER SYNTHESIS OF SIMPLIFIED ANTENNA**
0900   **ARRAY FEED NETWORKS**
              Randy L. Haupt
              Department of Electrical Engineering
              2354 Fairchild Dr, Suite 2F6
              USAF Academy, CO 80840-6236

Fourier analysis and synthesis of array antennas provides valuable insight to antenna design. This presentation shows two interesting extensions of Fourier synthesis: partially tapered arrays and joint sum/difference amplitude tapers. Partially tapered arrays have the center elements uniformly weighted while the amplitude tapered edge elements produce the low side lobe levels.

The Fourier series expansion for the partially tapered array is given by

$$f(\psi) = \frac{\dfrac{\sin(N\psi)}{\sin(\psi/2)} + 2\displaystyle\sum_{m=N+1}^{N+M} a_m \cos[(m-.5)\psi]}{2N + 2\displaystyle\sum_{m=N+1}^{N+M} a_m}$$

where $\Psi = kd\cos\phi$. The center 2N elements are uniformly weighted and the M elements on either edge are amplitude tapered. The desired far field sum pattern is specified via $f(\Psi)$ and the Fourier coefficients or array weights are found using a least squares solution. The figure below shows the amplitude weights and resulting far field pattern when N=5 and M=5. The dashed line is the desired Taylor far field pattern and the solid line is the approximated far field pattern.

The second application is the synthesis of both a sum and difference pattern using amplitude weights shared by the two channels. A Fourier cosine series represents the sum pattern and a Fourier sine series represents the difference pattern. The array weights or Fourier coefficients are identical for the two series.

1
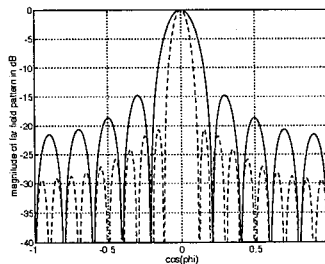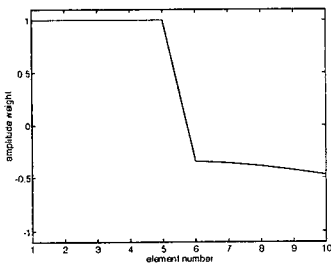
B1-2
0920
ENERGY PROPAGATION MODEL FOR LAND
BASED POSITIONING SYSTEMS
Dr Radha Telikepalli[1] and Dr J.M. Tranquilla[2]
[1] CAL Corporation, 1050 Morrison Drive
Ottawa/ON, CANADA K2H 8K7
[2] Department of Electrical Engineering
PO 4400, University of New Brunswick
Fredericton/N.B., CANADA E3B 5A3

The energy propagation from a typical antenna used for land based positioning systems is modelled using the analogy between fluid flow and electromagnetic energy flow. The velocities of propagation are modelled based on the concept of energy flow. Phase velocity and group velocity are used for distance calculations in radio positioning systems. The variation of the velocities of propagation from the velocity of light results in errors in range calculations.

The presence of pattern null corresponds to the presence of an eddy in fluid dynamics. Energy deflects around the null where the phase changes through 360^0. This paper discusses the behaviour of energy flow around the pattern nulls and the resulting distance errors due to the deviation of the energy flow from the assumed straight lines in this region.
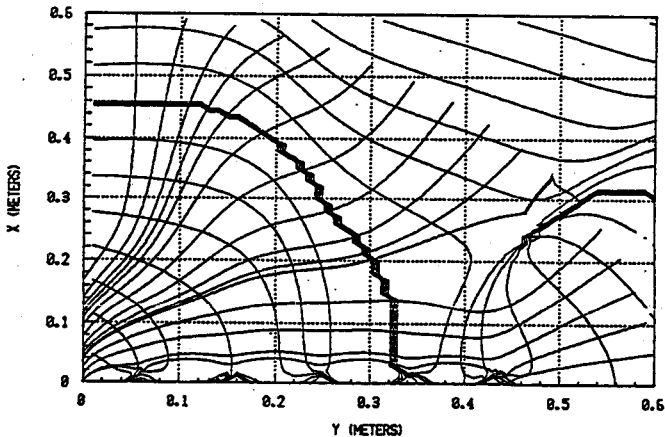
ILLUSTRATION OF ENERGY FLOW LINES AND PHASE CONTOURS OF YAGI AT 715 MHz

B1-3
0940
EFFICIENT COMPUTATION OF FRESNEL-ZONE FIELDS FOR CIRCULAR APERTURES

Steven L. Dvorak and Glen Evans
Department of Electrical and Computer Engineering
University of Arizona
Tucson, AZ 85721
Stephen A. Fast
Atlantic Research Corporation
P. O. Box 719
Fort Huachuca, AZ   85635

In this presentation, closed-form expressions are derived for the Fresnel-zone fields associated with common circular aperture sources. After assuming that the aperture electric field distribution is given by the parabolic taper on a pedestal,

$$E_x^n = -E_o \left[C + (1 - C) \left(1 - (\rho'/\rho_o)^2 \right)^n \right],$$

where ρ_o is the radius of the aperture, n is the order of the parabolic taper, E_o is the field strength, and C is the pedestal height, we find that the magnetic vector potential is given by

$$F_y^n(\mathbf{r}') = E_o \int_0^{\rho_o} \int_{-\pi}^{\pi} \left(C + (1 - C) \left(1 - (\rho'/\rho_o)^2 \right)^n \right) \frac{\exp(-jkR)}{R} \, d\rho' \, d\phi'.$$

The $n = 0$ distribution models plane wave diffraction through a circular aperture. Higher values of n are useful for studying parabolic reflector antennas.

Unfortunately, the above integrations cannot be carried out analytically. However, the Fresnel approximation allows the potential to be expressed in terms of an incomplete Lipschitz-Hankel integral of the first kind. This closed-form solution provides an efficient method for computing the Fresnel-zone fields since no numerical integration is required. The required incomplete Lipschitz-Hankel integrals are computed using the algorithm developed by Dvorak and Kuester, (*J. of Computational Physics, 87(2), 301-327, 1990*). The validity of the Fresnel approximation is demonstrated by comparing the Fresnel-zone fields with the "exact" fields which are obtained by numerical integration.

B1-4
1020

EXACT, CLOSED-FORM EXPRESSIONS FOR TRANSIENT FIELDS IN HOMOGENEOUSLY FILLED WAVEGUIDES

Steven L. Dvorak
Department of Electrical and Computer Engineering
University of Arizona
Tucson, AZ 85721

It is well known that transient electromagnetic fields exhibit dispersion in waveguides. Exact, closed-form expressions, which involve Bessel functions of the first kind, have been derived for the impulse response of homogeneously filled waveguides (R.E. Collin, *Field Theory of Guided Waves, Second Edition*, New York: IEEE Press, 1991), but exact, closed-form expressions for more complex pulses are absent from the literature. In this presentation, a contour integration technique is presented which allows for the analytical evaluation of the inverse Fourier transform representation for the transient fields in homogeneously filled waveguides. A continuous wave pulse is investigated, however, this technique can also be applied to a number of other transient waveforms in waveguides and lossy transmission lines. This general technique is applicable for transient sources which possess analytical Fourier transforms involving transcendental functions and pole terms. The branch cut integrals, which model the dispersive effects, present the most difficulty in the evaluation of the inverse Fourier transform representation. An integral identity, which is derived in (M.M. Mechaik and S.L. Dvorak, "Derivation of Series Expansions for the Incomplete Lipschitz-Hankel Integral $Je_0(a, z)$," paper submitted to *SIAM J. on Mathematics*.), is used to demonstrate that these branch cut integrals yield incomplete Lipschitz-Hankel integrals of the first kind. The algorithm outlined in (S.L. Dvorak and E.F. Kuester, "Numerical Computation of the Incomplete Lipschitz-Hankel Integral $Je_0(a, z)$," *J. Comput. Phys.*, vol. 87, No. 2, pp. 301–327, 1990) allows for the efficient compuatation of the transient fields inside waveguides. The exact, closed-form expressions are verified by comparing with results obtained by numerically integrating the pulse distribution multiplied by the known impulse response.

B1-5   COMPUTER AIDED DESIGN OF CORRUGATED HORNS
1040   Prof. A D Olver,
Queen Mary & Westfield College
Mile End Road
London E1 4NS
United Kingdom

The conical corrugated horn has become the prime choice for use as a feed for high performance reflector antennas in communications, radar and remote sensing systems. This is partly because the radiation characteristics are ideal with good co-polar pattern symmetry and low levels of cross-polarisation. It is also because corrugated horns can be designed, using a computer, with a high degree of reliability. The paper describes the computer aided design of corrugated horns and discusses the methods used to design horns in terms of their validation, accuracy, reliability and ease of use.

A hierarchy of techniques are available to predict the performance of corrugated horns. These range from a single equation which can be solved quickly on a small pocket computer to the powerful modal matching techniques which require long run times on fast computers. Generally the simplest methods are also the least accurate and the more sophisticated methods are the slowest in terms of computation time. The designer has to use a combination of initial fast approximate predictions followed by slow accurate predictions.

The approximate techniques are described in Clarricoats, P.J.B. and Olver, A.D.: 'Corrugated horns for microwave antennas', IEE Books, 1984. The modal matching technique (G.L. James, MTT-29, 1059-66, 1981) has been found to be a very powerful and accurate method of analysing conical horns because it enables the exact transverse fields at the horn aperture to be computed. The principle of the technique is to divide a horn longitudinally into short cylindrical waveguide sections. Modal matching is then used at the junction of each section to obtain the power coupled to the next section of the waveguide. A scattering matrix for the horn is obtained by cascading individual matrices for each junction progressively along the horn. The radiated fields of the horn are computed by Fourier transforming the aperture fields.

Modal matching differs from the simpler analysis techniques in that the behaviour of the fields are tracked along the horn from the throat to the aperture. This is particularly important for millimetrewave corrugated horns where the length of the horn can sometimes be such as to induce considerable amounts of higher order modes along the horn. In the other techniques, the horn is modelled as either a single cylindrical corrugated waveguide or a single conical corrugated horn. Only the aperture fields are computed and there is no information about the way in which the fields change along the horn. In addition to predicting the basic performance of a corrugated horn, a modal matching program is ideal for studying the tolerances on the geometry of a corrugated horn. Examples of the computer aided design of corrugated horns, including millimetrewave horns, will be discussed.

B1-6   ASYMPTOTIC EVALUATION OF THE FIELD
1100   RADIATED BY A LOOP

Bruno Stupfel
Commissariat à l'Énergie Atomique
Centre d'Études de Limeil-Valenton, D.MA / MCN
94195 Villeneuve St Georges cedex, France.

In this paper, we give the asymptotic expansion of the following integral

$$I_m \equiv I_m(\rho, z; \rho', z') = \int_0^\pi \frac{e^{-ikR(\varphi')}}{R(\varphi')} \cos(m\varphi')\, d\varphi'$$

(cylindrical coordinates are used) to three terms when $k \to \infty$. $m \geq 0$ is an arbitrary integer. $R(\varphi') = R_0 \sqrt{1 + b(1 - \cos \varphi')}$ with $b = 2\rho\rho'/R_0^2$ and $R_0 = \sqrt{(\rho - \rho')^2 + (z - z')^2}$. R is the distance between point $P = (\rho, z, \varphi = 0)$ and a point $P' = (\rho', z', \varphi')$ situated on a circular loop of radius ρ' and axis z. This integral appears when calculating the field radiated at point P by this loop on which an arbitrary, time harmonic, velocity distribution is prescribed and expanded in a Fourier series of the azimuthal angle φ'; m is then the Fourier mode number and k the wave number of the excitation.

Making use of the steepest descent method, and with the help of the software Mathematica (S. Wolfram, Mathematica, a system for doing mathematics by computer, Addison-Wesley Pub. Comp., 1988), we obtain the expressions, in closed forms, of the three first terms in the asymptotic expansion of I_m. These expressions depend on the value of the parameter $w = m/\gamma$, where $\gamma = k\rho\rho'/R_0$; they diverge when P is situated on the loop. When $b \to 0$, then the standard asymptotic expansions of the Bessel function $J_m(\gamma)$ are obtained ($w < 1$, $w = 1$, $w > 1$).

The numerical values of I_m derived from this asymptotic expansion are compared with the "exact" values computed with a Gauss-Legendre quadrature rule. Accurate results are obtained for sufficiently large values of k even when P is located near the loop, and a reliable estimate of the error is defined.

B1-7   **AN ARRAY-FED RECONFIGURABLE REFLECTOR**
1120   **FOR SPACECRAFT APPLICATIONS**

P.J.B. Clarricoats*, A.D. Monk* and Zhou Hai[+]
*Dept. of Electronic Engineering, Queen Mary & Westfield College,
University of London, Mile End Road, London E1 4NS, United
Kingdom
[+]South Bank University, London, United Kingdom

Introduction

Spacecraft antennas have been developed using array-fed paraboloidal reflectors and these can provide both regional and continental coverages. Shaped reflectors fed with a single high performance feed have also been developed to provide continental coverage and offer superior performance compared to the former.(S.J. Stirland et al, Proc. 14th AIAA Conf. Comm. & Sat. Sys., 1992). Because of changes in usage during the satellite lifetime, designers are interested in the possibility of changing the coverage while the satellite is in orbit. Reconfiguration of regional beams is possible with array-fed reflectors by utilising a switched beam-forming network and reconfiguration of a shaped beam reflector with a single feed has been demonstrated by the authors (P.J.B. Clarricoats et al.Proc. IEE Part H 138 No. 6, 485-496, 1991) using a reconfigurable mesh reflector. We now show that by using a small array feed in conjunction with a reconfigurable mesh reflector it is possible to achieve a very high degree of coverage flexibility. The paper provides a proof-of-principle backed by experimental results obtained using an antenna operating a frequency of 10 GHz.

Array-fed Mesh Reflector

A complete description of the reconfigurable mesh reflector has been given previously (P.J.B. Clarricoats et al.Proc. IEE Part H 138 No. 6, 485-496, 1991),(R.C. Brown et al, Proc. 19th EuMC, Paper A9.5, 1989) and the radiation characteristics of our 19-element array of conical horns has also been extensively investigated.(P.J.B. Clarricoats et al, Proc. IEE, Part H, 131, No. 3, 165-171, 1984). The new antenna comprises a reconfigurable mesh with an array feed. The array comprises 7 active single-mode horns surrounded by 12 passive elements to reduce the effects of mutual coupling.

To create high gain beams, the computer-controlled mesh reflector is configured as a paraboloid. The beam shapes are then determined by the element excitations but with a clean beam the copolar secondary pattern is circular. The position of the beams relative to the antenna boresight depends on the choice of excited elements but a reasonable scan can be achieved without unacceptable astigmatism.

To create a shaped beam the array is excited symmetrically about the centre element . The mesh is then configured to generate the desired pattern coverage. The advantage of using the mesh reflector to generate the shaped-beam compared to the use of an array with a rigid paraboloid lies in the reduced complexity of the beam forming network. The QMW mesh reflector utilises 52 actuators and a very high degree of flexibility in the shape of the coverage pattern is possible.

Experimental Results

Measurements of the patterns of both spot beams and shaped beams have been taken using the QMW Compact Antenna Range at frequencies centred on 10 GHz. Excellent agreement has been obtained between these patterns and those predicted using Physical Optics.

B1-8
1140

ELIMINATION OF UNWANTED MODES IN STRIPLINE-FED SLOT ANTENNAS

Catherine L. Levinson and Chalmers M. Butler
ECE Department
Clemson University
Clemson, SC 29634-0915

Paul D. Mannikko
M. I. T. Lincoln Laboratory
P.O. Box 73
Lexington, MA 02173

One type of low-profile antenna is the stripline-fed slot array. The stripline transmission line can be fed from the edge or from below. Undesirable parallel plate waveguide modes are excited by electric currents on bottom feeds or by equivalent magnetic currents in the slot. Shorting posts have been used to mitigate these modes while leaving the TEM propagation mode of the stripline relatively unaffected. Solid walls between the upper and bottom plate have also been proposed. These walls form a rectangular waveguide below cutoff for the frequencies of interest.

Measurements and MoM results will be presented for the case of a stripline-fed slot (array) that is end-fed and end-loaded. In this case the only coupling mechanism to the rectangular housing waveguide modes is through the slot, i.e., there is no electric current due to the feed which will couple to these modes. Numerical modelling has shown that the slot is tightly coupled to the rectangular waveguide modes and that most of the energy is lost to these modes, rather than coupled to the exterior region.

Experimental and MoM results will also be presented for the case of a stripline-fed slot (single element) that is bottom-fed and bottom-loaded. In this case the electric currents on the feed posts, as well as the slot can excite the rectangular waveguide modes that couple energy away from the slot and the stripline transmission line. At frequencies below the waveguide cutoff, however, the energy is not lost to these modes.

B2-1   COMPUTATION OF MONOSTATIC RCS AND SURFACE
0900   CURRENTS FOR A FLAT PLATE WITH PERFORATED APERTURES

K. L. Virga and Y. Rahmat-Samii
Department of Electrical Engineering
University of California, Los Angeles
Los Angeles, CA 90024-1594

The computation of monostatic RCS and surface currents for perforated apertures in a finite-size ground plane is an important electromagnetics problem. The geometry of a finite ground plane with triangular apertures resembles airplane and automobile windows. The size, shape, and location of the apertures can significantly affect the scattering signature and surface current distribution of the plate. It is essential to understand how the different geometry factors influence the scattering characteristics.

The method of moments (MoM) triangular surface patch formulation is used to compute the monostatic RCS and surface currents for a solid square plate and finite-size plates with several apertures. In this approach, the electric field integral equation is used in conjunction with the moment method to compute the induced currents on the plate. With this formulation, the characteristics of the triangular patch mesh can impact the accuracy of the computed results. Special consideration must be given to achieve good overall mesh quality to ensure that the time and convenience gained by developing the general MoM code is not lost in mesh construction and convergence tests. Once the currents on the plate are computed, they can be plotted and the scattered field can be determined by integrating these currents. Both the RCS and surface current results give useful insight and help identify the dominant scattering mechanisms of the perforated plates.

In this paper, the RCS and surface currents for a solid square plate, a finite-size plate with two widely spaced triangular apertures, and a finite-size plate with two closely spaced apertures will be presented. The RCS results obtained from measurements and the Method of Moments and Physical Optics simulations will be discussed. Emphasis will be placed upon how the aperture separation influences the RCS patterns. The effects of the specific mesh characteristics and overall mesh quality on the results will also be addressed. Additionally, comparisons of surface currents computed by the Method of Moments and Physical Optics will be presented. Special attention will be given to how the current distribution near the plate edges varies as a function of the aperture separation.

B2-2 MORE ON THE ILL-POSED NATURE OF HALLEN'S EQUATION

0920 Richard C. Booton, Jr.
Center for Microwave/ Millimeter-Wave Computer-Aided Design
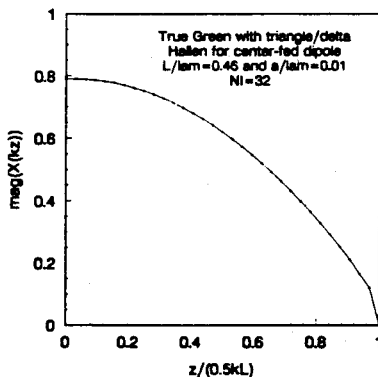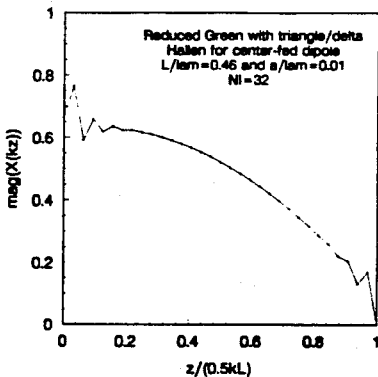Department of Electrical and Computer Engineering
University of Colorado
Boulder, CO 80309-0425

In a previous presentation (Booton, URSI Boulder 1993) numerical computations illustrated the ill-posed nature of Hallen's equation for scattering off thin cylinders. This ill-posed nature, the general characteristics of which were made clear by Sarkar (Radio Science 18, 29-38, 1983), was seen to result in increasingly large oscillations as the number of basis functions is increased past a certain number. An argument based upon approximation was made to demonstrate the source of the trouble in the lack of a singularity in the reduced Green's function.

This presentation investigates the more sensitive problem of determining the input impedance of a center-fed dipole. In contrast to the scattering situation, where the oscillations may result in large errors in the current without large errors in radar cross section, any oscillation may result in appreciable errors in input impedance. The results of numerical computation, a sample of which are shown in the figures below, are presented to illustrate the effects of the difference between the true Green's function and the reduced approximation for the center-fed dipole.

Determination of the true Green's function is well known to require a numerical integration with respect to angle around the cylinder. Analytic removal of the singularity and numerical investigation of the remainder suggests a useful approximation to the true Green's function without the lack of a singularity that causes the ill-posed caused oscillations.

B2-3 0940 ANALYSIS OF A WIRE PROBE MOUNTED ON THE NOSE OF A MISSILE-LIKE BODY OF REVOLUTION

Zhiqiang Qiu and Chalmers M. Butler
Department of Electrical and Computer Engineering
Clemson University, Clemson, SC 29634-0915

Interest in this paper focuses upon the electromagnetic analysis of a thin-wire probe mounted on the nose of a missile-like conducting body of revolution (*bor*). The wire is the extended center conductor of a small coax and lies on the axis of the *bor*. The end of the coax inside the *bor* is connected to a load or to a generator. Exterior to the bore-wire structure, all space is filled with homogeneous material characterized by (μ, ϵ). Excitations of interest are (1) a generator connected to the coax in which case the goal is to determine the resulting far-zone radiated field and (2) an exterior nearby elementary dipole or a plane wave in which cases the goal is to determine the signal at a load terminating the interior end of the coax.

An integro-differential equation is derived for the current induced on the structure, with full account taken of the coupling between the wire and *bor*. This equation is solved numerically for the wire/*bor* current due to the wire being driven at its base where it joins the *bor*. From knowledge of this current, the wire input admittance is determined and, subsequently, the input admittance at the interior end of the coax is computed. This information allows one to determine the current on the wire and *bor* due to a specified source applied to the interior end of the coax. With the wire and *bor* currents known, the radiated field caused by this interior source is found. To determine the signal on a load connected to the interior end of the coax, caused by an exterior source – an exterior dipole or a plane wave, one applies reciprocity to the data obtained from the above-described radiation computation.

Data depicting the current induced on the wire scatterer/antenna and the input admittance of the wire in the presence of the *bor* are presented for several *bor*-wire geometries. Also, values of input admittance at the interior end of the coax are presented and corroborated by measured results made on two laboratory models. Far-zone radiated field data are described as are data characterizing the behavior of the signal received by a terminal load at the interior end of the coax, when the structure is illuminated by a plane wave or by the field due to a nearby elementary dipole.

B2-4
1020

A NEW EFIE FOR HETEROGENEOUS DIELECTRIC BODIES OF REVOLUTION EMBEDDED WITHIN A STRATIFIED MEDIUM

Mark S. Viola
Department of Electrical Engineering
University of Akron
Akron, OH 44325-3904

Contemporary interest in electromagnetic phenomena associated with dielectric bodies immersed within a stratified medium encompasses a variety of applications. Rigorous quantification of such phenomena is commonly provided by an integral or integro-differential equation for the electric field. However, the presence of certain symmetries allows the formulation of an alternative integral equation having both computational and theoretical advantages.

In this paper, a novel electric field integral equation (EFIE) is developed for integrated heterogeneous dielectric bodies revolved about an axis aligned normal to the interfaces of the planarly-layered surround. It is assumed that the permittivity profile is azimuthally invariant. By exploiting the prevailing symmetry, straightforward analysis yields an EFIE of the form

$$\vec{E}_T = \vec{E}_T^i + \mathcal{L}\{\vec{E}_T\}.$$

Here, $\vec{E}_T$ is the component of total field transverse to the azimuthal component, $\vec{E}_T^i$ is the transverse component of an impressed field, and $\mathcal{L}$ is a volume-surface integral operator. This EFIE has the following salient features:

1) The azimuthal component of field is uncoupled from the remaining two (transverse components).

2) It is a rigorous pure integral equation for the transverse field components as opposed to an integro-differential one.

3) There are no highly singular kernels within $\mathcal{L}$.

It is believed that the new formulation should be an asset for both theoretical and computational endeavors. It enhances the efficiency of numerical computations by yielding a formulation for which the number of unknowns is reduced from three to two. Theoretically, it affords the luxury of providing a rigorous pure-integral equation description for which the singularity of the associated kernels are sufficiently weak. This avoids the necessitation of a principal-value integral (whose value depends upon the shape of the excluding region) and the corresponding depolarizing dyad.

B2-5
1040

**GUARANTEED ERROR BOUNDS FOR SOLUTIONS OF
INTEGRAL EQUATIONS OF THE FIRST KIND
IN SCATTERING PROBLEMS**

Edward F. Kuester
Electromagnetics Laboratory
Department of Electrical and Computer Engineering
Campus Box 425
University of Colorado at Boulder
Boulder, CO 80309

Fredholm integral equations of the first kind often arise in the formulation of electromagnetic scattering problems as well as in other areas of applied mathematics. The Galerkin method is frequently used to obtain an approximate numerical solution such integral equations, despite the fact that they are ill-posed in a certain sense, and generally are regarded as more poorly behaved than integral equations of the second kind. Practical experience nevertheless has shown good results from Galerkin solutions to first-kind integral equations. This is sometimes credited to the stationary (variational) properties known to be inherent in such solutions.

Up to now, however, it has not been possible to obtain rigorous error bounds for the Galerkin solution in any case but that of static problems. In this paper, we illustrate on the simple example of plane wave scattering from a thin conducting strip how to obtain guaranteed *a posteriori* error bounds for any linear functional of the induced current on the strip (for example, the far field radiation pattern). These bounds involve evaluation of the norm of the residual of the operator equation in the fractional-order Sobolev space $H^{1/2}$, and are a development of ideas presented in [G. C. Hsiao, R. E. Kleinman, R.-X. Li and P. M. van den Berg, *Computational Engineering with Boundary Elements* (S. Grilli, C. A. Brebbia and A. H.-D. Cheng, eds.), Vol. 1. Southampton, UK: Computational Mechanics Publications, 1990, pp. 73-83], and subsequent publications.

Computed results will be presented to illustrate the quality and accuracy of these bounds as the number of basis functions is varied, and extensions to more general problems will also be indicated.

B2-6 1100 A STUDY OF COUPLED PLANAR DIELECTRIC STRUCTURES USING THE INTEGRAL TRANSFORM TECHNIQUE

Kazem Sabetfakhri* and Linda P.B. Katehi
Radiation Laboratory
Department of Electrical Engineering and Computer Science
The University of Michigan
Ann Arbor, MI 48109-2122

An accurate full-wave analysis of coupled dielectric structures is a key factor in the efficient design of submillimeter-wave integrated couplers. The existing numerical methods tend to discretize the geometry into very tiny cells, thus introducing a huge number of unknowns. Such a fine discretization not only decreases the numerical efficiency in view of CPU time and memory requirements, but may also lead to numerical instability as the complexity of the structure increases. Moreover, some multilayered dielectric structures support leaky modes, which degrade the performance of the device significantly. Only those techniques that take into account the complete spectrum of open geometries are capable of predicting this leakage behavior accurately.

In this paper the integral transform technique, which was recently proposed for the analysis of planar dielectric structures (K. Sabetfakhri and P.B. Katehi, *IEEE MTT-S Dig.*, 1993, pp. 1523-1526), is extended to coupled structures. This technique introduces an appropriate integral transform to obtain an equivalent integral equation of reduced dimensionality in the transform domain. To this end, higher-order boundary conditions are enforced in conjunction with Taylor expansions of the fields. The reduced integral equation is solved numerically using the method of moments with a suitable entire-domain expansion basis.

Various coupled dielectric waveguides have been treated. It is seen that the integral transform technique leads to a considerable reduction in the number of unknowns as compared to the other discretizing methods. To study the leaky modes, a coupled strip waveguide consisting of two dielectric strips resting upon an infinite grounded substrate is treated and the effect of the separation between the two strips on the attenuation and phase constants of the waveguide is examined.
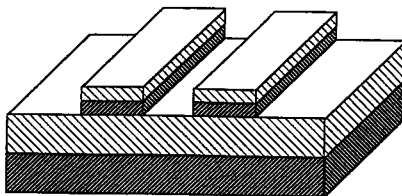
ANALYSIS OF APERTURE COUPLED PATCH ANTENNAS WITH A MIXED POTENTIAL INTEGRAL EQUATION

Richard C. Hall
Huber+Suhner AG, Mail Stop 456
CH-9100 Herisau, Switzerland
FAX: +41/71/53.45.90

Aperture coupled patch antennas (shown below with a bow-tie shaped aperture) provide wider bandwidth performance compared to conventional patch antennas while retaining most of their desirable properties such as low cost and physical robustness. The accurate analysis of aperture coupled elements, however, is more complicated due to the presence of the aperture and multiple dielectric layers.

In this paper a mixed potential integral equation is developed for the equivalent electric and magnetic currents on a multilayered aperture coupled antenna element. These currents are induced by a given excitation at one end of the feed line. The integral equation is solved by standard moment method techniques using sub-sectional basis functions that allow fairly arbitrarily shaped patches and apertures to be studied. Once the currents are known on the structure the antenna parameters of interest can be determined. Several methods to compute the input impedance will be discussed and compared to measured results. In addition, gain and efficiency calculations for various patch and aperture configurations will be presented.

FEED NETWORK   PATCH   SLOT
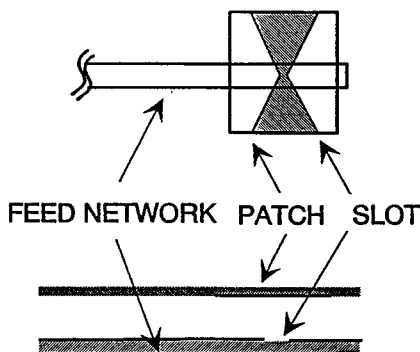
Numerical Dispersion Characteristics of the Two and Three Dimensional Frequency Dependent Transmission Line Modeling (FDTLM)

Fethi H. Bellamine* and Edward F. Kuester
Department of Electrical and Computer Engineering
Electromagnetics Laboratory: Campus Box 425
University of Colorado, Boulder 80309

A general formulation entailing the effficient treatment of first-order material dispersion (Debye relaxations) using the Transmission Line Modeling and entitled FDTLM has been presented (F. Bellamine and E.F. Kuester *Development of a Frequency-Dependent TLM*, 1991 North American Radio Science Meeting, London, Ontario, Canada, p.78). All discrete numerical techniques for wave propagation introduce unphysical dispersion and anisotropy, even if the material properties are frequency-independent. A study of numerical dispersion as well as the numerical anisotropy is important to understand the limitations of the discrete models, including the FDTLM in our case.

In this paper, the numerical dispersion charateristics of the two and three dimensional frequency dependent transmission line modeling (FDTLM) methods are treated for any first-order material dispersions (for the example of several commercial absorbers). Mesh losses in this type of medium are also evaluated and illustrated for different frequency dispersive materials. The results obtained pave the way to correct for the velocity error introduced by the time-domain FDTLM technique. It will also be shown that mesh losses in both two and three dimensional cases are not small contrary to the assumption made in the TLM literature.

MICROWAVE, MM AND SUB-MM INSTRUMENTATION

Chairmen: Robert Mattauch, Dept. of Electrical Engineering, Univ. of Virginia, Charlottesville, VA 22903; and Richard Bradley, National Radio Astronomy Observatory, Charlottesville, VA 22903-1797

D/J-1
0900

PLANAR AND WHISKERED GaAs SCHOTTKY DIODES FOR THz MIXING APPLICATIONS

### P.A.D. Wood, T.W. Crowe and W. L. Bishop

Semiconductor Device Laboratory
Department of Electrical Engineering
University of Virginia
Charlottesville, VA 22903

ABSTRACT

GaAs Schottky diodes are currently the most sensitive heterodyne receiver elements for applications above 1 THz which require high spectral resolution and broad bandwidth. We present results for several frequencies using whisker contacted GaAs Schottky diodes and an update on fabrication of submicron anode diameter planar Schottky diodes.

Receiver noise temperatures at 585 GHz, 803 GHz, 1.63 THz and 2.5 THz are presented for three high doped diodes (1T14 and 1T15, $N_d = 10^{18}$ cm^{-3}) and one low doped diode (1I7, $N_d = 3 \times 10^{17}$ cm^{-3}). A summary of these results are shown in the graph below. High doped diodes generally performed better than lower doped diodes with the same capacitance. At 2.5 THz we achieved a low DSB receiver noise temperature of 14300K, requiring 25 mW of LO pump power. At 1.63 THz the 1T15 again had the lowest receiver temperature, and only needed 1 mW of LO power. For 585 GHz and 803 GHz, the 1T14 diodes had the lowest receiver temperature (3400K at 585 GHz and 3100K at 803 GHz) and required about 1 mW of LO power.

Interest in electrically and mechanically robust diodes has motivated the research in planar diode fabrication. Planar diodes have large shunt and junction capacitances and so far have been limited to lower frequencies. The SA1T2, which was designed in collaboration with the University of Michigan, has an anode diameter of 0.8 microns. The receiver temperature of this diode at 762 GHz was 8900K, with 14.9 dB conversion loss[1]. This talk will summarize recent efforts to improve the performance of planar diodes.
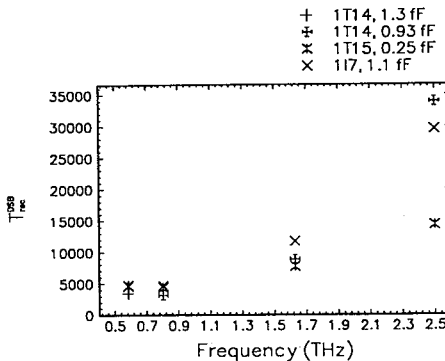
[1]S. S. Gearhart, J. Hesler, W. L. Bishop, T. W. Crowe, G. M. Rebeiz, A Wideband 760 GHz Planar Integrated Schottky Receiver, Fourth Intl. Symp. on Space THz Tech., pp. 516-521, March 1993.

TIME DOMAIN CHARACTERIZATION of WHISKER CONTACT

B. Houshmand, O. Boric, and T. Itoh
Department of Electrical Engineering
University of California, Los Angeles
Los Angeles, CA 90024-1594

ABSTRACT

Whisker contact and similar configurations are often used for diode mixers for radio astronomy. In addition, they are also used for two-terminal oscillators such as RTD (Resonant Tunneling Diode) and QWITT. In most circuits, these contacts are treated as inductive wire based on the quasi-static approximation. In this talk, we present a detailed analysis to characterize the electromagnetic behavior of these configurations. Since the outcome of this analysis gives rise to visually inspectable wave behavior along the configuration, it is possible to fine tune the whisker lengths, shapes and other parameters for a design objective.

Gate and Subthreshold Leakage Currents in GaAs- and InP-Based Heterostructure Field Effect Transistors

E. Martinez[*†], F. Schuermeyer[*], M. Shur[†], and C. Cerny[*]

[*]Solid State Electronics Directorate, Wright Laboratory
Wright-Patterson AFB, OH 45433-7319

[†]Dept. of Electrical Engineering, University of Virginia
Charlottesville, VA 22903-2242

ABSTRACT

Heterostructure Field Effect Transistors with very low leakage currents are desirable for high-speed, and low power applications. Several technologies on GaAs and InP substrates are being considered for the next generation of VLSI circuits. We present the results of a comparative study of the temperature dependencies of the gate and the subthreshold leakage currents in $Al_{.75}Ga_{.25}As/In_{.2}Ga_{.8}As/GaAs$ and $In_{.52}Al_{.48}As/In_{.53}Ga_{.47}As/InP$ Heterostructure Field Effect Transistors (HFETs). Our results show that the subthreshold leakage current in InP-based devices is larger than in the case of $Al_{.75}Ga_{.25}As/In_{.2}Ga_{.8}As/GaAs$ HFETs. At temperatures above 198 K, this subthreshold current behavior is consistent with the thermionic mechanism, in which both, the subthreshold slope and the ideality factor increase with temperature. At cryogenic temperatures (T=77 K), the ideality factor of the subthreshold current is larger than at 198 K, indicating the possible contribution of thermionic field emission. A similar behavior has been observed in GaAs MESFETs. However, in the case of GaAs MESFETs, electron tunneling starts playing a role at substantially smaller temperatures (around 40 to 50 K). This subthreshold current behavior in the InP-based devices is mainly a result of the n-type background doping in the indium-rich compounds. In order to suppress the subthreshold currents in the InP-based devices, compensating doping techniques are required.

Similarly, the gate currents for these devices have been compared. In the $Al_{.75}Ga_{.25}As/In_{.2}Ga_{.8}As/GaAs$ HFETs, thermionic emission of electrons over the barrier and electron tunneling contribute to the gate leakage current. In $In_{.52}Al_{.48}As/In_{.53}Ga_{.47}As/InP$ devices both mechanisms contribute to the gate current, with the exception that electron tunneling becomes dominant, especially at low temperatures. Therefore, the gate turn-on voltage for the InP-based devices is always lower than in the case of the GaAs-based devices. This increase in gate leakage current is explained based on the fact that the effective electron mass in the $In_{.53}Ga_{.47}As$ channel is smaller than in the case of a $In_{.2}Ga_{.8}As$ channel, increasing the probability of electron tunneling, especially in devices with high electric fields at the heterointerface. Observations of real-space electron transfer in the gate current also demonstrate that the smaller effective mass and the higher electron mobility in the $In_{.53}Ga_{.47}As$ channel contributes to the increase in gate current with drain voltage at a lower gate and drain biases than in the case of the GaAs-based devices. Evaluation of these technologies is being used to identify areas in which improvement is needed before successful implementations.

D/J-4   A BALANCED 600-1000 MHZ LOW NOISE AMPLIFIER
1000   Richard F. Bradley
           National Radio Astronomy Observatory
           2015 Ivy Road
           Charlottesville, VA 22903

The advantages of a balanced low noise amplifier over the conventional type LNA include a very good input match, an improvement in dynamic range, and the ability to cascade amplifiers and filters without degrading system performance.   Such amplifiers are particularly useful at VHF and UHF frequencies where input isolators are very large, or in situations where RFI is a problem and a filter may be required between two amplifier stages.   The amplifier described here is a prototype design for a complete set of amplifiers to cover 290-1200 MHz for use with the new Green Bank Telescope.

This prototype balanced amplifier design uses a pair of Toshiba JS8905-AS chip HFETs. Quadrature balance is provided by Lange couplers at the input and output.   For size reduction, Duriod 10.5 substrate was used in the microstrip components including the Lange couplers. Overall amplifier size is 7.1 cm long x 5.2 cm wide x 2.4 cm high.

The amplifier was evaluated at a physical temperature of 15 K. The minimum noise temperature was 3.5 K at 800 MHz. Additional measured data are given below:

Frequency Range:	680-920 MHz	600-1000 MHz
Noise Temperature:	3.6 ± 0.1 K	4.0 ± 0.5 K
Gain:	17.0 ± 0.7 dB	16.3 ± 1.4 dB
Input Match:	$\leq$ -15 dB	$\leq$ -15 dB
Output Match:	$\leq$ -23 dB	$\leq$ -20 dB
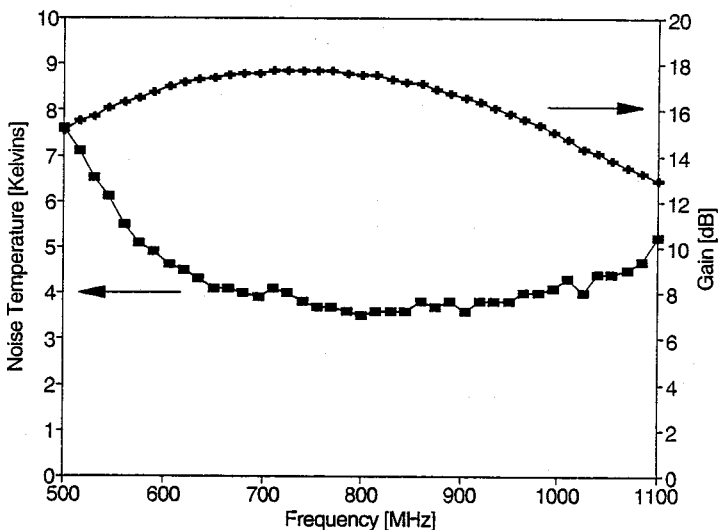
**OUTPUT POWER ANALYSIS FOR THE DESIGN
OF TRANSISTOR BASED OSCILLATORS**

R. D. Martinez, M. J. Vaughan, W. Wright, and R. C. Compton
School of Electrical Engineering
Cornell University
Ithaca, NY 14853

The rf power and efficiency of a three terminal oscillator can vary widely depending on the choice of the DC operating point, load impedance, and feedback network. The final operating point of these oscillators is usually determined numerically using a technique such as harmonic balance. A more intuitive and simplified solution can, however, be obtained using approximate techniques that originate from Lagrange's three-body gravitational studies in the 18th century.

Lagrange's techniques, which have been considerably enhanced by non-linear mathematicians in the last thirty years, provide accurate estimates for the final 'limit cycle' of an oscillator. In this paper, the use of these techniques to obtain stable trajectories for a variety of millimeter-wave oscillators will be described.
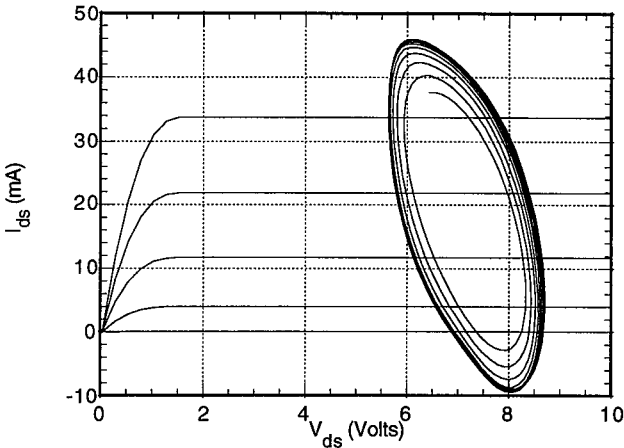
Figure 1. — I-V trajectory for a class-A MESFET oscillator superimposed on the DC I-V characteristics of the transistor.

D/J-6 1100 A Planar Transmission Wave Amplifier for Free Space Power Combining

Jon Schoenberg*   Jonathan Dixon   Zoya Basta Popović

Department of Electrical and Computer Engineering
University of Colorado, Boulder, Colorado 80309

A planar transmission wave amplifier is presented. Microstrip patch antennas provide input and output coupling from free space to the integrated pseudomorphic High Electron Mobility Transistor (PHEMT) amplifier. The amplifier consists of the radiating elements, PHEMT, matching and delay networks, and stabilization and bias circuitry as shown in Figure 1. Alternating ground planes on both sides of the substrate provide input/output isolation and allows arbitrary selection of input and output polarizations. The amplifier element may be integrated into an array for free space power combining. This configuration allows for inter-element spacing of less than one wavelength and integration of a delay network for a constrained lens application to minimize power spill-over ("Planar Three-Dimensional Constrained Lenses,", D. T. McGrath, IEEE AP-S, Vol. 34, January 1986). A 24-element polarization-preserving MESFET array is presented, and a constrained lens application to increase the efficiency and simplify the feeding of a transmission wave amplifier array is proposed.
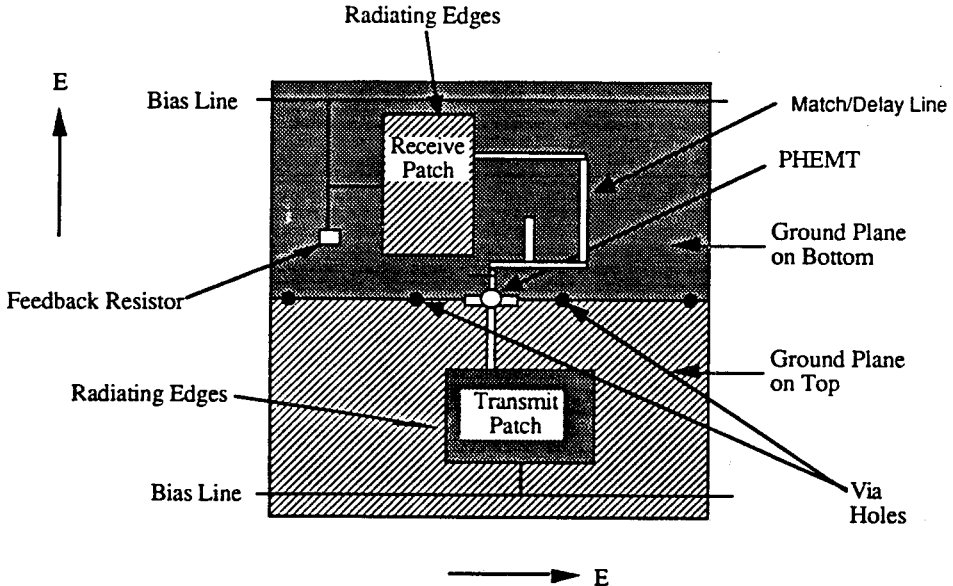
Figure 1: Transmission wave amplifier topology.

D/J-7
1120

EVANESCENT "CURRENT MODES" IN ACTIVE ANTENNA

Kuang Yi Chen   Steve Buchheit   Alan R. Mickelson
Dept. of Electrical Engineering
University of Colorado at Boulder
Boulder, CO 80309

It has been point out by Craven et al ("Evanescent Mode Microwave Components", Boston: Artech house, 1987), that evanescent modes are often the operating modes of antenna structures, especially those loaded by active devices. Here we will discuss how the current on an active antenna structure can take on the shape of an evanescent mode. Previously presented experimental results show that this is indeed the case.

An active antenna consists of a passive circuit structure loaded by an active device. The charge and current distribution along the line will appear as a "Maxwell like" distribution in the coordinate transverse to the line. The behavior of the current magnitude along the longitudinal coordinate of the line will determine the impedance seen by the active device. The current along the line, however, will also determine the impedance seen looking into the device from the line. If biased into a potentially unstable region, the transistor will emit broadband noise. As with any nonlinear system, the active antenna will satisfy a principle of self-organization. That is the system will pick the most comfortable mode of operation. Generally this mode will be oscillating. For a "short" dipole structure this will require an evanescent mode, as a typical short dipole antenna current presents a capacitive impedance to the feed point, and transistor requires an inductive load to oscillate in this configuration.

Most analytical techniques consider the passive antenna separately from the active device. It is difficult in such a manner to pick out the right mode of operation of the passive structure if right mode is not the "fundamental". In this paper, we will discuss from first principle, a technique in which we can analyze such "essentially active" structures.
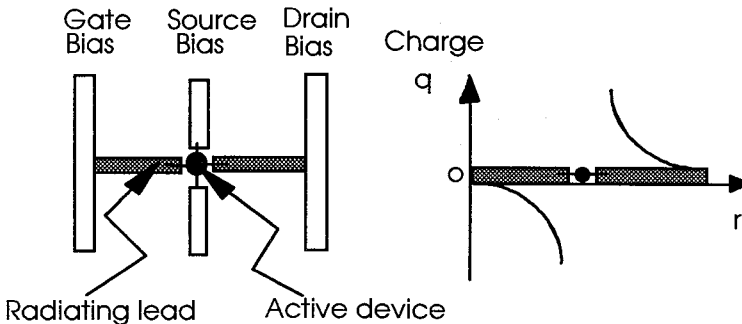
F1-1
0900

ACTS Propagation Campaign

F. Davarian
Jet Propulsion Laboratory
4800 Oak Grove Dr.
Pasadena, CA 91109

Because of a shortage of data regarding the propagation phenomenon in satellite links, the existing Ka-band propagation models are inadequate for accurately predicting tropospheric-induced effects on the slant path. To remedy this shortcoming, NASA has implemented the ACTS Propagation Program. This program consists of a campaign of experimental and analytical efforts where the ACTS satellite is used as the main vehicle for field measurements. The data collection phase of the campaign began October 1, 1993 and will last for at least two years.

The overall goal of this campaign is to expand the state of knowledge about all important Ka frequency impairments to Earth-space communications including rain attenuation, the effects of clouds, clear air, and tropospheric scintillation. Dynamic effects such as fade duration and fade rates are of particular interest to enable the design of compensation techniques based on power control and coding. Equally important is providing information critical to the design of efficient resource (power, coding, time pool) reserve strategies for future Ka band satellites. Rain rate and sky noise temperature measurements allow researchers to develop enhanced atmospheric and rain climate maps for prediction of propagation effects in those parts of the country which lack propagation data.

This paper reviews the ACTS propagation campaign. The campaign elements, logistics, and schedule are presented. Several types of experiments including fixed, mobile, and power control efforts are described. Some preliminary results are also shown.

F1-2   THE ACTS PROPAGATION EXPERIMENT TERMINALS
0920   Prof. W.L. Stutzman
            Bradley Department of Electrical Engineering
            Virginia Polytechnic Institute & State University
            Blacksburg, VA 24061-0111

The propagation experiment program is an important aspect of the Advanced Communications Technology Satellite (ACTS) which was launched on the Space Shuttle September 12, 1993. The ACTS beacons at 20 and 27.5 GHz provide the platform for a number of planned propagation experiments. Key to the success of this measurement program are ACTS propagation terminals which were constructed at Virginia Tech under NASA support. Seven terminals have been deployed across the United States and Canada.

The units consist of four components: antenna, radio frequency (RF) box, receiver box, and computer. The antenna is a 1.2-m offset parabolic reflector. The RF enclosure, located at the feed point on the antenna, houses the common RF front end for the two beacon and two radiometer channels operating at 20 and 27.5 GHz. The radiometers are of the total-power type, which permits the use of common front ends. The heart of the RF chain in each channel is a custom integrated downconverter, which consists of a low-noise amplifier, a mixer with a frequency doubler on the local oscillator port, postamplification, and filtering. The total-power radiometers require tight temperature control. Thermoelectric cooler/heater units together with custom control circuitry permit a constant temperature of $50^{\circ}C$ over an external temperature range of -40 to $40^{\circ}C$.

The receiver box houses the intermediate-frequency (IF) chain and digital receiver for the beacon channels, the radiometer receivers, the data acquisition and control system, and the power supplies. The 70 MHz signal from the RF box is divided between the radiometer and beacon channels. The radiometer receivers detect the incoming noise, integrate for 1 s, and output a voltage to the data acquisition and control system. The beacon IF amplifies, double downconverts to 455 kHz, and filters to a 200 kHz bandwidth. The digital receiver acquires the signal, resolves the spectrum in 1 Hz bins, and outputs the power in a 20 Hz bandwidth containing the carrier to the data acquisition and control system, which records the four power levels once per second. This system also acquires and stores weather and system status data and performs periodic functions, such as noise diode firing in the RF box for radiometer calibration.

The ACTS propagation terminal includes computing hardware and software. A personal computer is interfaced to the data acquisition and control system through fiber optic cable. The acquisition software allows the user to monitor the experiment hardware, to preview and route collected data to a printer, and to perform certain control functions such as calibrations. A second software package, the ACTS preprocessing code, uses the recorded raw data together with calibration information to output a preprocessed data set consisting of radiometric and beacon attenuation as well as weather and status information.

System performance tests that were performed include controlled signal input measurements with the on-orbit Olympus satellite 20 GHz beacon and measurements with the ACTS beacons in Princeton, NJ. Results have shown a system 31 dB dynamic range, which exceeds the goal of 25 dB.

F1-3
0940

ADVANCED COMMUNICATIONS TECHNOLOGY SATELLITE (ACTS) Ka-BAND PROPAGATION MEASUREMENTS AT COLORADO STATE UNIVERSITY

J. Beaver, J. Turk, and V.N. Bringi
Department of Electrical Engineering
Colorado State University, Fort Collins, CO 80523
(303)-491-7678; FAX (303)-491-2249
email: turk@longs.lance.colostate.edu

In September 1993, the National Aeronuatics and Space Administration's (NASA) Advanced Communications Technology Satellite (ACTS) was deployed into geostationary orbit, near 100°W longitude. The ACTS satellite employs two Ka-band beacons, one at 20.185 GHz and another at 27.505 GHz, where impairments due to rain attenuation and tropospheric scintillations will be significant a greater percentage of the time. The experiments are divided into two categories. The propagation experiments, or Class I experiments, involve multi-year attenuation measurements along the satellite-Earth slant path. Class II experiments deal with other aspects of propagation, such as multipath and blockage effects upon communications channels. We will discuss initial Class I propagation measurements made with Colorado State's ACTS propagation terminal (APT) located in northeast Colorado. Designed and built by Virginia Polytechnic Institute, the APT is designed to collect both beacon signals and radiometric sky noise brightness temperatures using a PC-based system at a 1 Hz rate in an unattended mode. For path attenuations under $\approx$ 10 dB, the brightness temperatures can be related to the attenuation, and this is used to set the "clear sky" attenuation reference level. A separate software package is used to edit the monthly datafile to remove periods calibration and bad data, and prepare cumulative distributions of attenuation and rain rate.

In order to gain more understanding about the cloud microphysics responsible for fades during wet, rainy conditions, the CSU-CHILL polarimetric radar is used to take radar measurements along the slant path. The Colorado Front Range experiences a variety of weather conditions throughout the year, ranging from upslope rain conditions to winter storms containing considerable supercooled liquid water. Examples will be shown from rain and snow events during late 1993 and early 1994.

F1-4   ACTS PROPAGATION MEASUREMENTS IN FLORIDA
1000   Prof. Henry Helmken
          Department of Electrical Engineering
          Florida Atlantic University, M.S. SE-450
          500 NW 20th Street
          Boca Raton, Florida 33431

The Space Communications Technology Center, a NASA sponsored Center for the Commercial Development of Space (CCDS) at Florida Atlantic University, is developing systems for digital satellite communication of voice, data and video. One commercial area of interest is the transmission of High Definition Television (HDTV) signals via wideband satellite communication links such as may become available at Ka band (20/30 GHz). For reliable transmission at Ka band, careful consideration must be given to models of channel characterization and propagation statistics. A series of tests are planned for the Ka band Advanced Communications Satellite (ACTS) to evaluate coding and compression algorithms via a real satellite channel. To support these tests, the CCDS is actively engaged in a propagation measurements program centered around the ACTS Propagation Terminals (APT) and a transportable receive only terminal.

To support the CCDS effort and participate in the ACTS collaborative propagation program, one of the seven NASA APT has been established at the University of South Florida campus in Tampa, Florida. The station has been operating since beacon turn-on and the initial data has been processed. Preliminary results from this station will be presented.

In addition to the NASA sponsored ACTS propagation terminal program in Tampa, ACTS channel characterization work is being performed using single and two tone in-band CW signals. A receive only transportable terminal has been built and signals have been transmitted via ACTS from Lewis Research Center in Cleveland to the site locations in Florida. In addition, the terminal will be be set adjacent to the ACTS propagation terminal to make beacon and in-band comparison measurements. Preliminary channel characterization results will be presented.

F1-5 ACTS Propagation Experiment:
1040 Observations in Oklahoma
Robert K. Crane
School of Meteorology
University of Oklahoma
Norman, OK   73019

The University of Oklahoma was one of seven sites selected by NASA for the
ACTS Propagation Experiment. Each site was picked to represent a different rain
climate region. In addition, some of the experimenters could provide auxiliary
meteorological data useful for the development of improved rain attenuation
prediction models. Oklahoma was selected because it is in a region of rapid
spatial change in rain rate climate parameters and because of the ready
availability of rain-rate data from the Oklahoma Climatological Survey and
weather radar data from NEXRAD (WSR-88D) radars and the NSSL Cimarron Dual
Polarization weather radar.

Observations to date have been mainly diagnostic. The satellite is up and
working but problems are still being worked out in the areas of receiver
operation and data processing. It is to early to talk about attenuation
statistics from the experiment. This talk will present the current status of
the observing program in Oklahoma and discuss system calibration and data
quality assurance.

F1-6   **MULTIPLE FREQUENCY SLANT PATH RAIN ATTENUATION**
1100   **MEASUREMENTS AT 13.5, 20 AND 27 GHZ**
              USING ACTS AND TDRS

Louis J. Ippolito
Stanford Telecom
Reston, VA

Stephen Horan
New Mexico State University
Las Cruces, NM

An evaluation of the effects of rain on satellite slant paths at White Sands, New Mexico, was initiated with the first acquisition of the Advanced Communications Technology Satellite (ACTS) propagation beacons in September 1993. ACTS beacon measurements, at 20 and 27 GHz, are utilized in conjunction with 13.5 GHz rain attenuation data obtained from Tracking and Data Relay Satellite (TDRS) space-to-ground links, operating at 13.5 GHz. The elevation angle to ACTS is 51°, and the elevation angle to the TDRS constellation (Atlantic and Pacific ocean locations) ranges from 7° to 14°. Radiometric measurements at 20 and 27 GHz, and rain guage and weather instrumentation are also monitored at the site.

The primary objectives of the measurements program are: a) the study and analysis of the dynamics of fading on slant paths, and b) the development of attenuation and scintillation prediction procedures for low elevation angle/low margin systems. The multiple frequency ACTS/TDRS measurements at White Sands offers a unique opportunity to evaluate the effects of rain and other propagation degradations over a wide range of frequencies and slant path conditions.

Results of the first three months of measurements are presented, with emphasis on the relative impact of rain attenuation, scintillation, and atmospheric absorption on slant path link performance. Long and short term attenuation statistics at the three frequencies are developed and compared with existing models.

F1-7   20/30 GHZ SLANT PATH PROPAGATION MEASUREMENTS AND
1120   MODELLING
            Asoka Dissanayake
            COMSAT Laboratories
            Clarksburg MD 20871

Advanced Communication Technology Satellite (ACTS) provides an excellent opportunity to conduct propagation research in the 20/30 GHz frequency band specifically aimed at exploiting the frequency band for communication applications. With this objective in mind, several ACTS related experiments will be conducted by COMSAT laboratories, one of which involves long-term observation of slant path attenuation and other impairments. The measurement system involves two 20/30 GHz beacon/radiometer receivers, rain gauges and other ancillary weather sensors. The collected data will be analyzed to extract following information:

> o cumulative distributions of single site attenuation, sky noise and rain
>   rate
> o site diversity statistics of same parameters
> o gaseous absorption and cloud attenuation statistics
> o tropospheric scintillation statistics

In addition, investigations pertaining to the development of theoretical models on slant path propagation will be made. In particular, determination of the effective rain height and characterization of the vertical inhomogeneity of rain will be undertaken. To this end, a vertically looking radiometer placed next to one of the Ka-band beacon receivers will be used. Another investigation will attempt to characterize the frequency dependence of the effective medium temperature used in the conversion of sky noise to path attenuation. As the frequency increases, scattering from rain drops will contribute appreciably to the measured sky noise and the rain cells producing path attenuation cannot be treated as black body radiators. Sky noise measurements made at 20 and 30 GHz frequencies will be augmented by appropriate radiative transfer modelling for this purpose. Figure 1. shows an example of a radiative transfer calculation made with a finite cylindrical rain cell model where the variability of the medium temperature is depicted at three different frequencies.
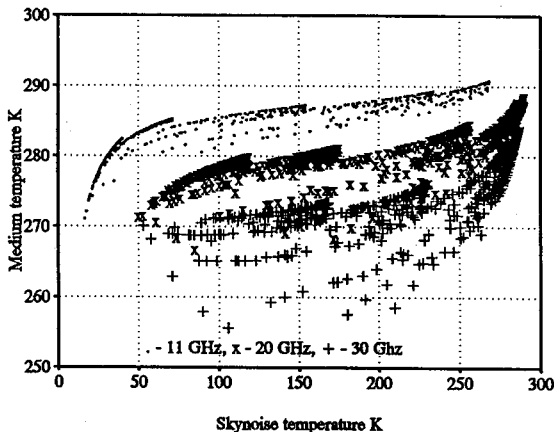

Figure 1 Radiative Transfer Simulation

F1-8   ONE YEAR OF NO PRECIPITATING ATMOSPHERIC ATTENUATION
1140   STATISTICS AT 20 GHz AND 30 GHz IN AVEIRO

Armando C. D. Rocha, José C. da Silva Neves, Júlio Nascimento
University of Aveiro
Department of Electronics

Atmospheric attenuation due to clouds and gases play an important rule for low fade margin satellite communications systems at 20 and 30 GHZ.

During the Olympus propagation measuring campaign, a dual frequency radiometer (21.3 GHz and 31.7) was installed near the propagation beacon receiver, in Aveiro a coastal city 300 Km north of Lisbon. While the main purpose was to use the radiometer to set the clear sky reference levels, radiometer data was also processed together with some meteorological data (ambient temperature, relative humidity and precipitation measured by drop-counter rain gauge) using in house developed Windows based Radiometer Data Analysis Program. Radiometer data files were unravelled, inspected and flagged either invalid , rainy or no-rainy .

Attenuation's at 21.3 GHz and 31.7 GHz were calculated and no-precipitating liquid water and also water vapour atmospheric contents were derived (Ed R. Westwater, Radio Science, 13, 677-685, 1978). The attenuation was scaled to 20 and 30 GHz and cumulative distributions obtained.

The well known Dintelman (F. Dintelman et al, Electronics Letters, 25, 1487-1488, 1989) and Altshuler (Edward E. Altshuler et al, IEEE Transactions on Antennas and Propagation, .37, 1473-1479, 1989) cloud attenuation prediction models were also evaluated at our site.

G1-1   SPATIAL CORRELATION OF IONOSPHERIC
0900   VARIAIBILITY
          R.A. Sprague
          Ocean and Atmospheric Sciences Division
          Research, Development, Test and Evaluation
          Division (NRaD)
          Naval Command, Control and Ocean
          Surveillance Center
          San Diego, CA 92152-5235

     The ionosphere is a highly variable medium on
many spatial and temporal scales. This variability
can have important consequences for all systems
which rely on transmission through or reflection
from the ionosphere. Study of these variations
requires ionospheric data collected with a time
resolution sufficient to resolve the shortest
periods of interest. It is also necessary to have a
relatively long sequence of such data in order to
adequately define the normal background variability
at these time scales. In this paper, some results
of a year long experimental campaign to determine
the magnitude and spatial correlation of
ionospheric variations will be presented. High
resolution (five minutes) time coherent digital
ionosonde data for this effort are being collected
at two sites, NRaD in San Diego and Utah State
University's Bear Lake facility near Logan, UT.
Examples of the correlation between ionospheric
parameters observed at San Diego and Bear Lake will
be presented.

G1-2   DIURNAL, SEASONAL AND SOLAR ACTIVITY
0920   VARIATIONS OF F-REGION PARAMETERS

Adolf K. Paul
7455 Brockway Dr.
Boulder, CO   80303
AND
R.A. Sprague
NCCOSC RDTE DIV, CODE 542
San Diego, CA   92152-5235

    Digital ionosondes combined with high quality
data processing methods permit the detection of
relatively small, but significant changes of
ionospheric parameters such as the critical
frequency of the F-region, the height of the
maximum, the half-thickness and the MUF(3000).
    The results to be presented are mainly based
on monthly median and upper and lower quartiles of
the parameters mentioned above, derived from
digital ionograms recorded at San Diego in five
minute intervals since March 1992.

G1-3   STATISTICAL DEPENDENCE OF AZIMUTH ANGLES OF
0940   ARRIVAL ON ELEVATION FOR MID-LATITUDE PATHS

W. M. Sherrill, Q. R. Black, and R. G. Reinhard
Southwest Research Institute
6220 Culebra Road
P.O. Drawer 28510
San Antonio, Texas 78228-0510

A large data base of DF Ionogram data has been collected over 24-48 hour periods for paths from 55 km to 3000 km in range. This large population of mode resolved DF data consistently exhibits increased azimuth spread about the great circle path with increasing elevation angle.

We present statistics of the azimuth angle of arrival vs elevation angle in four discrete time intervals for nominal 1000 and 3000 km mid-latitude ranges. Also included are azimuth statistics for 1E and various hop high and low ray F modes for the same paths. These DF ionogram results, representing examples of ionosphere limits to bearing accuracy, are briefly compared to existing standard representations of DF accuracy as well as to previously reported single mode azimuth spread statistics.

We discuss these results in terms of the achievable DF performance of mode resolving or mode separating direction finders when the lowest order propagation modes are used.

G1-4   IMPROVED HF PROPAGATION USING
1000   SATELLITE BEACON

Suman Ganguly
Center for Remote Sensing
P. O. Box 9244
McLean, VA 22102

A plan to improve the HF propagation prediction using the total electron content measurement is proposed. The ratio between the TEC and the maximum electron density is designated as slab thickness (T). This ratio shows much less variability than either the foF2 or TEC and can be used to predict the foF2 if measured TEC values are available.

The issues associated with the relative invariance of the slab thickness are addressed. The slab thickness is influenced by solar forces in a relatively indirect way and is mostly determined by the state of the neutral atmosphere. We propose schemes to model the slab thickness parameter for a better characterization of the ionosphere.

G1-5   ASSESSMENT OF foF2 SHORT-TERM VARIATIONS FROM
1040   TRANSIONOSPHERIC TIME-DELAY MEASUREMENTS

Z. Houminer
Asher Space Research Institute
Technion - Israel Institute of Technology
Haifa 32000, Israel

H. Soicher
Space and Terrestrial Communications Directorate
U.S. Army Communications-Electronics Command
Fort Monmouth, NJ 07703-5203

Both the total electron content of the ionosphere (TEC) and the critical frequency of the F2 layer (foF2) exhibit large day-to-day variations during quiet and active geomagnetic periods. It is of great interest to ascertain whether good correlation exists between TEC daily variability about the monthly mean and foF2 variations. With the availability of the global GPS constellation to provide instantaneous time-delay values such a correlation may enable the improvement of propagation predictions using passive monitoring of TEC.

In order to determine the correlation between the short-term variability of TEC and foF2, a pilot study was conducted using several months of TEC data taken in Haifa during 1980 and the corresponding foF2 measurements from Cape Zevgari, Cyprus. The TEC was determined from Faraday rotation observations using the signal of the Sirio satellite. The geographic subionospheric point corresponding to a ionospheric height of 350km is 30.3N and 28.9E. The geographic coordinates of Cape Zevgari are 34.6N and 32.9E.

Preliminary analysis indicates, that for large percentages of the time very good correlation exists between TEC and foF2 short-term variations.

G1-6   SEARCH FOR TEC MANIFESTATIONS OF CONVECTIVE
1100   STORMS, USING A VHF RADIO INTERFEROMETER

Y. Q. Li, R.C. Carlos, A. R. Jacobson, R. S. Massey and G. Wu
SST-7, MS D466
Los Alamos National Laboratory
Los Alamos, NM 87545

A satellite beacon-receiver array has been used to measure ionospheric disturbances in the Los Alamos area since January, 1993. This array includes 4 receiving stations which are separated with distances from 39 km to 81 km. The beacon signals from GOES-East (136.380 MHz) and ATS-3 (137.350 MHz) satellites were simultaneously monitored at all the stations, and ionospheric perturbations with period from 20 seconds up to hundreds of minutes were recorded.

It has been previously reported by other workers that wavelike disturbances were observed in the ionosphere with irregular periods around 3 minutes when severe thunderstorms occurred within a distance of 250 km. These disturbances were reported to last from a few minutes up to several hours. In the summer of 1993, there were many thunderstorm activities in the Los Alamos area; this provided us an opportunity to investigate the possible effects of thunderstorms in the ionosphere. Using the data from our beacon-receiver array, we studied the ionospheric perturbations we observed in the frequency range of 2 - 5 minutes in the active thunderstorm season. The power spectra were statistically studied for different local time and were compared with the months when there was no thunderstorm activity. We will report and discuss our study results in this presentation.

G1-7
1120

ACCURACY OF THE "SECANT-χ" CORRECTION IN THE
PRESENCE OF IONOSPHERIC IRREGULARITIES

E. Hernandez-Baquero and W.A. Pakula
c/o W.A. Pakula
Ionospheric Effects Division
Phillips Lab / GPIM
Hanscom AFB, MA 01731-3010

Total Electron Content (TEC) is the integral of ionospheric electron density (electrons/cm^3) along a path through the ionosphere, and is an important parameter in ionospheric physics. Measurements of ionospheric TEC are commonly made using techniques based on either the Faraday rotation or on the carrier phase advance(s) of radio signals from a passing spacecraft. The oblique, line-of-sight measurements of TEC are often corrected in some way to approximate a true-vertical TEC measurement at some point of interest between the ground station and the spacecraft position. Alternatively, the correction is made so as to approximate the vertical TEC at the point where the ray path(s) intersect some altitude of interest. In either case, the correction itself involves dividing the TEC measurement along a particular ray path by the secant of the angle between it and true vertical at the location of interest.

The purpose of this work is to quantify the accuracy of the "secant-χ correction" in the presence of regions of *smooth* gradients of electron density, such as a smooth variation with latitude, and regions of *sharp* gradients, such as enhancements ("blobs") or depletions ("troughs") of electron density. Fully analytic formulas are used to model the ionospheric regions of interest and comparisons are made between the true vertical TECs and the approximations at various locations.

INHOMOGENEOUS FLOWS AND THEIR STABILITY IN
LABORATORY AND SPACE PLASMAS

Chairman: M.C. Lee, Plasma Fusion Center, MIT, Cambridge, MA 02139. Organizers: G. Ganguli, Plasma Branch, Naval Research Laboratory, Washington, DC 20375; and M.C. Lee

H1-1
0900

INSTABILITIES DUE TO VELOCITY SHEAR

G. Ganguli
Beam Physics Branch, Code 6794
Plasma Physics Division
NRL, Washington DC 20375, USA

Magnetospheric boundary layers are characterized by strong velocity shear (Romero, et al., Geophys. Res. Lett., 17, 2313, 1990). Significant velocity shear is also observed in the ionosphere (Tsunoda, et al., J. Geophys. Res, 94, 15277, 1989). Strongly sheared flows are generated in chemical release experiments in space (Bernhardt, et al., J. Geophys. Res, 92, 5777, 1987), and in laser produced plasma jets in laboratory experiments (Peyser, et al., Phys. Fluids., B 4, 2448, 1992). Velocity shear can give rise to a number of instabilities in a broad frequency range which can significantly affect the dynamics and morphology of a plasma system.

It is well known that velocity shear can excite the low frequency long wavelength Kelvin-Helmholtz instability. However, in a number of space observations and laboratory experiments higher frequency (ion cyclotron frequency and higher) oscillations are reported which appear to be correlated with velocity shear. We (Ganguli, et al., Phys. Fluids., 31, 823, 1988; Ganguli, et al., Phys. Fluids., 31, 2753, 1988) find that when the shear frequency, w_s ($=V^0/L$, where V^0 is the peak value of the flow velocity and L is the scale-size of its gradient), is large enough to resonate with natural frequencies of the system, velocity shear can excite instabilities around these frequencies.

Numerical simulations and laboratory experiments show that nonlinear steepening of low frequency waves can lead to stressed regions characterized by large velocity shear. Also, observationally (and by global MHD simulations) it is found that stress can build up in the magnetosphere due to solar wind compression. Increasing stress can trigger the hierarchy of micro-instabilities described above. These instabilities relieve the stress and thereby play an important role in the dynamics and energy balance of a plasma system. Our PIC simulations (Nishikawa, et al., Phys. Fluids., 31, 1568, 1988; Nishikawa, et al., J. Geophys. Res, 95, 1029, 1990; Romero, et al., Phys. Rev. Lett., 69, 3503, 1992; Romero and Ganguli, Phys. Fluids. B, 5, 3163, 1993) show that the velocity shear driven instabilities are typically characterized by a broadband frequency spectrum, can provide significant viscosity and resistivity, lead to energization, and can affect plasma morphology. Implication of this on space and laboratory plasmas will be discussed.

H1-2
0920

HALL MHD SIMULATIONS OF THE KELVIN-HELMHOLTZ INSTABILITY

J.D. Huba
Code 6794, Plasma Physics Division
Naval Research Laboratory
Washington, DC 20375-5320

Hall MHD dynamics has received considerable attention in recent years regarding space and laboratory plasma phenomena. Inclusion of the Hall term in MHD theory extends the validity of the model to time scales faster than an ion cyclotron period ($\partial/\partial t > \Omega_i$) and length scales shorter than an ion gyroradius ($\rho_i > L$); however, the electrons are assumed to remain strongly magnetized (i.e., $\partial/\partial t < \Omega_e$ and $\rho_e < L$). Linear theory studies [Opp and Hassam, *Phys. Fluids B, 3*, 885, 1991; Fujimoto and Terasawa, *J. Geophys. Res., 96*, 15,725, 1991] indicate that the Hall term can modify the behavior of the MHD Kelvin-Helmholtz instability in two ways. First, a new, short wavelength mode ($kL > 1$) appears because of the Hall term, and second, the linear growth rate is a function of the sign of the vorticity (i.e., $\nabla \times \mathbf{V}$). We present 2D Hall MHD simulations of the Kelvin-Helmholtz instability to study these effects, and the nonlinear evolution of the instability. The simulation model describes the dynamics of the plasma and field transverse to the ambient magnetic field $\mathbf{B} = B(x,y)\,\mathbf{e}_z$; this is the most unstable configuration. The results are applied to several boundary layers in space plasmas (e.g., the earth's magnetopause, the Venus ionopause, the cometary ionopause).

H1-3   **SHEAR FLOWS IN THE SOLAR ATMOSPHERE**
0940   Judith T. Karpen
        Code 7675K
        Naval Research Laboratory
        Washington, DC 20375-5352

The Sun is a highly dynamic environment in which significant temporal and spatial variations in the velocity field are the rule rather than the exception. Both observations and theory show that shear flows in particular are ubiquitous throughout the solar atmosphere. In the high plasma β photosphere, the convection-driven horizontal flow pattern is predominantly convergent or divergent, except in the network where the granular cells meet; at such locations substantial shears are expected and have been measured down to the resolution limit of current instrumentation (Brandt *et al.* 1988, Nature 335, 238). Emerging magnetic flux also is likely to contain strong mass motions, yielding strong shears at the boundaries of the buoyant fluxtubes. Numerous jet-like phenomena are observed higher in the chromosphere and transition region, including spicules, surges, and the HRTS explosive events (*e.g.*, Dere *et al.* 1991, JGR 96, 9399). Understanding the dynamics of these events is essential to estimating the mass and energy balance of the solar atmosphere, as well as the transport of magnetic flux into the heliosphere. According to the wave–resonance theory of coronal heating (Hollweg 1984, ApJ 277, 392; Davila 1987, ApJ 317, 514), highly localized counterstreams driven at the global resonance frequency are associated with narrow absorption layers in coronal loops. A final example is the strong velocity gradient at the boundaries between high-speed and low-speed solar wind streams, and at selected sites where the solar wind interacts with the Earth's magnetosphere (*cf., e.g.,* Goldstein *et al.* 1989, in Solar System Plasma Physics, p. 113).

My colleagues at NRL and GSFC and I have been studying solar shear flows for the past few years, with particular emphasis on their stability, nonlinear evolution, and effects on fundamental solar activity. Our approach combines theoretical analyses and multidimensional numerical simulations, and utilizes available solar observations to initialize and test our models. In general, we find that shear flows in regions of weak parallel (or mostly transverse) magnetic field are indeed susceptible to ideal fluid or MHD instabilities, and hence can become filamentary or even turbulent within the characteristic timescales of the underlying activity. Although comparison with observations is difficult, due to the ~0.5-1 arcsec (350-700 km) resolution limit for most instruments, applicable data (*e.g.*, nonthermal spectral line widths in the corona) apparently confirm this scenario.

In this talk I will discuss three such investigations*:

- Kelvin–Helmholtz instability in photospheric shear flows at granule boundaries, and implications for direct-current coronal heating models (Karpen, Antiochos, Dahlburg, & Spicer 1993, ApJ, 403, 769)
- Transition to turbulence and secondary instability in MHD shear layers, and implications for solar surges (Dahlburg & Karpen 1993, in preparation)
- The stability and evolution of flows in resonance absorption layers in coronal loops, and effects on wave–resonance heating (Karpen, Dahlburg, & Davila 1993, ApJ, in press)

H1-4   Magnetohydrodynamic Turbulence in Cosmic Winds
1000   Dr. M. L. Goldstein
       Laboratory for Extraterrestrial Physics
       Code 692
       Goddard Space Flight Center
       Greenbelt, MD 20771

Turbulence involves the nonlinear interaction of various scalar and vector fields over a wide range of scales. The solar wind provides an ideal laboratory for the study of such processes because the space and time scales involved are relatively large, making it possible to sample relevant small scales, and the wind speed is much faster than signal propagation speeds, making it possible to treat time series of spacecraft measurements of particles and magnetic fields as spatial "snapshots." Here we review what is known about the solar wind as a magnetohydrodynamic (MHD) turbulence laboratory with an emphasis on what it can teach us about general processes occurring in such flows.

Initial observations of the solar wind magnetic field and moments of particle distribution functions (mainly density, velocity, and temperature) suggested that the solar wind might not be turbulent. The amplitudes of the observed fluctuations were relatively high, with the fluctuating magnetic field on the order of half the "mean" Parker field, and the spectrum of the fluctuations was nearly that of the "inertial range" of turbulence as predicted by fluid models, but the origin of most of the "waves" appeared to be the Sun. This was determined by observing that the dominant, Alfvén, wave mode was propagating nearly always away from the Sun thus implying its origin was almost certainly below the Alfvénic critical point where the wind speed became faster than the Alfvén speed. Moreover, pure Alfvén waves undergo no nonlinear couplings in incompressible, homogeneous MHD, and thus it seemed possible that most of the fluctuations were generated by turbulent processes near the Sun and advected outwards. Only where streams interacted, in this picture, would there be a substantial wave generation far from the Sun. As spacecraft observations became available far from the Earth's orbit, it became clear that while much of the initial power in the fluctuations was from the Sun, the observed evolution with heliocentric distance in power spectral shapes and the degree to which the fluctuations were Alfvénic, the heating of the medium, and the evolution of various other correlations all indicated that the wind was dynamically evolving. In light of this, the main questions become "What is the nature of the evolution?" and "What can the solar wind tell us about MHD turbulence?"

Roughly speaking, the solar wind plasma may be regarded as large scale flows ("streams" and related structures with an embedded nearly spiral large scale magnetic field) plus fluctuations about these large structures. The large scales can change the fluctuations due to "stirring" (shear), compression, and overall spherical expansion, and the small scales can react back on the large scales, perhaps significantly accelerating and heating the bulk plasma. Analytical approaches to the modeling of the solar wind typically take either the small or large scales as given by some simple construction and determine the effects of these simple fields on the other scale fields. This scale separation approach makes it possible to treat expansion effects and to isolate the contributions of particular terms in the equations. Computer simulation does not make any (ultimately artificial) scale division, but the limits of present computers force each model to focus on particular aspects of the overall problem. The complexity of the problem demands that we approach it from many avenues and continually check theory and simulation against the data. Present simulations have yielded power spectral and Alfvénicity evolution similar to that observed, and tend to support the conclusion from theoretical considerations that the dominant effects in the plasma are typically incompressive. Compressive effects, in this view, are largely forced by the incompressive fields. It is still an open question to what degree the Alfvénic, incompressive, fields will evolve due to interaction with quasi-static, nearly pressure balanced structures observed to be convected from the Sun. It is also not yet clear whether the effects of expansion alone can produce much of the observed evolution; the expansion will tend to enhance the role of structures with wave vectors nearly perpendicular to the spiral field, and this produces some effects similar to those observed. Overall, considerable progress has been made in understanding MHD turbulence, and the currently existing tools offer a rich variety of avenues of approach for resolving the many outstanding questions in solar wind turbulence research.

H1-5
1040

VELOCITY SHEAR FLOW AND VISCOUS TRANSPORT
AT THE MAGNETOPAUSE: AN OVERVIEW

D. Winske
Applied Theoretical Physics Division
Los Alamos National Laboratory
Los Alamos, NM 87545

The solar wind interaction with the Earth's magnetosphere occurs at a boundary known as the magnetopause. More than thirty years ago it was recognized that the magnetopause would be subject to the Kelvin-Helmholtz instability and the resulting viscous interaction could transfer momentum from the solar wind to the magnetosphere and create the observed boundary layer. In the first half of this talk, I will review the basic arguments for the existence of such processes and estimates of the importance of their effects. Moreover, some of the continuing controversies associated with viscous processes will be discussed. The second half of the presentation will involve recent observational and numerical modeling work at Los Alamos related to shear flow at the magnetopause and further upstream at the bow shock. This will include a description of accelerated flows at the magnetopause and anomalous flow events at the bow shock. Efforts to model these processes as well as to study the Kelvin-Helmholtz instability at the curved surface of the magnetopause by means of particle MHD and kinetic ion/fluid electron hybrid codes will also be discussed.

H1-6   SHEARS IN MAGNETOSPHERIC PLASMA FLOWS
1100   A. T. Y. Lui

          Applied Physics Laboratory, Johns Hopkins University
          Laurel, MD 20723-6099

     Shears in plasma flows represent an important free energy source to
drive dynamical processes in space plasmas. Plasma flows in the Earth's
magnetosphere can be measured accurately and have been studied quite
extensively. However, the non-uniformity in magnetospheric plasma flows
cannot be determined directly with a single satellite and thus is seldomly
assessed from these measurements. In this paper, we review observations
relating to shears in magnetospheric plasma flows and show some
observational hints suggesting that shears in plasma flows may play an
important role in many dynamical evolution of magnetospheric plasmas.

H1-7   STRUCTURE IN THE IONOSPHERIC DENSITY AND
1120   VELOCITY AT HIGH LATITUDES.

R. A. Heelis
Center for Space Sciences
University of Texas at Dallas
PO Box 830688 Richardson, TX 75083-0688

Measurements of the ionospheric number density and the ion
drift velocity at high latitudes have been made by the
Dynamics Explorer-2 satellite throughout the high latitude
region. Progress has been made in describing the spectral
characteristics of the density and velocity structures and in
relating the differences in the spectral characteristics to
each other. Here we report on initial studies aimed at
relating the varying nature of small-scale structures to the
larger scale morphology of the ionospheric density, motion,
and temperature. We describe some of the phenomenology of
the high latitude ionosphere by correlating the small scale
structures with the large scale behavior of the region. Such
studies lead to a discussion of the links between macro and
micro- scale processes wherein small-scale processes may be
responsible for larger scale behavior and large-scale
characteristics may be required to produce observed small-
scale structure.

Session A-1 1355-Wed. CR1-42
EM FIELD AND ANTENNA MEASUREMENTS
Chairman: Moto Kanda, NIST, Boulder, CO 80303

TIME-DOMAIN & FREQUENCY-DOMAIN CHARACTERIZATION
A1-1   **OF TWO SMALL, IDENTICAL TEM-HORN ANTENNAS**
1400   Dr. John F. Aurand
Sandia National Laboratories
High-Power Electromagnetics Department 1248
P.O. Box 5800
Albuquerque, NM 87185

Several experiments were recently performed with two identical, small transverse-electromagnetic (TEM) horn antennas. The purpose was to determine if it is possible to build simple antennas with sufficient bandwidth to have an effective step-equivalent risetime of less than 50 ps. This paper describes the antenna experiments, and compares three different methods for measuring the boresight/main-beam transmitting and receiving responses of TEM horns.

TEM horns are commonly used for wideband time-domain work because they offer minimum dispersion as a traveling-wave endfire structure which can be made fairly nonresonant.   Two nominally-identical 15-cm-long antennas were available and small enough to have a maximum geometrical time smearing on the order of 50 ps, so they were employed in this investigation. The two antennas were pointed directly at each other in a transmit-receive configuration, and the range between them was varied from 0.6 m to 4.6 m.

Two time-domain methods and one frequency-domain method were used for these experiments. The three basic instrumentation setups were as follows: 1) a time-domain setup utilizing a step generator for the transmitter and a 20-GHz digital sampling oscilloscope for the receiver, 2) a time-domain setup utilizing an impulse excitation of the transmitting antenna instead of a step excitation, and 3) a frequency-domain setup utilizing a 13-GHz vector network analyzer. In all cases, the primary goal of the experimental procedure was to measure the transfer function between antenna terminals, or equivalently, the input and output waveforms. The time-domain E and H-plane antenna patterns were also measured, as well as the effect of antenna separation on the time-domain waveforms.

The wideband performance of an antenna is most succinctly modeled in terms of frequency-domain transfer functions. The combination of transmitting and receiving antennas can be modeled as a cascaded network of the transmitting and receiving transfer functions, so that the complex ratio of input and output voltages is

$$S_{21}(f) = \frac{V_o(f)}{V_i(f)} = T(f,r)\,R(f),$$

where *T(f,r)* is the transmitting transfer function versus frequency and range, and *R(f)* is the receiving transfer function. For the double-antenna configuration here, where the transmitting and receiving antennas are assumed to have identical electromagnetic performance, then the sole measurement of S_{21} is sufficient to determine both transmitting and receiving transfer functions. This is based on the general reciprocity relation between the transmitting and receiving characteristics of an antenna. This was done with the data obtained from the three measurement techniques, and the results will be presented in this paper.

These small horns were found to have a transmitting step-equivalent risetime of 33 ps. This paper describes the antenna experiments which were performed, presents the resulting transmitting and receiving characteristics of the small TEM horn antenna (assuming two identical antennas), and compares the time-domain and frequency-domain antenna measurement techniques.

A1-2
1420
DE-EMBEDDING TECHNIQUES FOR MEASURING THE INPUT MATCH OF A LARGE PARALLEL-PLATE TEM-HORN ANTENNA

Dr. John F. Aurand
Sandia National Laboratories
High-Power Electromagnetics Department 1248
P.O. Box 5800
Albuquerque, NM 87185

A large TEM-horn transmitting antenna was recently designed and built for use in a high-power microwave transmitter. The antenna is 2.74-m long, with a parallel-plate input having a plate width of 1.22 m and a separation of 10 cm, yielding a surge characteristic impedance of 27 Ω. The parallel-plate input mates to a Blumlein pulser, which generates high-voltage pulses to be radiated by the antenna. This paper describes the measurement techniques which were developed and employed to characterize the input match of this antenna.

A TEM transmission-line transition had to be built to connect measurement instrumentation with 50-Ω coaxial connectors to the 27-Ω parallel-plate antenna input. Seven different versions of coax to parallel-plate transitions were constructed and evaluated for use, in an attempt to develop the best one for measuring the TEM horn antenna. The final version of the transition is a triangular parallel-plate assembly 4.1 m long, with a transverse SMA connector soldered to the input apex end of the two plates.

The goal of the antenna measurement task was to accurately measure the magnitude of the frequency-domain voltage reflection coefficient, $|\Gamma|$, at the parallel-plate input of the TEM horn antenna, over a frequency range of 100 MHz to 1 GHz. A vector analyzer was used, but the S_{11} measurement it makes is referenced to the coaxial input connector of the transition. Because every transition has some mismatch and insertion loss, the input reflection coefficient measured by the vector analyzer, ρ (= S_{11}), is different from the desired reflection coefficient at the output of the transition (the input of the antenna), $\Gamma(f)$. This is especially true of the type of transition required here. It must provide: 1) a dramatic change in the electromagnetic field geometry (from coaxial to parallel plate), and 2) a transformation of characteristic impedance from 50 Ω in the coaxial line to 27 Ω at the input of the antenna. These two conditions always limit the electrical performance of transmission line transitions. The worst problem was the mismatch at the coaxial feedpoint of the transition, which caused multiple reflections within the transition.

Three different de-embedding techniques were developed for estimating $\Gamma(f)$ from a measurement of $\rho(f)$ through a nonideal transition. Two techniques are direct S-parameter de-embedding methods, requiring characterization of the transition's S parameters. $\Gamma(f)$ can then be computed from the measurement of ρ:

$$\Gamma(f) = \frac{\left(\rho - S_{11}\right)}{S_{22}\left(\rho - S_{11}\right) + S_{12}S_{21}}.$$

The third technique, which could be termed 'time-gated normalization,' employs the built-in time-domain gating of vector analyzers to minimize the measurement errors introduced by the ringing caused by the coaxial-feedpoint mismatch. It then utilizes frequency-domain normalization of the desired load to both an open-circuit reference load and to a short-circuit reference load. This time-gated normalization method was found to work the best.

This paper describes the antenna measurement problem and the techniques which were developed to solve it. The types of transitions built will be shown, the de-embedding techniques will be described, and representative antenna input-match data will also be given.

A1-3
1440
A High Dynamic Range Time-Domain Shielding Effectiveness Measurement System

Arthur R. Ondrejka
Robert T. Johnk
Motohisa Kanda
National Institute of Standards and Technology
Boulder, Colorado

and

Kurt E. Mikoleit
Naval Surface Warfare Center
Dahlgren, Virginia

A wide variety of shielding effectiveness measurement techniques have been developed at the National Institute of Standards and Technology (NIST) over the years. One approach that has been particularly useful is to carry out the shielding effectiveness measurements in the time domain. The instrumentation requirements are quite modest, requiring two TEM horn antennas, a sampling oscilloscope with digitizing capability, a fast-risetime pulse generator, and a computer for signal processing. The measurement procedure consists of placing a panel of the shielding material between the two TEM horns, and time gating out the direct-path signal that penetrates through the material. The shielding effectiveness is then computed as a function of frequency through a deconvolution of the direct-path signal and a reference signal that is taken with the sample removed. The simplest version of this system can measure materials that have shielding effectiveness values up to 45-50 dB.

With the assistance and support of the Naval Surface Warfare Center (NSWC), the existing NIST measurement system has been modified to measure shielding effectiveness values as high as 75-80 dB. While the basic measurement procedure remains unchanged, the system dynamic range is significantly increased by the addition of an optical fiber trigger link and by the use of low-noise pulse amplifiers. A precursor problem associated with the use of the impulse generator is also remedied by the use of baseline diode clippers. Measurement results on materials with a high shielding effectiveness will be shown.

A1-4   **INFRARED MEASUREMENTS OF ELECTROMAGNETIC FIELDS**
1520   **IN SHAPED-END CIRCULAR WAVEGUIDE MICROWAVE ANTENNAS**

John Norgard[*], Joseph Sadler, Ronald Sega[**]
Ernie Baca, William Prather
Microwave Research Group
USAF Phillips Laboratory
3550 Aberdeen Avenue SE
Kirtland AFB, NM 87117-5776

An infrared (IR) imaging technique is used to measure the internal modes and the radiation patterns of a 30° bevel-cut circular waveguide antenna. An IR image of the electric field distribution is produced by the Joule heating that occurs in a thin lossy IR detector screen placed in the measurement plane, either in the cross section of the waveguide feed line or in the E or H plane outside the aperture of the antenna. The absorbed heat energy in the detector material is converted into conducted and convected heat energy and into re-radiated EM energy. The EM energy is concentrated in the IR band and is detected with an IR camera as the energy radiated from a "blackbody". The absorbed energy causes the temperature of the detector to rise above the ambient temperature of the waveguide by an amount proportional to the local electric field intensity (energy) at each point in the screen material. The temperature distribution in the screen material is a map of the intensity of the electric field distribution absorbed in the screen.

The antenna is fed with a coaxial TM_{01} mode for compact size and efficient operation. From symmetry, the TM_{01} mode does not radiate in the bore-sight direction; therefore, a mode converter/radiator is used to convert this mode to the dominant TE_{11} mode. A 30 degree bevel-cut radiator is examined. To improve the directivity of the antenna, the beveled end is shaped into a smooth contour. Near-field and far-field radiation patterns of the beveled-end and the shaped-end antenna are measured and compared.

---

[*] Also with the University of Colorado at Colorado Springs
[**] Also with NASA/JSC Houston

A1-5   **ELECTRONIC MODE STIRRING FOR REVERBERATION CHAMBERS**
1540   David A. Hill
        Electromagnetic Fields Division
        National Institute of Standards and Technology
        Boulder, CO 80303

Reverberation chambers (also called mode-stirred or mode-tuned chambers) are becoming increasingly popular for electromagnetic immunity testing. Such chambers can generate high field strengths using modest power sources. The goal of reverberation chambers is to create a statistically uniform field that eliminates the need to rotate the test object. A mechanical mode stirrer (paddle wheel) is usually used to vary the chamber boundary conditions in an attempt to obtain statistical field uniformity. Mechanical stirring can be quite effective, but it is fairly slow. It has been pointed out that rotating a mechanical stirrer continuously changes the resonant frequencies of the cavity modes and that mechanical stirring has some equivalence to frequency modulation of the source (D.I. Wu and D.C. Chang, IEEE Trans. Electromag. Compat., 31, 164-169, 1989). Statistical predictions of the field homogeneity achieved by frequency stirring have been made and compared with measurements using a band-limited, white, Gaussian noise source (T.A. Loughry, "Frequency stirring: an alternative approach to mechanical mode-stirring for the conduct of electromagnetic susceptibility testing," Phillips Laboratory, Pl-TR-91-1036, 1991).

In this talk we use the Green's function for a line source in a rectangular cavity to perform field uniformity calculations as a function of the source bandwidth and cavity parameters. The two-dimensional model is idealized, but it contains most of the relevant physics of the problem and has been shown to be useful in an analysis of mechanical stirring. We also derive an approximate expression for the power density in the cavity by using a uniform power density assumption of the type used in room acoustics. Numerical results show that for typical cavity dimensions good field uniformity (standard deviation less than 1 dB) can be obtained with a bandwidth of 10 MHz at a center frequency of 4 GHz. The bandwidth requirement is determined primarily by the number of modes excited, and higher frequencies can achieve the same field uniformity with a smaller bandwidth because of the higher mode density. The absolute field level calculated from the Green's function agrees well with the approximate field level derived from conservation of power.

We also examine the possibility of exciting the cavity with multiple sources (antennas) and calculate the field uniformity achieved from varying the relative phases of two sources (phase stirring).

A1-6   LIMITED-ANGLE-OF-INCIDENCE AND LIMITED-TIME
1600   ELECTRIC SENSORS
         Carl E. Baum
         Phillips Laboratory/WSR
         3550 Aberdeen Ave SE
         Kirtland AFB NM 87117-5776

     This paper considers two classes of antennas
which under the right conditions can be considered
as accurate time-domain sensors of an incident
electric field. One class gives an output pro-
portional to the incident time-domain field, while
the second class gives the time integral. As these
are electrically large but not infinitely large,
there is in general a limited time based on when
the truncation sends a signal to the output ter-
minal pair. Furthermore there are limitations on
the allowable angles of incidence of a plane wave
for ideal performance. They do not measure a
single component of the incident field, independent
of angle of incidence, in the manner of the
classical electrically small electric-dipole
sensor.

SCATTERING I

Chairman: P.L.E. Uslenghi, Dept. of Electrical Engineering and Computer Science, Univ. of Illinois, Chicago, IL 60680

B3-1   FULL WAVE SOLUTIONS OF ELECTROMAGNETIC WAVES
1400   SCATTERED FROM IRREGULAR STRATIFIED MEDIA
          Ezekiel Bahar and Yuzhi Zhang
          Department of Electrical Engineering
          University of Nebraska-Lincoln
          Lincoln, NE 68588-0511

The analysis of electromagnetic fields scattered from irregular stratified media can be applied to the problems of remote sensing, thin film analysis, and communications in stratified media. To this end, full wave solutions are derived for the vertically and horizontally polarized fields scattered from an irregular stratified structure consisting of three distinct media, air, coating material and substrate. The upper and lower interfaces are two dimensionally random rough surfaces. The thickness of the coating material is uniform. The waves are depolarized upon scattering, since the normal to the rough surface is not restricted to the reference plane of the incidence. Since the coating thickness is uniform the multiply reflected fields are not expressed as double infinite sums (E. Bahar, Radio Science, 23, 5, 749-759, 1988, E. Bahar and M.-A. Fitzwater, IEEE Trans. on AP, Vol.37, No.12, 1609-1615, 1989). The full wave solutions satisfy the duality and reciprocity relationships in electromagnetic theory and the surface element scattering coefficients are invariant to coordinate transformations.

The terms of the full wave solutions for the scattered fields from the irregular three media structure have simple physical interpretations. The first term is associated with waves scattered upon reflection from the upper interface. The second term is associated with waves that make multiple round trips in medium 1 before being scattered upon transmission into medium 0. The third term is associated with waves that are scattered upon transmission into medium 1 from medium 0 and make multiple round trips in medium 1 before they are transmitted back to medium 0. The fourth term is associated with waves that make multiple round trips in medium 1 before being scattered upon reflection from below the upper interface and then make multiple round trips in medium 1. The fifth term is associated with waves that are scattered upon reflection from the lower interface. These waves are multiply reflected in medium 1 before and after they are scattered by the surface element.

The full wave solutions for the scattered fields are used to derive expressions for the elements of the 4×4 modified Mueller matrix. The rough surface height and slope of the structure are assumed to be normally distributed.
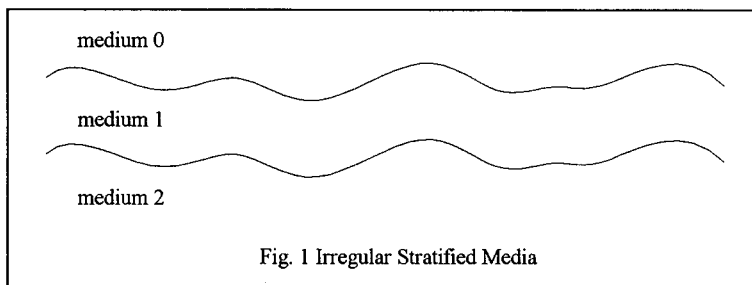

Fig. 1 Irregular Stratified Media

ELECTROMAGNETIC SCATTERING BY A SYSTEM OF TWO UNIFORMLY LOSSY DIELECTRIC PROLATE SPHEROIDS IN PARALLEL CONFIGURATION

Soumya Nag and B. P. Sinha
Faculty of Engineering and Applied Science
Department of Electrical Engineering
Memorial University of Newfoundland
St. John's, NF, A1B 3X5, Canada.

By means of modal series expansions of electromagnetic fields in terms of prolate spheroidal vector wave functions, an exact solution is obtained for the scattering by two uniformly lossy dielectric prolate spheroids in parallel configuration embedded in free space, the excitation being a monochromatic plane electromagnetic wave of arbitrary polarization and angle of incidence. Since the dielectric medium of the scatterers is complex in nature, complex eigenvalues have been evaluated for the spheroidal scalar wave function of transmitted components of E-field and H-field expansions.

$\overline{M}^{(a)}$ vectors for E-field expansion and $\overline{N}^{(a)}$ vectors for H-field expansion $[\overline{M}^{(a)} = \overline{\nabla}\psi(h;\xi,\eta,\phi) \times \hat{a}; \overline{N}^{(a)} = (1/k)\overline{\nabla} \times \overline{M}^{(a)}, \hat{a} = (\hat{x},\hat{y},\hat{z})]$ have been used in the present problem together with the Translational Addition Theorem for spheroidal vector wave functions (B. P. Sinha and R. H. MacPhie, *Quart. Appl. Math.*, **38**, 143-158, 1980). The Theorem which transforms the outgoing wave from one spheroid into the incoming wave at the other spheroid assume the simplest form for $\overline{M}^{(a)}$ and $\overline{N}^{(a)}$ vectors, because they translate like a scalar wave function $\psi(h;\xi,\eta,\phi)$.

By applying appropriate boundary conditions, the field solution is obtained in the form $\underline{S} = [G]\underline{I}$, where $\underline{S}$ and $\underline{I}$ are respectively the column vector of the unknown coefficients of the series expansions of the scattered and transmitted fields taken together and the column vector of the known coefficients of the series expansions of the incident field. $[G]$ is the system matrix which depends only upon the geometries of and spacing between the scatterers. The solution in the above form eliminates the need for repeatedly solving a new set of simultaneous equations in order to obtain the expansion coefficients of scattered and transmitted fields for a new angle of incidence. Numerical results in the form of curves for the Bistatic and Monostatic Radar Cross sections are given for a variety of two-body system of parallel uniformly lossy dielectric prolate spheroids having resonant or near resonant lengths and having different distances of separation.

B3-3   SCATTERING FROM CONES, WEDGES,
1440   AND HALF SPACES
           Carl E. Baum
           Phillips Laboratory/WSR
           3550 Aberdeen Ave SE
           Kirtland AFB NM 87117-5776

This paper considers the far scattering from
general cones based on the dilation symmetry of
such objects. These include not only perfectly
conducting cones, but also apply to various forms
of the constitutive parameters (dielectric cones,
etc.). The far-scattered field exactly factors
into a dyadic angular function times the time
integral of the incident field. Similar results
apply to wedges and half spaces with the same
dilation symmetry except that the frequency-
dependent (or s) part of the scattering is
proportional to $s^{\frac{d-1}{2}}$ where d is the number of
dimensions describing the expansion of the far
fields.

B3-4   SCATTERING FROM FINITE WEDGES AND
1500   HALF SPACES
Carl E. Baum
Phillips Laboratory/WSR
3550 Aberdeen Ave SE
Kirtland AFB NM 87117-5776

The far scattering from finite-length wedges and finite-dimensioned half spaces is developed based on dilation symmetry with respect to cones, wedges, and half spaces. This leads to a form (decomposition) of the scattering which is exact for early times, involving a few terms which are each real 2 x 2 dyadics times a simple temporal operation (integral, identity, derivative) on the incident plane-wave field. The time of validity is given by the first appearance of multiple scattering at the observer.

B3-5   EXACT RADIATION AND SCATTERING FOR AN OBLATE
1540   SPHEROIDAL CAVITY IN A GROUND PLANE
P.L.E. Uslenghi
Department of Electrical Engineering and Computer Science (M/C 154)
University of Illinois at Chicago, Box 4348, Chicago, IL 60680

Some exact solutions are obtained for acoustical and electromagnetic radiation and scattering boundary-value problems involving a cavity in an infinite ground plane. The cavity's shape is that of half an oblate spheroid, with its symmetry axis z perpendicular to the ground plane z=0. This shape is obtained by rotating half an ellipse of interfocal distance d about its minor axis; the resulting focal circle of diameter d in the plane z=0 is the hole coupling the cavity to the half-space z>0 (see figure).

The following frequency-domain boundary-value problems are solved exactly in terms of series of oblate spheroidal wave functions. For either acoustically soft or hard boundaries, the radiation of an arbitrarily located point source and the scattering of an obliquely incident plane wave are determined. In the electromagnetic case with perfectly conducting boundaries, the radiation of an electric or magnetic dipole located on the z axis and axially oriented is obtained. For all these cases, implications in low and high frequency approximations are discussed.

Aside from the two-dimensional case of a slotted semi-elliptical waveguide (P.L.E. Uslenghi, IEEE-APS Int. Symp. Digest, pp. 1849-1852, Chicago, July 1992), this study appears to contain the only available canonical solutions for boundary-value problems involving cavities in a ground plane.
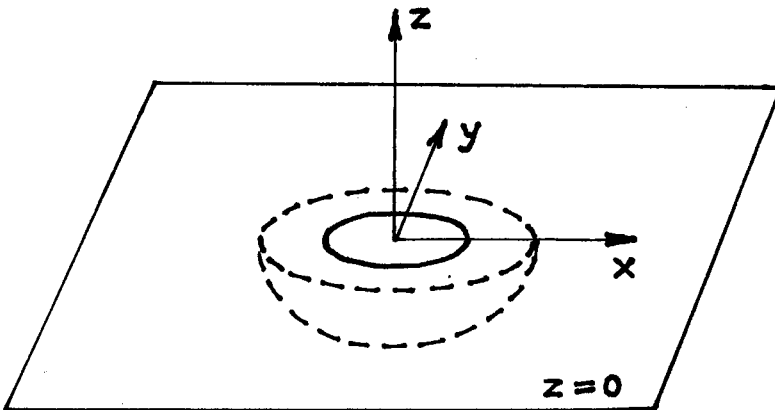
B3-6
1600

AN ITERATIVE METHOD FOR COMPUTING THE SCATTERED ELECTRIC FIELDS AT THE APERTURES OF LARGE PERFECTLY CONDUCTING CAVITIES

Daniel D. Reuster* and Gary A. Thiele
Department of Electrical Engineering
University of Dayton
300 College Park
Dayton, OH 45469-0227

The problem of electromagnetic scattering from large open-ended cavities has received much attention in research areas such as automatic target recognition and low-observable vehicle design. The cavity's large electrical size makes it a prime candidate for ray based or asymptotic techniques, while the cavity's geometrical complexities require more exact techniques such as the method of moments or the boundary integral approach. As a result of these diverse requirements, many hybrid techniques such as the generalized ray expansion (P.H. Pathak, *Radio Science*, Jan.-Feb. 1991) and the hybrid boundary-integral/modal method (H. Ling, *IEEE Trans. Antennas and Propagation*, Sept. 1990) have been developed in an effort to meet the computational challenges associated with the cavity problem. While these approaches show promise in the small to mid-size cavity range, their ability to effectively analyze large scale cavity problems is still a matter of debate, and the need for new approaches is evident.

In the theory presented, the equivalence principle is used to divide the cavity problem into an internal scattering problem and an external scattering problem. This is performed by sealing the cavity aperture with a perfectly conducting plate and an impressed magnetic current equivalent to the total electrical field at the aperture. Because of the cavity's assumed large electrical size, the electrical coupling between the internal and external problems is assumed negligible. The approximation breaks down for small cavities because the coupling between the edge diffracted fields and the aperture becomes an important scattering mechanism. Because these effects are small in comparison to the aperture reradiation for large cavities, the approximation provides valid results for cavities of large electrical size. Since the external scattering problem's geometry is usually much less complex than the internal scattering problem, it is assumed that standard asymptotic analysis may be applied here directly to the external problem; and thus, analysis of the external problem is not considered. The internal scattering problem, which normally requires a much more rigorous solution, is solved using a two stage iterative technique which utilizes both the magnetic field integral equation (MFIE) and the electric field integral equation (EFIE). The technique for the internal problem is an extension of previous work performed on external scattering problems (G.A. Thiele, *IEEE Trans. Antennas and Propagation*, Nov. 1985). For comparison purposes, the calculated scattered fields at the aperture are integrated to produce an approximate RCS for the cavity. The RCS prediction is approximate in the sense that the external scattering from the cavity is not included; however, the RCS predictions are accurate in the regions where the internal scattering phenomenon is dominant.

B3-7
1620

HYBRID FEM-MULTIFILAMENT CURRENT METHOD
FOR 2-D SCATTERING BY INHOMOGENEOUS
DIELECTRIC CYLINDERS

J. Wu and K. A. Michalski
Electromagnetics & Microwave Laboratory
Department of Electrical Engineering
Texas A&M University
College Station, TX 77843–3128

A hybrid approach is described for the analysis of two-dimensional (TM or TE) scattering from inhomogeneous material cylinders. In this approach, the interior inhomogeneous region is modeled by the finite element method (FEM) based on the E_z or H_z formulation, and the unbounded exterior region by the multifilament current method (MFCM). In the MFCM, the fields of fictitious electric or magnetic line currents are used to represent the scattered field (Leviatan and Boag, *IEEE Trans. Antennas Propagat.*, AP-35, 1119–1127, 1987; Leviatan *et al.*, *ibid.*, 36, 1026–1031, 1988). The coupling of the interior and exterior problems is accomplished by point-matching the (E_z, H_t) or (H_z, E_t) fields on the cylinder surface. A staggered point-matching scheme is employed, in which the continuity of the longitudinal (E_z or H_z) and transverse (H_t or E_t) field components is enforced at, respectively, the boundary nodes and the midpoints of the boundary segments. This FEM–MFCM procedure leads to a system of equations with a large sparse coefficient matrix that also comprises two much smaller full submatrices. This system is then efficiently solved using a general sparse matrix package. Compared with the more popular hybrid FEM–BEM procedure (Jin and Liepa, *ibid.*, 36, 1486–1490, 1988; Gong and Glisson, *ibid.*, 38, 60–68, 1990; Yuan *et al.*, *ibid.*, 38, 386–393, 1990) and the recently introduced bymoment method (Cangellaris and Lee, *ibid.*, 39, 1429–1437, 1990) the hybrid FEM-MFCM approach is more efficient and simpler to implement, mainly because it obviates the boundary integrals that arise in the former two techniques. It is also more accurate than the FEM combined with the absorbing boundary condition (Peterson and Castillo, *ibid.*, 37, 601–607, 1989). Sample numerical results are presented for several homogeneous and inhomogeneous material cylinders to illustrate the accuracy and generality of the proposed approach.

B3-8   RADAR ABSORPTIVITY OF PARTICULATE COMPOSITES
1640   Herbert Überall and Michael F. Stumborg
       Department of Physics, Catholic University
       Washington, DC 20064
       Barbara F. Howell and Eugene C. Fischer
       NSWC Annapolis Detachment
       Annapolis, MD 21402-5067

We perform numerical studies of the effective permittivity and absorptivity of composites, consisting of randomly distributed spherical inclusions with complex permittivity ε_s imbedded in a matrix of complex permittivity ε, at microwave frequencies 1-18 GHz. Results of effective field theory are used that include the effects of multiple scattering, as required for dense packing of the particles, but that so far are restricted to the case of particle sizes small compared to the wavelength (low-frequency approximation). Conditions for optimization of the absorptivity are obtained under variations of the particle density. Multiple scattering causes the appearance of imaginary parts of the permittivity (i.e. it causes an effective absorptivity) even if the matrix and inclusion have real permittivities. The magnitudes of these effects are discussed for representative examples of particulate composites.

D1-1
1400

TRANSISTORS OSCILLATORS AS VAN DER POL OSCILLATORS

Kuang. Yi. Chen   Alan. R. Mickelson
Dept. of Electrical Engineering
University of Colorado at Boulder
Boulder, CO 80309

As was pointed out by York (to be published in IEEE Transaction on Microwave theory and Techniques, Special Issue on Quasi-Optical Techniques), a useful method for analyzing power combining structures is by considering them as coupled Van der Pol oscillators. Nonlinear systems exhibit many commonalties of behavior independent of the specific detail of the underlying equations. The Van der Pol equation is a good model for a broad class of oscillating structures.

What we do in this work is to find in detail the relation between the parameters in Van der Pol's equation and the parameters used to characterize the transistor oscillator in the large amplitude limit. Experimental techniques for determination of the parameters are both proposed and carried out. We conclude that Van der Pol model is good if the parameters are experimentally calibrated.
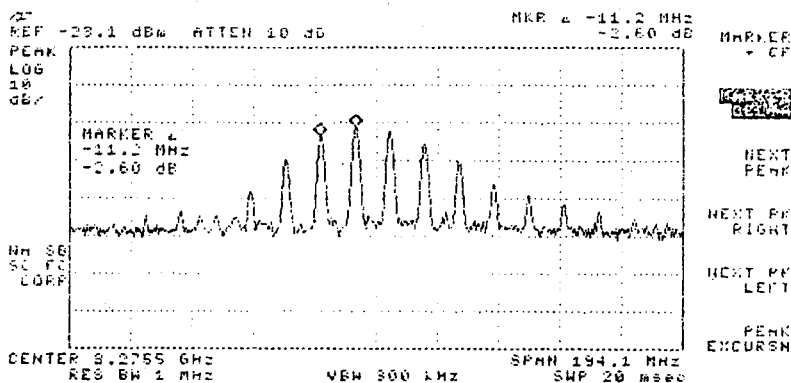
Fig. 1. Spectrum of the active antenna with triangular function of bias voltage at frequency 11.07 MHz. Bias condition Vgs= -0.3V, Vds(min) = 0.8V, Vds(max) = 1.1V.

Full-Wave Analysis of Grid Oscillators

Scott Bundy   Zoya Basta Popović

Department of Electrical and Computer Engineering
University of Colorado, Boulder, Colorado 80309

Grid oscillators (eg. *Popović et al., IEEE Trans. MTT-39, pp. 193-200*) are quasi-optical power combiners that can combine the output power of a large number of solid-state devices. The grid oscillators demonstrated to date consist of a narrow-strip metal mesh loaded with transistors, and feedback is provided by a metal mirror placed in parallel with the grid. These grids were modelled using the EMF method, which is only applicable to thin strip geometries. However, the metal geometry has a strong effect on power-combiner behavior. Here we present a method for determining the driving-point impedance between two points for an arbitrary metal geometry in a grid unit cell, such as the example shown in the figure below.

The relationship between the tangential electric field and the surface current density is formulated for such a unit cell. Galerkin's method with sub-domain basis functions is used to solve for the current due to a gap voltage excitation, yielding an impedance between the two points. In the case of a transistor, an equivalent two-port network for the grid connected to the device can be found, and this can be extended to an N-port for more active devices in the unit cell. Then the circuit can be analyzed using any linear or nonlinear technique. Reflection coefficients from arbitrary passive grids can also be found and are used as a verification tool. Comparison with measurement and other theories for some cases are given.
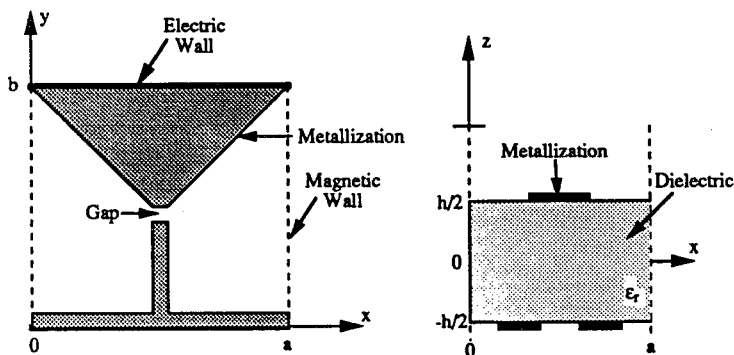
Figure 1: A grid unit cell with electric walls on top and bottom and magnetic walls on the sides. The metal geometry may have an arbitrary shape.

D1-3   ELECTROMAGNETIC MODELING OF ACTIVE CIRCUITS
1440   S. J. Buchheit and A. R. Mickelson
Guided Wave Optics Lab, EE 2-2
Department of Electrical and Computer Engineering
University of Colorado, Boulder, Co 80309-0425

Currently, it is fashionable in politics to discuss the creation of a vast "communications highway" to serve the "information age". Whether one believes this prediction of the path American society will take or not, it is clear that communications technology will be a major growth industry well into the twenty-first century. One of the key aspects of the technology is the desgin and fabrication of cheap high frequency circuits. These circuits will take the form of MMICs (Monolithic Microwave Integrated Circuits). However, cost of fabrication of these circuits must be reduced. This will require the use of a CAD tool that can accurately predict the performance of the devices before production, reducing iterations in the design.

Typically, microwave circuit design is performed using s-parameter matrix analysis tools, with some corrections for certain discontinuities. However, these are not always accurate and will become less so as circuit densities increase. Full-wave analysis techniques exist for this purpose though they require much more time than the s-parameter models. There is much need for a simulation tool that can predict the parasitic effects in a reasonable amount of time. Such a tool is currently under development here at the MIMICAD center. The method consists of a static solution followed by a dynamic solution that gives the frequency dependent behavior of the circuit. Results will be presented for several coplanar waveguide discontinuities as well as a structure that contains an active device.

High-Efficiency Microwave Amplifier Design

Thomas Mader   Zoya Basta Popović

Department of Electrical and Computer Engineering
University of Colorado, Boulder, Colorado 80309

At microwave frequencies, power-added efficiencies of 71% are achieved (*Duvanaud et al., IEEE MGWL-3, pp. 268-270*), but commonly manufactured high-efficiency power amplifiers have efficiencies of around 50%. Efficiency is important in portable systems for prolonging battery life and in all systems for reducing heat-sinking requirements. A high-efficiency circuit analysis approach will be presented. The transistor is heavily saturated, and is modelled as a controlled switch with a shunt capacitance, as shown in the figure. A sinusoidal approximation for the current flowing in the load network of the amplifier simplifies the nonlinear analysis of the circuit and allows for closed-form design equations. An S-band microstrip design example using MESFETs is presented; theory and measurements are compared.
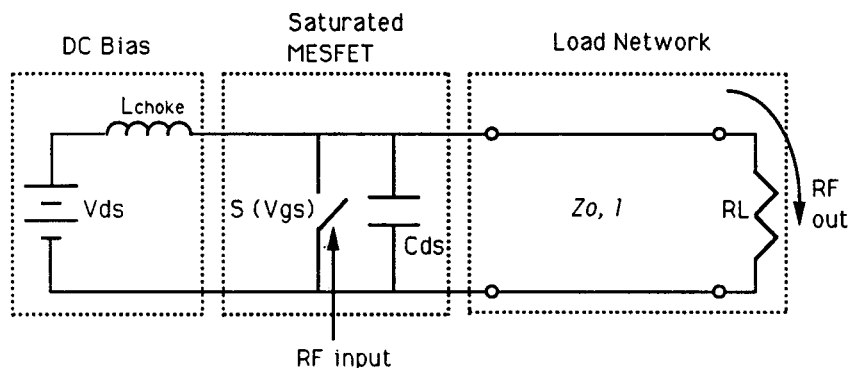
Figure 1: Equivalent circuit for the saturated-mode, high-efficiency S-band MESFET power amplifier. The MESFET is modelled as a switch in parallel with a shunt capacitance. A sinusoidal approximation is made for the current in the load network to allow closed-form design equations.

D1-5   OPTICALLY INDUCED EFFECTS IN MICROWAVE
1540   MESFETS: EXPERIMENTS AND ANALYSIS
         Sheryl M. Genco
         Professor Alan R. Mickelson
         University of Colorado
         Campus Box 425
         Boulder, Colorado   80309

Optical injection of microwave MESFET devices is used for phase locking, frequency tuning, and increasing the gain of amplifiers. We apply the locked MESFET devices to several system applications in particular phased array radar systems which uses the locked MESFET as the active antenna element. Our work takes advantage of a locked laser subsystem to provide optical mode stability prior to injecting into a MESFET. Experiments have been conducted to isolate the physics of optically induced changes to the MESFET. Direct measurements of standard MESFET characteristics, MESFET oscillator and MESFET amplifier have been completed. Increases in the current have been measured and analytically shown to be due to both photovoltaic and photoconductive processes. Analytic results will be discussed and compared with experiment.
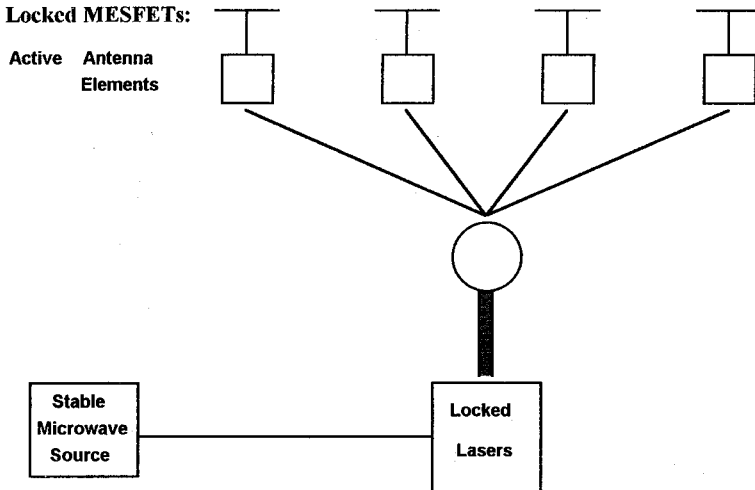
D1-6   FULL-WAVE ELECTROMAGNETIC MODELING
1600   FOR PARAMETER EXTRACTION
        Melinda Piket-May,
        ECE Dept.,University of Colorado at Boulder
        Boulder, CO, 80309-0425
        Kevin Thomas
        IS&T Dept., Cray Research, Inc.
        Eagan, MN
        Roger Gravrok
        Development Group, Cray Research, Inc
        Chippewa Falls, WI

"Parasitic" electromagnetic wave coupling, radiation, and ground loops in passive metallic interconnects and packaging can upset the operation of analog and digital electronic circuits. The finite-difference time-domain (FD-TD) numerical solution method for Maxwell's equations has shown particular promise for circuit simulation and design. FD-TD has already shown the ability to model ultra-complex passive interconnection and packaging geometries.

In this paper, we will show initial developments for a generalized FD-TD software which will naturally provide information on the electromagnetic wave parasitics. Eventually this work will lead to a unified, user-friendly capability for dynamic, full-wave electromagnetic modeling of passive interconnects along with the physics of the nonlinear voltage-current characteristics of the connected devices. The new solver, when fully developed, would permit time-stepping Maxwell's equations to obtain the dynamics of the operation of ultra-high-speed nonlinear analog and digital circuits mounted on modern multilayer boards and multichip modules. A wide range of applications well into microwave frequencies can be envisioned for this technique.

D1-7   ANALYSIS OF TRAVELLING WAVE ELECTRODES IN
1620   INTEGRATED OPTICAL DEVICES

R. Narayan and A. R. Mickelson
Guided Wave Optics Lab, EE 2-2
Department of Electrical and Computer Engineering
University of Colorado, Boulder, Co 80309-0425

We apply a novel numerical technique to analyze travelling wave electrode structures (see figure) in Integrated Optical (IO) devices. Numerical calculations for the overlap integral between the microwave and optical fields, switching voltages, switching bandwidth will be presented.

The algorithm [Radisic et. al., 1993 IEEE MTT-S International Symposium Digest, Vol. 2, pp 951) is based on the quasi-static approximation. First, a static solution for the charge distribution for the problem under study is calculated. A non-uniform transmission line problem is then formulated from the static charge distribution. This transmission line problem can be solved easily using the Riccati Equation. Thus the full dynamics of the problem can be extracted from essentially the static solution. The microwave field in the substrate is directly calculated with the knowledge of the static charge distribution and the appropriate Green's function for the problem under study. This approach does not impose any restrictions on the geometry of the electrode structure and hence takes into account all the parasitics involved in any particular design. Consequently, the calculated microwave fields will be a closer to the actual fields in the IO device.

optical channel · electrodes · L_1 · L_2

D1-8
1640
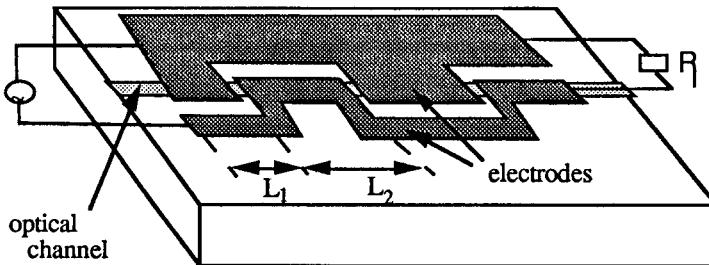
ANALYSIS OF A MULTI-LAYERED STRUCTURE OF NONLINEAR ORGANIC POLYMERS AND COPLANAR WAVEGUIDE ELECTRODES

Lori E. Rohlev and A. R. Mickelson

A model has been developed to determine the electric field distribution of coplanar electrodes buried between layers of anisotropic materials. Several configurations can be used to build electro-optic devices from nonlinear organic polymers. In all cases, the thickness of the metal is comparable to the thickness of the polymer layers and must be taken into account. The model is based on a quasi-static approach to solving the Laplace equation for the potential in each region of the structure. Results from the model have been used to determine the dielectric properties of the polymers at frequencies up to 40 GHz and to determine the electro-optic coefficient of polymers poled with coplanar electrodes.

NOISE MEASUREMENTS, MODELING, AND PREDICTION
Chairman: David B. Sailors, NCCOSC/NRaD, San Diego, CA 92152-5022. Organizers: D.B. Sailors, NCCOSC/NRaD, San Diego, CA 92152-5022; and E.F. Soderberg, Analysis and Technology, Inc., New London, CT 06320

E1-1
1400

THE AMPLITUDE-PROBABILITY DISTRIBUTIONS OF ELF/VLF RADIO NOISE

A.C. Fraser-Smith
STAR Laboratory, Stanford University,
Stanford, California 94305

It is often assumed, on good physical grounds, that the sferic noise measured at most (and perhaps all) locations around the world consists of two components: (1) a relatively low-amplitude Gaussian-distributed component from distant sources, and (2) a relatively high-amplitude, "spiky," component from nearby electrical storms [e.g., E.C. Field, Jr., and M. Lewinstein, *IEEE Trans. Commun.*, *26*, 83–87, 1978]. At high latitudes, where the electrical storm sources of the sferics are all distant, the assumption can still be considered to be valid provided allowance is made for an appropriate reduction of component (2) as latitude increases.

The above assumption is the basis for the present analytical models for ELF/VLF amplitude probability distributions (APD's) and the agreement between the theoretical and experimentally-measured APD's appears to be quite good in general. More specifically, a large number of measurements of ELF/VLF APD's have been made by Stanford University ELF/VLF radiometers located at various sites around the world, and there is often good agreement with the two-component sferic noise model. However, there are also a significant number of APD's that do not appear to agree well with the modeling, even though they incorporate a very large number of amplitude measurements and should be largely free from statistical variability. It is possible that the above APD assumption may need to be modified to incorporate an intermediate component of sferic noise: (3) a component of moderate amplitude from the lightning in electrical storms at intermediate distances.

E1-2   LIGHTNING-INDUCED DISTURBANCES
1420   OF THE EARTH-IONOSPHERE WAVEGUIDE

U. S. Inan
Space,Telecommunications and Radioscience Laboratory
Stanford University
Stanford, CA 94305-4055

The role of lightning discharges as a major source of noise for ELF/VLF/LF/HF propagation channels has been well recognized for many years. Recently, a new and possibly very significant effect of lightning on the propagation channel itself has emerged, in the form of the disturbances of the lower ionosphere. These disturbances are now known to occur in at least two ways. In one case, electromagnetic energy released in lightning discharges propagates upward to the earth's magnetosphere in the whistler-mode and precipitates energetic electrons out of the earth's radiation belts. The electrons penetrate to lower layers of the ionosphere and create enhanced ionization, light, heat and x-rays. An entirely different but possibly even more important effect occurs as a result of the direct interaction of intense electromagnetic pulses from lightning with the collisional lower ionospheric plasma. This highly nonlinear interaction of the EMP from lightning with the ionospheric gas results in intense heating and ionization of the nighttime lower ionosphere and leads to excitation of a variety of optical emissions. Recent theoretical and experimental results concerning these phenomena will be reviewed.

E1-3
1440

THE HIGH FREQUENCY ENVIRONMENT
AT THE
ROTHR AMCHITKA RADAR SITE

George D. Mc Neal
Code 5324
Naval Research Laboratory
Washington, D.C. 20375-5000

ABSTRACT

The successful performance of a High-Frequency (HF) Over-The-Horizon Radar (OTHR) is dependent upon the environment in which the radar must operate. This study investigates measured power levels of noise and signal characteristics in the HF environment of an operational OTHR system located in Amchitka, Alaska. These measurements were acquired by the Navy's AN/TPS-71 radar (ROTHR) spectrum monitor, and represent a new source of HF environmental measurements for noise characteristics, channel availability, and expected duration of various channel widths as a function of frequency, time-of-day and season-of-year. The analysis and results presented are based on HF environmental measurements obtained over the 5 to 28 MHz frequency band by a receiver with a very low noise figure, an efficient antenna, high dynamic range, and which was seldom internally noise limited. The analysis of this data has provided information on power levels associated with noise and HF users in the geographic region of the radar. Clear channel availability results are based on a threshold level defined by empirical distribution functions (EDF) of the measured power levels from the ROTHR site.

E1-4
1500

ELECTROMAGNETIC EMISSIONS ARISING FROM THE EARTHQUAKE SWARM OF APRIL TO JULY 1992 IN SOUTHERN CALIFORNIA

Jack Y. Dea and Peder M. Hansen
NCCOSC, RDT&E Division
Code 832
San Diego, CA 92152-5000

Wolfgang-M. Boerner
University of Illinois at Chicago
EECS
Communications and Sensing Laboratory
Chicago, IL 60680-4348

The last several years have seen a large number of investigators reporting on electromagnetic emisions preceding earthquakes. (e.g., Dea et al., Physics of the Earth and Planetary Interiors, 77, No. 1-2, pp 109-126, 1993). Yet, the reality of electromagnetic emissions preceding and even during earthquakes have been hotly debated during this time frame. This paper reports on direct observations of electromagnetic emissions during the earthquake swarm period of April to July 1992 in Southern California which included three major quakes registering greater than M=6.0 and more than 25,000 small quakes. The direct observations include,

(i) Three month elevation of magnetic emanations in the 0.1 to 5 Hz frequency band.

(ii) Large electromagnetic impulse train appearing 10 seconds before the ground shaking from the Big Bear quake on June 28, 1992 (M=6.0).

(iii) Noise spikes which began from the time of the Joshua Tree quake on April 22, 1992 (M=6.1).

(iv) Other evidence of electromagnetic emissions.

Recordings of some of the observations are shown. A model is presented to explain some of the observations.

NEW ADDITIONS TO THE LONG WAVE
TE/TM NOISE PREDICTION MODEL

C.R. Warber and E.C. Field, Jr.
Pacific-Sierra Research Corp.
2901 28th Street.
Santa Monica, CA 90405

Both vertical and horizontal polarizations are used for communication links between airborne terminals in the VLF/LF bands. Thus, the performance analysis of such communication systems requires knowledge of the naturally occurring noise in each polarization. There is good data on naturally occurring vertical noise; however, data on horizontal noise is extremely sparse. Therefore, based on a theoretical understanding of the physical processes that cause noise, we have developed a computer model that predicts both horizontally and vertically polarized noise in the ELF to LF band (10 Hz - 60 kHz). The model has undergone several revisions in response to user comments since its initial release. The third version has been recently completed.

Since naturally occurring radio noise in this band is produced by lightning in the lower atmosphere, and propagates to the receiver via the waveguide formed by the earth and the ionosphere, the model starts with the average lightning flash density as a function of season, time of day, and geographic location. It then turns this into radiated power density functions for horizontal and vertical noise using experimentally known frequency spectrums for those lightning flash components that radiate strongly in the long wave band. The noise power density is integrated over fairly large geographic areas into horizontal and vertical equivalent noise transmitters. The power radiated from each of these transmitters is then propagated to the receiver location using standard anisotropic waveguide algorithms.

From the received power, the model predicts RMS noise, standard deviation, voltage deviation V_d, and the amplitude probability distribution (APD) of the noise for both vertical and horizontal polarizations. For the third version, we have improved the V_d and APD predictions of the model by adding a more detailed lightning occurrence database, and have added the ability to produce noise value time series.

The model agrees well with experimental data over the entire frequency range treated by the model. We will briefly describe the physical basis of the model, demonstrate its agreement with noise data, and then discuss the new features that we have added to the model.

E1-6   PREDICTION PERFORMANCE
1600   OF VLF NOISE MODELS

R.R. Gupta and D.P.Frank
TASC
55 Walkers Brook Drive
Reading, MA 01869

        Three computer-based models have been developed
over the past twenty years to predict noise in the VLF band:
NTIA (CCIR 322-3), DECO, and LNP. This paper provides
an evaluation of the three models in the context of an effort
to develop signal coverage databases to be used to assess
the navigation performance of the Omega, U.S. Navy VLF,
and Russian ALPHA radionavigation/communication
systems. Evaluation of the models focuses on both their
prediction accuracy and computational requirements.
Prediction accuracy is determined using noise measurements
in the published literature. These include a portion of the
data used to develop the CCIR 322-3 model and data
collected by researchers from Stanford University. Results
and insights from this evaluation effort are presented.

E1-7 A DISCREPANCY IN THE CCIR REPORT 322-3 RADIO NOISE MODEL
1620 - A RECOMMENDED SOLUTION

David B. Sailors
Ocean and Atmospheric Sciences Division
Research, Development, Test and Evaluation Division
Naval Command, Control and Ocean Surveillance Center
San Diego, CA 92152-5235

Sailors (NCCOSC TD 2496, May 1993; Ionospheric Effects Symposium, May 4-6, 1993) reported the probable cause of a discrepancy in the CCIR Report 322-3 radio noise model. The basis for this discrepancy resulted from the procedure used to prepare the measured noise data for the determination of a global numerical representation of the 1 MHz data. In the development of the model, correction factors were determined for each measurement site. These correction factors were interpolated to 100-latitude by 84-longitude grid for each time block/season. The correction factors at each grid point were added to corresponding values for the old CCIR model, and finally the resulting data for each time block and season were numerically mapped.

Nineteen locations were used in the final model. Four sites used in the original CCIR model were not used. As no corrections factors were obtained for these locations or a correction factor of zero used to maintain the status quo, the interpolation algorithm used to obtain the 100-latitude by 84-longitude grid of correction factors supplied other values. For Byrd Station, Antarctica; Ibadan, Nigeria; and Thule, Greenland, the error is at some seasons and time of day serious. Examination of the geographical extent of these errors reveals that the error is not confined to the measurement location but in fact is very large. It was found that the error as a function of frequency is diurnally dependent. The absence of the data locations also affected the accuracy of the interpolation itself.

A recommended course of action to overcome this discrepancy includes (1) obtain correction factors for additional locations to increase the accuracy of the interpolation; (2) test the method of interpolation against a suitable bench mark; (3) Use the Zacharisen and Jones (Institute for Telecomm. Sciences Res. Report 2, 1970) numerical mapping technique applied in local time to develop a new 1-MHz model; (4) consider using a latitude transformation to increase the accuracy of the numerical mapping technique; and (5) submit a corrected model to the CCIR. Additional data include that for the four original locations not utilized in development of CCIR Report 322-3, for four locations from the former Soviet Union (Simferopol, Sverdlovsk, Tbilisi, and Kiev), and for one additional site at Ping-Cheng, Taiwan, China. To use this data it is necessary to remove the effects of man-made noise. Three methods to accomplish this that can be used together or alone are described. Sailors (National Radio Science Meeting, 1983) showed that an improvement in the accuracy of the numerical map can be made by transforming the latitude coordinates so that there is a more uniform variation of atmospheric noise as a function of the modified latitude than there is for the actual latitude. When used with the local-time Zacharisen and Jones mapping technique, it can be expected to work even better in improving the atmospheric noise model than when universal time was used in the mapping technique.

POLARIMETRIC OBSERVATIONS AND SCATTERING CHARACTERISTICS OF
THE OCEAN SURFACE

Chairmen: A.J. Gasiewski, Georgia Tech, Atlanta, GA 30332-0250; and E.R. Westwater,
Environmental Technology Laboratory, NOAA/ERL, Boulder, CO 80303

F2-1   Small-slope approximation for the microwave emission
1400   from the rough sea surface.

V.G.Irisov
CIRES/University of Colorado at Boulder
NOAA/ERL/Environmental Technology Laboratory
Boulder, Colorado 80303

The microwave thermal emission of a sea-like surface with some
model spectrum is the main point of interest of the paper. For this
purpose the absorption of the auxiliary electromagnetic plane wave
on the rough surface is considered. Due to Kirchhoff's law the
absorption is related to the emissivity of the surface. The
diffraction problem is solved to find the surface currents and the
energy flux through the surface.
    The solution is based on a small-slope expansion that includes
the first fourth-order terms of roughness amplitude. This gives the
first two terms of the emissivity expansion over the ocean wave
spectrum. The expansion is based on the integral formulation of the
diffraction problem that, in the limit of the long surface waves,
approaches an expansion over the slopes.
    The results show the increasing importance of the higher-order
terms of the expansion at grazing angles of observation. At the
same time in most cases the first order small-slope approximation
can be successfully used for near nadir sensing.
    Two cases of isotropic and absolutely anisotropic space
surface spectra are considered. For the last one the near nadir
polarization dependance is studied especially because of its
practical importance for passive microwave remote sensing of the
near surface wind speed and direction.

F2-2   AIRCRAFT–BASED OBSERVATIONS OF SEA STATE
1420   BY A DUAL–FREQUENCY MICROWAVE RADIOMETER

L. S. Fedor   V. G. Irisov
Environ. Tech. Lab.   CIRES/Univ. of Colorado
NOAA/ERL   NOAA/ERL/Environ. Tech. Lab.
Boulder, CO 80303   Boulder, CO 80303

The Environmental Technology Laboratory has developed an aircraft-based (King Air) dual-frequency microwave radiometer that measures upward and downward radiance at 23.87 and 31.65 GHz. The radiometer's antenna can operate in a variety of operator-selected modes. It can look continuously up, continuously down, or alternate between upward- and downward-viewing operations. When looking up, measured brightness temperatures can be processed to derive water vapor and cloud liquid overburdens. Measurements of the spatial variability of these quantities can provide fundamental information for climate, cloud, and radiation studies. When looking down, the measured radiation consists of surface emission, downward radiation reflected by the surface, and upward atmospheric emission. By flying the aircraft at various altitudes, and by alternatively measuring upward- and downward-flowing radiation, the surface emissivity can be measured (skin temperature would be measured by an infrared radiometer). Such aircraft measurements, when coordinated with satellite overflights, can provide data to assist satellite measurements of environmental parameters.

During September-October, the aircraft radiometer participated in the San Clemente Ocean Probing Experiment in San Clemente, California. By coordinating the aircraft overflights with in situ oceanographic data, and with ERS-1 satellite overpasses, a valuable set of data were obtained. In this paper, we present preliminary data from the aircraft radiometer, and also show some comparisons of measurements and theory of the polarized emission from the ocean surface.

F2-3 **Airborne Passive Polarimetric Observations**
1440 **of Ocean Wave Anisotropy at 92 GHz**
      During TOGA/COARE
      D.B. Kunkee, A.J. Gasiewski
      School of Electrical Engineering
      Georgia Institute of Technology
      Atlanta GA, 30332-0250

Airborne passive polarimetric measurements of sea surface brightness at 92 GHz were recently performed during the Tropical Ocean Global Atmosphere/Coupled Ocean Atmosphere Response Experiment (TOGA/COARE). A fixed beam fully-polarimetric radiometer was mounted on the NASA DC-8 airborne platform and flown in constant bank-angle turns at low altitude ($\sim$ 1.5 km), yielding azimuthal scans of the sea surface at fixed observation angles. Nadir video imagery was used to determine the dominant azimuthal angle of the surface gravity waves.

The measurements show significant azimuthal variations in the vertically and horizontally polarized brightness temperatures (T_v and T_h) for light sea and clear air conditions. At 65° from nadir, $\sim$ 3 K variations in T_v and $\sim$ 6 K variations in T_h over a full 360° scan were observed. Upwind/downwind brightness asymmetry was also observed; this is hypothesized to be the result of increased amounts of ocean foam on the leeward side of the wave. The data are consistent in amplitude and phase with the experimental findings of Wentz [Trans. Geosci. Remote Sensing (30), 5, 960-972, 1992] obtained using 19- and 37-GHz SSM/I satellite observations, and support the notion that an ocean wave direction signature is observable in passive polarimetric observations of the sea surface.

The consistency of the data from both this experiment and Wentz' suggest that a broadband emission mechanism is responsible for the wave azimuthal signatures. Accordingly, a tilted facet geometrical optics (GO) model of a sinusoidal water surface was developed to investigate striated surface emission. Laboratory measurements of polarimetric emission at 92 GHz from small-amplitude water waves corroborate this model.

F2-4   THEORY AND EXPERIMENTS IN POLARIMETRIC PASSIVE
1500   REMOTE SENSING

J. T. Johnson, J. A. Kong, and R. T. Shin
Department of Electrical Engineering and Computer Science
and Research Laboratory of Electronics
Massachusetts Institute of Technology, Cambridge, MA

L. Tsang
Electromagnetics and Remote Sensing Laboratory
University of Washington, Seattle, WA

Recent research in the passive polarimetric remote sensing of geophysical media has demonstrated some of the additional information available from this new technique. A large portion of this research has focussed on the third Stokes emission parameter, U, which has been shown to become large for azimuthally asymmetric fields of observation. Less interest has been given to the fourth Stokes parameter, V, but theoretical predictions have been made which show that V could be of use in the remote sensing of tilted gyrotropic media. Polarimetry should thus be useful in passive remote sensing in cases where there is interest in the underlying structure of the remotely sensed medium. One such case is the remote sensing of wind direction over the ocean: since a wind generated ocean surface has an azimuthally anisotropic structure, the third Stokes parameter, U, should give information as to the wind direction. This additional information could enhance the accuracy of previous non-polarimetric wind direction retrievals from satellite passive observations, such as from the SSM/I. This paper will review the authors' and their collaborators' theoretical and experimental work in developing theory and techniques for the retrieval of wind direction over the ocean using passive polarimetry. This work includes experimental measurements of the polarimetric brightness temperature from sinusoidal soil and water surfaces periodic in one direction, theoretical predictions for the polarimetric brightness temperatures of periodic surfaces, a Monte Carlo study of the polarimetric brightness temperature of randomly rough surfaces, and a model for the polarimetric brightness temperature of a surface rough in two directions.

F2-5   **OBSERVABLE DIFFERENCES IN OCEAN RADAR IMAGERY**
1540   **OBTAINED WITH HORIZONTAL AND VERTICAL POLARIZATIONS**

A.V. Smirnov, V.U. Zavorotny
CIRES/University Of Colorado
NOAA/ERL/Environmental. Tech. Laboratory
Boulder, CO 80303

The Environmental Technology Laboratory is evaluating a new radar ocean remote sensing technique based on microwave wavelengths, various polarizations, and new principles of signal processing, i.e., radar imaging. This technique exploits the K_u-band side-looking airborne radar having high surface resolution, and using the vertical and the horizontal polarization both in the receiving and transmitting modes.

It was observed that the images obtained using such a radar at different polarizations and at grazing angles are sensitive to different surface phenomena. The vertical polarization seems to image surface manifestations of atmospheric processes near the ocean surface such as a turbulent convection; the horizontal one seems better to image surface manifestations such as internal waves in the thermocline. At the same time, it was found that the Bragg two-scale model cannot explain these drastic differences between images on two polarizations.

To understand peculiarities of this phenomenon an analysis was completed of polarimetric airborne-radar images obtained in the US/Russian Joint Experiment in the New York Bight during July 1992. These radar images were classified into three major types with respect to their texture. A correlation was found between a certain image type and the state of sea-air interaction. For example, an occurrence of a significant number of spikes (the fluctuating bursts of a signal) strongly affects the image at horizontal polarizations. At the same time, the number of spikes is correlated with unstable atmospheric conditions in the near-water atmospheric layer.

A surface model which explains qualitatively polarization differences is suggested. This model takes into consideration the mechanism of wave breaking on a deep-water surface under unstable atmospheric conditions.

F2-6   **RADAR SCATTER CROSS SECTIONS FOR TWO-DIMENSIONAL**
1600   **RANDOM ROUGH SURFACES THAT ACCOUNT FOR HEIGHT/SLOPE**
       CORRELATIONS

Ezekiel Bahar and Bom Son Lee
Electrical Engineering Department
University of Nebraska - Lincoln
Lincoln, Nebraska 68588-0511

Using the full wave approach, the bistatic radar scatter cross sections for two-dimensional random rough surfaces are obtained. The expression for the radar cross sections for two-dimensional random rough surfaces involves 10-dimensional integrals (over the random surface heights h_1, h_2 and slopes h_{x1}, h_{x2}, h_{z1}, h_{z2} and the surface variables x_{s1}, x_{s2}, z_{s1}, z_{s2}). It is impractical and too time-consuming to carry out these integrations. At high frequencies (when the radii of curvature of the surface are large compared to the wavelength λ), it can be assumed that the surface slopes at two neighboring points are approximately the same as the slope at the center ($h_{x1} \approx h_{x2} \approx h_{xc}$ and $h_{z1} \approx h_{z2} \approx h_{zc}$). With this assumption, it is shown that for isotropic rough surfaces, the 10-dimensional integral can be expressed as a 3-dimensional integral (over the slopes h_x, h_z and the distance variable r_d). This integral accounts for the height/slope correlation through the use of the conditional joint characteristic functions (Bahar, IEEE Trans. on AP, Vol. 39, No. 9, Sep. 1991). These full wave results involving 3-dimensional integrals can be further simplified if the surface slopes are small. In this case, it can be assumed that the surface height and slopes are uncorrelated and the above 3-dimensional integral reduces to the product of a 2- and a 1-dimensional integral. Furthermore on applying a stationary phase (high frequency) approximation, the 3-dimensional integral reduces to a 1-dimensional (physical optics) integral or to a closed form (geometrical optics) expression.

These full wave results are compared with the associated small perturbation and physical/geometrical optics results. The full wave results are shown to reduce to the physical optics results in high frequency limit when the large radius of curvature assumption is made. It also reduces to the small perturbation results when $2\pi h / \lambda$ is of the same order of smallness as h_x and h_z. These results are also compared with the numerical results based on Monte Carlo simulation of rough surfaces.

HIGH FREQUENCY APPROXIMATIONS FOR THE MULTIPLE SCATTER CROSS SECTIONS OF ONE AND TWO DIMENSIONAL RANDOM ROUGH SURFACES

M. El-Shenawee and E. Bahar
Department of Electrical Engineering
Center for Electro-Optics
University of Nebraska-Lincoln
Lincoln, NE 68588-0511

Stationary phase approximations are used to simplify the full wave multi-dimensional integral expressions for the double scatter cross sections of one and two dimensional random rough surfaces. The full wave double scatter cross sections are expressed as six or ten dimensional integrals. For the two dimensional surface they involve a pair of surface variables, two pairs of slope variables and four wave vector variables. In the high frequency limit, the major contributions to the double scatter cross sections come from the neighborhoods of the specular points of the surface. In this work, it is assumed that $k_0 \rho >> 1$, (where k_0 is the free space wave number, ρ is the radius of curvature of the rough surface) and $\beta = 4k_0^2 \langle h^2 \rangle >> 1$, (where $\langle h^2 \rangle$ is the mean square height of the surface). The stationary phase approximations are used to reduce the expressions for the double scatter cross sections into two or four dimensional integrals (for the two dimensional surface they involve the four wave vector variables only).

The significant contributions to the double scattered intensities come from two different double scatter paths, the quasi parallel path and the quasi antiparallel path (E. Bahar and M. El-Shenawee, Proceedings of the IEEE AP-S International Symposium, Ann Arbor, June 1316-1319, 1993 and the Proceedings of the Computational of Electromagnetic Fields, Miami, October 1993).

The bistatic results exhibit a sharp peak in the backscatter direction. This enhanced backscatter is associated with the double scatter quasi antiparallel path.

F2-8
1640

**AN IMPROVED MODEL OF THE
OCEAN SURFACE WAVE SPECTRUM
AND ITS EFFECTS ON RADAR BACKSCATTER**

Dr. John R. Apel
The Johns Hopkins University
Applied Physics Laboratory
Laurel, MD 20723

Images of the ocean surface taken with active and passive microwave sensors often contain much information on near-surface and subsurface processes. However, their interpretations may depend on a detailed understanding of the physics of electromagnetic scatter and emission. In scattering theory, the surface hydrodynamics enters the equations via (1) the probability distribution function for either wave heights or slopes, and (2) the two-dimensional wave height/slope autocovariance or its Fourier transform, the wave vector spectrum.

This paper advances an improved model for the ocean surface wave vector spectrum based on recent work by Donelan, by Banner and by Jähne and their collaborators. The model addresses the range of surface wavelengths from fully developed wind waves to the gravity-capillary region. For GCW's, the spectral equation satisfactorily represents the observational data of Jähne et al. taken in tanks at large fetches, in the range from 20 to 2000 rad/m, to within the accuracy of the data. In the equilibrium region, the wave number dependence is taken as k^{-4}. It also models the angular distribution of the waves as given by Donelan and Banner with a simpler but improved spreading function.

The spectrum is inverse-Fourier-transformed to obtain the autocorrelation function of the sea surface, which Holliday's formulation of microwave radar backscatter from a Gaussian sea requires. The calculations quantitatively reproduce the absolute values of observational cross section data taken from aircraft and spacecraft over the open ocean at vertical polarization, for wind speeds from 1 to 24 m/s; at radar frequencies from approximately 5 to 35 GHz; and for incidence angles from 0° to greater than 60°. At horizontal polarization, although the theory captures the *range* of cross section variation with wind speed, it suffers from the same problem of underprediction of the *absolute* values of σ^0 as do all theories based on the Kirchhoff approximation. The effects on radar imaging of the ocean surface and wind scatterometry are assessed, and the impact of stability conditions and polarization dependencies is discussed.

G2-1 **WAVE PROPAGATION IN RANDOM MEDIA THEORIES**
1340 Prof. V.I. Tatarskii
University of Colorado/CIRES
& NOAA/ERL/Wave Propagation Laboratory
Boulder, CO 80309

We discuss some approaches in wave propagation theory which are useful for describing wave propagation in random media with dispersion and regular refraction. The possibilities and restrictions of different methods are discussed. We consider the following:

1. Geometrical optics
2. Small perturbation theory
3. Smooth perturbation method
4. Markovian approximation
5. Diffraction integral method.

G2-2   FINITE DIFFERENCE - TIME DOMAIN TESTS OF
1400   RANDOM MEDIA PROPAGATION THEORY

L. J. Nickisch
Mission Research Corporation
2300 Garden Road, Suite 2
Monterey, CA 93940-5326
P. M. Franke
University of Illinois at Urbana-Champaign
Department of Electrical and Computer Engineering
Urbana, IL 61801-2991

The recent extension of the Finite Difference - Time Domain (FDTD) method to frequency dependent media [Nickisch and Franke, IEEE Antennas and Propagation Magazine, Vol. 34, No. 5, October 1992] now allows FDTD to be applied to ionospheric propagation. The FDTD method solves the Maxwell equations directly in the time domain by temporal integration. No approximations beyond that of finite differencing are necessary, although the direct enforcement of certain approximations is possible. By doing so the method can be used to explore the effect of many standard propagation approximations. We consider several approximations typically applied to the problem of propagation in randomly structured ionization such as the neglect of polarization coupling and the assumption of small angle scattering.
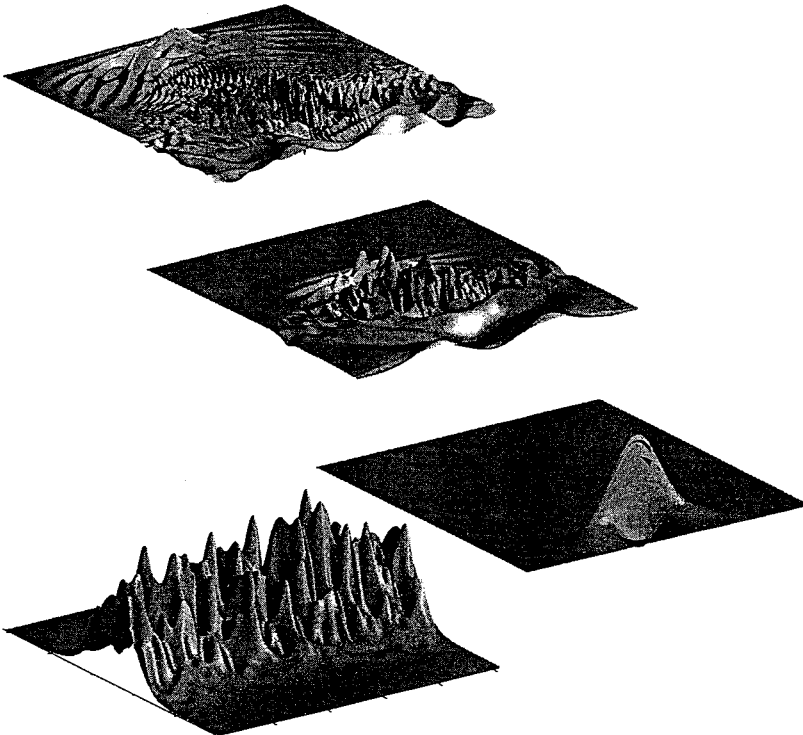
Time sequence of an electromagnetic pulse impinging on the region of gaussian distributed electron density shown on the lower left.

G2-3   MEASURED CHARACTERISTICS OF A HIGH LATITUDE
1420   HF RADIO SKYWAVE CHANNEL
           L.S. Wagner
           Information Tecnology Division
           Naval Research Laboratory
           Washington, D.C. 20375-5337

Channel probe observations of propagation conditions along a 1294 km transauroral path between Sondrestrom, Greenland and Keflavik, Iceland were made during the period from March 13 to April 3, 1992. The purpose of these measurements was twofold:(1) to support performance evaluation tests of a wideband HF Rake system on a high latitude channel and (2) to supplement the existing data base describing propagation conditions on the HF transauroral channel with data pertaining to a period around the time of solar maximum. Measurements were concentrated in a time period from late afternoon to one or two hours past local midnight since these were the times that were expected to pose the greatest challenge to wideband HF radio communication. Measurement events discussed here include a noontime measurement during a period ($K_p=3$) of unsettled to active magnetic conditions and during magnetically quiet nighttime conditions ($K_p<2$). Three types of signals are observed depending on time of day, magnetic activity, and frequency relative to the largest MUF observed on the path. These signals include isolated specular reflections from a quiescent ionosphere, specular multipath returns from horizontal gradients associated with strong patches of electron density in an irregular ionosphere, and scatter returns from weak field-aligned irregularities. Representative scattering functions for each of these three types of signals are presented along with their distinguishing characteristics.

G2-4   A TRANS-IONOSPHERIC RADAR CHANNEL MODEL
1440   Roger A. Dana
        Mission Research Corporation
        P.O. Drawer 719, 735 State Street
        Santa Barbara, California 93102-0719

Scintillation can degrade the performance of a radar in several ways: Amplitude fading can cause missed detections and reduced accuracy in measurements that depend on signal-to-noise ratio. Frequency selective fading reduces the signal power at the output of a matched filter and can cause multiple returns from a single target. Spatially selective fading (i.e., angular scattering) results in antenna scattering loss and random decorrelation of signals from multiple apertures. This latter effect is particularly important in monopulse systems where the phase difference of the signals from two apertures is used to measure angle-of-arrival.

Design, evaluation, and testing of trans-ionospheric radar systems that must operate in scintillation require an accurate channel model. Because radar scintillation is different from that on satellite communication links, due to the effects of the two-way path, one-way channel models are not appropriate for the radar problem.

This paper describes a radar channel model used to generate realizations of the impulse response function for the sum and difference beam outputs of a monopulse radar. The radar channel model is based on a general model for one-way radio frequency propagation through structured ionization (Dana and Wittwer, *Radio Science* 26, 1059-1068, 1991), and it is applicable to the case where the scintillation on both paths (from the radar to the target and from the target back to the radar) is separately described by Rayleigh statistics.

The method of constructing two-way impulse response functions from one-way realizations and the application to phase comparison monopulse radars are briefly described. Examples are then given that illustrate the effects of two-way amplitude fading on target detection, the effects of frequency selective fading on range accuracy and resolution, and the effects of spatially selective fading on phase comparison monopulse angular measurement accuracy.

G2-5 **A NEW APPROACH TO HF CHANNEL MODELING AND SIMULATION**
1500

J. A. Hoffmeyer and L. E. Vogler
National Telecommunications and Information Administration
Institute for Telecommunication Sciences
Boulder, Colorado 80303

Numerous narrowband channel simulators have been developed based on the narrowband channel model originated by Watterson (Watterson et. al., IEEE Trans. Comm. COM-18, 792-803, 1970). This model is valid only for narrowband propagation. Other restrictions on these models (such as their ability to represent only stable channels) further limit their usefulness. As Watterson clearly indicates, this model was validated only for channel bandwidths of 12 kHz or less using selected data that represented only undisturbed propagation conditions. Unfortunately, with the passage of time, these restrictions on the validity of the model have sometimes been forgotten.

Current interest in direct sequence spread spectrum HF communications has led to the requirement for an improved channel propagation model which accurately represents the HF transmission media for bandwidths of the order of one MHz. The objective of the modeling and simulation research described in this paper is not only to develop a model having wide bandwidth capabilities, but also to eliminate other restrictions of current HF channel propagation models.

The newly developed wideband channel propagation model that is presented here simulates the effects of the ionosphere on a signal transmitted over an HF sky-wave channel. It includes the key characteristics that describe the received signal: the delay time spread and amplitude shape, the Doppler frequency shift and spread, and the effects of scattering from diffuse multipath and of Doppler variation with delay time. It also simulates multilayer and multimode conditions by specifying independent values in each layer for the parameters associated with the key characteristics. The primary differences of the new model in comparison with the Watterson Model are the addition of delay spread, the use of Lorentzian as well as Gaussian Doppler spreads, and the ability to model disturbed as well as undisturbed paths.

The figure below provides a comparison of output from the new model with propagation data provided courtesy of Dr. Wagner of the Naval Research Laboratory (MilCom '89 Conf. Record, Vol. 3, 48.2.1 - 48.2.10). The measured data in Part (a) of the figure were collected on a 126-km path in California in Winter 1993. The delay scale in (a) and (b) have an arbitrary zero offset.

a) Measured data   b) Simulated output from new model
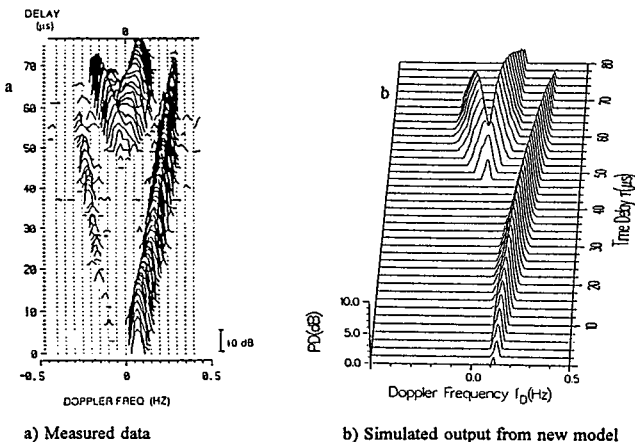
G2-6
1540
THE TWO-FREQUENCY CORRELATION FUNCTION OF THE SINGLE PATH HF CHANNEL. THEORY AND COMPARISON WITH THE EXPERIMENT.

S.V. Fridman, O.V. Fridman, K.H. Lin, and S.J. Franke
University of Illinois at Urbana-Champaign
Department. of Electrical and Computer Engineering
3rd Floor North CSRL, 1308 W. Main, Urbana, IL 61801-2307

We estimate statistical characteristics of the HF electromagnetic field fluctuations caused by the ionospheric irregularities in the oblique radiopath. First we apply the single scattering approximation (Born's approximation). This approximation is valid only for weak field fluctuations. Then we extend our theory to stronger field fluctuations by applying the Rytov's approximation in a manner proposed by Zernov (N.N. Zernov, Radiophys. Quantum Electron., Engl. Transl., 23(2), 151-158, 1980).

For the wide band HF communication applications the quantity of considerable interest is the correlation function of the channel $B_u(\omega,\Omega,t) = \left\langle u^*(\omega,t_1) u(\omega+\Omega,t_1+t) \right\rangle$, where $u(\omega,t)$ is the complex amplitude at the receiver of the radiowave transmitted at a frequency ω. We obtained an expression for this correlation function and found that this particular quantity behaves as though there are no diffraction effects (no Fresnel filtering effects). Thus the correlation time τ_0 of $B_u(\omega,0,t)$ is close to Λ/v regardless of whether the size of irregularities Λ is smaller than or greater than the Fresnel length (v is the component of the drift velocity perpendicular to the ray path). The typical scales for the two-frequency mutual correlation function are also quite obvious. For example, the correlational bandwidth, Ω_c of $B_u(\omega,\Omega,0)$, is such that the rays connecting the transmitter and receiver at ω and $\omega+\Omega_c$ are separated from each other (in the vicinity of the reflection point) by a distance of the order of Λ.

We developed a procedure which allows us to extract the size of irregularities and components of plasma drift from two measured functions $B_u(\omega,0,t)$ and $B_u(\omega,\Omega,t)$, $\Omega \neq 0$. This procedure was applied to measurements from the U of I Sounder (transmitter is located in Platteville, Colorado, receiver in Urbana, Illinois). We found that in the examples considered irregularities with a size of the order of a few hundred meters drifting with a velocity 20-100 m s^{-1} can explain the fading. The observed magnitude of fading may be ensured by the irregularities with and amplitude of the order of a few tenths of one percent.

G2-7   APPLICATION OF METHODS FOR PREDICTING CHAOTIC
1600   DYNAMIC PROCESSES TO HF FADING. METHODS
       FOR PREDICTING CHAOTIC DYNAMIC PROCESSES AND
       SHORT TERM FORECASTING OF THE HF FADING.
       S.V. Fridman, O.V. Fridman, and S.J. Franke
       University of Illinois at Urbana-Champaign
       Department. of Electrical and Computer Engineering
       3rd Floor North CSRL, 1308 W. Main, Urbana, IL 61801-2307

There exist two major mechanisms which are responsible for the fading phenomenon at HF propagation. They are multipath interference and distortions due to ionospheric irregularities. The fading time series produced by the first of these mechanisms alone should typically represent a multi-periodical process. This type of signal might be produced as well by an autonomous dynamical system.

The character of the time series produced by the second mechanism depends on the nature of the ionospheric irregularities. Traditionally, small scale irregularities are treated as a random field. Recently, however, evidence has been obtained that sometimes the ionospheric turbulence on equatorial and middle latitudes represents a low-dimensional, deterministic chaotic process (A. Bhattacharyya, K.C. Yeh, and S.J. Franke, Space Sci. Rev., 61, 335, 1992; V.N. Zvezdin and S.V. Fridman, J. Atmos. Terr. Phys., 54, 957, 1992).

These facts suggest that in many cases the fading time series has a deterministic nature and is, therefore, predictable. We apply the chaotic time series predicting technique proposed by J.D. Farmer and J.J. Sidorovich (Phys. Rev. Lett., 59, 845, 1987) to amplitude measurements obtained in the University of Illinois HF Sounder. It is found that for some time series this technique allows reasonably good forecasting on a few correlation times. We discuss possible criteria (such as time stationarity, fractal dimensionality) for determining whether a particular process is predictable by the chosen method.

G2-8
1620

THE NEW GREENLAND PRD/METEOR RADAR SYSTEM
S. K. Avery[1], M. F. Larsen[2], R. Tsunoda[3], J. Avery[1], J. Buonicore[3], L. Connor[1], R. Jacobson[2], B. Livingston[3], C. Odom[2], T. Valentic[1],
[1]Dept. of Electrical Engineering, University of Colorado, Boulder, CO
[2]Dept. of Physics, Clemson University, Clemson, SC
[3]SRI International, Menlo Park, CA

In September 1993, construction and installation of a new partial reflections drifts radar operating at 2 MHz and a meteor radar operating at 30 MHz was completed at Søndre Strømfjord, Greenland. The new system is located in the vicinity of the large 1290 MHz incoherent scatter radar system which has operated at Søndre Strømfjord for over ten years. The transmitter, radar controller, and receivers used in the system are part of a frequency agile radar that can transmit at frequencies between 2 and 30 MHz. The peak transmitted power is 16 kW. Pulse coding and decoding can be implemented in software. Both the PRD and meteor radar systems have redundant receiver antennas along two baselines. The separation of the antennas for the 30 MHz radar is 0.5 λ and 1.0 λ along each baseline so that the location of the meteor trails providing the scatter can be determined unambiguously. The 2 MHz system also has three receiving antennas along each baseline with a separation of 0.5 λ between adjacent antennas. The advantage of the multiple receiving antennas is that various techniques for extracting the horizontal winds in the mesosphere can be implemented and compared. Specifically, spaced antenna analysis can be carried out using various combinations of receiving antennas. In all, there are ten combinations of triangles and crossed baselines. True Imaging Doppler Interferometry analysis is also possible since there are redundant receiving antennas along each baseline. The collocated 2 and 30 MHz systems also allow comparisons of meteor scatter and partial reflections drifts winds. The flexible software implementation of coding schemes makes it possible to test schemes for eliminating the total reflection echoes from the E region at 2 MHz by eliminating the range sidelobes. The latter, if successful will make it possible to increase the number of coherent integrations significantly. The system will be described and first results will be presented.

G2-9
1640

A PERFECTLY REFLECTING GTD MODEL OF THE HF IONOSPHERIC COUPLING WINDOW: IMPLICATIONS FOR GROUND-BASED DETECTION

Prof. Thomas A. Seliga
Electromagnetics and Remote Sensing Laboratory
Department of Electrical Engineering FT-10
University of Washington
Seattle, WA 98195

This paper examines the feasibility of detecting the narrow penetration or coupling window of a high frequency ordinary wave incident upon a horizontally stratified ionosphere and propagating in the magnetic meridian near the critical coupling angle (Seliga, Radio Science, 20, 565-574, 1985; Abali and Seliga, J. Wave-Material Inter., 1, 381-396, 1986). This is done by employing a perfectly conducting/reflecting two-dimensional model of the ionosphere along with a GTD solution of the field amplitude at a point of interest P. An infinite $\mathbf{E}$ or $\mathbf{H}$ field line source is assumed located at the origin, and an open slit of width d, beginning at an assumed critical launch angle of Θ_c from the vertical, is used to model the strong coupling region. The simulation examines the total field, consisting of the superposition of line of sight L, reflected R and diffracted D fields as a function of distance from the line source (transmitter). The results show that normally expected 'ionospheric coupling holes' of the order of 1° should be readily detected on the ground by a receiver tuned to the sky wave during transit north or south along the meridian away from the source.

INHOMOGENEOUS FLOWS AND THEIR STABILITY IN
LABORATORY AND SPACE PLASMAS
Chairman: G. Ganguli, Plasma Branch, Naval Research Laboratory, Washington, DC 20375.
Organizers: M.C. Lee, Plasma Fusion Center, MIT, Cambridge, MA 02139; and G. Ganguli

H2-1   THE ROLE OF FLOW VELOCITY SHEARS DURING
1400   ELECTRON ATTACHMENT CHEMICAL RELEASES
           W. A. Scales
           Bradley Dept. of Elec. Eng.
           Virginia Tech Blacksburg
           VA 24061-0111, USA

Artificial ionospheric electron density depletions and
negative ion plasmas may be created by electron attachment
chemical releases. During the past few years, three NASA
sounding rocket experiments, NICARE 1 and 2 and CRRES AA-4,
have been successful at creating electron density
depletions by releasing these materials. Common to these
experiments was the creation of a very sharp boundary layer
at the edge of the depletion at early times (less that 0.1
seconds). An initially highly sheared localized electric
field and subsequent small scale plasma density and
electric field irregularites were also observed at the
depletion boundary. Theoretical and numerical simulation
investigations of the electrodynamics and plasma physics of
the electron attachment release will be described. It will
be shown that a highly sheared electron flow velocity
develops in the boundary layer. This ultimately leads to
structuring and irregularity development.

H2-2   ON THE IMPORTANCE OF SHEARED FLOWS
1420   IN MAGNETIZED PLASMAS
        Prof. F. Skiff
        Laboratory for Plasma Research
        University of Maryland College Park
        College Park, MD   20742

Recent experimental and theoretical research on magnetized
plasmas in the laboratory and in space indicate the
importance of both parallel and cross-field sheared flows.
According to the circumstances, sheared flows may either
enhance or degrade plasma stability.   We will briefly
review recent advances in the study of sheared flows in
magnetized plasmas, and then discuss a particular
laboratory experiment which demonstrates the importance of
the parallel shear flow instability to plasma cross-field
transport.

In magnetized plasma, the Kelvin-Helmholtz instability is
suppressed for parallel flows below Alfvenic speeds.
Plasma compressibility, however, results in a shear flow
instability for flows at acoustic speeds. This instability
is at zero real frequency in the plasma frame, and can
result in significant cross field particle transport. We
describe a laboratory experiment involving a linear
uniformly magnetized plasma column with a shear in the
parallel (field aligned) plasma flow. Plasma flow is
observed by two different methods which can be thought of
as Eulerian and Lagrangian respectively.

Eulerian measurements involve Doppler shifted laser induced
fluorescence (LIF) of plasma ions as a function of space
time and velocity in laboratory coordinates. Lagrangian
techniques involve following the particle trajectories by
the use of test particles.   Test particles are created
experimentally by optical pumping of plasma ions to
selectively change the quantum state densities of the ions.
Such ions have the same charge to mass ratio, and thus
dynamics, as unlabeled ions and may be selectively detected
by LIF.

H2-3   ELECTROSTATIC ION-CYCLOTRON WAVE TURBULENCE
1440   EXCITED IN A NARROW VELOCITY-SHEAR LAYER
M.E. Koepke, W.E. Amatucci, J.J. Carroll III, and T.E. Sheridan
Department of Physics, West Virginia University,
Morgantown, WV 26505-6315

Inhomogeneous energy-density driven (IEDD) waves (G. Ganguli and P. J. Palmadesso, *GRL* **15**, 103, 1988) have been observed in a Q machine plasma column ($n \approx 10^8$ cm^{-3}, $m_i/m_e = 7\times10^4$, $B = 1.5$ kG, $\rho_i = 2$ mm, $r_{plasma} = 3$ cm, $T_e = T_i \approx 0.2$ eV) containing a radially localized, radial electric field produced by a segmented disk electrode (M. E. Koepke and W. E. Amatucci, *IEEE Trans. Plasma Sci.* **20**, 631, 1992), heated to avoid the effects of surface contamination. The 2-cm-diameter electrode, located on axis at the end of the plasma column, consists of an inner button segment and a surrounding coplanar annular segment (radial extents $> \rho_i$), electrically separated by a gap ($\approx \rho_i$).

When the segments are biased to support a sufficiently large magnetic-field-aligned current (FAC), the current-driven electrostatic ion-cyclotron (CDEIC) mode (Motley and D'Angelo, *Phys. Fluids* **6**, 296, 1963) is observed. The electrode segments can be biased to generate a large radial electric field (≤ 10 V/cm) in the gap region which introduces shear in the $E \times B$ flow velocity. The shear augments the destabilization of IEDD waves at values of FAC subcritical to the CDEIC instability. The broadband fluctuations are in the ion-cyclotron frequency range (M. E. Koepke *et al.*, in *Auroral Plasma Dynamics*, AGU Monograph, in print) and propagate azimuthally in the direction of the $E \times B$ drift with $k_\theta \rho_i \approx 0.4$ and a peak oscillation amplitude in the gap region. Values of $k_z/k_\theta \geq 0.02$ rule out the Kelvin-Helmholtz instability as a possible explanation for these waves (G. Ganguli *et al.*, *Phys. Fluids* **31**, 823, 1988). Mode characteristics near and beyond the instability threshold will be compared, and interpreted using theoretical calculations.

The capability of exciting ion cyclotron waves in plasma with such a low electron drift velocity has implications in the ionosphere. These results impact the interpretation of the high level of ion heating in the low-altitude ionosphere as indicated by thermal-ion upwelling into the magnetosphere (G. Ganguli *et al.*, *GRL* **12**, 643, 1985; R. T. Tsunoda *et al.*, *JGR* **94**, 15277, 1989; G. Ganguli *et al.*, *JGR*, submitted) and support the idea that waves associated with transition regions in the magnetosphere may be caused by small-scale density and/or potential structures (H. Romero *et al.*, *GRL* **17**, 2313 (1990); G. Ganguli *et al.*, in *Micro- and Meso-Scale Phenomena in Space Plasmas*, AGU Monograph, submitted; H. Romero and G. Ganguli, *Phys. Fluids B***5**, 3163, 1993).

H2-4
1500

LABORATORY STUDIES OF WHISTER AND ALFVÉN WAVES

Walter Gekelman, James Bamber, James Maggs, David Leneman,
Steve Rosenberg, Steve Vincenna (The LAPD group)
Department of Physics UCLA, 1000 Veteran Ave, Rm 15-50
Los Angeles, California 90024-1696

The interaction of obliquely propagating whistler waves and field aligned density striations is of fundamental interest in auroral physics. When electromagnetic whistler waves encounter sharp density gradients, mode conversion generates electrostatic whistlers whose large electric fields and slow phase velocities can lead to fast particle generation. This interaction has been studied in the LAPD device, a machine constructed to study the physics of plasma processes which occur in space. The LAPD plasma column is 10 meters long and 50 cm in diameter with an axial magnetic field ranging from 20 G to 2.5 kG. A magnetic loop antenna is used to launch whistler wave radiation ($\lambda_\parallel \approx 15$ cm, $\omega/\omega_{ce} \approx 0.1$, n $=7.0 \times 10^{11}$ cm^{-3}) near an 8.0 cm diameter, 8.0 m long density depletion having a steep gradient ($n/\nabla n \approx 1$ cm) perpendicular to B_0 (≈ 500 G). The plasma density in the depletion is five times less than the background density. Vector electric and magnetic wave fields are measured, both with and without the striation. Nearly-electrostatic whistlers are observed to be generated in regions of steep gradient and escape the striation. Electromagnetic whistlers are seen to reflect from the striation.

Alfvèn waves are fundamental to many physical processes in Space plasmas. They have been launched and detected in the LAPD in a highly ionized He Plasma with B = 1.25 kG and n $\approx 4 \times 10^{12}$ /cm^3. A phase coherent tone burst below the ion cyclotron frequency is launched from a wire grid antenna several ion Larmor radii in diameter. The launched waves are detected by three orthogonal magnetic pickup loops which can be moved anywhere in the plasma volume. Antenna radiation patterns for the shear Alfvèn mode are measured as a function of space and time. The wave polarization is measured as a function of position, time and wave amplitude. The measured fields are compared to theoretical predictions.

H2-5   ALFVEN WAVE IN LABORATORY PLASMAS
1540   Prof. Noah Hershkowitz
          University of Wisconsin
          Department of Nuclear Engineering & Engineering Physics
          1500 Johnson Drive
          Madison, WI 53706-1687

There is no doubt that Alfven waves are important in space. The study of Alfven waves and waves near the ion cyclotron frequency requires plasma densities $> 10^{19}\text{m}^{-3}$, or very long devices, or both. At lower frequencies, even higher densities or longer devices are required. The Phaedrus-T tokamak provides a regime in which high plasma density is relatively easy to achieve at electron temperatures of 500-800eV in order to reduce the collisionality. Laboratory Alfven wave experiments require the excitation of appropriate modes within the plasma, away from the device walls. This is accomplished by employing mode conversion of magnetosonic modes, which can be excited near the device walls to shear Alfven or kinetic Alfven waves. The presence of several plasma species provide a natural way for mode conversion to occur.

Alfven wave experiments carried out with multi-species plasmas in the Phaedrus-T tokamak have demonstrated both electron heating and Alfven wave electron current drive. These recent results will be compared to those obtained in the Phaedrus-B tandem mirror.

H2-6   IONOSPHERIC CHAMBER EXPERIMENTS WITH THE VERSATILE
1600   TOROIDAL FACILITY (VTF)

M.C. Lee, D.T. Moriarty, D.F. Beals, J.M. Sorci,
S.M. Murphy, and R.R. Parker
Plasma Fusion Center, MIT, Cambridge, MA 02139

Laboratory experiments have been conducted with the
Versatile Toroidal Facility (VTF) that is a large toroidal
plasma device constructed for simulating the wave propagation
and interactions with the ionospheric plasmas. The VTF plasmas
are primarily generated by the injected microwaves via the
electron cyclotron resonance heating (ECRH) process. The ECRH
plasmas are mainly imposed by a toroidal magnetic field that
can simulate the Earth's magnetic flux. Nevertheless, a small
vertical field is added to the toroidal field, forming a
spiral configuration of magnetic field. This spiral field can
increase the confinement time of plasmas from microseconds up
to milliseconds. Further, the spiral field can guide electric
current to flow from the bottomside to the topside of the
plasma chamber. The electric current is produced by a hot
cathode electron beam drive system. Microwave propagation and
attenuation in the turbulent magnetoplasmas were investigated,
showing anomalous absorption of the injected waves due to the
nonlinear mode conversion and scattering off the plasma turbu-
lence. The plasma turbulence appears inherently with the ECRH
generated plasmas and is enhanced by the injected electron
beam. We will discuss our recent studies of the wave-plasma
interactions and the plasma modes produced by the intense
microwaves and the magnetic field-aligned electric current.

H2-7 1620 On the Spectrum of a High Power Microwave Pulse Propagating in a Self-generated Plasma*

A. Ren and S.P. Kuo

Weber Research Institute and Department of Electrical Engineering
Polytechnic University, Route 110, Farmingdale, NY 11735, USA

An intense microwave pulse can cause the breakdown of the background air. Thus frequency spectrum of the pulse can be modified significantly during its propagation through the self-generated plasma which is a rapidly space-time varying dielectric medium.

In this work, a chamber experiment is performed to demonstrate the frequency shift phenomenon. The experiment of pulse propagation is conducted in a vacuum chamber filled with dry air (~0.2 torr), the chamber is made of a 2 ft. cube of Plexiglas. A rectangular microwave pulse (1 μs pulse width and 3.27 GHz carrier frequency) is fed into the cube through an S-band microwave horn placed at one side of the chamber. A second S-band horn placed at the opposite side of the chamber is used to receive the transmitted pulse. The spectra of the incident pulse and transmitted pulse are then compared. As the power of the incident pulse is only slightly (<15%) above the breakdown threshold power of the background air, the peak of the spectrum of the transmitted pulse is upshifted from the carrier frequency 3.27 GHz of the incident pulse. However, as the power of the incident pulse exceeds the breakdown threshold power of the background air by 30%, a different phenomenon appears. The spectrum of the transmitted pulse becomes to have two clearly peaks. One is upshifted and the other one downshifted from the single peak location of the incident pulse. The amount of frequency downshift is comparable to that of the upshifted frequency.

A theoretical model describing the experiment of the pulse propagation in a self-generated plasma is developed. There are excellent agreements between the experimental results and computer simulations based on this theoretical model, which is also used to further carry out computer experiments for identifying the role of collisional loss on the frequency downshift phenomenon.

H3-1 **RADIO SOUNDING OF THE MAGNETOSPHERE:**
1400 **OVERVIEW**

William W. L. Taylor
Nichols Research Corporation
1700 N. Moore St., Suite 1820
Rosslyn, VA 2209
and the Radio Plasma Sounding Team

Over the past few years the *ad hoc* Radio Plasma Sounding Team has investigated the possibility of using radio waves to image the magnetosphere. In the thirty five years of space physics research, ionosondes, auroral and geocorona instruments, and energetic neutral detectors have been able to remotely sense some parts of the magnetosphere and ionosphere. A new type of magnetospheric imaging, radio plasma imaging will allow large portions of the magnetosphere to be studied, using data taken over only a few hours. For example, the dynamics of the plasmapause and magnetopause will be able to be investigated because remote imaging will allow the investigator to visualize the surfaces, not just make single point measurements while passing through the surfaces.

Radio sounding will be reviewed, along with the ionospheric understanding that ground based and topside sounders have brought us over the years. Ground based (bottomside) sounders were necessary to the understanding of the lower ionosphere as topside (satellite) sounders were to the upper ionosphere.

To see how the extension of the ionosphere sounder to the magnetosphere will work and what kind of data will be available, the Team has assembled a comprehensive magnetospheric model and coupled it with a model of a realistic radio plasma sounder, and a ray tracing code. The results give simulated magnetospheric plasmagrams, which are plots of echo delay as a function of wave frequency.

The simulated plasmagrams will demonstrate how plasmagrams from a radio plasma imager on a magnetospheric spacecraft will be able to further our understanding of plasmapause evolution, plasmasphere filling, magnetopause structure and motion, auroral cavity formation and stability, cusp structure and ring current dynamics.

H3-2
1420

FEASIBILITY OF RADIO SOUNDING IN THE MAGNETOSPHERE

W. Calvert, R. F. Benson (GSFC), D. L. Carpenter (StarLab, Stanford), S. F. Fung (GSFC), D. L. Gallagher (MSFC), J. L. Green (GSFC), P. H. Reiff (Rice Univ.), B. W. Reinisch (Univ. of Mass, Lowell), M. F. Smith (GSFC), and W. W. L. Taylor (Nichols Research Corporation)
Department of Physics and Astronomy
University of Iowa
Iowa City, Iowa 52242 USA

Providing remote density measurements of unprecedented accuracy and coverage, pulsed radio sounding in the magnetosphere would permit almost continuous observation of the plasmapause and magnetopause, along with complete cross-sectional density images of plasmasphere, cusp, and auroral plasma cavity. This technique would thus revitalize magnetospheric research and answer many important questions that cannot be addressed by local measurements.

Using modern digital techniques and operating at frequencies of 3 kHz to 3 MHz, a magnetospheric radio sounder would require 500-meter tip-to-tip dipole antennas and a transmitter peak pulse power of ten watts or less. This sounder would be equipped with three-axis electric antennas to measure echo directions, including two long-wire antennas in the spacecraft spin plane and a short, tuned dipole receiving antenna along the spin axis. The plasmagram cycle, during which echo delays and directions are measured as a function of frequency, would require only a few minutes and include both range-gate and doppler integration to enhance the echo signals. Density versus distance profiles could thus be calculated at intervals of roughly two degrees along a satellite orbit at 6 R_E, using techniques previously developed during the Alouette and ISIS Topside-Sounder Programs [see Franklin and Maclean, *Proc. IEEE, 57,* 897-928, 1969; J. E. Jackson, *ibid,* 960-975].

Considering spatial attenuation, focusing, and competing natural and instrumental noise sources, such a sounder is found to be quite feasible and practical. It is therefore considered an outstanding candidate for future missions to remotely image the magnetosphere.

H3-3   SIMULATIONS OF MAGNETOSPHERIC RADIO
1440   SOUNDINGS
        Robert F. Benson, W. Calvert (Univ. of Iowa), D. L.
          Carpenter (StarLab, Stanford Univ.), S. F. Fung
          (GSFC), D. L. Gallagher (MSFC), J. L. Green (GSFC),
          P. H. Reiff (Rice Univ.), B. W. Reinisch (Univ. of Mass.,
          Lowell), M. F. Smith (GSFC), and W. W. L. Taylor
          (Nichols Research Corporation)
        Code 692
        Goddard Space Flight Center
        Greenbelt, MD 20771

This paper will present the results of simulations of global mag-
netospheric sounding from a space-borne radio sounder located
between the plasmapause and the magnetopause. Three-
dimensional ray tracing was performed using diffusive equilibrium
electron density N_e and plasmapause models (Angerami and
Thomas, J. Geophys. Res., 69, 4537 , 1964; Aikyo and Ondoh, J.
Radio Res. Labs., 18, 153, 1971, respectively) combined with a
maxwellian N_e fall-off from the magnetopause boundary. This
boundary was determined using the model of Roelof and Sibeck
(accepted in J. Geophys. Res., 1993) which is based on the IMF B_z
and the solar wind dynamic pressure.

The ray tracing results for frequencies from 30 to 90 kHz are
summarized on simulated magnetospheric plasmagrams (records of
echo delay time vs. frequency), similar to the ionograms from
ionospheric sounding which have been studied for the last three
decades. The similarities include the ability to interpret multiple
echoes from different directions that appear on the same record. The
differences include the predominance of curved reflection surfaces in
magnetospheric sounding as compared with the usually justified
assumption of horizontal stratification in the case of ionospheric
sounding. The curved magnetospheric surfaces can result in
defocusing near the plasmapause and focusing near the mag-
netopause. Such focusing and defocusing can also result from
boundary irregularities. Magnetopause irregularities will lead to
multiple reflections from the same general direction. A smooth mag-
netopause, on the other hand, will yield several echoes from signifi-
cantly different directions. The capability to interpret such multiple
echoes means that it will be possible, from such a sounder mission,
to monitor the global configuration of the magnetopause while pro-
viding nearly simultaneous radial N_e profiles in different directions in
order to yield unprecedented 3-dimensional information on the mag-
netopause and plasmasphere.

H3-4 TOPSIDE WAVE-INJECTOR
1520 Suman Ganguly
Center for Remote Sensing
P. O. Box 9244
McLean, VA 22102

For the ponderomotive force induced effects to be manifested in the space plasma, a fluence of around 100 mW/m^2 is needed. This is beyond the reach of any ground based facility. A Satellite based wave injection experiment in the ionosphere/magnetosphere is proposed, where a high power ≈500 KW, pulsed (<secs), multifrequency (several Hz to tens of MHz) transmitter with extremely low duty cycle (average power of tens of watts) could provide significant jolt of electric field over reasonable area of the ionosphere (≈10 Km).

The range of experiments are diverse and include numerous plasma instabilities, non-linear wave effects, ion and electron acceleration, ion cyclotron effects, AKR, triggering of magnetic storm, airglow, cavitons, etc. With the addition of a simple receiver in a second satellite, this could be a unique ionospheric/magnetospheric sounder for mapping plasma properties and wave propagation studies. The proposed satellite would be a valuable addition to HARRP facility and could be an international platform for wave injection experiments.

H3-5
1540

DIFFUSE KILOMETRIC RADIATION AS OBSERVED BY
GALILEO DURING THE SECOND EARTH ENCOUNTER

J. D. Menietti, W. S. Kurth, and D. A. Gurnett
Department of Physics and Astronomy
The University of Iowa
Iowa City, IA 52242

The Galileo spacecraft made its second Earth encounter on December 8, 1992. During this flyby kilometric radiation was observed with two distinct morphologies. The first is in the frequency range of about 100 kHz to near 1 MHz and typically has a discrete structure as expected for auroral kilometric radiation. The second component, observed while the spacecraft was in the magnetosheath, is more diffuse and typically occurs at lower frequencies, $f \leq 200$ kHz. Using ray tracing, we have examined a number of possible source regions for this emission assuming both O-mode and R-X mode. The data appears to be most easily explained by R-X mode emission from sources located in the nightside auroral region. The magnetosheath can act as a wave guide that channels the emission tailward; "scattering" from plasma inhomogeneities within the magnetosheath may be responsible for the diffuse nature of the emission.

H3-6
1600

PROPAGATION OF ELECTROMAGNETIC WAVES PARALLEL TO THE MAGNETIC FIELD IN THE NIGHTSIDE VENUS IONOSPHERE

J.D. Huba and H.L. Rowland
Code 6794, Plasma Physics Division
Naval Research Laboratory
Washington, DC 20375-5320

A theoretical and numerical analysis of the propagation of electromagnetic waves in the nightside Venus ionosphere is presented. The special case of propagation parallel to the magnetic field is considered. The model assumes a source of electromagnetic radiation in the Venus atmosphere, such as produced by lightning, and specifically addresses wave propagation for realistic ionospheric parameters in the altitude range $z = 130 - 160$ km at the four frequencies detectable by the Pioneer Venus Orbiter Electric Field Detector (OEFD): 100 Hz, 730 Hz, 5.4 kHz, and 30 kHz. The results are summarized as follows. The $f = 100$ Hz and 730 Hz waves can propagate as whistler waves, provided $f < f_{ce}$, where f_{ce} is the electron cyclotron frequency, and provided that the ionospheric electron density is sufficiently small that the waves are not strongly attenuated by collisional effects (i.e., Pedersen conductivity). The attenuation length scale λ_0 associated with the Pedersen conductivity is $\lambda_0 \sim 2(c/\omega_{pe})[\Omega_e{}^3/\omega(\nu_{en} + \nu_{ei})^2]^{1/2}$; for parameters typical of the nightside Venus ionosphere above 140 km, electron-ion collisions are more frequent than electron-neutral collisions and are therefore responsible for the attenuation of the waves. A parameterization of the wave intensities and Poynting flux as a function of magnetic field and peak electron density is presented. The waves are found to propagate most easily for high magnetic field and low electron density conditions (i.e., ionospheric holes); this result is consistent with observational data. The incident Poynting flux at the bottom of the ionosphere ($z \simeq 130$ km) is estimated to be $S \simeq 0.1$ W/m^2 for the 100 Hz waves. The $f = 5.4$ kHz and 30 kHz cannot propagate through the nightside Venus ionosphere, as expected, because $f_{pe} > f > f_{ce}$.

J1-1   SPACEBORNE ANTENNA TECHNOLOGY FOR RADIO ASTRONOMY
1400   Mr. Robert E. Freeland
              Jet Propulsion Laboratory
              4800 Oak Grove Drive, Mail Stop 157/507
              Pasadena, CA 91109

ABSTRACT

Large size space antennas are needed for a variety of applications that include mobile communications, radiometry, active microwave sensing, radio astronomy, and space based radar. Since current NASA planning does not include any meaningful orbital assembly capability, essentially all near term large size antenna structures will have to be based on self deployable structural concepts. There are a large number of different space antenna structural concepts at this time. They range in maturity from simple configuration designs to a small number of proven space flight designs. However, the antenna user community has their own stringent criteria for selection of antenna concepts for specific applications. The selection criteria common to all users are low cost, light weight, high reliability and usable surface precision. Therefore serious interest from this community will depend on realistic demonstrations and validation of concept capability. This means building large size, flight quality hardware for demonstration of deployment reliability and thermo/mechanical performance in a realistic environment. Consequently, the number of candidate deployable antenna concepts, for any application, with potential for meeting the user criteria is small. The opportunity for realistic performance validation of exceptional concepts is extremely limited.

Since there are no validated large size space antenna concepts for radio astronomy at this time, this paper identifies technology development options for structures up to 30 meters in diameter for radio astronomy. These options include (a) modifications and/or advancements of existing concepts, (b) hybrid concepts based on desirable features of existing concepts and (c) new and unique technology approaches. Examples will be given with emphasis placed on new and innovative concepts such as the inflatable deployable antenna concept that has tremendous potential for accommodating an affordable radio astronomy mission. System configuration studies for determining the applicability of this unique concept for space VLBI have been initiated. The technology maturity of this concept will be demonstrated and evaluated by the space flight experiment of a 14 meter diameter antenna, scheduled to be launched in late 1995. The results of these activities are expected to significantly reduce user risk.

J1-2   THE SPACE VLBI PROJECT RADIOASTRON
1440   L.I. Gurvits
            National Astronomy and Ionosphere Center
            Arecibo Observatory, P.O.Box 995, Arecibo, Puerto Rico 00613
            and
            Astro Space Center of P.N.Lebedev Physical Institute
            Leninsky Pr. 53, Moscow, 117924, Russia

The RadioAstron project is aimed to create a Space–Ground VLBI (Very Long Baseline Interferometry) system. The orbiting element of this system, a radio telescope onboard the spacecraft "Spectr-R", will be launched with "Proton" launcher on high-excentricity near-one day orbit. Such a period provides a maximal baseline of about 80,000 km. Scientific objectives of the mission imply studies of galactic and extragalactic radio sources with an angular resolution approximately 10 times higher than achieved with global ground VLBI networks.

The main feature of the RadioAstron design is the 10-m parabolic antenna. It will be launched in folded state and then will be deployed in the orbit. The reflector surface is formed by 27 solid petals and the central 3-m diameter part. The antenna petals are produced from carbon-fiber composite material which provides high solidity under strong weight and thermal deformation requirements.

RadioAstron will have the simplest optical scheme with feeds in the prime focus of the main reflector. Such a scheme allows to avoid some extra weight and design problems comparably with two or more reflectors scheme. But at the same time this single reflector scheme put some specifical requirements for feeds design and operational logics.

Radioastronomical receivers will be placed inside the focal package. They will operate in both circular polarizations at all four operational frequencies 0.327, 1.6, 5, and 22 GHz. The bandwidth in each polarization at three highest frequencies will be 32 MHz, and 8 MHz at 327 MHz.

Another basic part of VLBI data flow equipment will be placed inside the service module – the main body of the spacecraft. The standard 500 MHz IF signal will come to video converters and than digitized and formatted. The output of formatter will be connected with data down-link system with two 32 MHz channels. The mission will operate in two VLBI standards, VLBA and S2.

The mission will be available for the astronomical community as an open facility. A peer-review process and proposal evaluation, as well as the project implementation and the scientific operation will be supervised by the RadioAstron International Scientific Council (RISC).

The RadioAstron project is been developing by joint efforts of experts from Australia, Canada, Finland, Germany, Hungary, India, Italy, Kazakhstan, The Netherlands, Russia, Sweden, Ukraine, United Kingdom, USA, Uzbekistan.

J1-3   AN AFFORDABLE ADVANCED SPACE VLBI MISSION
1540   J. S. Ulvestad, J. G. Smith, D. L. Meier, D. W. Murphy, R. A. Preston
            Jet Propulsion Laboratory
            California Institute of Technology
            Mail Code 264-664
            Pasadena, CA 91109

We propose a high-sensitivity Space VLBI mission as a successor to the VSOP and Radioastron missions that will be flown in the late 1990s. This future mission has science goals similar to those of the International VLBI Satellite (IVS) that was proposed in the late 1980s. It will take advantage of significant technology advances in the last five years to enable a mission with a total cost expected to be less than $500 million.

The most important attribute of the proposed mission will be a greatly enhanced sensitivity. Interferometer baselines to the same ground radio telescopes as those used by VSOP and Radioastron will produce a factor-of-50 sensitivity enhancement over those missions at frequencies of 1.6, 5, and 22 GHz, with coverage of the 43-GHz band also likely. The highly sensitive centimeter-wavelength mission is preferred over one operating at much shorter wavelengths because of the much greater expense of constructing a space radio telescope (and co-observing ground telescopes) with sufficient sensitivity at frequencies of 86 GHz and higher. The high sensitivity would be achieved by (1) orbiting a telescope in the 30-m class, compared to the 8–10-m antennas of VSOP and Radioastron; (2) making use of a data rate of 1–2 Gigabit/s instead of the 128-Megabit/s rate for the 1990s missions; and (3) flying cryogenically cooled receivers providing total system temperatures of 10–20 K, compared to values of 70–200 K for VSOP and Radioastron. The technologies necessary for these improvements are available now, or will be in the very near future. Antenna technology is described in the paper by R. Freeland in this session, and the data-recording and correlation capability will exist in the Mark IV VLBI system that has been developed by the Haystack Observatory with some contributions from the European VLBI Network. Some technology development work still is necessary for the required long-lived, space-qualified, cryogenic cooling systems.

The root-mean-square noise on baselines between the spacecraft and a 25-m ground telescope will be less than 1 mJy, and will be 0.2–0.3 mJy for ground telescopes in the 100-m class. Such noise levels will allow mapping of the centimeter-wavelength radio emission (including polarization) of active galactic nuclei at a resolution of 0.1 milliarcsecond with extremely high sensitivity and dynamic range. Observations of the cores of nearby, low-brightness-temperature extragalactic sources such as Seyfert galaxies will be possible on scales at or below the sizes of their accretion disks. A number of extragalactic water masers will be accessible, with determination of statistical parallaxes of those objects leading to an improved value for Hubble's constant. The low noise levels also will enable observations of radio stars in both their flaring and quiescent states.

J1-4   LOW FREQUENCY RADIO ASTRONOMY IN SPACE
1600   Kurt W. Weiler

Namir E. Kassim
Andrew W. Clegg
Naval Research Laboratory
Code 7215
Washington, DC 20375-5351

At the lowest radio frequencies (≤ 30 MHz), the Earth's ionosphere transmits poorly or not at all. This relatively unexplored region of the electromagnetic spectrum is thus an area where high resolution, high sensitivity observations can open a new window for astronomical investigations. Also, extending observations down to very low frequencies brings astronomy to a fundamental physical limit where the Milky Way becomes optically thick over relatively short path lengths due to diffuse free-free absorption.

To obtain data at these frequencies requires the difficulty and expense of placing radio telescopes in space, but the scientific rewards of space missions are likely to be great. Even without considering the serendipitous discoveries which have always accompanied the opening of a new realm of frequency, resolution, or sensitivity in astronomy, a low frequency telescope in space can: (1) map the entire sky, with emphasis on the galactic background non-thermal emission, with high resolution and sensitivity; (2) determine the distribution of galactic diffuse ionized hydrogen by surveying its absorption of discrete background sources and the galactic background radiation; (3) study of the interstellar plasma by investigating its scattering and refraction; (4) study individual source spectra for energy production and absorption mechanisms; (5) study the correlation between low frequency, steep spectrum clusters of galaxies and their enhanced x-ray emission; (6) search for "fossil" radio components in "radio quiet" objects at the low frequencies where synchrotron lifetimes approach the age of the universe; (7) image individual sources with high resolution to investigate spectral index changes across source components and to search for extended halos; (8) study the impulsive emission from Jupiter and the Sun and search for similar radiation from other Solar System bodies; and (9) search for the coherent radiation common from Solar System bodies but apparently rare in larger systems.

A program of development from a single interference monitoring satellite in low earth orbit through arrays in high earth orbit to synthesis telescopes on the near- and far-side of the moon will be described.

J1-5   THE SUBMILLIMETER WAVE ASTRONOMY SATELLITE - SWAS
1620   Paul F. Goldsmith
          National Astronomy and Ionosphere Center
          Cornell University

The SWAS satellite has been designed to observe molecular and atomic species of critical importance to chemistry and physical conditions in dense interstellar clouds. It will be able to observe simultaneously the ground state transition of water (H2O) at 557 GHz, atomic carbon (CI), and low-lying transitions of carbon monoxide (13CO) and molecular oxygen (O2). It will also be possible to observe the isotopic variant of water, H218O, which will be of interest if the abundance of water is relatively high.

As a group, and especially in conjunction with species observed from the ground, these transitions are important diagnostics of conditions in interstellar clouds. The water molecule is expected to play a major role in cooling the gas in these regions, thus allowing their density to increase, and enhancing the formation of new stars. The abundance of carbon in atomic form is a sensitive probe of the penetration of ultraviolet radiation into dense regions, which gives us important information about inhomogeneities in the distribution of material.

SWAS is a part of NASA's SMALL EXPLORER PROGRAM, designed to enable relatively inexpensive space missions on an accelerated time scale. SWAS has been designed to use available hardware, but has proven to be a significant driver in advancing technology for future space missions.

The SWAS telescope is an off-axis Cassegrain, with aperture dimensions 71 cm by 55 cm. Switching the position of the beam on the sky can be accomplished by a chopping secondary, for angular shifts up to 10 arcminutes, and by repointing the entire spacecraft for larger shifts. The latter can be carried out in less than 10 seconds for a several degree change in pointing. The front end consists of two Schottky diode second harmonic mixers passively cooled to 150 K. The noise temperature achieved is less than 3000 K (SSB). The two IF's are combined and fed to an acousto-optical spectrometer with a total bandwidth of 1400 MHz and frequency resolution of 1 MHz (0.5 km/s).

SWAS has been configured to be placed in orbit by an enhanced PEGASUS launch system. The orbit altitude will be ~ 550 km, inclined by approximately 60 degrees and the design mission lifetime is 3 years. SWAS is presently scheduled to be launched in June 1995. The SWAS project has been implemented by scientists at the Center for Astrophysics, the University of Massachusetts, Amherst, Cornell University, Johns Hopkins University, the National Air and Space Museum, the University of Cologne, and NASA Ames Research Center. The submillimeter front end is being built by the Millitech Corporation, and the overall instrument by Ball Aerospace Corporation.

0815-Thurs. CR2-28
PLENARY SESSION

0815 Introduction: David Chang, Chair, USNC/URSI, Dean, College of Engineering and Applied Sciences, Arizona State Univ., Tempe, AZ 85287-5506

0825 Student Paper Competition: Charles M. Rush, Chief Scientist, NTIA, U.S. Department of Commerce, Washington, DC 20230

0945 NEW DEVELOPMENTS IN ENHANCED BACKSCATTERING: Walter A. Flood, Jr., Director, Geosciences Division, U.S. Army Research Office, Research Triangle Park, NC 27709

1025 APPLICATION OF COMMUNICATION AND ELECTRONICS IN TRANSPORTATION: Donald Dodson, Vice President, R & D, TRW Transportation Electronics Division, Farmington Hill, MI 48335

1105 NATIONAL INFORMATION INFRASTRUCTURE INITIATIVES: Charles M. Rush, Chief Scientist, NTIA, U.S. Department of Commerce, Washington, DC 20230

1145 Student Paper Award

Session B-4 1355-Thurs. CR2-28
INVERSE SCATTERING
Chairman: Louis Fishman, Dept. of Mathematical and Computer Sciences, Colorado School of Mines,
Golden, CO 80401

B4-1   DIRECT AND INVERSE WAVE PROPAGATION
1400   IN THE FREQUENCY DOMAIN VIA THE
         DIRICHLET-TO-NEUMANN OPERATOR SYMBOL

Louis Fishman
Department of Mathematical and Computer Sciences
Colorado School of Mines
Golden, CO 80401

This talk is concerned with both direct and inverse elliptic (fixed-frequency) wave propagation problems. The fundamental idea is to combine wave field splitting, invariant imbedding, and phase space methods. Wave field splitting, invariant imbedding, and phase space methods reformulate the Helmholtz wave propagation problem in terms of an operator scattering matrix characteristic of the modeled environment. The subsequent equations for the reflection and transmission operators are first-order in range, nonlinear (Riccati-like), and, in general, nonlocal. The system allows for well-posed marching of the elliptic scattering problem. The reflection and transmission operator symbol equations are stiff and oscillatory with a subtle (fixed and movable) singularity structure. This apparent numerical difficulty is partly overcome by reformulating the calculations in terms of the Dirichlet-to-Neumann operator symbol which generally has a much smoother behavior, and is consequently more easily computed. The physically necessary reflection and transmission operator symbols then follow from a transformation formula. The reflection and transmission operator symbol equations provide the framework for constructing inverse algorithms, based on, in principle, exact solution methods. Again, transformation to the Dirichlet-to-Neumann operator symbol is a crucial step in the analysis. For both the direct and inverse formulations, the mathematical framework and computational algorithms will be examined and compared with exactly soluble, multidimensional model problems designed to illustrate the theory and provide numerical benchmarks. The direct approach is particularly appropriate for large-scale propagation models, while the development of robust, numerical algorithms for multidimensional inversion based on exact solution methods is clearly a desirable goal since the computational algorithms currently being employed in these areas often involve either perturbative methods (an initial linearization of the problem) or massive optimization (search) algorithms.

B4-2
1420

IMAGE RECONSTRUCTION FROM STRONGLY SCATTERING OBJECTS USING A DIFFERENTIAL CEPSTRAL FILTER

J. B. Morris,[*] F. C. Lin, R. V. McGahan[*] and M. A. Fiddy
Department of Electrical Engineering, University of
Massachusetts-Lowell, Lowell, MA 01854
[*]Rome Laboratory, Hanscom AFB, MA 01731

Inversion methods using linearized approximations such as the Born or Rytov approximation for diffraction tomography typically require that the object either be weakly scattering or small in size compared with the illuminating wavelength. Based on these approximations, the inversion methods become simply Fourier inversion procedures.

In this paper, we present a novel approach, using the differential cepstral filtering technique which is also computationally simple and straightforward, to reconstruct the structure of strongly scattering objects having permittivity fluctuations with scales comparable with the illuminating wavelength. A quantitative image which is the product of the permittivity distribution function of the object and the internal field is first obtained by backpropagating the measured scattered field data into the object domain. Then, this backpropagated image is filtered, in the differential cepstral domain, by removing the contribution due to the internal field in order to reconstruct the permittivity distribution function.

We will show reconstructions from both simulated and real microwave scattered data. More importantly, we will illustrate that this approach is particularly effective for objects which are strongly scattering but slowly varying on the scale of the illuminating wavelength.

B4-3
1440
AN INVERSE SCATTERING APPROACH TO CALCULATION OF EFFECTIVE PERMITTIVITY OF RANDOM COLLECTIONS OF SCATTERERS

M. Moghaddam[*,1] and B. Houshmand[2]
[1] Jet Propulsion Laboratory
California Institute of Technology
4800 Oak Grove Drive
Pasadena, CA 91109

[2] Department of Electrical Engineering
University of California at Los Angeles
Los Angeles, CA 90024

ABSTRACT

Characterization of scattering by multiple objects is of importance in several areas such as remote sensing, random media, and mixing laws. Here, we utilize inverse scattering to calculate the equivalent dielectric constant of a random mixture of two-dimensional scatterers. Without loss of generality, we assume that the scatterers have circular cross sections. First, we use the recently developed fast algorithms for scattering by multiple objects (e.g., see Chew, W. C., *Waves and Fields in Inhomogeneous Media*. New York: Van Nostrand Reinhold, 1990) to find the average scattered field from a collection of randomly distributed cylinders with arbitrary, random dielectric constants. The scattering problem is then solved several times, each time with a new arrangement for the location of the randomly distributed cylinders. The scattered field is found at many points around the simulation region by statistically averaging the field due to each arrangement. Normal plane wave incidence is assumed. If the cylinders have low permittivity such that they are weak scatterers, we can use a number of linear inverse scattering techniques to find the equivalent dielectric constant of an object with the same scattered field as the above collection of cylinders. Here, we use diffraction tomography for linear inversion. The results of this approach will be presented. For the case where scatterers are not weak, it is also possible to carry out a nonlinear inversion using the Born iterative method.

B4-4
1500

FAST ISAR IMAGE FORMATION OF COMPLEX TARGETS
USING THE SHOOTING AND BOUNCING RAY METHOD
R. Bhalla and H. Ling
Department of Electrical and Computer Engineering
The University of Texas at Austin
Austin, TX 78712-1084

The shooting and bouncing ray (SBR) method is a high frequency electromagnetic simulation technique for predicting the radar returns from realistic aerospace vehicles and the scattering by complex media (H. Ling et al, IEEE Trans. Antennas Propagat., 37, 194, 1989; J. Baldauf et al, IEEE Trans. Antennas Propagat., 39, 1345, 1991; H. Ling et al, IEEE Trans. Antennas Propagat., 39, 1412, 1991). The basic idea behind the SBR method is very simple. Given the geometrical description of a target, a large set of geometrical optics rays is shot towards the target. Rays are traced according to the laws of geometrical optics as they bounce around the target. At the exit point of each ray, a ray-tube integration is performed to sum up its contribution to the total scattered field. While the basic idea behind the SBR methodology is simple, when combined with CAD tools for geometrical modeling and fast ray-tracing algorithms developed in computer graphics, this technique becomes a very powerful tool for characterizing the scattering from large, complex targets. One such development is the general-purpose SBR code, Xpatch (S. W. Lee and D. J. Andersh, 9th Annual Review of Progress in Applied Computational Electromagnetics, Monterey, 1993), which is currently used by the Air Force and the aerospace industry in programs related to target identification and low-observable vehicle design.

In this work, we will address the issue of fast inverse synthetic aperture radar (ISAR) image formation of complex targets using SBR-based codes such as Xpatch. Contrary to the conventional approach where the ISAR image is obtained by inverse Fourier transforming the computed scattered field data over frequency and aspect, a simple image-domain ray-tube integration formula is derived to account for the contribution of each ray to the overall ISAR image directly. This image-domain ray-tube integration formula is determined in closed form under the small angle approximation and utilizing the bistatic-monostatic equivalence. Simulation results using the SBR-based code "Xpatch" show that the direct image domain method results in good image quality and superior time performance when compared to the conventional frequency-aspect approach.

B5-1
1520

LEAKY DOMINANT MODES ON MICROSTRIP-TYPE STRUCTURES

David Nghiem, Jeffery T. Williams, David R. Jackson

Department of Electrical Engineering
University of Houston
Houston, Texas 77204-4793

Arthur A. Oliner

Weber Research Institute
Polytechnic University
Brooklyn, NY 11201

For a conventional microstrip with an isotropic substrate, it has recently been reported (D. Nghiem et al., IEEE MTT-S Digest, 3, 1291-1294, 1993) that an independent leaky dominant mode exists at high frequencies in addition to the customary bound dominant mode (where "dominant" implies that the strip current is similar to that of the TEM mode existing when the dielectric is air). This leaky dominant mode has leakage into only the fundamental TM_0 surface wave on the grounded substrate. For both the dominant bound and leaky modes, the corresponding field distributions are very similar around the strip region and, therefore, the modes are expected to be excited with comparable amplitudes by conventional microstrip feeds. This expectation has been verified experimentally. It has also been shown experimentally that the leaky dominant mode causes additional loss and spurious performance, such as crosstalk between circuit elements and interference with the bound mode.

In this presentation, the formulation for determining the propagation wavenumber of the dominant bound and leaky modes on a general microstrip structure with an arbitrary number of uniaxial-anisotropic layers, using the spectral domain moment method, will be discussed briefly. The basic properties for both the dominant bound and leaky modes will be also reviewed. For a conventional microstrip, the characteristics of the dominant leaky mode which has leakage into only the TM_0 surface wave will be presented, including the effects of varying strip width, strip location, anisotropy ratio, etc. Dominant-mode leakage effects have also been investigated for other microstrip-type structures, such as suspended microstrip, inverted microstrip, and embedded microstrip. Finally, possible ways to suppress the leaky dominant modes will be discussed.

RADIATION FROM DIELECTRIC LEAKY-WAVE ANTENNAS OF FINITE SIZE

H. Ostner, J. Detlefsen
Lehrstuhl für Hochfrequenztechnik
Technische Universität München, 80290 München, Germany

D. R. Jackson
Department of Electrical Engineering
University of Houston, TX 77204–4793, USA

Planar high-gain millimeter-wave antennas are required in many applications. One possible type of antenna is a leaky-wave antenna consisting of multiple dielectric layers over a ground plane. If the layer thicknesses are properly dimensioned, large radiating apertures resulting in narrow-beam patterns can be achieved by simple sources such as a line current in the one-dimensional case or a Hertzian dipole in the two-dimensional case, respectively. Due to the simple feeding structure these antennas do not suffer from the losses of a feeding network needed for microstrip element arrays, and hence higher efficiency and gain can be obtained.

In the first part of this presentation the different types of wave components that comprise the total aperture field of a dielectric leaky-wave antenna excited by a line source are studied. The aperture field is first decomposed into a radiation-field part and a surface-wave part. A further decomposition of the radiation field into a leaky-wave field and a space-wave field is then made, using a defined transition function based on the complex power radiated by the leaky waves. The influence of each individual wave component on both the aperture field and the radiation pattern is shown. For moderate scan angles the aperture field is dominated by a weakly attenuated leaky wave, which primarily determines the radiation pattern. However, for scan angles approaching the horizon the space-wave field dominates the total aperture field. The effects of a finite aperture on the radiation pattern are investigated by Fourier transforming the truncated aperture field.

In the second part, a practical dielectric leaky-wave antenna with a finite cylindrical aperture operating at 62 GHz is investigated. The structure is excited by a waveguide-fed slot, which is modelled theoretically by a horizontal magnetic dipole. The theoretical background for the antenna radiation analysis is given and the effects of the finite-size aperture on the radiation pattern are discussed. Experimental results validate the theoretical model and demonstrate good efficiency and high gain.

B5-3
1600

AN ASYMPTOTIC ANALYSIS
OF A
LEAKY PARALLEL-PLATE WAVEGUIDE

M.F. Pasik and D.G. Dudley
Electromagnetics Laboratory
ECE, Building 104
University of Arizona
Tucson, AZ 85721, USA

The method of steepest descents is applied to a parallel-plate waveguide where one of the plates is a bonded wire mesh modeled by a sheet impedance boundary condition. The structure is excited by a magnetic line source exterior to the waveguide. We present several interpretations of the Fourier integral representation of the magnetic field and evaluate the integral asymptotically by steepest descents. The case of a leaky-wave pole near the saddle point is examined in detail.

In this analysis, the parameters of the wire mesh are adjusted to exploit the contributions of the leaky-wave poles in the near far-zone radiation pattern. The use of the asymptotic expressions in this region is justified by comparisons with results obtained by numerical integration.

We study the transient response of the structure by FFT methods applied to the frequency domain results. An alternate representation of the magnetic field, computationally efficient in early time, is derived. Numerical results for a double-exponential pulse excitation of the line source are presented.

B5-4 SPECTRAL GAPS AT THE TRANSITION BETWEEN
1620 SURFACE WAVES AND LEAKY WAVES
ON DIELECTRIC LAYERS

A. A. Oliner   **D. R. Jackson**
Polytechnic University   University of Houston
Brooklyn, NY   Houston, TX

It is not generally known that the transition region between the surface-wave and the leaky-wave solutions for guided modes on dielectric layers contains some very interesting fine structure, and that in fact the solution is *nonphysical* over a certain frequency range. We are calling this nonphysical range a *spectral gap*. Evidence is mounting to indicate that some type of spectral gap is present at all such transitions, on any type of guiding structure. Dielectric layers are selected here for exposition because they constitute a simple and well-known class of guiding structures, and they serve well to illustrate the principal features of the spectral-gap region.

The first part of the talk will review the behavior of surface waves on dielectric layers, show how the surface waves change into leaky waves as the frequency is decreased, and summarize the properties of these leaky waves as a function of frequency. It will also be seen that, for a dielectric layer on a ground plane, the lowest mode (TM_0) always remains a surface wave, while the TE_1 mode becomes an improper (nonspectral) real solution that is nonphysical below the surface-wave cutoff frequency, and never becomes a leaky mode. All other higher-order surface waves turn into leaky modes at lower frequencies, after passing through a spectral-gap region. For single dielectric layers, the leaky waves decay very rapidly in the transmission direction, but, for pairs of layers arranged to satisfy the high-gain condition (to be reviewed), the decay rate can be very small, resulting in different physical behaviors, both in wavenumber and in radiation pattern. Most of this material is already known, but it constitutes essential background information.

The second half of the talk is concerned with the nature of the spectral gap that appears in the transition region between the surface-wave and the leaky-wave eigenvalue solutions. The width in frequency of the spectral gap is larger when the decay rate of the leaky wave is larger, so that for single layers the spectral gap is rather large whereas for pairs of layers satisfying the high-gain condition the spectral gap is quite narrow. The need for such spectral gaps will be explained physically, and the detailed wavenumber behavior within the gaps will be shown on both the longitudinal-wavenumber plots and the steepest-descent plane. Comments will also be made that address the nonphysical nature of the spectral gap, and how this dilemma is approached in the next paper in this session.

1640 Round Table

Session E/A 1355-Thurs. CR1-40
HPE GENERATION, MEASUREMENT AND SHIELDING
Chairmen: R.L. Gardner, Phillips Laboratory, Kirtland AFB, NM 87117-5776; and Sedki M. Riad,
Dept. of Electrical Engineering, Virginia Polytechnic Institute and State Univ., Blacksburg, VA 24061.
Organizers: Robert L. Gardner; E.F. Soderberg, Analysis and Technology, Inc.,
New London, CT 06320; and S.M. Riad

E/A-1   **RADIATION FROM SELF-RECIPROCAL APERTURES**

1400   Everett G. Farr   Carl E. Baum

Farr Research   Phillips Laboratory

614 Paseo Del Mar NE   3550 Aberdeen Ave. SE

Albuquerque, NM 87123   Kirtland AFB, NM 87117

We define here a new symmetry operator called reciprocation. Apertures that remain unchanged after reciprocation are called self-reciprocal, and have a number of unique properties. When excited by a step-function voltage, a self-reciprocal aperture becomes an antenna. This antenna is an approximation to a TEM horn, to a lens IRA (TEM feed + lens), or to a reflector IRA (TEM feed + reflector).

Because of the unique properties of self-reciprocal apertures, these antenna configurations have radiation characteristics that are of a particularly simple form. In particular, the radiated field on boresight is proportional to the electric field at the center of a self-reciporcal aperture. Thus, one can avoid the surface integral or contour integral that is normally required for predicting the aperture field on boresight.
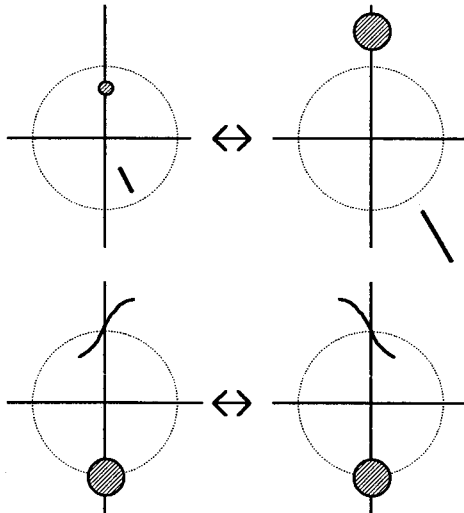
Figure 1. Some examples of apertures and their reciprocals.

120

APPLICATION OF HYBRID TRANSMISSION LINE TECHNIQUES TO SYSTEM ASSESSMENT

Robert L. Gardner
Phillips Laboratory
PL/WS
3550 Aberdeen SE
Kirtland AFB, NM 87117

One of the pressing problems of high power electromagnetics (HPE) research is the prediction of the penetration of electromagnetic fields deep into real systems. Interest in making these predictions has increased with the complexity of HPE threats. Candidate threats include lightning, other systems (EMC), high power microwaves, and the currently less interesting nuclear EMP. A number of techniques have been applied to the problem, including statistical methods, large numerical simulations, and topological decomposition. In this paper, we will discuss an application of the BLT equation to system assessment presented six years ago [Paxton and Gardner, Proceedings of EMC Zurich 1987, page 58J4] and its application to current problems.

A lumped-junction matrix method is derived for the reduction of a complicated network of branching cable bundles to an equivalent uniform section of multiconductor transmission line between two lumped junctions. The lumped junctions are represented by matrices that entirely characterize the conductors beyond the uniform section. This technique is applied systematically to a sample problem of current injection in a real communications satellite.

E/A-3
1440

COMPARISONS OF THE LOW LEVEL CW ELLIPTICUS AND HIGH LEVEL PULSE HPD CURRENTS ON THE EMPTAC AIRCRAFT

D. Lawry, W.D. Prather, R. Torres and T. Tran
Phillips Laboratory, WSR
S. Langdon, S. Gutierrez and W. Walton
Phillips Laboratory, WSM
Kirtland AFB, NM
S. Kokorowski, J. Martinez and D.P. McLemore
Kaman Sciences Corporation, Dikewood Division
Albuquerque, NM and Santa Monica, CA

The Phillips laboratory has recently designed and constructed a CW, low-level simulator (ELLIPTICUS) for use in determining coupling of electromagnetic energy to aerospace systems.(D. McLemore, J. Martinez, G. Sower, C. Baum, T. Tran, and W. Prather, "The Phillips Laboratory Broadband, High Frequency CW Simulator," National Radio Science Meeting, Boulder, CO, 1993). This antenna is designed to make the field patterns similar to those produced at the high level pulse simulator, HPD.

The HPD antenna with the HAG I pulser, at Kirtland AFB, was used to obtain the high level pulse responses on the EMPTAC aircraft. Although this simulator was capable of producing energy above the noise level up to well above 100 MHz; however, the high frequency fiber optic system dynamic range effectively limited the measurement bandwidth to 100 MHz.

Figure 1 shows the excellent frequency domain comparisons of the measured and CW predicted responses of test point 2142, a relatively well shielded bulk current measurement in the midsection of the aircraft.
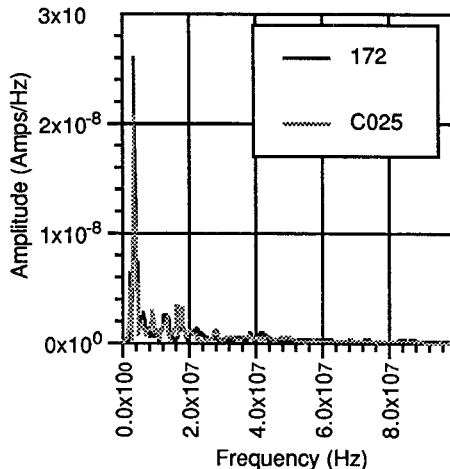
Figure 1. A Frequency Comparison of the Ellipticus Prediction (C025) and HPD (172) Responses for EMPTAC

E/A-4
1500

A SIMPLE HIGH FREQUENCY, NOISE GENERATED DIRECT DRIVE SIMULATOR

S. Gutierrez, S. Langdon, D. Lawry, W.D. Prather, R. Torres and
T.Tran, and W. Walton
Phillips Laboratory, WSR
Kirtland AFB, NM
G. Hoffer, S. Kokorowski, D.P. McLemore and V.D. Peckham
Kaman Sciences Corporation, Dikewood Division
Alameda, CA, Santa Monica, CA, Colorado Springs, CO and
Albuquerque, NM

Damped sinusoid, direct drive techniques on interconnecting cable bundles
between military subsystems have long been used to test the susceptibility of these
subsystems to electromagnetic transients. Questions arise, however, about the
adequacy of this method in assuring subsystem strength against broadband threats

In recent years, arbitrary waveform generators (AWG) have been used in
the area of EMP to duplicate simulator measured waveforms on cable bundles with
a high degree of fidelity. Unfortunately, with the advent of MIL-STD-2169A, the
operating speed of AWGs does not allow the extension of this approach to address
the new threats. A novel, alternative approach for generating these signals on cable
bundles is to use white noise sources. Because noise generators are inexpensive
and broadband, high frequency capabilities for the induced transients can be
achieved with little technology development.

A diagram for a system to create fast transient, broadband test signals is shown in
Figure 1. Most of the equipment shown in Figure 1 is "off-the-shelf" and offered by
multiple venders. The filters can be assembled for specific groups of waveforms.
Phillips Laboratory has developed couplers in the past which are capable of
coupling signals up to 1 GHz on subsystem interface cable bundles.
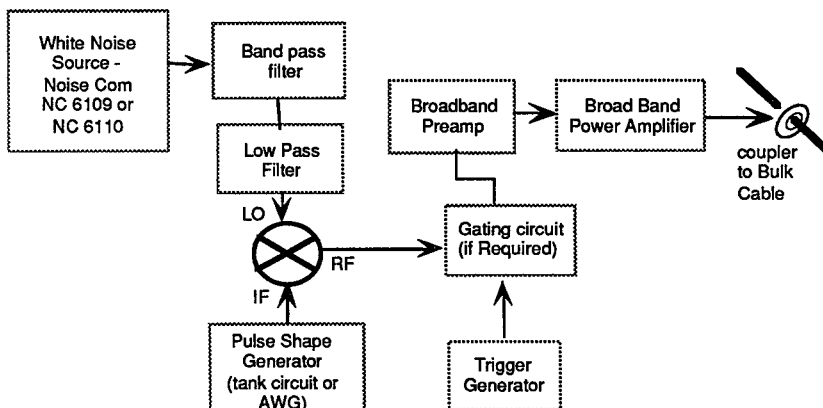
Figure 1. A Noise Generator Based Direct Drive System

A STUDY OF LASER INDUCED
DIPOLE LAYERS AND FIELDS

William E. Page
Phillips Laboratory
Kirtland AFB, Albuquerque NM.

LASER light incident on a metal surface can eject
electrons by photoelectric emission or other
processes. The boundary layer formed by the
ejected electrons approximates a dipole layer. The
variations of the dipole moment for various
emission parameters and modulations of the
incident light have been modelled and studied
computationally. The resulting near and far field
terms of the dipole moment and their variations
with modulation frequency and format have been
computed parametrically. These results are
presented and their scaling laws are discussed.
The radiated field pattern for an extended
modulated dipole patch is also computed and
discussed.

E/A-6
1600

METAL CONDUIT REDUCES 60Hz MAGNETIC FIELDS

Dr. D.N. March, Professor, Montana State University
Mr. Mark Major, Graduate Student, Montana State University

High current carrying wires that take 60Hz current to and from a load can be closely spaced but the currents in the wires generate a magnetic field that can be measured. The current carrying wires were placed in a rigid steel conduit; the magnetic fields were reduced by at least 90%. The fields were reduced by at least 75% when the wires were put in EMT conduit, which is lighter steel conduit. By placing the wires in two concentric conduits, the fields were reduced by more than 98%. The magnetic field reduction using other types of conduit was investigated. Single phase and three phase wires were considered. The induced currents in the conduit cancel each other without I^2R heating. The conduit did not reduce the field from the net current component, i.e. when the summation of currents was not zero in the wires. Further, the conduit heats due to induced currents from the net current. The field reduction was shown to be inversely related to the reluctance of the conduit (in a circular sense). Examples are given where steel conduit should be used to reduce magnetic fields.

E/A-7
1620

**APERTURE EXCITATION OF ELECTRICALLY LARGE,
LOSSY CAVITIES**

David A. Hill and Mark T. Ma
Electromagnetic Fields Division
National Institute of Standards and Technology
Boulder, CO 80303

In many electromagnetic interference (EMI) problems, the important electronic systems are located within a metal enclosure with apertures. In such cases it is important to know the shielding effectiveness (SE) of the enclosure so that we can relate the interior fields to the external incident fields. For example, the high intensity radiated fields (HIRFs) that commercial aircraft can encounter are calculated to be in the 1000 to 7000 V/m range for frequencies above 400 MHz, the frequencies used by most radars.

The purpose of this talk is to describe a mathematical model for the shielding effectiveness of electrically large enclosures that contain apertures and interior loading. The method that we present uses a power balance approach and yields a simple, approximate expression for the average field strength throughout the cavity enclosed. This method does not yield the fine detail of the interior fields as would be obtained by a numerical method, but it has the advantages of being applicable to both cw and pulsed fields and not requiring all the geometrical details of the enclosure, the apertures, and the loads. The theory is similar to that developed for reverberation chambers, where the average power density is assumed to be uniform throughout the chamber.

The calculated quantities include SE, cavity Q, and cavity time constant. The losses included in the Q calculation include wall loss, aperture leakage, absorption by internal lossy objects, and power extracted by any receiving antennas. The cavity time constant for pulsed rf excitation (like a radar pulse) depends only on the cavity Q and the carrier frequency. The SE calculation uses aperture theory and power conservation to determine the ratio of the internal and incident power densities. The aperture(s) can be either electrically small or large.

We have constructed a rectangular metal box with a circular aperture and loaded it with salt water spheres. Mode stirring with a metal paddle wheel was used to obtained uniform fields. Measurements of SE, Q, and time constant have been performed for frequencies from 1 to 18 GHz, and good agreement has been obtained with theory. Particular effort was required to account for all the losses in order to obtain accurate Q values.

E/A-8
1640

Time–Domain Measurements of the Reverberation Characteristics and Shielding Effectiveness of a Small Aircraft

Robert T. Johnk
Arthur R. Ondrejka

National Institute of Standards and Technology
Boulder, Colorado

The effects of electromagnetic interference (EMI) on aircraft is becoming increasingly important, particularly as aircraft systems are employing more and more electronics and computers. Two issues that must be addressed are the effects on aircraft electronics of internally and externally generated EMI. These must be well understood in order to assess the possible effects that EMI could have on aircraft safety.

At the request of and under the sponsorship of the Federal Aviation Administration (FAA), the National Institute of Standards and Technology (NIST) performed a series of time-domain electromagnetic measurements on a civilian aircraft at the Naval Surface Warfare Center (NSWC) in Dahlgren Virginia. Both external penetration as well as internal electromagnetic measurements were performed using a time-domain system consisting of a fast risetime (broadband) pulse generator, two TEM horns, a digitizing sampling oscilloscope, and a computer for signal processing. The external penetration measurements yielded the shielding effectiveness characteristics of the aircraft, while the internal measurements yield characteristics that are quite similar to an electrically large reverberation chamber.

Using the time domain in conjunction with broadband pulses permits the rapid and efficient evaluation of aircraft shielding effectiveness as well as the internal cavity Q. In fact, the cavity Q can be computed without having to know the interior volume of the aircraft. Data are presented that are averaged over stirrer position along with frequency-averaged results that do not require a mechanical stirrer. The time-domain represents a method from which data can be rapidly and accurately obtained.

F3-1 MEASUREMENT OF CLOUD DROPLET SIZE SPECTRA BY
1400 DOPPLER RADAR

Earl E. Gossard
Cooperative Institute for Research in Environmental Sciences
(CIRES)
University of Colorado/NOAA
Boulder, CO 80309

A new technique is examined for using Doppler radars to extract information about the size spectrum of cloud droplets too small to have fall velocities large enough to be resolvable by the radar. If the drops are very small, motions of the drops are dominated by turbulent fluctuations in the medium rather than their fall velocity. Their motion is then the convolution of the fall velocity with the turbulent velocity probability density function (PDF), and size information about the population can be obtained only by deconvolving the spectra. Doppler radars can extract this velocity and size information, as well as cloud liquid and liquid flux, using a surprisingly simple and accurate technique assuming some functional form (e.g., gamma) for the drop number density spectrum. The method also allows Doppler radars to extract dropsize information independent of up/downdrafts in the medium in which they are embedded. Various gamma and log-normal functions are compared, and the influence of a "Stokes range" of dropsizes is included and found to be important, especially when the median dropsize lies within the Stokes range. Examples are shown and errors are discussed.

F3-2   SUMMARY OF THE MARINE AEROSOL PROPERTIES AND
1420   THERMAL IMAGER PERFORMANCE TRIAL (MAPTIP)
         Organized by NATO AC/243 Panel 4/RSG.8 on
         Atmospheric Propagation Effects on Electro-
         Optical Systems (Oct 11 - Nov 5, 1993)

D. R. Jensen
Tropospheric Branch, Code 543
Naval Command, Control and Ocean Surveillance Center, RDT&E Division
San Diego, CA 92152-7385

G. de Leeuw & A. M. J. van Eijk
TNO Physics and Electronics Laboratory
Oude Waalsdorperweg 63
2509 JG The Hague
The Netherlands

During the fall of 1993 a field experiment was conducted by NATO AC/243 Panel 04/RSG.8 and 04/RSG.5, in the Dutch coastal waters entitled Marine Aerosol Properties and Thermal Imager Performance Trial (MAPTIP). The objectives of the trial are: 1) To improve and validate vertical marine aerosol models by providing an extensive set of aerosol and meteorological measurements, within a coastal environment, at different altitudes and for a range of meteorological conditions, 2) To make aerosol and meteorological observations in the first 10 m of the ocean surface with a view to extending existing aerosol models to incorporate near-surface effects, and 3) To assess marine boundary layer effects on thermal imaging systems. Calibrated targets at different altitudes will be observed to the maximum observable range under a wide variety of conditions in both the 3-5 and 8-12 μm bands. These data will be used for the development and validation of IRST models and IR ship signature models with the view of determining the effects of marine-generated aerosols, turbulence and meteorological profiles on their performance.

Aerosol and meteorological instruments, as well as thermal imagers and calibrated targets, will be utilized on the Dutch Meetpost Noordwijk (MPN) tower, at a Katwijk Beach Station, the Hr. Ms. Tydeman oceanographic vessel, on a Lynx helicopter, on a Dutch P3 Orion, on the NCCOSC RDT&E Div airborne platform, and on buoy systems. This network of instrumentation will be used for obtaining a comprehensive data base of aerosol size distribution profiles and relevant meteorological variables throughout the marine atmospheric boundary layer. Thermal imagery will also be included to provide ground truth for assessing the low-level propagation effects near the ocean surface. Measurements will be made of atmospheric turbulence and refractivity effects in the IR and RF bands, to assess the marine boundary layer effects on the degradation of thermal images.

A summary of the MAPTIP trial will be presented and initial results discussed.

F3-3   THE NASA/JPL TOPOGRAPHIC SAR (TOPSAR) PROGRAM
1440   Thomas W. Thompson
          Jet Propulsion Laboratory
          California Institute of Technology
          Pasadena, California

During the last few years, JPL has developed a C-band (5.67 wavelength) aircraft radar system that acquires interferometric maps of the earth. This is an adjunct to the NASA/JPL AIRcraft Synthetic Aperture Radar (AIRSAR) system that acquires multi-polarization SAR images at P-band (70cm wavelength), at L-band (25cm wavelength) and at C-band. The TOPSAR/AIRSAR system routinely flies on the DC-8 Airborne Laboratory operated by the NASA Ames Research Center. This TOPSAR/AIRSAR system is implemented such that the C-band interferometry can be acquired simultaneously with the P-band and L-band polarimetry data.

The TOPSAR system is implemented via two antennas mounted vertically with a 2.6 meter spacing on the left side of the aircraft. Interferometric maps of the surface are constructed by comparing the phase differences between SAR images from the two antennas. Statistical elevation errors for the TOPSAR system range from 2.0 meters for flat land to 5.5 meters for mountainous areas. Typical data acquisitions are for areas of 10 km across-track (i.e. in range) and 40 to 50 km along track (i.e. in azimuth). However a recent observations of Isla Fernadina in the summer of 1993 demonstrated that these 10 km * 50 KM topographic maps could be mosaicked together for an area of about 40km * 40km.

During the summer of 1993, we experimented with "repeat pass" interferometry in an attempt to acquire phase-coherent SAR images from two separate, but nearly identical, aircraft flight paths. Also, these aircraft observations are a precursor for a possible earth-orbiting TOPgraphic SATellite (TOPSAT).

F3-4
1500

SENSITIVITIES OF DENSE BULK RANDOM AND REGULAR STRUCTURE MODELS TO ITS GEOPHYSICAL PARAMETERS

Dr.Eugenia A.Skirta, Laboratory S2HF, IRESTE, University of Nantes, La Chantrerie, CP 3003, 44087 Nantes, Cedex 03, FRANCE

The electrodynamic method to investigate dielectric properties of bulk anisotropic structures leads to a deeper insight into the relationship between the geometric and dielectric characteristics of media and the elements of its scattering matrices. A physical basis to study volume scattering from a dense dielectric medium is provided by the calculation of multiple electromagnetic interactions between scatterers in a spatial structure and/or between particles into a complex scattering center. Proceeding from the known spatial packing, geometrical shape and dimensions of dielectric inhomogeneities, the averaged dielectric permittivity tensors for the structures, which can serve as models of some earth covers, are calculated.

We investigated the sensitivities of the regular and random medium physical models to its dielectric and geometrical parameters to specify the scattering properties of these structures. It is shown that the shape of scatterers is the most essential at valuable densities ($v > 0.3$) when their size tends to the size of the "elementary volume" of averaging. The structural effects manifest themselves in dispersion properties of bulk anisotropic media in a rather peculiar way. For example, a regular dielectric with a nonuniform spatial distribution of scatterers, having a large permittivity with losses, possesses a negative dispersion property in the resonance region due to the complex structure of a medium.

The application of this method is shown on the example of calculations of the averaged dielectric permittivities of sea ice. We analysed two types of sea ice at X-band frequencies: underformed first-year ice as a random three-phase model and multi-year ice as an anisotropic quasiregular structure. Special attention is consentrated on the investigation of several types of volume packing of dielectric inhomogeneities for the finite-width multi-year ice layer. The dependence on a shape of inclusions (air bubbles and saline water pockets) is analysed. Saline water pockets are considered having the shape of cylinders or spheres with geometrical dimensions being the fluctuating quantities. Backscattered intensities are sensitive to dielectric losses and to the shape and volume fraction of dielectric scatterers, especially, for multi-year sea ice model.

F3-5
1540

COMPARISON OF WIDEBAND PROPAGATION IN THE 902-928 AND 1850-1990 MHZ BANDS IN VARIOUS MACROCELLULAR ENVIRONMENTS

Jeffery A. Wepman, ITS.S3
U.S. Department of Commerce
Institute for Telecommunication Sciences
325 Broadway
Boulder, CO 80303

Michael E. Hughes
Bell Atlantic Mobile, Inc.
180 Washington Valley Rd.
Bedminster, NJ 07921

This paper discusses a PCS propagation experiment to conduct impulse response measurements in the 902-928 and 1850-1990 MHz bands simultaneously. The measurements were taken in four different macrocells (with radii ranging from 3 to 11 km) in the Philadelphia, PA area. The cells were chosen to represent typical semi-rural, suburban, urban, and urban high-rise environments. Measurements were taken in all four cells using vertically polarized transmit and receive antennas. In the suburban and urban high-rise cells, measurements were also taken using circularly polarized transmit antennas (the receive antennas were vertically polarized).

The impulse response measurement system consisted of a transmitter placed at existing cellular base station sites and a receiver located in a measurement van. Impulse response data were recorded as the measurement van travelled along predetermined routes within each cell. The routes were chosen to provide a representative characterization of the propagation behavior in each cell.

The impulse response data were analyzed to provide RMS delay spread, correlation bandwidth, and various other multipath power statistics. The results of this data analysis provided a comparison of wideband propagation between the two frequency bands, the two transmit antenna polarizations, and between the different cell types. Major differences in the propagation behavior between the two frequency bands were not seen. The urban high-rise cell exhibited the most multipath, showing higher power and more delayed signals with longer delays than in the other cells. Propagation behavior in the suburban and urban cells was very similar. The semi-rural cell, however, displayed more multipath than the suburban and urban cells, probably due to hilly terrain (in the semi-rural cell). An improvement in propagation (less multipath) was seen when using the circularly polarized transmit antennas instead of the vertically polarized ones for 1920 MHz. This trend was not apparent for 915 MHz. These results suggest that the detrimental effects of multipath propagation may be reduced by using circular polarization in place of vertical polarization in the transmit antennas of a PCS system operating in various macrocellular environments. Additionally, the results suggest that these benefits obtained by changing the transmit antenna polarization may be more significant for 1920 MHz than for 915 MHz. Further polarization studies are recommended to investigate these possible benefits.

F3-6
1600

MEASUREMENT AND THEORETICAL MODELING OF PROPAGATION LOSS, RADAR SEA BACKSCATTER(CLUTTER) AND FORWARD SCATTER(MULTIPATH) FROM 40 mHz TO 300 mHz AT GRAZING ANGLES LESS THAN 1°

R. H. Ott[1]*, M. A. Pollock[2], R. J. Dinger[2], and T. E. Tice[2]

(1) GRC/SWL
1601 Randolph Rd. S. E.
Suite 200 (south)
Albuquerque, NM 87106

(2) NRaD
San Diego, CA 92152

Measurements of low-grazing -angle radar sea backscatter and multipath in the frequency range form 40 mHz to 400 mHz, along with the supporting theoretical modeling, have been relatively lacking because of the practical difficulties (primarily related to antenna size and frequency allocation) associated with fielding radars in this band. An ultra-wideband radar that radiates waveforms encompassing this band has recently been installed at a seaside location near San Diego,CA.

The theoretical model is based upon an integral equation solution for the surface fields. The surface fields are then integrated to obtain either the forward scatter(multipath) of backscatter(clutter) . The surface fields are obtained using a new mathematical derivation for the integral equation for the surface fields(R. H. Ott, <u>Radio Science</u>,27,867-882,1992). This new integral equation extends the frequency range of the former algorithm,WAGNER, to the VHF band. The new computer algorithm is named RING(<u>R</u>adio <u>IN</u>tegral over <u>G</u>round).
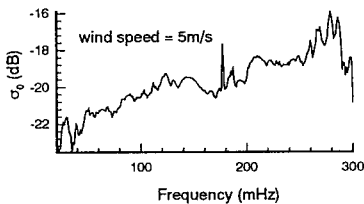
F3-7
1620

A SPINNING FLAT REFLECTOR FOR MILLIMETER-
WAVE RADIOMETRY

Mark D. Jacobson
NOAA/ERL/WPL, R/E/WP5
325 Broadway
Boulder, CO   80303

Millimeter-wave radiometers are often required to operate under all weather conditions, including those under which an exposed surface of the antenna system becomes wetted by rain or wet snow. A dry reflector surface is required during precipating conditions to avoid contamination of the atmospheric data (M. D. Jacobson, "Wet Reflectors in Millimeter-Wave Radiometry-Experiment and Theory," IEEE Trans. Geosci. Remote Sensing, vol. GE-24, 784-791, 1986 and B. B. Stankov, "Remote Measurements of Supercooled Integrated Liquid Water during WISP/FAA Aircraft Icing Program," Jour. Aircraft, vol. 29, 604-611, 1992). One way to accomplish this is to spin the exposed reflector so that particles falling on the rapidly rotating disk will be thrown off, thereby reducing the liquid water layer buildup on the exposed flat.

Here we discuss the case of a spinning wetted-flat reflector, with energy at 20.60 and 31.65 GHz linearly and othogonally polarized at an incidence angle of 45°. This spinning reflector is an integral part of the National Oceanic and Atmospheric Administration's (NOAA) Platteville radiometer. The brightness temperatures produced by the spinning wet reflector and overhead water spray combination are measured for various water spray rates and reflector speeds. The water on the spinning reflector is dispersed in about 5 to 10 seconds for speeds between 250 and 1000 RPM. Furthermore, for a constant water spray rate, the liquid layer formed on a spinning reflector is thinner than that formed on a stationary reflector. We selected the reflector's speed by these results. The present reflector speed is 300 RPM. A follow-up experiment will determine if this is the optimal speed.

F3-8
1640
PERFORMANCE PREDICTION OF DIRECT SEQUENCE
MODEMS IN THE INDOOR CHANNEL

R.J. Achatz
Institute for Telecommunication Sciences
325 Broadway
Boulder, Co.   80303

The indoor radio channel is degraded by multipath because of reflection, refraction, and diffraction of the transmitted power by the building's walls, floor, ceiling, and furnishings.   Multipath causes intersymbol interference (ISI) in digital modems. Direct sequence (DS) modulation suppresses ISI with its code correlation properties and has been proposed as a modulation method for this channel. This report investigates the ability of DS modulation to suppress ISI introduced by the multipath channel. To predict performance, software was written to simulate a DS modem operating in the indoor channel. Measured impulse responses were used to characterize the indoor multipath.

The simulated DS modem is binary phase shift keyed (BPSK) modulated, has a center frequency of 1.5 GHz, and uses a 7 chip maximal length spreading code. Simulations were performed for data rates ranging from .9 to 14 Mbps. Perfect carrier synchronization was assumed, however, symbol sample timing was computed.

Indoor channel impulse response measurements of an office building at 1.5 GHz were used in the simulation (Papazian, "Wideband Propagation Measurements for Wireless Indoor Communication", NTIA Report 93-292, January 1993). The measurements were obtained using a 200 MHz null to null bandwidth slipped correlator channel probe. The measurements sample the impulse response every fifth of a wavelength over eight evenly distributed paths in a large (25x25 meters) office area.

Three prediction methods are used in accessing the performance. The performance prediction methods provide 1) probability of an outage (P_o) over a large area, 2) P_o over a small area, and 3) average probability of error (P_e). The P_o is the cumulative distribution of the per cent of locations that exceed a P_e for each signal to noise ratio and data rate. Average P_e is computed from the entire ensemble of impulse responses for each signal to noise ratio and data rate.

G3-1   **OCEAN MONITORING WITH HF**
1340   **OVER-THE-HORIZON DEFENSE RADARS**
         T. M. Georges
         NOAA Environmental Technology Laboratory
         Boulder, CO 80303-3228
         J. A. Harlan
         CIRES/University of Colorado/NOAA
         Boulder, CO 80309-0216

For more than 20 years, NOAA has been evaluating the potential of hf over-the-horizon (OTH) or skywave radar for monitoring weather conditions over very large data-sparse ocean areas. Although the physical concepts have been demonstrated using experimental radars, the main obstacle to deploying affordable operational OTH sea-state radars has been the cost of overcoming the spectral distortion caused by ionospheric motions and multipath. It has turned out that multiple strategies are required: large-aperture phased antenna arrays more than a kilometer long; transmitting powers of hundreds of kilowatts; systems to monitor the ionosphere and hf spectrum usage in real time; development of FMCW modulation; and sophisticated signal-processing schemes to remove and avoid ionospheric distortion of the sea-echo spectrum.

During the 1980s, the Defense Department developed large OTH radar systems for air defense that employ all these strategies. With the end of the Cold War and the disappearance of the threat these radars were designed to warn against, the future of these huge facilities is being reevaluated and alternative missions considered that focus on environmental monitoring. Recent tests with the U. S. Navy ROTHR and the Air Force OTH-B east- and west-coast radar systems have shown that it is possible to map surface wind direction over areas as large as 20-million square kilometers, revealing synoptic weather patterns. The east-coast OTH-B radar in Maine has also focused on smaller areas to track hurricanes Claudette and Andrew more than 2000 km away. Minor modifications would permit wind-speed and parameters of the ocean-wave spectrum to be measured. It is now clear that these radars could be modified for routine ocean monitoring for less than 1% of the cost the taxpayers have already paid for them.

G3-2   **EFFECT OF THE IONOSPHERE ON SATELLITE**
1400   **COMMUNICATIONS SYSTEMS**
          Allen L. Johnson
          Wright Laboratory
          WL/AAAI Bldg 635
          2185 Avionics Circle
          Wright-Patterson AFB OH 45433-7301

ABSTRACT:
        The use of Satellite Communications (SATCOM) by the Department Of Defence (DOD) has moved for a test curiosity to a standard (and often preferred) mode of communications. Users particularly appreciate the distance independent aspect of SATCOM over other media such as High Frequency (HF), troposcatter, or microwave relay. The applications of SATCOM have moved from simple 75 bit-per-second teletype record copy to computer-to-computer links and slow scan video. The DOD has made a commitment to support a three segment SATCOM architecture with Ultra High Frequency (UHF) for the mobile tactical applications, Super High Frequency (SHF) for the fixed, high data rate users, and Extremely High Frequency (EHF) for the protected traffic users.

        The primary effects that natural ionosphere has on SATCOM propagation is to scatter and delay the signal to and from the satellite. An ionosphere disturbed by a nuclear detonation will exhibit attenuation in addition to severe scattering and delays. The ionospheric delays affect precision measurements, such as the Global Positioning System (GPS), but have only a minor effect on communications. However, the scattering causes severe scintillation fading that can disrupt critical communications systems.

        This paper discusses the characteristics of ionospheric scintillation fading, such as frequency, time, and location dependence, suggests mitigation techniques, and explores the effects on representative SATCOM systems.

G3-3   USE OF GPS IN SATELLITE TRACKING: REAL-TIME
1420   ESTIMATION OF IONOSPHERIC REFRACTION
Dr. A. J. Coster
M . I . T . Lincoln Laboratory
Millstone Hill Radar
244 Wood Street
Lexington, MA 02173-9108

The ionosphere can produce significant effects on RF propagation for ground-based space surveillance.   In particular, the ionospheric total electron content (TEC) along a ray path introduces an error in the measurement of radar range, Δr, which is dependent on the radar frequency, f,

$$\Delta r \; = \; \frac{40.3}{f^2} \; \int_0^R N_e \, dr$$

where N_e is the local electron density and R the radar range. This range error is significant in satellite tracking and can be mitigated to a large extent by improved modeling and real-time measurement of the ionosphere. The total electron content can vary significantly with time of day, geomagnetic activity, and look direction. A real-time synoptic ionospheric monitoring system has been developed at Millstone using data acquired from a TI4100 GPS receiver. The TI4100 GPS receiver can track up to four GPS satellites at any one time. Each GPS satellite transmits signals at two different L-band frequencies, L1 (1575.42 MHz) and L2 (1227.6 MHz). The total electron content (or TEC) along the path to each satellite can be determined by combining the two frequency pseudo-range and phase data. If it were not for the problem of multipath, the TEC could be determined directly from the GPS pseudo-range data. The integrated phase data, which only provides a relative measurement of the range, is not as susceptible to multipath and is therefore used to smooth the pseudo-range data. At Millstone, the TEC is measured every three seconds for each GPS satellite in view. Using a Kalman filter, coefficients are then fit to a model with azimuth and elevation dependence. This model allows us to account for the variation in look angle of the TEC. The coefficients for this model are sent to the Millstone satellite tracking computer, and the model is applied in real-time to account for the path delay due to the ionosphere. The results of using this ionospheric monitoring system at Millstone will be discussed, and our results will be compared with ionospheric measurements obtained from other techniques: Faraday rotation using data from the Hamilton polarimeter and incoherent scatter data from the Millstone UHF radar.

G3-4
1440

EFFECTS OF SCINTILLATION ON UHF RADAR PERFORMANCE

Dennis L. Knepp
Mission Research Corporation
2300 Garden Road, Suite 2
Monterey, CA 93940-5326

UHF ground-based radars that must detect, acquire and track targets whose lines-of-sight intersect the equatorial or polar-region ionosphere are likely to suffer performance degradation due to signal scintillation. Signal scintillation or fading is caused by propagation through random structure or inhomogenities in the ionosphere, and is observed as rapid fluctuations in the received amplitude and phase.

Although mild scintillation can degrade radar performance, strong scintillation is likely to have a severe impact on radar systems that are designed with insufficient margin. This talk utilizes ALTAIR VHF and UHF measurements of equatorial scintillation as a focus to summarize the effects of ionospheric scintillation on radar detection and tracking performance. Detection performance is given for both M-out-of-N combining and noncoherent combining. Results for tracking performance are calculated from a high-fidelity Kalman filter simulation that includes the effects of scintillation through the use of statistical signal realizations generated to possess Nakagami-m statistics.

Future UHF radars may have to perform coherent processing of the returns from a number of pulses in order to satisfy requirements for detection of small targets at long range. If the duration of the burst of coherent pulses exceeds the ionospheric signal decorrelation time, then the output of the radar coherent integrator is reduced, resulting in degradation in detection preformance.

This talk summarizes all the above issues and suggests operational strategies that might help to reduce the degrading effects of the ionosphere.

G3-5   A COMPARISON BETWEEN A DYNAMIC MODEL AND
1500   UHF RADAR OBSERVATIONS OF THE AURORAL
         CLUTTER ENVIRONMENT

D. B. Odom and F. E. Daum
The Raytheon Company, Equipment Division
Wayland, MA 01775
K. M. Groves and J. A. Klobuchar
Ionospheric Effects Division
Phillips Laboratory
Hanscom AFB, MA 01731

For either ground-based or satellite radar systems the effect of the auroral clutter environment is governed by a systems sensitivity to the apparent size, granularity and motion of this dynamic phenomenon at the frequencies chosen for the observation. In order to characterize the radar system sensitivity to the scattering characteristics of this clutter background, a set of observations was made in the UHF band using a narrow pencil beam generated by a large phased array to map the fine structure of the aurora which was observed looking north from the CONUS during the peak of the most recent solar cycle. These measurements are compared with a dynamic model of the auroral clutter environment which was developed to describe the effects of the auroral scattering on radar systems in space. This model predicts the diurnal motion of the major scattering centers in the auroral zone and the regions of space where a radar system of a given configuration will see the greatest concentration of scatterers.

For the current set of measurements, which were taken from a ground based CONUS radar site, the phenomenon is observed in the evening at long ranges in the northeastern quadrant. As time progresses, the moving clutter returns appear over a wider range window, positioning themselves nearer to geomagnetic north later during the night. A comparison between the radar measurements at UHF and the dynamic model for the auroral scattering is provided, with a description of the details of the ionospheric disturbance structure which is obtained from these measurements.

G3-6   **INCOHERENT SCATTER RADAR AND RADIO RESEARCH**
1540   **FACILITIES OF THE FORMER SOVIET UNION**

Dr. John C. Foster
Atmospheric Sciences Group
M.I.T. Haystack Observatory
Westford, MA 01886

Ionospheric radio research facilities of the Former Soviet Union have become increasingly accessible to Western scientists during the past year. Site visits have provided details of existing scientific research facilities in Russia and Ukraine and, in addition, a number of former military facilities are being reprogrammed for scientific research. Brief descriptions of several facilities will be presented as well as an overview of current and proposed ionospheric research activities.

The Institute of the Ionosphere in Kharkov, Ukraine has operated VHF incoherent scatter radars (ISR) over a period of 25 years. The principal ISR system operates at 2 MW and 150 MHz using a 100-meter, fixed, zenith directed, parabolic antenna. A two-pulse technique is used to determine ion-line electron and ion temperatures and vertical Doppler velocity at altitudes between 150 km and 1000 km. Concurrent electron plasma-line observations are often made with a separate 2 MW, 150 MHz system which uses a 25-meter diameter, fully steerable antenna. This second system is used primarily for diagnostics during experiments involving the co-located ionospheric HF heating facility, which operates in the frequency range 5-12 MHz with 150 kW mean output power and a 300-m x 300-m antenna array. Also located near Kharkov is the UTR-2 radio telescope, a 2-km x 1-km "T-shaped" array of over 2000 wide-band dipole elements operating in the decameter band at frequencies between 10 MHz and 25 MHz. The UTR-2 is proposed as the principal bi-static receiver for the magnetospheric radar initiative, which involves a new transmit antenna array at the Russian Sura heating facility.

World Day ISR observations are being made near Irkutsk, Russia by the Institute of Solar-Terrestrial Physics using a 2.4 MW, 155 MHz radar with a 3000 sq-m sectorial horn antenna, phase steerable over 30° about the zenith in the N-S meridian. The massive 70-meter diameter deep-space command antenna at Yevpatoria, Crimea, Ukraine has also been made available for scientific research.

G3-7   FREQUENCY-AND-ANGULAR IONOSPHERIC SOUNDING
1600   USING THE UTR-2 RADIO TELESCOPE

V. S. Beley, V. G. Galushko, and Yu. M. Yampolski
Institute of Radio Astronomy
Ukrainian Academy of Sciences
Kharkov, Ukraine

The paper is an analysis of the potential of some new methods for reconstructing plasma parameters of the terrestrial ionosphere. All the methods to be considered are based on precise frequency and angular measurements of HF signals reflected by the ionosphere. The problem of restoring the regular electron density profile, maybe within some model, by means of measuring the signal trajectory parameters near the skip distance is enunciated and solved. Reconstruction of travelling ionospheric disturbances (TIDs) based on long term precise measurements of HF signal elevation angles, azimuths and Doppler shifts is described. Algorithms for TID visualization have been developed in the models of a perfectly reflecting surface and density waves propagating through the ionospheric layer. Finally, the problem of frequency-and-angular sounding of the ionosphere is considered within the integral approach for a plane-stratified model of the ionized layer. All the original methods have been tested in numerous experiments performed by the authors with the use of the large HF phased array of the UTR-2 radio telescope. The ionospheric measuring complex, as well as the UTR-2 radio telescope are also described in detail in the paper.

G3-8
1620

THE FREQUENCY-AGILE RADAR: A MULTI-FUNCTIONAL APPROACH
TO REMOTE SENSING OF THE IONOSPHERE
R.T. Tsunoda, J.J. Buonocore, R.C. Livingston, and A.V. McKinley
Geoscience and Engineering Center
SRI International
Menlo Park, CA 94025

We will describe a new kind of diagnostic sensor for ionospheric research that features multifunctional capabilities through frequency agility, system modularity, comprehensive resource management, and a user-friendly control interface. This sensor, which we call the frequency-agile radar (FAR) was designed specifically for the researcher and has the following characteristics. It is frequency agile from 1.5 to 50 MHz. Its hardware is controlled by an AT-bus personal computer (including an array processor) using instructions written in C which are communicated through an IEEE-488 standard interface bus. Because of its modular nature, the FAR can be reconfigured easily for various applications of interest through the proper selection of radar parameters, power amplifiers and an appropriate antenna system. It is easily transportable for participation in field experiments anywhere in the world. Its unique value comes from the synergism that often can result from the availability of multiple capabilities. We will present examples of various kinds of measurements that have been made with the FAR while operating as: an ionosonde; an HF multifrequency radar for barium ion cloud tracking and backscatter from the equatorial E and F region irregularities, a VHF radar for investigations of backscatter from midlatitude sporadic E, and, most recently, as an MF partial-reflection radar and VHF meteor-scatter radar for D-region wind measurements.

G3-9   THE SAPPHIRE COHERENT RADAR SYSTEM
1640   J.A. Koehler and G.J. Sofko
            Institute of Space and Atmospheric Studies
            University of Saskatchewan
            Saskatoon, Sask., Canada
            S7N 0W0

In the autumn of 1993, the SAPPHIRE (Saskatchewan Auroral Polarimetric PHased Ionospheric Radar Experiment) radar went into operation. This bistatic coherent radar operates at a wavelength close to 6 meters and observes meter scale turbulence in the auroral E-region over a region in northern Saskatchewan. This radar uses DDS techniques and a very sophisticated data analysis and collection system to produce very high temporal and frequency resolution spectra in real time.

Because this radar observes E-region turbulence in a region which is in the field of view of the SuperDARN radar system, the combined data from these two systems will produce synoptic information about the E-region irregularities simultaneously with knowledge of the E-fields which produce them.

The design of the SAPPHIRE system will be discussed and some of the first observations will be shown.

H4-1   THE FIRST MISSION OF THE TETHERED SATELLITE
1400   FROM THE ON BOARD CREW PERSPECTIVE.
Dr. Franco E. Malerba, Payload Specialist STS-46
Agenzia Spaziale Italiana
NASA Johnson Space Center CB
NASA Road One
Houston, Texas 77058

The Italian "Tethered Satellite" has been operated for the first test flight
during the the STS-46 mission of the Space Shuttle Atlantis, July 31-Aug 8,
1992. The first mission of the Tethered Satellite (TSS-1) was a novel
experiment, which concentrated in the planned four-day mission a large
number of engineering and operational challenges for the ground controllers,
for the scientists, and for the astronauts:

* the engineering verification of a new system and the first utilisation of a
  scientific instruments ensemble installed both in the Tethered Satellite and
  in the Shuttle's payload bay
* the developement of new rendez-vous and formation flight techniques
  for a flexible orbiting system - the tether -of unprecedented length and
  unpredictable behaviour when slack
* the host of concurrent scientific and technological research themes
  spanning the dynamics of the tether, the electrical energy generation
  experiment and the in orbit generation of elecromagnetic waves for local
  detection by ground stations
* the coordination and synchronisation of the scientific experiment
  sequences to match the changing enviromental conditions, the spaceship's
  activities, orbital position and attitude

This communication outlines the on board operational environment for the
TSS-1 active electrodynamic experiment, some of the techniques developed
before the flight and the lessons learned during the mission in the areas of
satellite visibility, attitude determination and control, flight techniques and
slack tether management, active science instruments operation and related
training.

EXCITATION OF WHISTLERS FROM ELECTRODYNAMIC TETHERS AND LARGE MAGNETIC LOOP ANTENNAS

R.L. Stenzel, J.M. Urrutia and C.L. Rousculp
Department of Physics
University of California, Los Angeles, CA 90024-1547

There is considerable interest in the excitation of ULF to VLF waves in the ionosphere. Attempts to fly large loop antennas (Russian ACTIVE mission) and long electrodynamic tethers (US-Italian TSS1 mission) have not been successful yet. In order to test theoretical and numerical predictions laboratory experiments have been performed at UCLA (R. Stenzel et al., IEEE Trans.Plasma Sci.**20**, 787,1992; Phys. Fluids B **5**, 325, 1993). This work has been concentrated on detailed diagnostics and physical concepts.

In a large , uniform afterglow plasma ($1m\perp B_0$, $2m \parallel B_0$, $n_e \leq 10^{12} cm^{-3}$, $kT_e \geq 1eV$, $B_0 = 20$ G, Ar 2×10^{-4} Torr) a model electrodynamic tether (20 cm insulated tether wire $\perp B_0$ with $\approx$1cm diam collecting/emitting end electrodes) and an insulated loop antenna ($\approx$5cm diam) have been inserted. Single current pulses ($\Delta t_p \approx 0.1$ μs, I$\approx$0.1A) applied to these structures excite time-varying magnetic fields which are measured with probes in a large plasma volume at $\approx$15,000 positions in space and in time (resolution $\Delta r \approx 1.5$cm, $\Delta t \approx 10$ns). The pulsed magnetic field propagates as a dispersive wave packet. By 4-D Fast Fourier Transformation of $B(r,t)$ into $B(k,\omega)$ it is shown that the packet consists of plane waves obeying the dispersion and polarization properties of, in general, oblique, low frequency whistler waves. The inductive and space-charge electric fields are solved in Fourier space, the former from Maxwell's equations and the latter from Ohm's law, then inverse transformed so as to obtain $E(r,t)$ within the wave packet. The separation of the electric field into rotational and divergent contributions, which cannot be achieved by single-point electric field measurements, is of intrinsic importance for understanding the observed magnetic fields, currents, and space charge distributions within the wave packet. The Poynting vector $S(r,t)$ is obtained and analyzed in terms of radiation, energy storage and dissipation.

The basic studies of stationary, pulsed exciter structures are extended to moving sources relevant to active space experiments. This is accomplished by a linear superposition of delayed pulse responses emitted from displaced source positions which, according to Huygen's principle, yields wave fronts (R. Stenzel and J.M.Urrutia, Geophys. Res. Lett. **16**, 361,1989). A moving electrodynamic tether excites "whistler wings" not only from its charged electrodes but also from the tether wire with its moving magnetic field. Current closure and radiation drag will be discussed. A rapidly moving magnetic dipole generates a "whistler wake". Antenna radiation patterns distorted by motional effects (satellite motion or plasma flows along or across B_0) will be shown.

H4-3   ELECTRODYNAMIC TETHER WORK IN OEDIPUS C
1440   H. Gordon James
          Communications Research Centre
          Ottawa, ON K2H 8S2

          Wynne Calvert
          Department of Physics and Astronomy
          University of Iowa
          Iowa City, IA 52242

The flight of the tethered sounding rocket OEDIPUS A in 1989 met a number of novel objectives in the areas of ionospheric plasma physics and tether technology. The Canadian Space Agency and NASA have agreed to fly a second experiment, OEDIPUS C, in winter 1994-1995. Using a double payload like A's, OEDIPUS C will return to the active wave subjects of OEDIPUS A and address some of the questions that it uncovered. A central theme is again bistatic propagation using a transmitter HEX at one end of the tether and a synchronized receiver REX at the other. The study of the payload mechanical dynamics has prominence because of the complexity of the payload motion observed on OEDIPUS A. In addition, the payload will be equipped for the passive observation of auroral plasma processes.

The OEDIPUS-C flight scenario calls for a launch on a Black Brant XII rocket from Poker Flat, Alaska to an altitude of 800 km over an active aurora. The launch and flight conditions are somewhat different from those of A because of a desire for greater heights, and, in the second half of the flight, disconnection of the tether at both subpayloads. The goal will be to investigate dc and ac electric fields in the more tenuous plasma existing at heights attainable with the Black Brant XII. The HEX output power has been increased over OEDIPUS A and the associated dipoles lengthened from 5 to 16 m tip to tip. To better understand the differences between plane-wave and sheath-wave propagation, it is planned to cut the tether on the downleg and to concentrate on plane-wave propagation between the dipoles. Detectors of thermal and energetic particles will provide information on the interaction of particles with waves and with the body of the payload. Flux-gate magnetometers and plasma sensors will monitor the state of the auroral ionosphere in the vicinity. These sensors include an instrument that operates the tether and two subpayloads as a large double electrostatic probe. Collaborative experiments using radio equipment on the ground will attempt to observe payload transmissions. This controlled experiment may shed light on the reception of emissions triggered by auroral particles. Extensive study of the mechanical stability of the tethered payload throughout the flight has guided the payload design, and has produced theoretical models that will be compared with payload-motion sensor data after the flight.

H4-4   **IONOSPHERIC EFFECTS ON TSS-1 SWITCHING TRANSIENTS**
1500   S. G. Bilén, B. E. Gilchrist, V. M. Aguero
      Space Physics Research Laboratory
      University of Michigan
      2455 Hayward
      Ann Arbor, MI 48109-2143
    E. Melchioni, M. Dobrowolny
      IFSI/CNR
      Via G. Galilei, Casella Postale 27
      00044 Frascati, Italy

The first mission of the Tethered Satellite System (TSS-1) deployed an electrically conductive 1.6 m diameter Italian built satellite to a maximum distance of 267 m above the Space Shuttle Atlantis. The satellite was connected to the shuttle via an electrodynamic tether — an electrically conducting, insulated wire — across which a potential was induced due to its interaction with the geomagnetic field. The Shuttle Electrodynamic Tether System (SETS) measured this induced potential and also the current flow as resistive loads were selectively placed between the tether and the Shuttle's electrical ground. Due to the large inductance ($\approx$ 12 H) presented by the almost fully wound tether reel, large transients occurred as these resistive loads were switched out. The SETS experiment measured these transients by selectively sampling the tether voltage in high speed (32 kHz) bursts.

These transients, which can be described by an underdamped second order response, are influenced by the surrounding plasma environment. Specifically, it was found that the decay constant of these transients is dependent on the local ionospheric plasma density which was provided by the Research on Electrodynamic Tether Effects (RETE) experiment. (See Figure 1) The peak transient voltage, however, is not dependent on plasma density but only on initial tether current as previously reported [S. G. Bilén, *et al.*, URSI National Radio Science Meeting, Boulder, CO, Jan. 1993]. There are also preliminary indications that the transient nature is affected by Shuttle charging as well. The mechanisms behind these dependencies will be discussed.

This research may have an impact on other large systems in the ionosphere, electrodynamically tethered or otherwise, which intend to switch or pulse current.
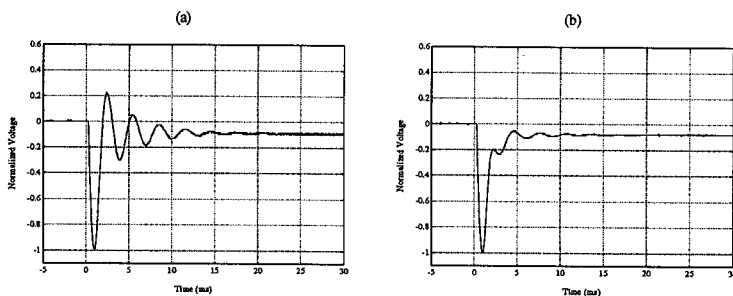
Figure 1 Normalized switching transients showing that decay constant is dependent on plasma density. Transients taken under the following conditions: (a) day pass with $1.29 \times 10^{+12}$ N_e/m^3, collected at 218/21:18:45, -4.9° lat., 226.7° long., 223.63 m deployed tether, 10.24 mA initial current, -319.2 V peak transient; (b) night pass with $4.87 \times 10^{+11}$ N_e/m^3, collected at 218/18:59:56, -1.6° lat., 70.3° long., 224.15 m deployed tether, 16.38 mA initial current, -492.3 V peak transient.

H4-5
1540

CHARGE TRANSFER REACTIONS OF
METASTABLE BA(I) AND SR(I) IN THE
CRRES G-11b CHEMICAL RELEASE

D. E. Hunton
Geophysics Directorate
Phillips Laboratory (AFMC)
Hanscom AFB, MA 01731

During the summer of 1991, the Combined Release and Radiation Effects Satellite (CRRES) was used to perform five chemical release experiments in the ionosphere over the Caribbean Sea. In four of these experiments, a Ti-B thermite reaction was used to vaporize barium metal doped with a small amount of strontium metal at a distance of around 5 km from the spacecraft. In addition to extensive ground based observations of the releases, the satellite itself carried several instruments that were used to make in-situ measurements of ion composition, plasma density and VLF waves.

One of the in-situ instruments was the Quadrupole Ion Mass Spectrometer built by the Air Force Phillips Laboratory. We used this instrument to measure mass resolved fluxes of Ba^+ and Sr^+ ions produced from the released metal vapor. The flux of Sr^+ relative to Ba^+ in each experiment was more than 100 times larger than was expected based on known photoionization rates and estimated charge transfer cross sections of the ground state metals.

In a proposed mechanism to account for the large Sr^+ fluxes, the neutral metal atoms are excited to low-lying metastable states by electron-atom collisions early in the expansion of the neutral cloud. These metastable atoms are then ionized by near-resonant charge exchange reactions with ambient O^+ and by photoionization after the cloud had expanded sufficiently to reach the spacecraft. Rough estimates of the rates of the charge exchange reactions for each state are shown to give total ionization levels consistent with the measured fluxes for the case of the G-11b release experiment in darkness. This proposed mechanism offers support for the existence of a population of energetic electrons early in the expansion of the barium cloud similar to what would be expected if a Critical Ionization Velocity (CIV) process were occurring.

H4-6
1600

ELECTRON HEATING PHENOMENA ASSOCIATED WITH IONOSPHERIC BARIUM RELEASES

F. T. Djuth[1], M. P. Sulzer[2], P. A. Bernhardt[3], J. H. Elder[1], and K. M. Groves[4]
[1]Geospace Research, Inc., 550 N. Continental Blvd., Suite 110, El Segundo, CA 90245
[2]Arecibo Observatory, Arecibo, Puerto Rico 00613
[3]Plasma Physics Division, Naval Research Laboratory, Washington, D.C., 20375
[4]Phillips Laboratory, Hanscom Air Force Base, MA 01731

During the NASA/CRRES *El Coqui* rocket campaign, several rocket-borne releases of Ba took place in the ionosphere to the north of Arecibo Observatory, Puerto Rico. All releases were performed within the viewing limits of the Arecibo incoherent scatter radar. In this presentation, attention is focused on 430-MHz radar observations made during the three largest *El Coqui* Ba releases. These releases, designated AA-1, AA-2, and AA-7, were performed under dawn solar illumination conditions to facilitate ground-based optical measurements. As part of the AA-2 project, approximately 35 kg of Ba doped with 148 gm of Sr, 260 gm of Eu, and 24 gm of Li were released near 252 km altitude. The AA-1/AA-7 experiments were very similar. Each consisted of the release of ~22 kg of Ba and 276 gm of Sr at 255 km altitude. It is estimated that 14 kg of Ba vapor was produced during the AA-2 release and roughly 9 kg of Ba vapor was generated during the AA-1/AA-7 releases.

During two of the three experiments, the Arecibo radar beam was pointed a significant distance (~10 km) away from the ionospheric release point. With this viewing geometry, the first event observed is a large (factor of 2) enhancement in the temperature of the background electron gas. The bulk heating phenomenon is detected several seconds after the release and precedes the arrival of the Ba ion cloud in the radar beam. After the appearance of the Ba ions, the hot electron gas is most evident below the cloud. This initial heating event lasts for approximately 30 s. Over time scales of minutes following the AA-1 and AA-7 releases, enhanced electron temperatures are observed to develop above and/or behind the Ba ion cloud. These enhancements persist throughout the period of radar observations, which typically lasts 15 min or longer. The late-time electron temperature enhancements appear to be accompanied by a reduction in background electron concentration. Currently, the origin of the early time bulk electron heating is not well-understood and remains a topic of continuing investigation. The late time heating is thought to be a product of the photochemistry but may be influenced by electrodynamic processes.

J2-1   **A 1024-LAG CORRELATOR CHIP**
1400   **AND ITS USE IN RADIO/RADAR ASTRONOMY**

J. Hagen, NAIC Laboratory
  124 Maple Ave. Ithaca, NY 14850
M. Davis, NAIC Arecibo Observatory
  PO Box 995, Arecibo PR 00612
J. Canaris, U. of New Mexico-NASA SERC
  2650 Yale SE, Albuquerque. NM 87106

A 1024-lag correlator chip is now being fabricated for use in a number of
radio astronomy projects. This chip, containing about 1 million 0.8 micron CMOS
transistors, implements the traditional correlator architecture wherein each of the
1024 on-chip "lag modules" computes and accumulates products of an "A" data
stream times a delayed version of a "B" data stream.
If the A and B data streams are the same the chip calculates the autocorrelation
function of this steam. The maximum rate for input data (and clock rate for the
chip) is at least 100 Ms/sec. Each lag unit has its own 32-bit accumulator and 32-
bit holding register to allow accumulated data to be read out while new data is
being processed. Chips can be cascaded to form longer correlator chains. The
input data can be either 2-level (1-bit) or 3-level (1.6 bits). Output data is via a 32-
bit tri-state bus which can be clocked as fast as 20 Mhz.

Spectrum analyzers for radio astronomy will use these chips together with
several multiplexing schemes to increase the clock rate and/or increase the
number of input quantization levels from two or three to nine.

These chips and multi-chip modules can and will be used for the transversal
filtering operation used in pulse compression for radar astronomy at Arecibo. In
this application the received data is cross-correlated with a copy of the 1-bit
pseudo-random code used to phase-encode the transmitted signal. The output
data from successive correlator channels corresponds to successive ranges on the
target.

J2-2   THE GBT SPECTROMETER
1420   R. P. Escoffier
          National Radio Astronomy Observatory*
          2015 Ivy Road
          Charlottesville, VA   22903

The NRAO is developing a spectrometer for use on the 100-meter radio astronomy Green Bank Telescope (GBT) now being constructed by the National Radio Astronomy Observatory in Green Bank, WV.

This instrument will analyze up to eight 1 GHz baseband outputs of the GBT. A total of 262,144 correlation lag channels will be provided. The instrument will alternatively analyze the output of up to 32 baseband signals up to 62.5 MHz in bandwidth.

An Application Specific Integrated Circuit (ASIC) is being developed for use in the GBT spectrometer by the NASA Engineering Research Center for VLSI System Design at the University of New Mexico. This ASIC has 1024 lag channels, short-term integration and is specified for a 100 MHz clock rate. The GBT spectrometer will have 256 such ASIC's in its design.

The design differs from a conventional correlator design in that the low speed ASIC's process the 2 GHz digital output of the A/D converter using fast RAM memories and a linear array of processing ASIC's. This approach stands in contrast to the conventional method of using a square array of processing ASIC's.

A 2 GHz A/D is being developed for use with the GBT spectrometer. This device is a 2-bit, 3-level converter and uses standard ECL integrated circuits.

J2-3   **A WIDEBAND ANALOG CORRELATOR FOR RADIO**
1440   **ASTRONOMY**

S. Padin
California Institute of Technology
Owens Valley Radio Observatory
Big Pine, CA 93513

Although digital signal processing techniques are now widely used in radio astronomy, analog correlators are still attractive for very wideband systems. Indeed, for bandwidths in excess of a few GHz analog correlators may currently be the only affordable option.

A new analog correlator has recently been developed for the Owens Valley Millimeter Array. The correlator processes two 1-2 GHz bands for a six telescope array and is currently used for simultaneous dual-wavelength continuum observations in the 1 and 3 mm bands. Each cross-correlator uses a pair of microwave mixers (fed in phase quadrature from one telescope and in phase from the other telescope) to realize a complex multiplier. The multiplier outputs are amplified, integrated for 5 ms and then digitized. Further integration and demodulation of the quadrature phase-switching cycle impressed on the first local oscillator in the receiver system is handled by a computer.

The sensitivity of the analog correlator is limited by passband errors and noise generated in the amplifiers which follow the multiplier. Low-frequency signals (in particular 60 Hz and its harmonics) which are coupled to the amplifiers can also degrade the sensitivity of the correlator if they are not completely rejected by phase-switching the first local oscillator. In the Owens Valley analog correlator a 20 KHz 180° phase-switch is used in addition to the 200 Hz first local oscillator phase-switch to increase the rejection of unwanted low-frequency signals.

J2-4   THE VLBA CORRELATOR: LESSONS LEARNED
1520   Joseph H. Greenberg, Electronics Engineer
              National Radio Astronomy Observatory
              P.O. Box O, Socorro, NM 87801-0387
              Email: jgreenbe@nrao.edu

Introduction

The Very Long Baseline Array (VLBA) FX Correlator processes
eight channels from twenty stations. Twenty-four tape
drives are multiplexed into the twenty correlator inputs.
FX means the FFT is done before the cross multiplication.
The hardware is divided into three sections: the playback
interface, the FFT section, and the cross multiply or MAC
section. The hardware occupies 4 large racks. An ASIC was
designed to serve a double purpose of doing FFT's or MAC's.
Most of the lessons we learned are applicable to any large
digital system, instead of being specifically due to the FX
nature of the design.

Hardware Lessons Learned

*   Use heavy duty power and ground distribution
         with a substantial ground plane.
*   Keep wires away from power cables to avoid voltage spikes.
*   To avoid cross talk, do not bundle signals.
*   Avoid chips that are likely to soon be out of production.
*   In ASIC design, expect multiple cycles of prototypes.
*   Have the ASIC serve a dual function, as opposed
         to having two ASIC designs.
*   Design the ASIC so there are uniform, non-excessive setup
         and hold times.
*   On large cards, buffer signals near the connectors.
*   Problems with large wirewrap boards:
             -Install VCC and Ground clips on all F type logic.
             -Shorts develop from chafing of wire insulation.
             -The boards are hard to work on.
*   Clock distribution.
             -Use sine wave clock distribution to the boards.
             -Use clock drivers designed for that purpose.
             -Have short clock runs on the boards.
*   Use a single type of microprocessor in the system.
*   Do not over-specify the impedance of PC board runs.
*   On the PC board layout, place bypass capacitors
         under the centers of Pin Grid Arrays.
*   Extensively use PALs and Xilinx chips to make changes easy.
*   Place cooling fans in the bottoms of the racks.

Software Lessons Learned

*   Avoid revamping the software methodology midstream.
*   Allow adequate processor capacity for when the full system
         configuration is implemented.
*   Have an extensive system test to aid in debugging.

General Lessons Learned

*   Beware building so much flexiblity into the system
         that it becomes unworkably complicated.
*   Build test fixtures for card checkout and testing.
*   Use bar code readers to identify the tape reels.
*   Store the microprocessor software in ram for easy changes.

J2-5   COHERENT DISPERSION REMOVAL PROCESSOR
1540

D. C. Backer, D. J. Werthimer and M. Dexter
Astronomy Department and NSF Center for Particle Astrophysics
University of California
Berkeley, CA 94720

J. M. Rabaey
Department of Electrical Engineering and Computer Sciences
University of California
Berkeley, CA 94720

and

A. A. Kapadia
Hewlett Packard Corporation
Cupertino, CA

Pulsars are rapidly rotating, highly magnetized neutron stars that emit sharp pulses each rotation period. The signals we receive are faint, and highly dispersed in the intervening column of interstellar electrons. The unwanted dispersion can be removed from the received electric field, or voltage, by convolution with the appropriate restoring function. This predetection, or coherent, technique is essential for precise timing of millisecond period pulsars at decimeter wavelengths. We are constructing a multichannel, digital signal processor – the Coherent Dispersion Removal Processor – that removes the dispersion within many subbands of the received signal. The processing kernel for each subband is a finite impulse response (FIR) filter implemented in a full-custom, application specific integrated circuit (ASIC). The maximum number of taps is 1024 for subband widths of 1 MHz or less. Modes with 512 taps at 2 MHz and 256 taps at 4 MHz are available. Low bit quantization is used, as in other radio astronomical digital processors. This leads to minimal loss in sensitivity and dynamic range when observing noise dominated signals.

The ASIC chip uses a partially parallel and pipelined approach to implement the 7.2×10^9 operations per second computational requirement of the filter. The internal clock speed is up to 32 MHz. The datapath consists of 32 complex multipliers and a binary adder-tree followed by accumulators that sum up the 1024 products to produce the convolution result. The chip has been fabricated in the MOSIS 1.2 micron process. The die size is 7.4mm × 8.4mm and the pin count is 132. The chip has been successfully fabricated, lab tested and used to observe real astronomical signals.

We are constructing a 128 channel Coherent Dispersion Removal Processor for use on NRAO telescopes in Green Bank, WV. Input signals with total bandwidths of (up to) 64 × 4 = 256 MHz for orthogonally polarized IFs will be split into SSB baseband signals 40 MHz wide using standard analog video converters and filters. A digital filter bank VME board has been built to subdivide these signals into 8 adjacent bands of 4 MHz width. A dedisperser VME board has been built to first remove dispersion in the custom chip described above, then detect and average synchronously with the pulse period. A total of 16 board pairs in two VME crates is required. A timing board will provide PC interface, pulse arrival time monitoring, and clocks for all boards. First telescope tests with a single channel were performed in 1993 June.

J2-6
1600

A VLSI CORRELATOR CHIP FOR RADIO ASTRONOMY

W. Aldrich
MIT Haystack Observatory
Route 40
Westford, MA 01886

The Haystack observatory, in conjunction with its sponsors, is developing a VLSI correlator chip to form the basis of a number of new correlators for radio astronomy applications.

The level of integration which is now available from the semiconductor industry allows the consideration of a "system on a chip" in which many of the features of existing correlators migrate inside the chip. In addition, the economics of chip development have required that the chip development costs be shared between several projects. Thus the sometimes competing requirements of multiple projects must be resolved in the chip design.

We have chosen to base our chip design on the architecture developed by Bos (A. Bos, IEEE Transactions on Instrumentation and Measurement, Vol. 40, No. 3, pp 591-595, June 1991) but to augment it with full support for very long baseline interferometry. In addition, a flexible means of interconnecting sections within the chip as well as from chip to chip has been provided to make the chip useful for connected-element applications.

The chip architecture and specifications will be presented as well as a snapshot of the current development status. The first silicon is expected to be available for testing in mid 1994.

J2-7   **THE SERENDIP III AND IV INSTRUMENTATION**
1620   Dan Werthimer, David Ng, Stuart Bowyer, Charles Donnelly

Space Sciences Laboratory
University of California
Berkeley, CA 94720

The SERENDIP program is an ongoing search for narrow band radio signals from extraterrestrial civilizations. In this paper we discuss the hardware design of the SERENDIP III and IV instruments. SERENDIP III is a four million channel FFT-based spectrum analyser which has been operating in a sky survey mode at NAIC's 305 meter radio telescope in Arecibo, Puerto Rico since April 1992. The spectrum analyser covers a 2.4 MHz instantaneous bandwidth at 0.6 Hz resolution. Building on the SERENDIP III design, SERENDIP IV is a 160 million channel spectrum analyser, covering a 96 MHz bandwidth, also with 0.6 Hz resolution and a 1.7 second integration time. SERENDIP IV incorporates a bank of digital mixers and filters to separate the 96 MHz band into fourty 2.4 MHz sub-bands. Each 2.4 MHz sub-band is further broken down into 0.6 Hz bins by means of a four million point Fast Fourier Transform. The resulting power spectra are analysed by 40 high speed signal processors. Narrow band signals having power significantly above background noise levels are recorded, along with telescope coordinates, time, and frequency.

J2-8
1640

SIMULATIONS OF SAMPLER ERRORS AND THEIR EFFECT ON DIGITAL CORRELATORS

Andrew V. Dowd

60 Garden St., MS 78

Smithsonian Astrophysical Observatory

Cambridge, MA 02139

Improvements to astronomical radio receivers have created the need for increases in backend performance. In one respect, astronomical spectrometers and correlator have keep pace with these developments by increasing bandwidth and resolution. This paper will examine a different set of performance issues with respect to astronomical spectrometer, namely dynamic range and linearity. The goal is to understand several undesirable aspects of a practical sampler as it pertains to astronomical backends, and to minimize their impact on instrumental performance.

Very small distortions introduced in the signal processing can have dire consequences to astronomical observations. The sampler technique ("flash-converter") used in digital spectrometers is essentially non-linear with post processing necessary to convert the measured values into a unbiased estimate of input statistics. This post processing, (the *clipping correction*), relies on assumptions about the sampler. Errors are introduced when practical samplers deviate from the assumed model.

An ideal sampler is an impractical construct. The structure of a flash converter relies upon a voltage comparator. An ideal voltage comparator would require infinite gain to detect a transition across a threshold level. Other practical problems cause significant deviation from the assumed comparator model such as digital leakage and hysteresis. A model for a practical comparator is presented and described. Next, this model is used in simulations to predict their impact on an astronomical observation. The results of these simulations are compared to data measured with the NRAO 12 meter Hybrid Spectrometer.

This work is directed to creating a valid model of sampler behavior. With a valid model, the design of a sampler can be evaluated before final construction of the correlator. Also, an understanding of sampler issues can be used to improve the design of an astronomical sampler.

Session J-3 1955-Thurs. CRO-30
COSMIC MICROWAVE BACKGROUND
Chairman: Mark Birkinshaw, Dept. of Astronomy, Harvard Univ., Cambridge, MA 02138

J3-1
2000

FUTURE OBSERVATIONS OF THE CMBR WITH THE MSAM

P. T. Timbie, K. H. Farooqui, G. W. Wilson. J.-W. Zhou
Brown University, Department of Physics
Providence, RI 02912

L. Piccirillo, R. Schaefer
Bartol Research Institute, University of Delaware
Newark, DE 19716

C. A. Inman, S. S. Meyer, J. L. Puchalla, J. Ruhl
University of Chicago, Enrico Fermi Institute
Chicago, IL 60637

E. S. Cheng, D. A. Cottingham, D. J. Fixsen, M. S. Kowitt,
and R. F. Silverberg
NASA/ GSFC, Code 685
Greenbelt , MD 20771

L. A. Page
Princeton University, Department of Physics
Princeton, NJ 08544-0708

The Medium-Scale Anisotropy Measurement (MSAM) is a balloon-borne telescope which has detected signals consistent with anisotropy in the CMBR at angular scales near 0.5 degrees There are 4 spectral bands, centered at 190, 300, 550, and 750 GHz, for rejection of signals from interstellar dust emission. A future flight of this experiment will carry a new detector system to extend the spectral coverage of the MSAM to lower frequencies to provide improved rejection of foreground sources, such as galactic free-free emission. MSAM II will observe the same spots as earlier MSAM flights, with bands centered at 70, 100, and 150 GHz. The total of 7 spectral bands will allow spectral decomposition of each spot observed for most anticipated sources of confusion. The new system uses single-mode optics in order to under-illuminate all optical surfaces of the telescope while achieving the same beam size and sensitivity as the higher frequency channels. The detectors are waveguide-coupled bolometers cooled to 0.1K.

J3-2   PROSPECTS FOR INTERMEDIATE-SCALE ANISOTROPY
2020   MEASUREMENTS FROM SPACE

C. R. Lawrence
Space Physics and Astrophysics
Jet Propulsion Laboratory
Pasadena, CA 91109

The fluctuation spectrum of the Cosmic Background Radiation (CBR) on angular scales from $0\overset{\circ}{.}5$ to $\sim 10°$ is both crucial to our understanding of structure in the Universe and poorly constrained by the COBE measurements on larger angular scales. The success of future intermediate-scale experiments will depend not only on their sensitivity and freedom from systematic errors, but also on how well they can separate confusing anisotropies from foreground sources (i.e., everything else in the Universe) from those of the CBR itself. A feasibility study conducted at JPL during the last year suggests that a space mission could achieve the necessary performance at moderate cost. The technology developments required to achieve the necessary instrument performance could be tested on ground and balloon platforms, and thereby help to decide whether a space mission is really required.

J3-3   RECENT RESULTS ON THE SUNYAEV-ZEL'DOVICH EFFECT
2040   Dr. Mark Birkinshaw
            Smithsonian Astrophysical Observatory
            60 Garden Street
            Cambridge, MA 02138-1596

The 40-m telescope at the Owens Valley Radio Observatory has been used to measure the angular structures of the Sunyaev-Zel'dovich effects from three clusters of galaxies. The quality of the one-dimensional cuts across the clusters is limited by residual systematic errors, but the data clearly show the signature of extended inverse-Compton scattering from the same gas that produces the X-ray emission from the clusters, and measure the amplitudes of the effects with good precision.

These data have been used to study the properties of the clusters, and to measure the value of the Hubble constant, H_0. The result, $H_0 = 55 \pm 17$ km s^{-1} Mpc^{-1}, tends to support the long distance scale for the Universe, but may be biased low by an orientation effect (which is not likely to exceed a factor of 1.4). Further work on the Hubble constant using Sunyaev-Zel'dovich effect and X-ray data demands the observation of a cluster sample without an orientation bias. The strategy for selecting such a sample, and the prospects for obtaining more precise values of the Hubble constant, will be discussed.
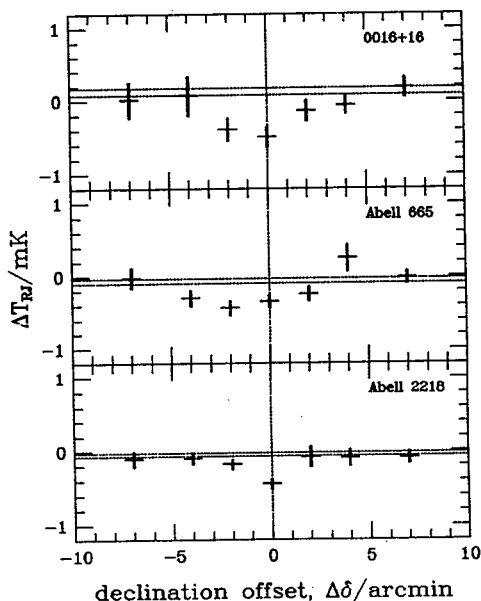
J3-4 **RESULTS FROM THE COBE MISSION**
2100 Dr. Stephan Meyer
Department of Astronomy and Astrophysics
University of Chicago
5640 S. Ellis Avenue, Chicago, IL 60637

The COsmic Microwave Background Explorer (COBE) satellite has completed its data taking lifetime. The Diffuse Microwave Radiometer (DMR) maps from the first year of operation have been used to detect anisotropy in the Cosmic Microwave Background Radiation (CMBR) in three frequencies. The analysis of the second and subsequent years is in progress and will provide improved signal to noise measurements of the large-scale anisotropy. The Far-InfraRed Absolute Spectrophotometer (FIRAS) has measured the spectrum of the CMBR and the diffuse sub-millimeter galactic emission. Continuing refinement in the calibration of the instrument has led to new limits on the CMBR spectrum and to results on the galactic emission. The Diffuse InfraRed Background Experiment (DIRBE) has mapped the sky in 10 wavelength bands covering the entire infrared spectrum. Analysis of these data have led to information on the morphology of our Galaxy and the planetary dust cloud. The data will also provide limits on the strength of the Cosmic Infrared Background (CIB).

J3-5
2120

CO Absorption In The Outer Galaxy: Abundant Cold Molecular Gas
----

R. J. Allen, Space Telescope Science Institute
J. Lequeux, Observatoire de Meudon
S. Guilloteau, Institute de Radio Astronomie Millimetrique

We have detected absorption in the CO(1-0) and CO(2-1) spectra of two
very-low-latitude radio continuum sources. Little CO emission is found
in the immediate regions of these sources. The results, obtained with
the 30m IRAM radiotelescope, have been confirmed with the IRAM
interferometer for one of the sources in CO(1-0) absorption. There is
only one absorption feature from the local gas, but at least 3 features
are detected from gas at about 12 kpc from the Galactic center. This is
an unbiased survey, whereas present CO emission surveys preferentially
detect warm (more than 10 K) molecular gas associated with recent massive
star formation. We conclude that we have found evidence for the
existence of significant amounts of cold molecular gas in the outer
Galaxy; there may be 4 times more molecular gas than atomic gas at 12
kpc radius. The fraction of molecular gas can only increase at larger
Galacocentric distances, and we suggest that cold molecular gas may
make a significant contribution to the dark matter required by
dynamical studies of spiral and irregular galaxies. Another consequence
of our observations is that both the electron and proton components of
cosmic rays must decrease strongly at large radii, pointing to a
Galactic origin for GeV cosmic rays.

Session A/D 0835-Fri. CR1-9
ELECTROOPTIC DEVICE CHARACTERIZATION
Chairman: Robert Gallawa, NIST, Boulder, CO

A/D-1   CHARACTERIZATION OF X-CUT LINBO3 PLANAR WAVEGUIDES
0840   Milica Popovic
           Steven L. Kwiatkowski
           Alan R. Mickelson
           Department of Electrical and Computer Engineering
           University of Colorado
           Boulder, CO   80309-0425

Studies and experiments have shown that the process of Ti-indiffusion in X-cut LiNbO3 is coupled with the process of Li-outdiffusion. Both of these processes produce changes in distribution of the refractive index of the substrate, however, with different spatial distributions. This combination leads to a composite index profile which is more complex than that due to either alone. This is undesirable from the standpoint of achieving single spatial mode operation. In general, the greater depth of the lithium outdiffusion leads to extra weakly guided modes deep in the substrate. In order to determine how to achieve single mode operation, a number of LiNbO3 X-cut samples have been processed with three variable parameters: titanium layer thickness, indiffusion time, and temperature. These samples are tested by the m-line measurement in order to observe the effect of change of parameters on the number of modes.
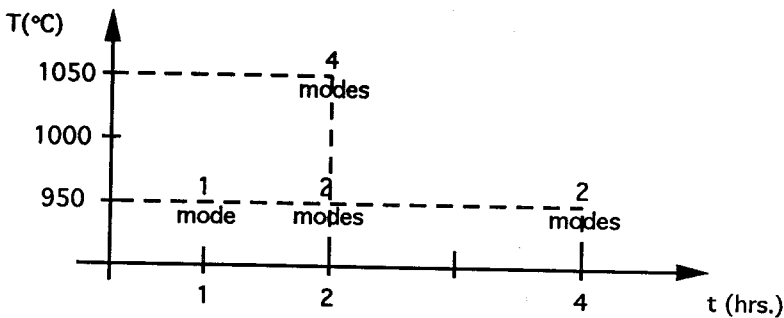
Ti thickness = 250 Å

A/D-2   EFFECTS OF THE PRISM-WAVEGUIDE COUPLING STRENGTH ON
0900   EFFECTIVE INDEX MEASUREMENT ACCURACY.

Stephen L. Kwiatkowski and Alan R. Mickelson
Department of Electrical and Computer Engineering
University of Colorado
Boulder, CO 80309-0425

Jeff Margolies
The Institute of Optics
University of Rochester
Rochester, NY 14627

The subject of this presentation is the accuracy of mode effective index measurements in a dielectric optical waveguide using a prism out-coupler. A prism with index of refraction greater then the waveguide is clamped to the surface of the waveguide and causes the guided modes to radiate away from the waveguide. At a distance from the prism the optical intensity distribution associated with each radiated mode appears as a distinct line and is referred to as a 'm-line'. According to one model, which utilizes the phase matching condition, the radiation angle of a m-line depends upon the effective-index of the mode. Thus, a measurement of the radiation angle should yield a value for the mode effective index. However, this model does not include the perturbation effects of the prism on the waveguide. The perturbation locally affects the boundary conditions of the waveguide, thus changing the properties of the mode and the characteristics of the m-line. Other models are used to predict the effects of the prism perturbations. One such model uses solutions to the transverse resonance condition for the leaky-waveguide. In this model the prism coupler is analyzed as a leaky-waveguide that is formed by placing a prism half-space above the nonperturbed waveguide. We have investigated the perturbation effects using a local normal mode expansion of a composite waveguide which is formed by the prism and the nonperturbed waveguide. We will present results from these theoretical models and compare them to our experimental observations of perturbed m-line characteristics .

165
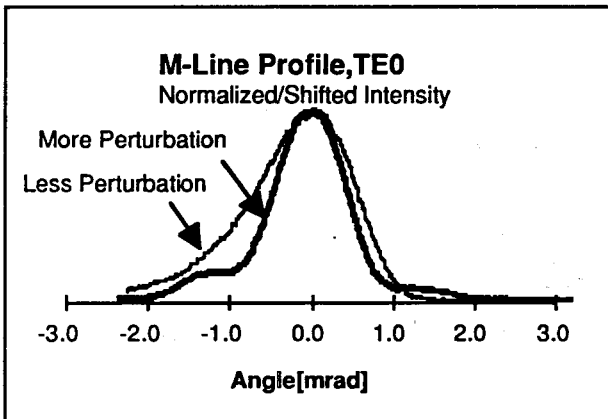
A/D-3
0920

OPTICAL SAMPLING FOR DETERMINATION OF MATERIAL CHARACTERISTICS

Paul Biernacki and Prof. Alan R. Mickelson
Department of Electrical & Computer Engineering
University of Colorado
Boulder, Colorado 80309-0425

An optical sampling technique developed here at the University of Colorado can be used to map out two dimensional charge and current distributions on planar electrodes of microwave circuits. Knowledge of the longitudinal variation of the current gives a complete description of the local S parameters of the circuit, thereby giving a complete device characterization. However, there is still more information present in the two dimensional distributions. Here we propose to use this information to determine characteristics of the homogeneity of the material underlying the electrode.

A prime test case for determining the efficacy of our technique is the ohmic contact. Since defects present themselves inherently during the fabrication process of ohmic contacts, optical sampling measurements can possibly provide direct correlation of the perturbing effects due to these defects to the anticipated measured anomalies of the charge and current distributions. Test structures for measuring the effects of different length ohmic contacts and different metalization techniques are shown in fig. 1. Ohmic contacts of different lengths will be constructed by placing heavily doped gaps in regions along coplanar transmission lines built on electrooptic GaAs.
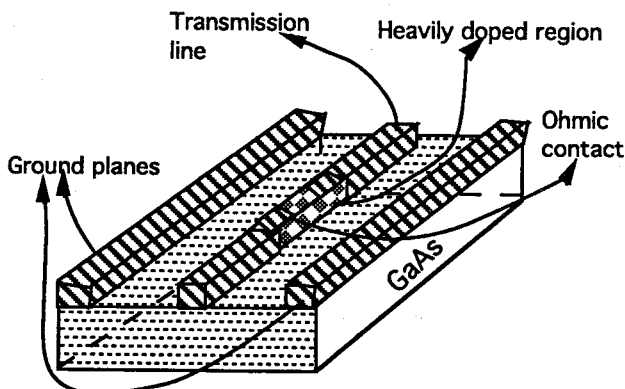
Figure 1 Coplanar transmission line with an ohmic contact

A/D-4
0940

PHOTONIC ELECTRIC-FIELD PROBE WITH 6 GHZ FREQUENCY RESPONSE

K. Masterson, A. Bazin[+], M. Kanda, D. Novotny
Electromagnetic Fields Division, 813.07
National Institute on Standards and Technology
325 Broadway
Boulder, CO   80303

A photonic electric-field probe consisting of a three-port directional coupler fabricated by Ti:LiNbO$_3$ indiffusion and having electrodes formed by resistively tapered dipole elements deposited directly on the crystal surface is characterized. Operation is at an optical wavelength of 850 nm. Testing was done in both the time and frequency domains and with both a free-field environment and by directly injecting electrical signals to the dipole elements. The optical output from the downlink fiber was directly detected by an optical sampling oscilloscope with a 30 GHz bandwidth.

The frequency response extends from 1 Hz to beyond 6 GHz. The V_π voltage for the modulator is 10 V and the E_f field strength is 8 kV/m. Preliminary determinations for the antenna factor and drive point capacitance for the dipole are 0.0012 m and about 8 pF respectively. These values will be compared to the results of numerical calculations and presented together with more details of the probe testing and characteristics.

[+] A. Bazin's affiliation is with DGA, Centre D'Études de Gramat, France.

A/D-5   PROPAGATION LOSS OF POLYMERIC THIN FILM OPTICAL
1020   WAVEGUIDES
        W. Feng, S. Lin, H.B. Hooker, and A. R. Mickelson
        Department of Electrical and Computer Engineering
   University of Colorado at Boulder
        Boulder, CO 80309

Nonlinear optical (NLO) polymers have been proven to be promising materials for high speed electro-optic devices due to their optical and microwave properties. However, optical propagation losses in these materials are usually higher than those in the inorganic EO materials, such as LiNbO3, especially when making optical channel waveguides and making the material electrically active. Optical losses are from material absorption and light scattering, which are usually increased either when chromophores are added into the polymer, films are exposed to UV light to build optical channel waveguides, or when high electrical field is applied to the NLO film heated to its glass transition temperature (electrical poling). There are many ways of measuring losses. Since it is usually hard to prepare the endface of a polymer film to the surface quality close to that of other materials (i.e. LiNbO3, glass), and since we are interested in the loss of slab wave guide (simplifying the causes of loss in order to find out the loss mechanism of the material), the three prism coupling technique is used. This technique has advantages over techniques which utilize the scattered light along the streak of an optical waveguide because of sensitivity. It's drawback is that the prisms contact the surface of the waveguide. The NLO polymers under study are PMMA/DR1 copolymer and Ultem/DEDR1. Optical propagation losses of the planar waveguide (unbleached, bleached, poled) are measured, which show a significant increase in loss when samples are bleached or poled. Sources of losses are discussed. Losses of optical channel waveguides are also studied. Measuring wavelengths are 0.83 μm and 1.3 μm.
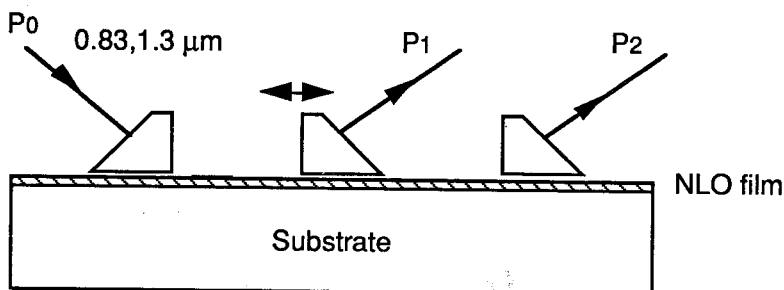
A/D-6 CHARACTERIZATION OF POLYMERIC OPTICAL CHANNEL
1040 WAVEGUIDES AND THEIR APPLICATIONS IN HIGH SPEED
ELECTRO-OPTIC DEVICES

W. Feng, S. Lin, H.B. Hooker, A.R. Mickelson
Department of Electrical and Computer Engineering
University of Colorado at Boulder
Campus Box 425
Boulder, CO 80309

Nonlinear optical (NLO) polymers are promising materials for high speed electro-optic devices because of their potenially large electro-optic coeficients, low dielectric constants, and their potential multilayer applications. Polymeric optical channel waveguides can be formed in various ways, such as UV light bleaching, laser ablation, reactive ion etching, etc. UV light bleaching and coplanar electrode poling are more interesting because they are better adapted to the multilayer applications. Properties of the NLO polymer will be changed under these processes (i.e. index changes of the bleached and poled films, optical loss increases, film shrinkages, etc.). Characterization of some of these properties seems to be improtant for further applications. Effective index and optical field distribution are two of the basic parameters of an optical channel waveguide. They can studied by using M-line measurement and near-field measurement.

In this presentation, we report on measurements of the effective indices of optical channel waveguides formed by UV bleaching and study of the effects of coplanar electrical poling. UV bleaching can be done either at room temperature or at elevated temperatures. Differences between room and elevated temperature bleaching are seen in terms of birefringence, film shrinkage, edge effects on the boundary between bleached and unbleached regions. Measurement and prediction made by effective index method are compared, and the causes of the discrepancies between prediction and measurement are discussed. Application of single mode optical channels on Mach-Zehnder interferometers and directional couplers is reported.
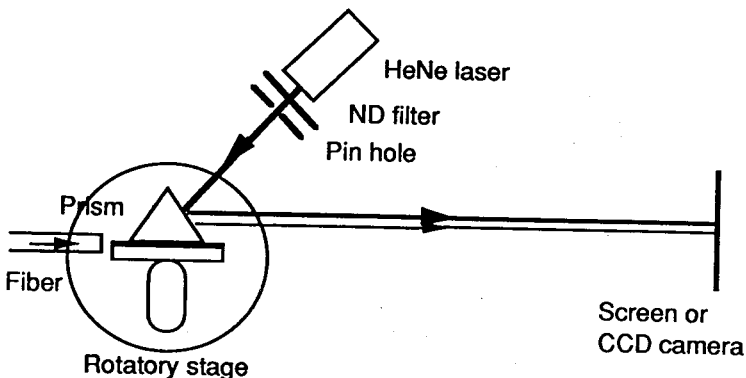
A/D-7
1100

MODELING PHOTOBLEACHED OPTICAL POLYMER WAVEGUIDES

Jiong Ma, Sihan Lin, Wei Feng and Alan R. Mickelson
Department of Electrical and Computer Engineering
University of Colorado
Boulder, Colorado 80309

One of the most efficient ways to prepare non-linear optical polymer channel waveguides is by photobleaching. The photobleaching method is the one which is most compatible with planar technology, and the one most suitable for integrated multilayer optical interconnect applications. In order to precisely control the index profile, modeling the photobleaching process is important. The ultimate goal of this modeling is to build a CAD tool based phenomenological model that will predict the optical properties of the polymer waveguides.

In this paper, the properties of th bleached photopolymer for a given set of fabrication parameters will be discussed. A simulation tool based on Beer's law and a local chemical reaction equation will be presented. Fitting techniques will be discussed and compared using experimental data. The use of Kramers-Kronig relation to predict the index profile of the polymer waveguides will also be addressed. We have experimented with PMMA based side-chain and polyimide based guest-host non-linear optical polymer materials and with the high chromophore concentrations, the model shows that the bleaching is non-uniform. Once the index profile of the optical polymer channel waveguides is determined, it is possible to calculated the optical field distribution and loss as well as design active electro-optical modulators.

index profile at 830 nm
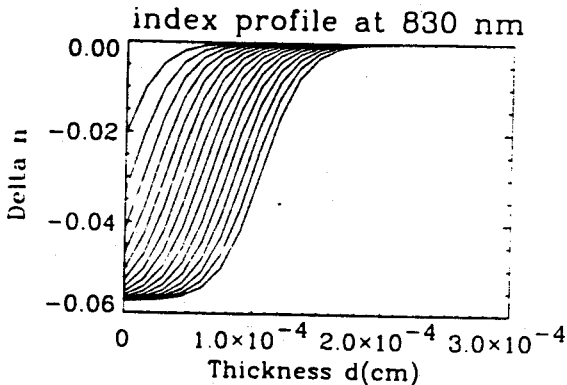
UV BLEACHING OF NLO POLYMERS FOR FORMATION OF CHANNEL WAVEGUIDE

Sihan Lin, Jiong Ma, Wei Feng

H. Brian. Hooker, and Alan R. Mickelson

Department of Electrical and Computer Engineering

University of Colorado at Boulder

Boulder, Colorado 80309-0425

The knowledge of the index profile of a UV bleached polymer film is crucial in designing optical guided wave devices. In this paper we present a method to obtain the index profile of a bleached polymer film from its absorption spectrum. The narrow-band and the broad-band UV-bleaching experiments on both PMMA-based side-chain and polyimide-based guest-host NLO polymer systems have been studied. The absorption measurements showed that the different wavelength UV bleaching sources cause the same kind of change in the absorption spectrum, however the shorter wavelength UV light bleached NLO polymer faster than that of the longer one. Based upon this point, we introduced a pseudo bleaching source for each wavelength and developed a white bleaching model. The absorption at each wavelength for different bleaching times and different thicknesses of the film can be solved from a set of absorption spectra of the films at several different bleaching times. The absorption at unmeasured wavelength region has been modeled. The M-line measurements showed that the polyimide-based polymer has larger birefringent effect than the PMMA-based polymer, this is explained by the inhomogeneity of the polyimide. The effects have been studied and modeled on the absorption due to the shrinkage and the coloring of the base polymers. An index profile of a bleached film has been determined by using the Kramers-Krönig relation. This generic approach is material independent, and is easy to use to predict the index profile of a bleached film with any thickness and bleaching time. The predicted effective indices of the films agreed with the measurements.

A/D-9
1140

ERBIUM DOPED SILICON LUMINESCENCE
Prof. R.J. Feuerstein, Prof. J.I. Pankove, J. Torvik,
L. Nichols, B. Willner
Department of Electrical Engineering
University of Colorado
Boulder, CO 80309-0425

The success of erbium doped optical amplifiers are one example of the utility of rare earths in glasses. In recent years there has been increasing interest in rare earth doped semiconductors. The inner 4f shell electronic transitions in these materials provide for fixed luminescence bands which are almost host independent. With electronic pumping of the rare earths in semiconductors, there would be no need for an extra optical source for pumping the rare earths. This electrically pumped device (shown below) would be an integrated optoelectronic source or amplifier. We will discuss the issues for rare earths in semiconductor materials and their potential for applications in optoelectronics. Specifically we will present data on the 1.54 um luminescence of Er doped Si. This data will be contrasted with behavior in rare earth doped insulating crystals and glasses.

Reactive Ion Etched Rib Waveguide
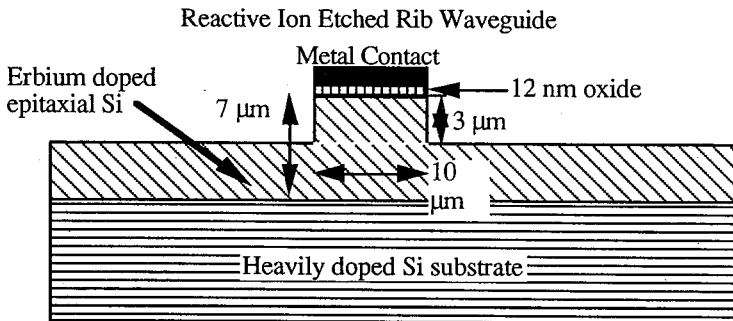
Electrons injected through thin oxide layer achieve energies of about 10 eV, enough to impact excite the Er ions.

B6-1   PETR BECKMAN A RENAISSANCE MAN
0900   Frank S. Barnes
Department of Electrical and Computer Engineering
University of Colorado at Boulder
Boulder, CO 80309-0425

In this brief paper we will review some of Petr's activities outside the field of the scattering of electromagnetic waves. Petr was an artist, a musician, a linguist, a humorist, a scientist, a mathematician, an educator, a political historian, a publisher, a rancher and a strong advocate for free enterprise and nuclear power. In short he was an active contributor to the world he lived in and his contributions covered a far broader range of intellectual activity than most of us in this era of specialization are able to read about let alone contribute to.

B6-2   **BECKMANN'S CONSTRUCTION OF NON-GAUSSIAN**
0920   **TWO-DIMENSIONAL PROBABILITY DENSITY**
          FUNCTIONS FROM THEIR MARGINALS AND
          CORRELATION COEFFICIENTS

Ezekiel Bahar
University of Nebraska-Lincoln
Lincoln, Nebraska 68588-0511

Petr Beckmann, in his book on Orthogonal Polynomials for Engineers and Physicists (The Golem Press, Boulder, Colorado 1973) developed a technique to construct two-dimensional probability density functions $p(x,y;\tau)$ from their marginals $p(x)$ $p(y)$ and correlation coefficients $R(\tau)$ with the aid of orthogonal polynomials. Beckmann's shows that the joint probability density function he constructs decorrelates into the product of the marginals when $R(\tau \rightarrow \infty) \rightarrow o$ and for $R(\tau=o) = 1$, $p(x,y;o) = \delta(x-y)p(x)$ (where $\delta(.)$ is the Dirac delta function). Furthermore $R(\tau)$ is equal to the ratio of the covariance and the variance of the identically distributed random variables. Thus the joint probability density function constructed by Beckmann is very useful for analyzing scattered electromagnetic fields from random rough surfaces.

Of particular interest are the family of joint probability density functions whose marginals are chosen to be the gamma functions of order K. The gamma function of order K=1 corresponds to the exponential probability density function. For K>>1 the gamma function corresponds to a Gaussian probability density function with a non-zero mean. However, since the range of the random variable is $(0,\infty)$ the gamma function is not symmetric about the mean . When the Gamma functions are used for the marginals, the associated orthogonal polynomials are the Laguerre polynomials. In his book on orthogonal polynomials, Beckmann also uses his construction of the joint probability density function $p(x,y;\tau)$ to derive the expression for the probability density function of the derivative of the random variable $p(x')$. Thus Beckmann's work on non-Gaussian probability density functions can be used to analyze scattering from realistic models of random rough surfaces. In addition his work is particularly suited to modeling problems of scattering from random rough surfaces that are coated by dielectric materials. Use of Gaussian probability density functions to model coated rough surfaces leads to convergence problems since the thickness of the coating material can never be negative.

B6-3
0940

THE SCATTERING OF LIGHT FROM TWO-DIMENSIONAL, RANDOMLY ROUGH, PERFECTLY CONDUCTING AND METALLIC SURFACES
P. Tran
Code CO 2313
Naval Air Warfare Center - Weapons Division
China Lake, CA 93555
V. Celli
Department of Physics
University of Virginia
Charlottesville, VA 22901
A. A. Maradudin
Department of Physics
and Institute for Surface and Interface Science
University of California
Irvine, CA 92717

We present results of computer simulation studies of the co-polarized and cross-polarized, in-plane and out-of-plane, scattering of a finite beam of p-polarized light incident normally on large rms height, large rms slope, two-dimensional, randomly rough, perfectly conducting and metallic surfaces. The scattered electromagnetic field is expressed in terms of the surface magnetic current and the surface magnetic and electric currents, respectively, through the use of the Franz equations. The Stratton-Chu equations are used to obtain the inhomogeneous integral equations satisfied by the independent components of these surface currents. These integral equations are converted into matrix equations that are solved by the Neumann-Liouville iterative method for each of 100-150 realizations of the randomly rough surface that are generated numerically on a 64×64 grid covering an area $L^2 = 16\lambda \times 16\lambda$ of the xy-plane, where λ is the wavelength of the incident light. Thus a system of 8192 equations in 8192 unknowns has to be solved for scattering from the perfectly conducting surface, while a system of 24576 equations in 24576 unknowns has to be solved for scattering from the metallic surface. The rms height of the surface is λ, while the transverse correlation length of the roughness is 2λ. Convergent results are obtained when terms through the 10th iterate are retained in the solution for the perfectly conducting surface, while terms through the 6th iterate are retained in the solution for the metallic surface. In both cases the results display the phenomenon of enhanced backscattering.

B6-4
1020
PETR BECKMANN, HIS THEORY ON WAVE SCATTERING FROM
ROUGH SURFACE, AND MISCELLANEOUS OTHER SUBJECTS
Prof. V.I. Tatarskii
University of Colorado/CIRES
& NOAA/ERL/Wave Propagation Laboratory
Boulder, CO 80309

I will discuss Beckmann's pioneering works in the theory of wave scattering from rough surface and his activity in some other branches of knowledge and areas in which he was a contributor.

B6-5   STATISTICAL DISTRIBUTION
1040   OF
        ELECTROMAGNETIC FIELDS (BECKMANN)
        APPLIED TO
        ANTENNA ARRAY ERROR ANALYSIS

D.G. Dudley
Electromagnetics Laboratory
ECE, Building 104
University of Arizona
Tucson, AZ 85721, USA

Results from the statistical distribution of the amplitude and phase of electromagnetic fields (P. Beckmann, *J.Res. NBS* 66D, 231-240, 1962; P. Beckmann and A. Spizzichino, *The Scattering of Electromagnetic Waves from Rough Surfaces*, MacMillan, New York, 1963) have been applied by the author to the analysis of errors in antenna arrays. We review two cases.

The first is the case of phase errors in end-fed traveling wave arrays (D.G. Dudley, *Radio Science* 3, 1132-1143, 1968). The expectation of the Fraunhofer power response is derived and the complete probability distribution in the sidelobe region is obtained, based upon the formalism in the Beckmann paper and the subsequent book with Spizzichino. Results are verified by Monte Carlo methods.

The second is the case of two-dimensional arrays of waveguide line source antennas (D.G. Dudley, *Canadian J. Phys.* 48, 852-858, 1969). The errors are assumed to have been caused by dissimilarities in waveguide cross section. Again the expectation of the Fraunhofer power response is derived, followed by the complete probability distribution in the sidelobe region. Results are verified by Monte Carlo methods.

Although the author never met Professor Beckmann, his dissertation and early work at the Autonetics Research Center was based on Beckmann's results for rough surface scattering, as reviewed above. It is interesting that the author's application was in a field quite different from the field of Beckmann's study.

SEA SCATTER IN THE SMALL

L. B. Wetzel and M. Sletten
Naval Research Laboratory
Washington, D.C. 20375

ABSTRACT

In view of the complexity of the sea surface, sea scatter has generally been approached as a statistical problem, in which the scattering behavior is expressed primarily in terms of variances and spectra. On the other hand, this very complexity poses a challenge to understand the fundamental nature of the scattering process at a surface which is, after all, controlled by hydrodynamic laws and is subject to close experimental scrutiny. In this paper we discuss some of the recent work conducted at NRL in ultra-high-resolution investigations of scattering by disturbed water surfaces in the wave tank, showing how the temporal evolution of both the polarization state and the ultra-wide-band scattering transfer function reflect the rapidly changing morphology of the surface scattering elements. In addition, we describe bench measurements of rigid scatterers that help explain some of the phenomenology. The characteristic spikiness of sea scatter observed with high-resolution probes is attributed to the origin of the scattered signal in localized geometrical events such as regions of high surface curvature, or reentrant structures associated with microbreakers and other non-linear surface objects. The difficult problem of incorporating this behavior into a general characterization of sea scatter is discussed in terms of the various analytical models available.

SPECTRUM ISSUES FOR THE EMERGING WIRELESS SERVICES
Chairman: Richard D. Parlow, NTIA, Washington, DC 20230
Organizers: R.D. Parlow; D.J. Cohen, NTIA/OSM, Annapolis, MD 21401; and George H. Hagn,
Information, Telecommunications and Automation Division, SRI International,
Arlington, VA 22209-2192

E2-1
0900

OVERVIEW OF SPECTRUM ISSUES FOR THE
EMERGING WIRELESS SERVICES
R.D. Parlow, Associate Administrator
National Telecommunications and Information
Administration, Room 4009
U.S. Department of Commerce
14th & Constitution Avenue,N.W.
Washington, D.C. 20230

Spectrum issues are an important element for the future
implementation of the emerging wireless services. This talk discusses
these issues, particularly emphasizing regulatory matters such as
spectrum allocation. The issues to be discussed include: (1) the recent
rulings by the FCC on the division of the 2 GHz PCS bands into various
size spectrum blocks to satisfy the various user classes and the
auctioning of the PCS spectrum, (2) the reallocation of Federal spectrum
to the private sector to support future emerging wireless services, (3)
the NTIA "refarming" initiatives, and (4) the current thinking of the NTIA
Strategic Planning Initiatives on the spectrum needs to support the
emerging wireless services. Other timely spectrum issues will also be
discussed.

E2-2
0920

SPECTRUM CONSIDERATION FOR WIRELESS
LOCAL AREA NETWORKS AND PRIVATE BRANCH
EXCHANGES

Lawrence A. Wasson, Electronics Engineer
Office of IRM Policy, Planning, and Oversight
U.S. Department of Energy
HR-425, Room C108
Germantown, MD 20874

This paper provides an overview of the current efforts and findings on wireless devices with emphasis on the spectrum management aspects and presents areas that deserve future consideration by the spectrum management community.

In early 1990, one of the Energy Department facilities proposed using a wireless LAN to assist scientists requiring communications between remote PCs and a mainframe computer. Correspondence with the user indicated that the wireless LAN was viewed as simply a "walkie talkie" with no safeguards in place, thus interim policy to address environmental health and electromagnetic compatibility factors, security, and work force concerns was hastily put into effect. Since comprehensive management or operational plans or controls had not been formulated for devices that would shortly support a variety of Federal Government businesses while authorized under the low power rules, it was obvious that some longer term Departmental effort should be focused in this area.

During February 1991, a report entitled, "Wireless Information Systems," was distributed within the Department of Energy to solicit IRM and Spectrum Managers' comments on planning and use of wireless transmission technology that provide integrated radio and information system services. Efforts associated with this document raised awareness of this new technology, assisted in identification of potential environmental problems and served as a catalyst to gain insight on wireless devices by conducting evaluations of wireless LANs and PBXs.

E2-3   SPECTRUM EFFICIENT AND COST EFFECTIVE USE
0940   OF THE LAND MOBILE INFRASTRUCTURE
            David J. Cohen
            U.S. Department of Commerce
            National Telecommunications and Information
            Administration
            179 Admiral Cochrane Drive
            Annapolis, MD 21401

The National Telecommunications and Information Administration (NTIA) was required by the NTIA Organization Act (November 1992) to develop and commence implementation of a plan for Federal agencies to use wireless mobile technologies that are spectrum efficient and cost effective. As background, preliminarily, NTIA, assisted by the Federal user agencies, performed an analysis of the current Federal land mobile infrastructure and identified candidate methods to improve spectrum efficiency and cost effectiveness. This talk discusses the technical and economic findings from the analysis.

The analysis demonstrated that certain techniques such as trunking, rechannelization of frequency channels, digital coding, voice compression and multiple access techniques (FDMA,TDMA,CDMA) have the potential to improve spectrum efficiency for Federal land mobile systems.   Also, computerized analysis methods combined with appropriate data bases can determine operational spatial separations which are spectrally efficient.

Also addressed was an examination of methods which would assure that the Federal telecommunications land mobile infrastructure is cost effective. It is shown that the inclusion of "economy of scope" in the design of the land mobile infrastructure may be an important attribute to help realize both cost effectiveness and spectrum efficiency. "Economy of scope" exists when the cost of a single network is less than the cost of several individual networks.

E2-4   SPECTRUM   ISSUES   FOR   INTELLIGENT   VEHICLE
1000   HIGHWAY SYSTEMS
        K.C. Allen, Acting Deputy Director, Spectrum
        Institute for Telecommunication Sciences
        325 Broadway
        Boulder, Co.   80303

On December 18, 1991, President Bush signed the Intermodal Surface Transportation Efficiency Act of 1991 (ISTEA). The purpose of the Act is stated as: "... to develop a National Intermodal Transportation System   that   is   economically   efficient   and environmentally sound, provides the foundation for the Nation to compete in the global economy, and will move people and goods in an efficient manner." The Act funds the Intelligent Vehicle Highway Systems (IVHS) program consisting of a range of advanced technologies and concepts which, in combination, can improve mobility and transportation productivity, enhance   safety,   maximize   the   use   of   existing transportation facilities, conserve energy resources, and reduce adverse environmental effects.

The   application   of   advanced   technology   and concepts to the transportation infrastructure will increase the requirement for information interchange and processing, not only within the infrastructure, but between vehicles, and between vehicles and the infrastructure.   The ubiquitous application of telecommunications will be required. Initial steps are already underway to develop and deploy IVHS systems.   A list of 27 user services are being developed   cooperatively   by   the   Department   of Transportation, and industry, to satisfy the needs of IVHS.   The user services range from pre-trip travel information to route guidance, and from collision avoidance to fully automated vehicle operation. The current efforts for implementation of IVHS systems include development of a national architecture to support the 27 user services, and small scale operational testing of concepts and equipment for early deployment of some systems.

IVHS communications will be accomplished using a range of systems, from existing and emerging wireless commercial services to dedicated IVHS systems. IVHS will increase the spectrum usage of both commercial services and private systems. It is essential that radio spectrum be available for IVHS through all its stages, now during its initial experimental stage through the time when it becomes an essential part of our national infrastructure.

E2-5
1040

MONITORING THE NEW PERSONAL COMMUNICATIONS SERVICES (PCS) BANDS

G. H. Hagn
Information, Telecommunications and Automation Division
SRI International
1611 N. Kent Street
Arlington, VA 22209

Through the initiative of Rep. John D. Dingell (D–MI) and others in the Congress, the Omnibus Budget Reconciliation Act of 1993, signed by President Clinton last summer, authorized the National Telecommunications and Information Administration (NTIA), acting on behalf of the President, to identify and transfer a minimum of 200 MHz of Federal Government spectrum to the Federal Communications Commission (FCC) for use by industry for new and emerging technology, including Personal Communications Services (PCS). The technical and economic successes of citizens' band (CB) radio in the 1960s and 1970s and cellular radio in the 1980s led the Congress to believe that the economic value of the spectrum (see H. J. Levin, *The Invisible Resource, 1971*) could be quantified and also could be used to benefit the U.S. Treasury if it was auctioned. The experience with cellular radio frequency assignments (an administrative law judge for the top 30 markets, and then a lottery) indicated that the next logical step in the evolutionary assignment process was an auction. The Congress included the requirement for auctions in the legislation. On 23 September 1993, the FCC decided on how to implement the new law. Meanwhile, the NTIA is deciding on which 200 MHz will be transferred to the FCC.

SRI International pioneered spectrum occupancy measurements to document usage while working with the FCC in the late 1960s, the Office of Telecommunications Policy (OTP) and the Office of Telecommunications (OT) in Commerce in the early 1970s--and their successor organization, the NTIA. SRI worked with NTIA to develop a definition of channel occupancy as a random variable (A. D. Spaulding and G. H. Hagn, *IEEE Trans. EMC* , 1977), and this definition achieved international acceptance (*CCIR Report 660*, 1978). This paper explores the use of spectrum monitoring for channel and band occupancy using several inexpensive remotely–controllable equipments in each major U.S. population center to document changes in spectrum usage in the evolving PCS bands. Some observations are offered on the use of spectrum occupancy data to better define the technical and economic spectrum efficiency improvements.

E2-6   SPECTRUM EFFICIENCY OF MOBILE RADIO SYSTEMS
1100   Robert J. Matheson

U.S. Department of Commerce, NTIA/ITS.S
325 Broadway
Boulder, Colorado 80303

There is a great increase in demand for many types of mobile/personal radiocommunication services. These services include cellular telephone, personal communication services (PCS), wireless LANs, conventional mobile radio, and others. The demand has caused substantial crowding in the available frequency bands, and much effort is underway to find more spectrum-efficient methods to provide these services.

Various mobile radio systems utilize a wide variety of architectures and technologies, producing a substantial difference in spectrum efficiency (i.e., erlanges/kHz/km^2). Although it is difficult to directly calculate spectrum efficiency, an approximate comparison of spectrum efficiencies can be fairly easily performed. This paper defines a method to compare spectrum efficiency of mobile system. This method is used to compare the spectrum efficiency of about 20 contemporary mobile/personal radio systems to conventional analog FM voice radio.

A somewhat surprizing conclusion is that systems in use today and planned for use in the immediate future cover a very wide range of spectrum efficiencies-- from 10,000 times more efficient than conventional mobile radio to 40 times less efficient.

E2-7   ELECTROMAGNETIC COMPATIBILITY OF 404 MHZ WIND PROFILERS
1120   Russell B. Chadwick
          Profiler Program Office, Forecast Systems Laboratory
          NOAA Environmental Research Laboratories
          Boulder, Colorado   80303-3228

Introduction

Wind Profilers are upward looking, highly sensitive Doppler radars. They are specifically designed to measure vertical profiles of the horizontal wind by using the energy scattered from half wavelength refractive index inhomogeneities in the clear atmosphere. Profiles of vertical wind, scattered power, turbulent energy dissipation, and temperature are also made. NOAA has deployed a network of thirty 404.37 MHz wind profilers in the central United States and is operating it for operational and research purposes. There are some unique electromagnetic compatibility issues associated with this wind profiler network and this paper discusses two of them.

Site Selection

Prior to deploying the profilers an extensive site selection activity was planned and carried out. This involved: detailed site selection criteria; calculated interference levels at each site; a preliminary on-site RF spectrum measurement; and a final RF survey at selected sites which involved a 96 hour on-site measurement. Experience has shown that this site selection activity was successful as the installed profilers have proven to be free of interference from off-site sources. The site selection criteria and the RF surveys are described and several examples of data collected during the final surveys are presented.

Spectrum Sharing

Spectral sharing occurs routinely between the profiler network and a satellite based system. NOAA's Search and Rescue Satellite Aided Tracking (SARSAT) system has receivers at 406.1 MHz carried aboard polar orbiting satellites. When the satellite passes through the main beam of a wind profiler, energy from the side bands of the profiler transmitted signal can cause interference to the SARSAT system. However, because of the two different ways that the Profiler and the SARSAT system use the radio frequency spectrum, there is opportunity for spectral sharing. This allows for normal operation with no impact to SARSAT and only minor impact to the Profiler. The operational procedures that bring about this spectral sharing are described and simulation results illustrating it presented.

PROPAGATION AND ENVIRONMENTAL MEASUREMENTS RELATED TO PROPAGATION
Chairman: Julius Goldhirsh, APL/JHU, Laurel, MD 20723-6099

F4-1   THREE YEARS OF C-BAND FADE, DIVERSITY
0840   AND DURATION STATISTICS FOR OVER-WATER,
         LINE-OF-SIGHT PROPAGATION LINKS
         IN THE MID-ATLANTIC COAST REGION
         G. Daniel Dockery, Julius Goldhirsh, and Bert H. Musiani
         The Johns Hopkins University, Applied Physics Laboratory
         Johns Hopkins Road, Laurel, Maryland 20723-6099

Three years of fade statistics are described for two over-water, line-of-sight propagation links in the Mid-Atlantic coast of the United States operating at 4.7 GHz. The 44 km and 39 km links are comprised of a single transmitter located at Parramore Island, Virginia and two receiver sites on Assateague Beach, Virginia. The receiver sites are separated by approximatey 5 km. Single terminal and joint fade and fade duration statistics derived from time-series of received signal losses due to refractive and diffractive effects are described for combined years, annual, and monthly cases. In particular, year to year and month to month variabilities in the statistics, and the efficacy of employing space diversity for the two links to mitigate fade margin requirements are examined. The meteorology associated with sustained deep fades (SDF) which biased the annual statistics are described in a companion paper.

The salient results for both links are as follows: [1] SDF events due to severe subrefraction during the three-year period tended to dominate the statistics. These events simultaneously occurred at both sites during the period November–July and did not occur during August–October. [2] The peak probability months over which SDF events simultaneously occurred at both sites were December through March. [3] The year-to-year variability in the annual fade statistics were relatively small. [4] The yearly variability in the monthly statistics were large, especially during April–July with June exhibiting the maximum spread. [5] The August–October probabilities versus fade values may be approximated by exponential decaying functions. [6] September was the "best" month showing smallest fades and December was the "worst" month experiencing maximum fading. [7] During the months of November–July, space or route diversity techniques proved to be ineffective for the two links. [8] The months November–July (SDF months) showed minimal probability changes in the fade durations during the first 120 seconds for fade thresholds ranging from 15 dB–35 dB, whereas the August–October (non-SDF months) period showed considerable variability in probability changes. [9] SDF events exhibiting fades in the range 20 dB–60 dB were simultaneously observed at both sites for durations as large as 48 hours.

F4-2
0900

METEOROLOGY ASSOCIATED WITH SUSTAINED DEEP
FADES AT C-BAND FOR OVER-WATER, LINE-OF-SIGHT
PROPAGATION LINKS IN THE MID-ATLANTIC COAST
Julius Goldhirsh, G. Daniel Dockery, James H. Meyer
The Johns Hopkins University, Applied Physics Laboratory
Johns Hopkins Road, Laurel, Maryland 20723-6099

The morphology of deep and long lived fades for line-of-sight, over-water propagation links in the Mid-Atlantic coast are examined. Such events, known as *sustained deep fades (SDF)*, are analyzed employing weather maps, in situ measurements from radiosondes, an instrumented helicopter, and sensors on coastal platforms. These events occurred during the contiguous nine-month period October–July and none were simultaneously observed at both links during August–September for each of the three years in which fade statistics were amassed. The SDF events biased the three year fade statistics described in a companion paper.

The results have demonstrated that synoptic weather conditions created by a sustained high pressure system over the subtropical Atlantic and/or a sustained low pressure system whose center lies west of the coastal region results in a steady flow of warm, humid air at altitude. When coupled with colder water conditions, such a flow results in a surface temperature inversion, an increase of water vapor pressure with altitude, and a positive lapse rate of the radio refractivity. This highly unusual condition causes severe subrefraction resulting in fades ranging from 20 dB to 60 dB for durations in excess of 2 hours and lasting as long as two days. Propagation modeling using a refractivity profile derived from sensors on board a helicopter during an SDF event confirmed the range of fades measured during that period.

F4-3
0920
ENVIRONMENTAL MEASUREMENTS AND
REFRACTIVITY MODELS FOR OVER-WATER
PROPAGATION
John R. Rowland and James H. Meyer
The Johns Hopkins University, Applied Physics Laboratory
Johns Hopkins Road, Laurel, Maryland 20723-6099

A series of fixed boat measurements of temperature and humidity were made off the coast of California, in the vicinity of San Nicholas Island and off the coast of Wallops Island, Virginia. These measurements were made at fixed heights above the ocean surface of 2 cm, 1 m, 2 m, 10 m, and 30 m. In addition, a kytoon was employed which extended these measurements from 30 m to 300 m. The temperature and humidity values were converted to radio refractivity profiles which were compared with those derived from three different evaporation duct profile models referred to as models #1, #2, and #3. Model #1 employs a knowledge of the refractivity only at the 6 m level. Model #2 uses the refractivity at heights of 2 cm and 6 m, and model #3 requires the refractivity at 6 m and the surface water temperature. Each of the models were tested through comparison of the measurements made at the other altitudes.

In this paper are given (1) a description of the above measurement system, (2) a review of the three evaporation radio refractivity profile models employed, and (3) a description of how well each of the models performed in predicting the radio refractivity profiles through comparisons with the refractivity values measured at the other heights.

F4-4   COASTAL ATMOSPHERIC REFRACTION AND
0940   REMOTE MEASUREMENTS
           K. L. Davidson and C. H. Wash
           Department of Meteorology, Code MR
           Naval Postgraduate School
           Monterey, CA 93943-5000

Calibration/validation studies were performed on airborne and ground-based remotely sensed marine atmospheric boundary layer and ocean surface conditions. Inferred boundary layer and surface dynamic and thermodynamic properties have been related to in situ measured refractive properties. The studies were performed in coastal regions or in regions with persistent sea surface temperature (SST) fronts. They were in the vicinity of a subtropical front in the west North Atlantic (FASINEX-1986), off the west Norwegian coast during ERS-1 pre-, and post-launch experiments (NORCSEX-1988 and - 1991), off the central California coast (GB-HIS and -1992), and off the southern California coast (VOCAR - 1993).

In situ calibration/validation and ground-based remotely measured (GB-HIS) data were obtained from ship mounted systems. Other remotely sensed data were obtained both from aircraft (FASINEX and NORCSEX'88) and from operational (FASINEX, VOCAR, NORCSEX'88 and '91) and research (NORCSEX'91) satellite borne sensors. A wide range of atmospheric boundary layer and ocean surface conditions occurred in these studies.

Near-surface refraction conditions were assumed to vary with remotely sensed variations in near-surface turbulence (wind speeds) , in surface temperature (SST), and in overlying air dryness. All of these are detectable in operational and research remote sensors. Gradient properties at the top of the boundary layer, determined from radiosondes, were related to cloud type as detected by airborne sensors and to the GB-HIS, a ground-based infrared High Resolution Interferometer Sounder (HIS) system, detected changes of thermal and moisture structure of marine boundary layer.

In all cases, remotely sensed information does not provide the vertical detail possible with in situ data. The remote data describe horizontal and temporal variations not described by the point measured in situ data. The latter are important in the coastal and SST front regions.

F4-5   **VARIABILITY OF COASTAL ATMOSPHERIC REFRACTIVITY**
1000   **(VOCAR) EXPERIMENT RADIO MEASUREMENTS**
        Ted Rogers
        Tropospheric Branch, Code 543
        Naval Command, Control and Ocean Surveillance Center, RDT&E Division
        San Diego, CA 92152-7385

       Variability of the atmospheric refractive structure changes the detection range of active and passive electromagnetic sensors. Present air/sea sensing technology assumes range independent refractive profiles. In coastal areas however, range independent profiles may be the exception rather than the rule. From June 1, 1993 until September 5, 1993 radio measurements were made on the paths illustrated in figure (1). CW transmitters installed on the northeast end of San Clemente Island and existing VHF and UHF Automatic Terminal Information System (ATIS) transmitters at NALF San Clemente Island, John Wayne Airport, Tustin MCAS and NALF San Clemente transmit signals whose intensity is measured at NAWCWPNS Point Mugu and NRaD San Diego. Time series and correlations are used to assess temporal and spatial variability for the described paths.
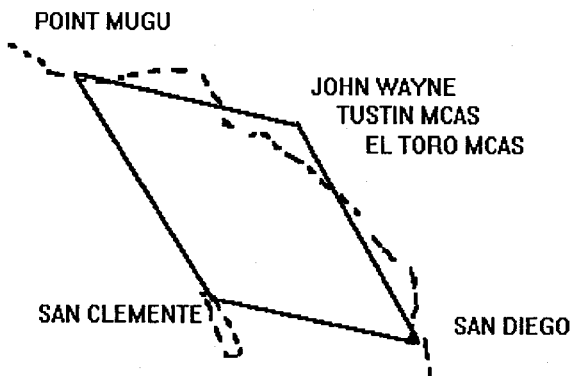
Figure (1) . Paths in southern California bight.

F4-6   9.6 GHZ PROPAGATION IN THE EVAPORATION DUCT: MODEL
1040   PREDICTIONS AND COMPARISONS TO DATA

Richard A. Paulus
Tropospheric Branch, Code 543
Naval Command, Control and Ocean Surveillance Center, RDT&E Division
San Diego, CA 92152-7385

In 1972, a series of radio propagation measurements in the 1 to 40 GHz frequency range was performed in the eastern Mediterranean. A 35.2 km over-the-horizon propagation path was established between the islands of Naxos and Mykonos in the Aegean Sea. Although measurements were conducted during four different periods throughout the year, only the last period, in November 1972, included meteorological measurements on both islands. Measurements of air and sea temperature, relative humidity, and wind speed were made hourly at the receiver site at Ornos Beach on Mykonos. On Naxos, air temperature and relative humidity were measured hourly, wind speed was recorded every three hours, and sea temperature was measured twice daily at a Greek meteorological station. A qualitative comparison of evaporation duct heights for these two sites showed reasonable agreement and the trends in duct height agreed with trends in the radio data (Richter and Hitney, NOSC TD 1209, 1988, NTIS acc. no. AD-A192311/9/XAB). These data have been re-analyzed quantitatively with the Engineer's Refractive Effects Prediction System (EREPS), the Radio Physical Optics (RPO) propagation model assuming horizontal homogeneity of the evaporation duct as characterized by the Mykonos meteorological data, and RPO utilizing the data at both Mykonos and Naxos. To accomplish the latter, the Naxos wind speed and sea temperature data were linearly interpolated to hourly values. Comparisons of predicted propagation loss by the three approaches to the observed data show the influences of the EREPS single mode assumption, surface-layer stability, and range-varying evaporation ducting. Despite the limitations in the meteorological data, correlations of predicted to observed loss exceeded 0.76 for an X-band link that had 77 dB signal variation during the 15 day period. A sample comparison is shown below.

Greek Islands 1972 Experiment
(range-dependent environment)

191
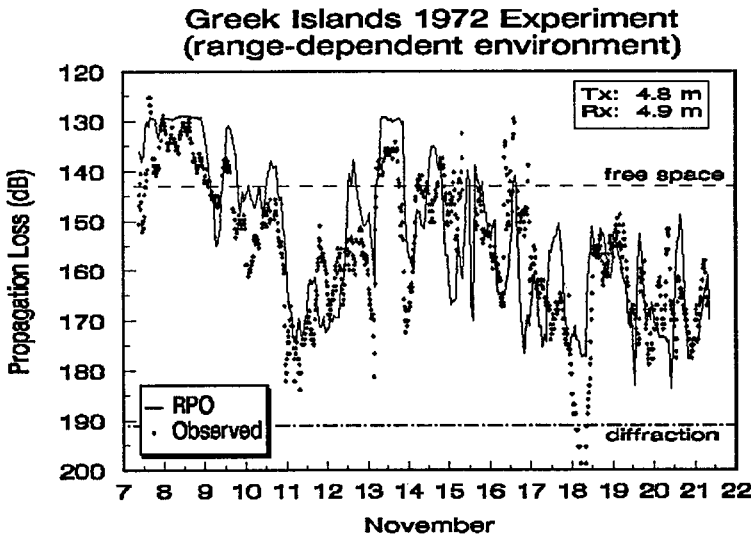
F4-7   **RADAR DETECTION OF LOW-ALTITUDE TARGETS IN A**
1100   **MARITIME ENVIRONMENT: FINAL ANALYSIS**

Kenneth D. Anderson
Tropospheric Branch, Code 543
Naval Command, Control and Ocean Surveillance Center, RDT&E Division
San Diego, CA 92152-7385

Final results from an analytical and experimental effort to assess radar detection of low-altitude, short-range targets over the ocean are presented. A moderate power X-band radar was used to measure signal return from a set of calibrated targets which were carried on a high-speed ocean-going boat. In addition, surface and upper air meteorological sensors were used to monitor both vertical and range dependent refractivity conditions. From these observed refractive conditions, the NRaD RPO model is used to predict maximum target detection ranges for comparison to measured ranges.

The accompanying figure presents a summary of the measured detection ranges. The four symbol curves show the measured detection range for four one-way propagation loss thresholds. A 125 dB threshold is a typical propagation loss limit for a moderately capable radar; A 130 dB threshold corresponds to a limit for a state-of-the-art radar system; The 135- and 140 dB thresholds are possible limits for detection of targets that will be built in the future. The horizontal dashed lines on this figure represent the detection ranges expected in a standard atmosphere. For the moderately capable radar (125 dB threshold), nearly all of the detections occurred close to the range expected in a standard atmosphere. For the state-of-the-art radar, nearly half of the detections were at ranges *less* than expected. Detection ranges for the 135 dB threshold are sometimes much *greater* than expected but are generally about what is predicted for a standard atmosphere. For the 140 dB threshold, detection ranges are usually *greater* than expected.
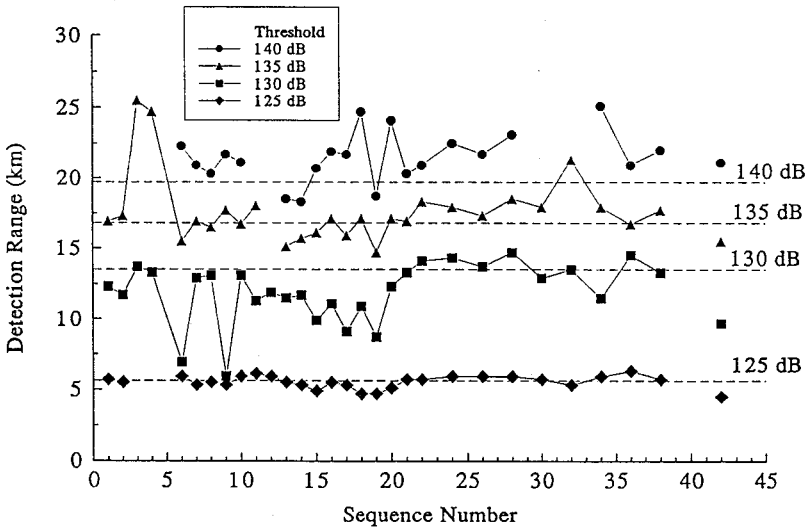
F4-8 **A COMPARISON OF ROUGH SURFACE**
1120 **PARABOLIC EQUATION MODELS**
Amalia E. Barrios
Tropospheric Branch, Code 543
Naval Command, Control and Ocean Surveillance Center,
RDT&E Division
San Diego, CA 92152-7385

Several parabolic equation models currently exist that model radiowave propagation over the ocean. Few of these models can accurately account for rough surface effects over an ocean environment. Several techniques to account for these effects, implemented within the split-step parabolic equation (PE) algorithm, are investigated.

Two of the rough surface algorithms to be discussed were originally developed to model acoustic wave fields incident on a rough boundary. The first model (M.E. Moore-Head, E.S. Holmes, JASA, 86(1), 247-251, 1989) is based on an angle-dependent surface loss function that is applied to the field in a layer near the surface. The second model (Tappert, private communication) does not depend on incident angle, but instead modifies the PE by including the impedance boundary condition as a singular index of refraction. The third method uses the mixed transform algorithm (J.R Kuttler, G.D. Dockery, Radio Sci., Mar.-Apr., 381-393, 1991), in which the impedance boundary condition is directly applied to the field at each range step. This method relies on an equivalent rough surface reflection coefficient, which is angle-dependent. The final method simply modifies the starter field by multiplying the rough surface reflection coefficient and the reflected field.

All of the above models will be compared with a reference waveguide model that is shown to agree well with signals measured in the presence of slight to moderate sea states.

F4-9 **AN APPROXIMATE MODEL FOR VERTICAL POLARIZATION AND**
1140 **SURFACE ROUGHNESS USING THE PARABOLIC EQUATION**

Herbert V. Hitney
Tropospheric Branch, Code 543
Naval Command, Control and Ocean Surveillance Center, RDT&E Division
San Diego, CA 92152-7385

An approximate method is presented that allows vertical polarization and sea surface roughness effects to be included in parabolic equation (PE) radio wave propagation models. This method was implemented in the hybrid Radio Physical Optics (RPO) propagation model, and several comparisons of RPO results to waveguide results are presented.

The simplest and fastest running PE models use fast Fourier sine transforms. These models give exact results for horizontal polarization, but only approximate results for vertical polarization. In addition, there is no known simple method to correctly simulate rough sea surface effects in PE models using sine transforms. For low elevation angles, waveguide models show vertical polarization and rough surface effects to be important primarily for surface duct or surface-based duct conditions, because of the strong interaction between the ducting and reflecting mechanisms. The method presented here is an empirical model that makes simple adjustments to the PE method for ducting cases, such that the PE results match the waveguide results.

The PE method is modified to account for surface-interaction loss by multiplying the magnitude of the lowest PE field value by a factor between 0 and 1 just prior to each PE range step. Comparisons of this technique show remarkably good matches to waveguide results, provided the proper loss factor is applied. Several methods have been used to determine the appropriate loss factor based on the modified refractivity profile for the duct. The figure below shows propagation loss versus height for a strong evaporation duct for the cases of horizontal and vertical polarizations over a smooth sea, and for vertical polarization over rough seas corresponding to wind speeds of 10 and 20 meters per second.

24 Meter Evaporation Duct
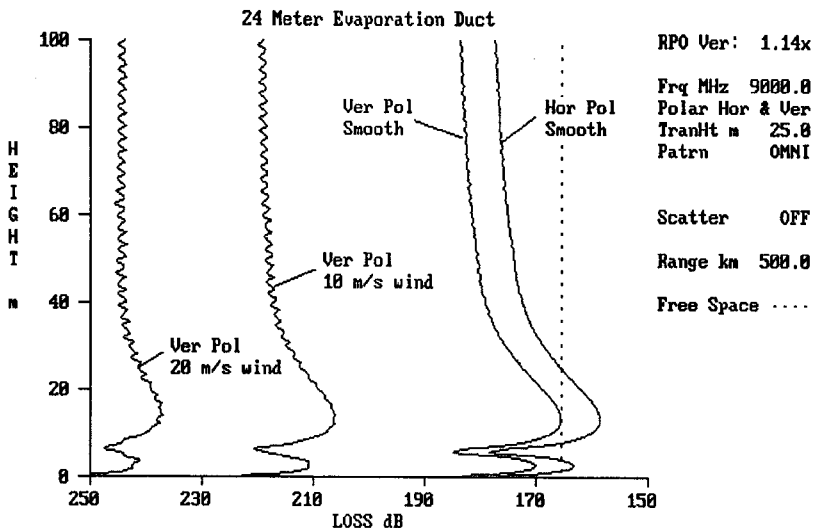
F4-10   SIGNAL FADING AND ANGLE-OF-ARRIVAL MEASURE-
1200   MENTS ON LINE-OF-SIGHT MICROWAVE PATHS.

Alan R. Webster, Thang Tieu and William K. Wong,
Department of Electrical Engineering,
The University of Western Ontario,
London. ONT. N6A 5B9.

Introduction.

Extensive observations on the signal fading on terrestrial line-of-sight links have been conducted over several consecutive fading seasons. Central to this exercise has been the operation of a system designed to resolve the incoming signal energy into individual rays, giving a measure of both the amplitude and, particularly, the angle-of-arrival (AOA) of these components. The system operates as CW at a frequency of 16.65GHz and the receiving system consists of a vertical wide-aperture array (666λ) with 16 equally spaced elements. Sampling the complex amplitude across this array, repeated once per second, leads in a straightforward manner to the desired AOA spectrum; the resolution is approximately 0.1°. Recent observations have been augmented by the operation of an acoustic sounder to provide some indication of the atmospheric structure which is the root cause of the fading.

Results and Discussion.

The original raw data has been processed to investigate the behaviour of the strongest rays encountered at a particular time. Up to three rays are chosen subject to the criterion that a limit of 20dB down from the amplitude of the strongest for that record be imposed. Under almost all circumstances, signal fading is associated with an elevated AOA for the strongest ray, ranging up to $+0.5^\circ$ relative to the normal value with a typical change of $+0.2^\circ$. From the behaviour of the AOA spectum with time, it is clear that two basic mechanisms are involved. Much of the time, the direct ray from transmitter to receiver is attenuated and elevated by a ground-based layer of more negative refractivity gradient than normal, the familiar "radio-hole" effect. This single direct ray then interacts with small amplitude ground reflected rays causing sharp deep fades on top of the more general slowly varying attenuation due to the de-focussing of the main ray. Less often, though not infrequently, an elevated anomalous layer results in true atmospheric multipath propagation in which a strong elevated refracted ray is seen at the receiver in addition to the "normal" path.

Evidence is also presented from the operation of the acoustic sounder in support of this scenario. In particular, elevated layers are often seen to grow out of the nocturnal ground based layer around dawn, producing the effects described above.

G4-1 GRAVITY WAVE SEEDING OF EQUATORIAL SPREAD F
0900

D. L. Hysell and M. C. Kelley
National Radio Science Meeting
School of Electrical Engineering
Cornell University
Ithaca, NY 14853

We will investigate the relationship between the day-to-day variability of equa-
torial spread F and the influence of internal gravity waves. Spread F is almost always
present in the post-sunset F region over Jicamarca during equinox periods, usually
taking the form of narrow bottomside scattering layers. Such layers, which may be
related to bottomside sinusoidal structures (BSS), are thought to represent the quasi-
normal mode of the collisional interchange instability with the fastest linear, nonlocal
growth rate. The horizontal wavelength of this mode is typically a few km. The
instability also gives rise to large-scale irregularities, but only if an external driver or
seed mechanism is initially present to enhance the growth rate of the long-wavelength
mode. The large-scale irregularities then enter the nonlinear phase of their growth,
ultimately producing the rising depleted regions and radar plumes characteristic of
topside spread F.

We will examine the ability of internal gravity waves to act as the seed mech-
anism. VHF radar data from Jicamarca and from Kwajalein show that the radar
plumes in spread F are often regularly spaced, with wavelengths that are larger than
any characteristic scale size of the ionospheric interchange instability but which are
within the realm of likely gravity wave scale sizes. We will discuss under what condi-
tions a gravity wave can drive plasma advection and how strong the seeding must be
to overwhelm nonlinear saturation and the kilometer-scale normal mode.

G4-2   DAY TO DAY VARIATIONS OF EQUATORIAL
0920   IRREGULARITIES

Jules Aarons
Center for Space Physics
Boston University
725 Commonwealth Avenue
Boston, MA 02215

Although the general pattern of equatorial F-layer irregularities as a function of latitude, longitude, and geophysical conditions is in hand, the day to day variations are still difficult to evaluate. The forcing functions for day to day variations appear to be neutral winds and electric field conditions. The data indicate that at times in "the irregularity season", irregularities are produced day after day. However nights of irregularities are at other times followed by one or more nights with an absence of irregularities.

For the equatorial region, using scintillation data at 136 MHz, we have correlated the occurrence of irregularities at several stations along a relatively narrow range of longitudes at various latitudes in the Pacific sector. The sites used are in the Philippines, Taiwan, and Korea. The correlation of daily occurrence was poor. For example at magnetically quiet times there are irregularities noted at a station such as Osan, Korea (dip latitude 30°) with little irregularity activity at Manila (dip latitude 5°), relatively close in longitude.

For latitudes somewhat higher that the anomaly region, the problem arises of separating polewards effects of the equatorial plumes and the equatorwards motion of irregularity development originating in the auroral region during severe magnetic storms.

A possibility exists for the generation of another class of F-layer irregularities at mid-latitudes with a body of data from Japan, Port Moresby, Osan, and Palehua, Hawaii. This is suggestive that at least in the Pacific region there is a low latitude generation of irregularities distinct from equatorial or auroral mechanisms.

G4-3   **MODEL STUDIES OF THE LONGITUDINAL VARIATION**
0940   **OF THE LOW LATITUDE AND EQUATORIAL IONOSPHERE**
          Amanda J. Preble, Phillips Laboratory
            PL/LIAF 3550 Aberdeen Ave, SE
            Kirtland AFB, NM 87117-5776
          David N. Anderson, Phillips Laboratory
            Hanscom AFB, MA 01731-3010
          Bela G. Fejer, Department of Physics/CASS
            Utah State University
            Logan, UT 84322
          James A. Whalen, Phillips Laboratory
            Hanscom AFB, MA 01731-3010
          Phil J. Wilkinson, IPS Radio and Space Services
            West Chatswood NSW 2057, Australia
          Roland T. Tsunoda, SRI International
            Menlo Park, CA 94025

We use results from the recently developed global equatorial vertical **ExB** drift model [Fejer, B.G., E.R. de Paula, R.A. Heelis, and W.B. Hanson, J. Geophys. Res., submitted 1993] as an input to the Phillips Laboratory Ionospheric Model (PLIM) and compare the calculated results with measurements made at Kwajalein (4° dip N) and Vanimo, Australia (10° dip S) as well as at Jicamarca, Peru (2° dip N) and Bogota, Columbia (16° dip N). The Phillips Lab model is a time-dependent, theoretical model which solves the coupled continuity and momentum equations for O^+ concentrations every two degrees dip latitude and every half hour local time from 160 to 1600 km in altitude. Differences have been observed between the Pacific and American sector diurnal vertical drift patterns and are especially apparent during evening prereversal enhancement and at night. Comparisons are presented in each sector both near the magnetic equator (Kwajalein and Jicamarca) and near the crests of the equatorial anomaly (Vanimo and Bogota) for June solstice, solar maximum conditions to investigate the effects of these longitudinal drift differences on the electron density distributions.

G4-4   PLASMA INSTABILITY GROWTH RATES IN
1000   THE EQUATORIAL NIGHTTIME IONOSPHERE

David N. Anderson
Geophysics Directorate
Phillips Laboratory
Hanscom AFB, MA   01731-3010

It is well known that the pre-reversal enhancement in upward E x B drift at the magnetic equator after sunset raises the ionospheric F layer to altitudes in the neighborhood of 500 to 700 km. At these altitudes the bottomside of the layer may become unstable to Rayleigh-Taylor and/or gradient drift plasma instability processes if proper seeding mechanisms are present. This paper examines the sensitivity of these instability growth rates to variations in the vertical E x B drift velocity, the transequatorial neutral wind pattern and the underlying ionization densities between the E and the F layer. The ambient (O^+) and electron density distributions are calculated by solving the coupled, time-dependent ion momentum and continuity equations, numerically. Required inputs include production, loss and diffusion rates, a neutral density, wind and temperature model, electron and ion temperatures and a vertical E x B drift pattern. Ion and electron density profiles are calculated as a function of latitude and local time for each set of input parameters. Given ambient ionospheric density distributions, flux tube integrated quantities such as tube content and flux-tube integrated Pederson conductivity are easily calculated. Plasma instability growth rates are dependent on these quantities and their gradients. The sensitivity of these growth rates to the daily variability in vertical E x B drift and neutral wind patterns are presented and discussed.

G4-5   ON THE VARIABILITY OF EQUATORIAL F REGION
1040   PLASMA DRIFTS

Bela G. Fejer and Ludger Scherliess
Center for Atmospheric and Space Sciences
Utah State University, Logan, UT 84322-4405

We use incoherent scatter radar observations from Jicamarca and Ion Drift Meter data from Dynamics Explorer-2 to study the variability of the equatorial F region vertical and zonal plasma drifts. During magnetically quiet periods, the variability of the vertical plasma drifts decreases with increasing solar flux. The solar minimum evening drifts near June solstice increase noticeably with magnetic activity. This effect is probably responsible for the corresponding increase of spread-F activity. The solar maximum evening drifts do not show a clear response to magnetic activity. The night sector shows velocity upward perturbations which maximize between midnight and dawn. The Jicamarca and DE-2 data show the absence of magnetic activity effects on the daytime zonal drifts. The nighttime zonal drifts show noticeable westward perturbations associated with disturbed conditions with the largest effects a few hours after the peak in magnetic and high latitude current activity.

G4-6   THE CHARACTERISTICS OF HIGH ALTITUDE BUBBLES
1100   Prof. W. B. Hanson
           Center for Space Sciences
           University of Texas at Dallas
           P. O. Box 830688 MS/FO22
           Richardson, TX 75083–0688

The DMSP F-10 spacecraft is in a 98° inclination round orbit near 830 km altitude. Its ascending node commenced about 19:30 LT and drifted from a solar zenith angle near 110 degrees to over 120 degrees during 1991, its first year in orbit. Surprisingly, this orbit has provided a rather large data base of equatorial bubble signatures obtained from the drift meter and scintillation meter, approximately 2 per day on average (out of ~15). The seasonal dependence of their occurrence on longitude will be presented. In addition, several rather unexpected features of the data will be discussed, i.e., smooth depletion regions associated with upward drift, the apparent break up of these features into structured plasma, the rather common high (>1km s^{-1}) vertical velocities, and also the high east and westward plasma drift velocities. The high latitude extent of some features is also noted.

G4-7 **MODIFIED GEOSTROPHY IN THE THERMOSPHERE**
1120

M. F. Larsen[1] and R. W. Walterscheid[2]
[1]Dept. of Physics, Clemson University, Clemson, SC
[2]The Aerospace Corp., Los Angeles, CA

We present a theory for modified geostrophic balance in the high latitutude thermosphere that includes the effects of both the Pedersen and Hall drag components on the neutral flow. The resulting balance between the Coriolis force, the pressure gradient, and the two drag components leads to predictions of large neutral flow velocities in the lower thermosphere around 110-120 km altitude. The direction of the neutral flow is oppositely directed to the plasma and the predicted flow velocity has typical magnitudes of 100-150 m/s. A further prediciton of the theory is that large shears are to be expected on the bottom side of the wind maximum. Finally, the balanced flow equations suggest that large convergence/divergence in the neutral flow is to be expected on the equatorward/poleward side of the auroral oval so that large vertical velocities are anticipated in those regions.

We present examples of diverse observations supporting the theoretical predictions, and we discuss the possible implications of the results for radar observations of the lower E region.

G4-8
1140

LIGHTNING-INDUCED HEATING
OF THE LOWER IONOSPHERE:
COMPARISON OF THEORY AND DATA

U. S. Inan
Space,Telecommunications and Radioscience Laboratory
Stanford University
Stanford, CA 94305-4055

Intense heating of the lower ionospheric electrons, by the electromagnetic pulses released in lightning discharges, has recently emerged as a new means of thermal, electrodynamic and aeronomic coupling between the troposphere, the mesosphere and the ionosphere (U. S. Inan et al., *Geophys. Res. Lett., 18*, 705, 1991). Fully kinetic modeling of the electrodynamic coupling has allowed detailed predictions concerning the measurable manifestations of the heating, namely the impact ion-ization of the neutrals and production of enhanced airglow (Y. N. Taranenko et al., *Geophys. Res. Lett., 20*, 1539, 1993a). Experimental data in the form of lightning-associated subionospheric VLF signal changes constituted the first observations of this effect and motivated the theoretical modeling. Observations of enhanced air-glow from the Space Shuttle (W. L. Boeck et al., *Geophys. Res. Lett., 19*, 99, 1992) are found to be consistent with the predictions of the kinetic model of the in-teraction (Y. N. Taranenko et al., *Geophys. Res. Lett.,* (in press), 1993b). Although the mechanism of heating, ionization and production of optical emissions by light-ning EM radiation appears to be generally consistent with experimental findings, no direct comparison of data with theoretical predictions has yet been done. In this paper, we undertake such a comparison using correlated VLF and lightning data (U. S. Inan et al., *Geophys. Res. Lett., 15*, 172, 1988; U. S. Inan et al., *Geophys. Res. Lett.,* (in press), 1993) and also discuss other possible optical signatures of this phenomenon.

IONOSPHERIC MODIFICATION BY HIGH POWER RADIO WAVES
Chairman: Lewis M. Duncan, Univ. of Tulsa, Tulsa, OK

G/H1-1
0900

THE SCATTERING CROSS SECTION OF HEATER INDUCED
FIELD ALIGNED IRREGULARITIES

T. L. Arce, M. C. Kelley and D. L. Hysell
School of Electrical Engineering
Cornell University
Ithaca, NY 14853
M. Sulzer
Arecibo Observatory
Arecibo, PR 00612

In the summer of 1992, a sounding rocket carrying high resolution plasma density and electric field detectors was launched into the Arecibo Heater Beam. A preliminary analysis of the plasma probe data has been completed and will be briefly reviewed. Over 180 deep filamentary plasma density depletions were traversed at altitudes both above and below the reflection point of the 5.1 MHz beam. These structures had a mean separation of 15 meters and their full width at half maximum was approximately 8 meters. The mean depletion depth of the filaments was 6%. A Fourier analysis of the data shows local maxima at scales of 15 meters, several hundred meters and several kilometers. At high k, the one-dimensional spectrum falls off as k^{-4}. In this paper, we use these data to predict the scattering cross section as a function of wave number for heater induced field aligned structures. The calculation will be compared to measurements at Platteville and Arecibo.

G/H1-2   **HF WAVE-PLASMA INTERACTIONS IN A BARIUM**
0920   **PLASMA**

F. T. Djuth[1], M. P. Sulzer[2], J. H. Elder[1], and K. M. Groves[3]
[1]Geospace Research, Inc., 550 N. Continental Blvd., Suite 110, El Segundo, CA 90245
[2]Arecibo Observatory, Arecibo, Puerto Rico 00613
[3]Phillips Laboratory, Hanscom Air Force Base, MA 01731

The NASA/CRRES El Coqui rocket campaign was successfully carried out in Puerto Rico during the period 18 May through 12 July 1992. A total of eight rockets were launched into the ionosphere within view of the Arecibo incoherent scatter radar. In this presentation, we describe results from the so-called AA-2 chemical release performed on the last day of the campaign. The purpose of the AA-2 experiment was to study the interaction between the Arecibo HF beam and a high ion mass (Ba^+), "collisionless" plasma. Approximately 35 kg of Ba doped with 148 gm of Sr, 260 gm of Eu, and 24 gm of Li were explosively released near the center of the Arecibo HF beam at 252 km altitude. This was the largest Ba release of the CRRES experiments; it produced a distinctive ionospheric layer having a maximum plasma frequency of 11 MHz. At early times (less than one minute after the release), the Arecibo HF beam produced the strongest Langmuir waves ever detected with the Arecibo 430 MHz radar. Initially, resonantly enhanced Langmuir waves were observed only at the upshifted plasma line (i.e., near 430 MHz + f_{HF}, where f_{HF} is the frequency of the modifying HF wave); no HF-excited waves were apparent at the downshifted plasma line (430 MHz - f_{HF}). At the time of maximum upshifted plasma line backscatter, the power asymmetry between the upshifted and downshifted lines was greater than 10^6. The upshifted plasma line was accompanied by strong HF-enhanced ion acoustic waves that were present only at the downshifted acoustic sideband. A few minutes after the release, HF-induced, field-aligned irregularities were first detected with a 50 MHz radar interferometer deployed on the island of Antigua. At Arecibo, moderate amplitude echoes were detected at the downshifted plasma line coincident with the appearance of the field-aligned irregularities. With increasing time, the amplitude of the echoes at the upshifted plasma line decreased, and the strengths of the upshifted and downshifted lines became approximately equal. In general, the plasma line observations of AA-2 are difficult to interpret within the context of any current theory. The experimental results seem to indicate that the so-called parametric decay instability is excited in an extremely asymmetric manner; that is, the counterstreaming of induced Langmuir waves is not symmetric relative to the HF wave electric field. However, in a stationary, homogeneous plasma, the parametric decay instability is by definition symmetric. New approaches aimed at resolving this dilemma are currently being explored; particular attention is being paid to the role played by steep plasma gradients in creating asymmetries.

G/H1-3
0940

LATE-TIME DEVELOPMENT OF HF-INDUCED LANGMUIR TURBULENCE AT ARECIBO

F. T. Djuth and J. H. Elder
Geospace Research, Inc., 550 N. Continental Blvd., Suite 110,
El Segundo, CA 90245

Recent radar experiments at Arecibo Observatory have provided compelling evidence that elements of the strong turbulence (ST) approximation to the Zakharov model equations [DuBois *et al.*, *J. Geophys. Res.*, *95*, 21,221-21,272, 1990; DuBois *et al.*, *Phys. Rev. Lett.*, *66*, 1970-1973, 1991] are applicable to measurements of HF-induced Langmuir turbulence. When the HF beam is turned on in a cold background ionosphere, the consistency between ST theory and the experimental findings is rather striking for the first 50 ms of modification. Thereafter, the Langmuir turbulence exhibits characteristics attributable to much weaker states of turbulence. The reason for this rather abrupt transition in the plasma is currently not known, but it may be related to the generation of irregularities in the plasma. Two types of HF-induced irregularities are known to develop very quickly in the plasma following turn-on of a powerful HF beam: horizontally stratified irregularities and short-scale, field-aligned irregularities. These irregularities alter Langmuir wave propagation and may directly influence the instability process itself. Over time scales of 30 s and longer, large-scale (100-500 m) structures develop in the plasma. The large-scale structures apparently contain packets of smaller-scale (3 - 30 m) irregularities. The embedded irregularities greatly complicate the interpretation of Langmuir wave data. In this presentation, an experimental view of the development of Langmuir turbulence will be presented with particular emphasis on late time (> 50 ms) spectral features measured with the Arecibo 430 MHz radar. These observations are supported by direct measurements of HF-induced, field-aligned irregularities made with a mobile VHF radar. The goal is to develop a test strategy for identifying physical processes that influence the development of ST. It is hoped that this will provide the basis for new theoretical initiatives in studies of Langmuir turbulence.

G/H1-4   SIMULTANEOUS EXCITATION OF PARAMETRIC DECAY
1000   CASCADES AND THE OTSI IN 1D NUMERICAL
          SIMULATIONS BASED ON ZAKAROV'S EQUATIONS

R.A. Sprague
NCCOSC RDTE DIV, CODE 542
San Diego, CA   92152-5235
AND
J.A. Fejer
Department of Electrical and Computer
Engineering
University of California, San Diego
La Jolla, CA   92093

Plasma wave spectra observed during ionospheric heating experiments are generally classified as being of two main types, the 'cascade' type or the 'broad' type, although instances of the apparent co-existence of the two types is also observed. Cascade type spectra are thought to be produced by the parametric decay of the heating (pump) wave into lower frequency Langmuir waves and low frequency ion acoustic-like density oscillations. Broad type spectra are believed to be produced by the repeated cycle of nucleation, collapse and burnout of localized density depletions. The physical processes involved in the two cases are thus quite different.

A feature of the cascade type spectra which is often observed under particular experimental conditions is a narrow bandwidth, zero frequency offset 'line'. This feature is thought to be produced by the 'purely growing' or 'oscillating two-stream (OTSI)' instability which is known to be excited under conditions similar to those which produce the cascade. In this paper we present results from numerical simulations, based on Zakarov's equations, which show that, for relatively low pump powers, the OTSI is stabilized by the presence of the cascade and thus can co-exist with the cascade. Examples of both frequency and wavenumber spectra will be presented, along with plots showing the evolution of the total power in the Langmuir spectrum.

G/H1-5   DYNAMICS OF HF-INDUCED ELECTRON
1040   ACCELERATION PROCESSES IN THE IONOSPHERE

Keith M. Groves
Ionospheric Effects Division, Phillips Laboratory
Hanscom AFB, MA 01731-3010
Frank T. Djuth
Geospace Research Inc.
El Segundo, CA 90245

High power HF modification experiments were conducted in conjuction with the CRRES rocket campaign at the Arecibo Observatory during the summer of 1992. Near their reflection point in the ionosphere, intense HF pump waves excite a turbulent spectrum of Langmuir waves which accelerate a relatively large number of electrons to energies at least 100 times greater than the bulk plasma thermal energy. The majority of these suprathermal electrons subsequently escape upward along geomagnetic field lines exciting electrostatic fluctuations (i.e., electron plasma waves) as they stream through the background plasma. By monitoring the enhancement of plasma waves on the magnetic field lines which map into the heated volume near the HF wave reflection layer with the UHF incoherent scatter radar, one can infer the spatial distribution and temporal evolution of suprathermal electron fluxes across the HF beam. When nighttime ionospheric heating was performed at full power (~ 80 MW ERP) enhanced plasma lines were observed with the 430 MHz incoherent scatter radar tens of kilometers above, and on magnetic field lines mapping into, the HF heater wave reflection layer at 295-300 km. Energetic electrons with energies of about 14-17 eV are responsible for the enhanced waves. The acceleration region is observed to shift magnetically southward during the first 4-5 minutes following heater turn-on at speeds of 40-60 m/s. After this, electron acceleration becomes sporadic temporally and spatially for 1-2 minutes before reorganizing near the original source region and exhibiting a distinct amplitude periodicity for the last few minutes of the experiment.

A Theoretical Model for the Broad Up-Shifted Maximum in the Stimulated Electromagnetic Emission Spectrum*

J. Huang and S. P. Kuo
Weber Research Institute and Department of Electrical Engineering
Polytechnic University, Route 110, Farmingdale, NY 11735

A second order four wave interaction process including two pump photons, an upper hybrid plasmon and an electron Bernstein plasmon is studied. The pump is the second harmonic of the HF heater in the plasma. It is found that, when the heater wave frequency is above a harmonic of the electron cyclotron frequency, frequency up-shifted upper hybrid waves and frequency down-shifted electron Bernstein waves can be excited above the upper hybrid resonance layer via the considered process. The process occurs in a local region where the heater wave frequency is about the mean of the upper hybrid wave frequency and the electron Bernstein wave frequency. It is also found that the field strength of the excited upper hybrid wave is much larger than that of the electron Bernstein wave. Moreover, in this interaction process, a low frequency electrostatic oscillation in the frequency range of the lower hybrid wave is generated through the nonlinear coupling of the HF heater wave with the excited high frequency electrostatic waves. However, this wave does not satisfy the linear dispersion relation of the lower hybrid wave and is, thus, a driven wave.

The exited frequency up-shifted upper hybrid waves can then scatter off the field-aligned density irregularities to generate o-mode emissions with frequencies around $2f_0 - nf_c$ consistent with the observation of the broad up-shifted maximum (BUM) feature in the stimulated electromagnetic emission (SEE) spectrum. The concomitantly excited frequency down-shifted electron Bernstein waves are found to have much smaller amplitudes, hence, their scattering products are also relatively weak. This explains why only BUM lines are detected. Furthermore, the driven low frequency fluctuations can also be the scatterers to convert the upper hybrid waves into emissions with frequencies around $f_{BUM} + f_{LH}$ and $f_{BUM} - f_{LH}$. This is suggested to be the generation mechanism of the 2nd BUM feature which appears when the shoulder of the BUM feature is not very high.

G/H1-7   INVESTIGATION OF   STIMULATED ELECTROMAGNETIC
1120   EMISSIONS IN THE IONOSPHERE

P.A. Bernhardt[1], L.S. Wagner[1], J.A. Goldstein[1],
V.Yu. Trakhtengerts[2],   E.N. Ermakova[2], V.O.
Rapoport[3], G.P. Komrakov[3], A.M. Babichenko[3]
[1]Naval Research Laboratory
Washington, DC 20375-5000, USA
[2]Institute of Applied Physics and
[3]Radiophysics Research Institute
Nishni Novgorod, USSR

Stimulated electromagnetic emissions (SEE) have been
recorded when powerful O-mode electromagnetic waves were
launched vertically from   ground based   transmitters in
Norway, Puerto Rico, Alaska, and   Russia. The generation of
the downshifted maximum (DM) in the SEE spectrum is thought
to result from linear mode coupling to upper hybrid waves
and field aligned irregularities below the reflection level.
The upper hybrid waves parametrically decay into a lower
hybrid wave and a downshifted electromagnetic wave. To test
this theory, experiments were conducted in March 1993 at the
SURA facility in Russia. The DM intensity was found to have
a power-law dependence on   transmitter strength.   The
threshold for the parametric decay instability was not
detected. Two frequency transmissions showed that the SEE
associated with one frequency may be enhanced by 2dB with
the   transmission of a   second,   higher   frequency.   This
amplification of SEE has been attributed to the generation
of plasma inhomogeneities by the second wave that enhances
the linear mode coupling of the first wave.   The two
frequency technique allows the experimenter to distinguish
between nonlinear parametric decay and linear mode coupling
for generation of SEE.
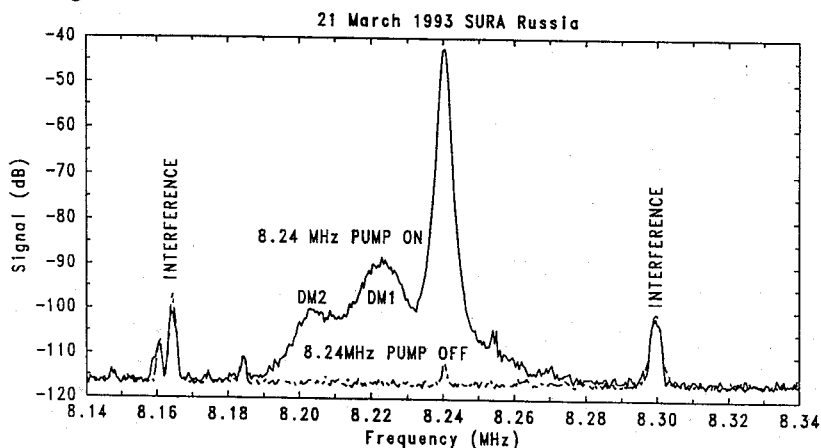
SEE spectrum showing two downshifted maxima DM1 and DM2.

G/H1-8   **ANALYSIS OF IONOSPHERIC MODIFICATION BY HIGH POWER**
1140   **OBLIQUE HF HEATING**

Yuming Huang and Gary S. Sales
University of Massachusetts Lowell
Center for Atmospheric Research
450 Aiken Street
Lowell, MA 01854

Several theoretical investigations have been carried out over the past two decades to understand the mechanisms for oblique, underdense heating of the ionosphere by high power HF transmitters and its potential to enhance or degrade the performance of HF communication and radar systems. Most theories rely on F-layer focusing and defocusing caused by changes in electron density in the F region to explain the "observed" changes of amplitude, frequency and angle of arrival of a probe signal. Most of these earlier oblique ionospheric modification experiments were made in the former Soviet Union. However, the most recent USAF-VOA experiments revealed changes only in the amplitude of the received signal; no changes in the frequency and angle of arrival correlated with the high power heating were detected. These observations indicate that the F-region theory cannot explain all the observed heating effects and an alternative explaination is required.

This paper presents a theory based primarily on the changes of electron temperature which in turn affects the effective electron collison frequency, the recombination rates, the electron diffusion rate and ultimately the electron density. The research shows that the effects of ionospheric heating are different in daytime compared with the nighttime. The observed amplitude changes are explained in terms of heating-induced absorption in addition to focusing and defocusing. The changes in frequency and angle of arrival result from changes in the refractive index and the observation of these effects depends on the time constant of the electron density changes which have a significant diurnal variation. This theory is able to explain both the earlier Soviet and our VOA experimental results.

211

REMOTE TELESCOPE OPERATIONS

Chairman: Philip R. Jewell, National Radio Astronomy Observatory, Tucson, AZ 85721-0655

J4-1   REMOTE OBSERVING CAPABILITIES OF THE OVRO
0840   MILLIMETER WAVE ARRAY

Stephen L. Scott
California Institute of Technology
Owens Valley Radio Observatory
PO Box 968
Big Pine, CA 93513

The OVRO millimeter wave array consists of five 10.4m telescopes that is accessed remotely on a routine basis. The scientific program of the instrument is primarily aperture synthesis in the 1mm and 3mm bands in both continuum and spectral line. Remote access modes include both active control of the array and passive monitoring. All observing is done by Caltech scientific staff, students, and their external collaborators; there are no telescope operators. Typical use of the instrument involves both highly interactive use for optimization and calibration and a repetitive mode for collection of the synthesis data.

The system architecture uses diskless microprocessors embedded in the telescope and receiver hardware and in the data collection systems. These machines handle all of the high duty cycle realtime work. A workstation is used as the host machine for the Server program that runs the array and for the Client programs that handle the user interfaces. The system design is tightly coupled as opposed to a loose toolkit approach. The Server is the central component of the system and handles arbitration of control by the Client programs, synchronization and communication with the micros, error detection and logging. Each observer runs a Client program that executes in the observer's own context. All data is recorded in a commercial RDBMS with several years of data kept online at all times. Remote observing is supported by the features described below.

Simultaneous access by multiple users allows monitoring of the instrument while a single user controls the instrument. It also allows for a seamless transition from one remote location to another and can be used in training novice observers.

The user interface is based on an nx80 (n≥24) character cell screen layout. The text terminal is still the common denominator so the user interface permits remote access from almost anywhere. Command line input supports minimum match, nine datatypes and limit checking.

A realtime monitoring window containing instrumental parameters, status, and recent continuum data shares screen space with command input. The realtime update rate is 1Hz. More than 300 different pages may be selected for display in the window. These pages are the most critical part of the interface with the observer and must be carefully designed, providing views that range from the most global to the most detailed. Pages are tailored toward a specific category of user, such as astronomer, receiver expert, hardware engineer or programmer.

A scheduler accepts text files with the same syntax as keyboard commands. All files are checked for syntactic correctness upon submission to avoid runtime errors. The scheduler has additional looping, nesting and time conditionals (UT or LST) that allow for simple construction of complex schedules. The scheduler queue holds 8 files.

J4-2
0900

REMOTE OPERATION AND IMAGING
WITH THE BIMA MILLIMETER ARRAY

Melvyn Wright, Radio Astronomy Laboratory,
University of California, Berkeley, CA 94720

The Berkeley-Illinois-Maryland Association, BIMA, operates a 6-antenna millimeter synthesis array located at Hat Creek California. The array can be operated remotely by remote login to the Hat Creek computers over standard networks. The array is usually operated by submitting an observing command file which contains a sequence of observations and calibrations necessary to complete an 8-12 hour aperture synthesis observation of a source, such as observations of molecular line emission from a stellar envelope. The remote control includes pointing the telescopes, controlling frequency synthesizers, and setting up the correlator to alternately observe the molecular line source in several spectral lines, and quasar sources which are used to calibrate the antenna gains. The remote observer can run various programs to monitor the control of the array and inspect the data as it is acquired.

An 8-12 hour observation with 6 antennas is sufficient to to make aperture synthesis images with a few hundred pixels and a dynamic range greater than 100. More extended images are obtained from multiple configurations of the 6-antenna array. The array is currently being expanded to nine antennas which will increase the speed and dynamic range by a factor 2.4. Images are made automatically by fitting the antenna gains to the quasar data and deconvolving the instrumental response from the source data. These images are typically displayed at the remote terminal using X-windows. The data are also transferred automatically to disk and archive storage at the NCSA, Illinois where they are available for further processing.

J4-3   INTERACTIVE REMOTE OBSERVING -
0920   REMOTE USAGE OF THE 3.5m APACHE POINT OBSERVATORY

R. F. Loewenstein, Brian Yanny [†], & Russell Owen[‡]
Yerkes Observatory, The University of Chicago
Williams Bay, Wisconsin 53191, USA
[†]Institute for Advanced Study; [‡]Astronomy Dept., University of Washington

The Astrophysical Research Consortium (ARC) has constructed a 3.5m telescope at Apache Point Observatory (APO) located in the Sacramento Mountains of New Mexico. The entire observatory (telescope, enclosure, surveillance cameras, and instruments) has been designed from the outset to be remotely controlled with minimal on-site support. Remote experts are able to maintain the software systems. Each of a variety of instruments may be rapidly switched on-line by the remote observer. Primary connection to APO is by the Internet (64 Kbps) with a high speed 42bis MNP10 modem (30 Kbps) as backup. While scripting and automated operations are possible, we have concentrated on implementing an interactive remote control environment.

Centralization of control was avoided in favor of distributed processing; thus time-critical tasks are resident in machines closest to the devices they control. The observatory consists of a heterogeneous system of various computers (SUN, DEC, Macintosh, and stand-alone, single-board systems), operating systems (UNIX, VMS, Mac OS), and languages (C, Fortran, Forth). Each instrument has its own Instrument Computer (ICC, consisting of smaller robotics controllers, if necessary) which communicates to a Master Computer (MC). The ICC program must, however, conform to a well defined low level message protocol for interfacing to the MC. This creates a modular architecture that easily absorbs new computers and instruments. A Unified Command Language to control all instruments is available on the MC.

After several years of testing many remote observing implementations, we have identified what we believe to be pertinent design fundamentals for creating a successful telescience environment: (1) Suitably designed hardware (forgiving, minimal maintenance); (2) Adequate bandwidth of data links to the remote site; (3) Minimal latencies; (4) Open loop commanding (once a command is issued, the connection to the site may be broken with no disastrous results); (5) Timely and informative feedback; (6) Well designed protocol for asynchronous communications between computers; & (7) Intuitive and easy-to-use user interface.

Many users at various sites around the country have routinely observed singly or collaboratively on the APO telescope during the 1991-92 season using a Graphical User Interface (GUI) on a Macintosh computer. The GUI requires minimal prior knowledge of the system, and is used by both professional astronomers and undergraduate students alike. The user environment must create the 'feel' that the observer is connected to the observatory and that what is supposed to be happening *is* happening. After evaluating many incarnations of the GUI we can summarize certain desirable attributes: (1) Easy to learn and use; (2) Intuitive and obvious functionality; (3) As modeless an environment as possible; (4) Timely and meaningful feedback; (5) Audible as well as visual cues; (6) Minimal required keyboard use; (7) Control panel simulation; & (8) Uncluttered displays.

The year's usage has provided insight into making remote observing more effective. Collaborative remote observing, a by-product of our system, is one of the more interesting areas to pursue.

J4-4   REMOTE OBSERVING AT THE SOUTH POLE
0940   R. F. Loewenstein, Dir. of Computing and Communications
            CARA, Yerkes Observatory, The University of Chicago
            Williams Bay, Wisconsin 53191, USA

The South Pole is located on a high plateau (10,000 ft. pressure altitude) 800 miles from the nearest coastal station on an uninhabited, frozen continent at the bottom of the world; it is one of the coldest and driest places on Earth. These attributes make it perhaps one of the most difficult yet best places on Earth to carry out Infrared and Submillimiter astronomical observations. The Center for Astrophysical Research in Antarctica (CARA) was created in 1991 to exploit these characteristics and explore the potential of the Antarctic Plateau for astrophysical research over a spectral range extending from the near infrared to millimeter wavelengths.

Four projects comprise CARA's plans, addressing problems in star formation, evolution of galaxies, and the distribution of matter in the early universe. These surveys can be conducted effectively with moderate size telescopes operated in both automated and remote modes. They include: COBRA, a cosmic background anisotropy experiment at 90 GHz; AST/RO, a 1.7m submillimeter telescope with a 230 GHz receiver; SPIREX, a 60cm telescope with a 256x256 2.4 μm camera; and an Advanced Telescope Project to measure the site characteristics for future large (7.5m) telescopes sensitive to these wavelengths. While COBRA has been operational during Austral summers in some incarnation since 1987, AST/RO and SPIREX will be deployed within the next two years for year-round operations.

Because of its hostile environment, limited access in the summer, and inaccessibility in the winter, remote operation of the various instruments will greatly enhance the capability of the experiments. But while the South Pole's location makes it advantageous for astronomy, it also causes it to be uniquely unsuitable for satellite communications. Being at 90° S latitude, no geostationary satellite can be seen at the pole. Therefore normal communication satellites are unusable for data transfers, instrument control, or even email and telephone connections. In addition, no single satellite can supply twenty four hour coverage.

For the past twenty-five years, communications to the Amundsen-Scott South Pole Station has made use of short wave radio. Large amounts of data had to be flown out in the form of magnetic tape or other storage media. More recently, communications to the pole has taken advantage of two errant geostationary satellites (ATS-3 and LES9) that pass above the horizon for a few hours each day. These aging satellites provide 1200-2400 baud communications for a few hours per day, yielding a data throughput of about 4 Mbytes/day with non-loss compression techniques. Telephone and delayed email services are available when these satellites are visible, but no reliable interactive logins from remote computers is possible. In order to implement true remote operations, we are investigating ways to bring the Internet to the South Pole.

An inclined NOAA satellite (GOES-2) is visible at the pole for about 3 hours a day, offering a possible data rate of 56 Kbps to 256 Kbps, which will transmit 60-240 Mbytes per day. Each year GOES-2 rises 0.7° higher above the South Pole horizon, increasing the time available for communications. In the 1993-94 Austral summer season, we will attempt to establish a connection between the South Pole and CONUS using this satellite. During the same season, experiments will determine if LES-9 may be used at higher bit-rates up to 38 Kbps. Because it is available for about 7 hours a day, data rates over LES-9 may achieve up to 100 Mbytes per day. In addition to data transfers, these satellites offer a way to bring the Internet and ultimately true remote observing to the South Pole.

J4-5   REMOTE OBSERVING AT THE NRAO 12 m -- RETROFITTING
1000   FOR REMOTE OPERATION

P. R. Jewell, D. T. Emerson, T. W. Folkers, and J. R. Hagen
National Radio Astronomy Observatory
Campus Building 65
949 North Cherry Avenue
Tucson, AZ 85721-0655

Remote observing has become an important and much-requested capability at the NRAO 12 m millimeter-wave telescope. We discuss the motivation, the benefits achieved, and the potential pitfalls of remote observing with this telescope. We outline how remote observing now works at the 12 m. We discuss some of the particular difficulties presented when both state-of-the-art and older equipment are present, and discuss additional goals.

The essential motivations for remote observing at the 12 m are efficiency and flexibility, both of which affect the scientific productivity of the telescope. For example, remote observing has provided a cost-effective way of utilizing small blocks of unassigned time left between requested LST blocks on the telescope schedule. Because millimeter and submillimeter-wave observations depend critically upon weather conditions, we also expect remote observing to allow flexible scheduling. Particular advantages to us will be in $\lambda \le 1.0$ mm observing in the winter months and $\lambda 3-4$ mm observations during the summer monsoon season. Another valuable use of remote observing is by a collaborator unable to attend the run in person.

The 12 m remote observing system supports X Windows displays on a variety of workstations, or on ANSI text and TEK 4010 graphics terminals. The system has these specific features: an Internet connection at near-T1 data-rates supporting remote logins and file transfers; remote on-line data analysis; remote display of the control system status screen; a system monitor window showing error messages; a network "talk" window for communication with the telescope operator; an electronic chart recorder displaying switched and total power traces for the receiver channels; a display of site weather information; and, selected video images of the control room, the telescope, and the sky above the site. The capability exists to configure and execute all observations remotely, although some pieces of hardware must be configured manually.

The equipment and physical plant at the 12 m present some special challenges for remote observing. For example, most of the SIS receivers used at the 12 m have two mechanical tuning shorts with single or double sideband options. Although we will soon be able to tune receivers remotely, tuning will require experts. On-site aid will continue to be necessary and will be provided; we choose not to compromise performance for simplicity. On the other end of the scale, much of our mechanical equipment is over 25 years old, and not all of it can be readily interfaced or made robust enough for unsupervised use. An example is the dome, which is steered by an analog differential tracking system and is not positioned or sensed by the computer.

Future enhancements will include more control by observers, more monitor points, and programmable scripts.

J4-6   REAL-TIME OPERATIONS WITH THE IUE OBSERVATORY SATELLITE
1040   Dr. A.G. Michalitsianos, IUE Deputy Project Scientist
           NASA Goddard Space Flight Center
           Laboratory for Astronomy and Solar Physics, Code 684.1
           Greenbelt, MD 20771

The International Ultraviolet Explorer (IUE) undoubtedly has been the most productive space astronomy observatory since its launch on January 26, 1978. After fifteen years of guest observer operations, IUE together with its extensive archive of nearly 100,000 ultraviolet spectra, continues as a strong and vigorous facility for astronomical research in the vacuum ultraviolet. The advantages realized from geosynchronous operations is central to the scientific productivity of the mission that achieves about 60% observing efficiency. High earth orbit spacecraft operations has enabled IUE to operate with a very flexible observing schedule, critical to responding to targets-of-opportunity (novae, supernovae, cataclysmic variables, solar system phemonena), observing UV spectral variations in astronomical sources over a wide range of timescales (phase critical observations of interacting binaries, intrinsic variables, monitoring variability in Active Galactic Nuclei), and coordinating observations with ground-based as well as other spaceborne observatories. The geosynchronous 24-hour orbit affords direct communication between the observer and spacecraft during the course of observations. This real-time capability greatly facilitates target recognition and track using the Fine Error Sensor (FES), which together with the flexible attitude and control system of the spacecraft, affords an efficient means of tracking moving targets, such as natural satellites, asteroids and comets. High earth orbit has also provided a stable thermal environment which has been critical for achieving high photometric stability of the UV detectors over their nearly two decades of operations. As a consequence, IUE spectra are often used as standards for photometric calibration of other spaceborne instrumentation that operate in the vacuum ultraviolet (HST-Goddard High Resolution Spectrograph and Faint Object Spectrograph, ASTRO-I Ultraviolet Imaging Telescope, and numerous sounding rocket experiments). The choice of high earth orbit operations for future space astronomy missions posses important tradeoffs, such as limiting telescope aperture and spacecraft weight for currently available launch vehicles. However, the important advantages realized with IUE operations are being applied to the development of the Far-Ultraviolet Spectroscopic Explorer (FUSE) which is planned to be inserted into a highly eccentric 24-hour geosynchronous orbit for launch in 2000. FUSE borrows significantly from the heritage learned with IUE by baselining real-time communications. As in the case with IUE, a dedicated ground-antenna station for FUSE that eliminates the need for command uplink and telemetry downlink through the TDRS satellite system, significantly reduces the complexity of scheduling the transmission of spacecraft commands and telemetry of data. Real-time operations is also identified as a cost savings, both in the development of the ground system, and the life cycle cost of operating the spacecraft for the baseline mission lifetime.

J4-7   MESOSPHERIC WATER VAPOR MONITORING
1100   FROM A REMOTE SITE

T. Pauls, R. Bevilcqua, W. Waltman,
D. Thacker, M. Gomez and G. Nedoluha
Code 7200
Remote Sensing Division
Naval Research Laboratory
Washington, DC 20375–5351

The Naval Research Laboratory has recently developed a broadband microwave monitoring system to observe the 22.2 GHz line of water vapor. This system, controlled by a personal computer, uses a cooled HEMT amplifier frontend combined with multi–channel spectrometers developed for space flight as part of the Millimeter–wave Atmospheric Sounder shuttle experiment. This system has a total bandwidth of nearly 400 MHz, which sets the lower limit to the measurement altitude at about 20 km. The instrument is being deployed in the field as part of the NASA Network for Detection of Stratospheric Change (NDSC), and, therefore, must be capable of extended operation at a remote site.

For a simple experiment controlled by a personal computer, there are two options for remote operation, assuming the remote link is a telephone line. Either the telephone modem control is built into the application software, or one of the commercial remote emulation programs can be used. We feel that commercial emulation programs offer a number of advantages:

- *Remote Screen and Keyboard Emulation.*
- *Authentication.*
- *File Transfer.*

Several design considerations should be kept in mind when developing software for remote control applications:

- *Text Display Only.*
- *Simple User Interface.*
- *Auxiliary Files.*
    - Log Files.
    - Configuration Files.
- *Raw Data Mode.*
- *Shell to OS.*

Finally, it is imperative that the instrument start in a known state when the control computer is turned on, to handle power failures gracefully. This is done by preparing batch files that are executed at start–up.

The first NRL monitoring system has been operating at the Table Mountain Observatory of the Jet Propulsion Laboratory near Pasadena, California since July, 1991. A second system operated at Lauder, New Zeeland from November, 1992 to February, 1993. Both systems are currently operating on Table Mountain. Occasional on–site help is necessary for system check–out and to perform hot–cold calibrations. The current systems are in continuous operation, and the data is copied to NRL approximately once per day for further analysis. The data transfer takes about 4 minutes at 9600 baud.

J4-8 **A REMOTE OBSERVING CENTER FOR MULTIPLE**
1120 **TELESCOPES**

D.T. Emerson   R.N. Martin
NRAO[1]   Steward Observatory
949 N. Cherry Ave.   University of Arizona
Tucson, AZ 85721   Tucson, AZ 85721

Many radio and optical telescopes already support remote observing; the observer has a choice between going to the telescope to carry out the observations, or staying at his home institute and controlling the telescope and accessing data from there. In both cases, it may be possible to make real-time decisions on observing strategies. Both alternatives have advantages and disadvantages.

If the observer travels to the telescope, he or she may have much closer contact with the equipment and its environment. The best observing decisions can be made, based on equipment performance and current weather conditions. The close contact with engineering and maintenance staff is important in resolving any perceived or actual difficulties with the telescope and its instrumentation. The observer is also away from the day-to-day distractions, such as teaching or administrative responsibilities, which might exist at the home institute. He or she can concentrate single-mindedly on obtaining the best science from the telescope.

The main disadvantage of on-site observing is the inconvenience of travel; the telescope is often at a relatively inaccessible site, such as an isolated mountain-top, and may take many hours to reach. The site itself may be inhospitable; the thin air on a high mountain-top may cause bad observing decisions to be made. Remote observing avoids these difficulties.

A third option, that of a **Remote Observing Center**, could combine many of the advantages of both on-site and remote observing (D.T. Emerson & R.N. Martin, Observing at a Distance, 291-296, World Scientific Publishing Co., 1993). In this concept, an Observing Center is set up in some easily accessible location, such as at a university with a strong astronomy department, in or near a city with particularly good access by air or other means of transport. The one Center may support several telescopes at different sites, and would offer high-bandwidth links to each telescope, providing full real-time telescope control, monitoring and data transfer. Expert help - friends of the telescopes and specialized engineers - would be readily available for consultation, more so than might be possible at an isolated telescope site. The visiting observer would be able to avoid the distractions inevitably present at his or her home institute, but would have much better access to libraries and other support facilities than would be possible at the remote telescope site. There would be opportunities for interaction with the local astronomy faculty, to the benefit of the observing program. By supporting several telescopes, the facilities and support staff could be shared, making the Remote Observing Center most cost effective.

In future, the option of travelling to such a **Remote Observing Center** may be the preferred choice for observers, offering better support and more convenience than either on-site observing or remote access from the home institute.

J4-9   CAN REMOTE OBSERVING BE GOOD OBSERVING?
1140   Felix J. Lockman
         National Radio Astronomy Observatory
         P.O. Box 2
         Green Bank, WV 24944

We are now building the 100 meter diameter, unblocked-aperture, Green Bank Telescope, which is scheduled to begin operations in early 1996. Its monitor and control system is designed using standard UNIX network protocols, so anyone with access to internet will have the same monitor and control facilities as an on-site observer. This capability brings us into the wild world of remote observing and forces us to face a number of interesting issues:

1. What are the goals of an observing program?
2. How does the "remote" observer judge data quality?
3. Who is responsible for the correctness of data taken remotely?
4. Can a creative experiment be run remotely?

In principle, by making the distance between user and instrument completely arbitrary, remote observing frees us from the tyranny of geography and gives astronomers and observatories great flexibility in scheduling facilities. In practice, the experience of remote observing is that it often places an "observer" between the astronomer and the telescope and thus separates those who ultimately receive and use the data from those who have the skill to acquire the data. Very talented astronomers who (remotely) use the Hubble Space Telescope are currently complaining that getting the data is not enough, that they need "... a kind of caretaker and guide. 'We need a person at the institute responsible not only for the beaucratic paper maze by also the meaning of the observations' ... someone who understands the ultimate goal of a project and makes sure the researchers get the data they need" (*Science*, 1993, Vol. 260, p. 1716). In short, remote astronomers need local astronomers, because good science involves more than a final data product.

Challenges similar to those posed by remote observing have been faced in endeavors as different as truck driving and warfare. We have much to learn from the experience of others (I discuss some instances in *Observing at a Distance*, proceedings of a workshop on remote observing, ed. Emerson and Clowes, 1993, in press). The best use of remote observing capabilities will probably be for routine projects run by very experienced astronomers using techniques that are long established and that require little or no flexibility.

Friday Afternoon, 7 January, 1335-1700

Session A-2 1355-Fri. CR1-42
MATERIAL CHARACTERIZATION
Chairmen: James Baker-Jarvis and Claude M. Weil, NIST, Boulder, CO 80303

A2-1
1400

OVERVIEW OF RF/MICROWAVE MEASUREMENT METHODS FOR DIELECTRIC AND MAGNETIC MATERIALS

Eric J. Vanzura and Claude M. Weil
Electromagnetic Fields Division, NIST 813.08
National Institute of Standards and Technology
325 Broadway, Boulder, CO 80303-3328

A number of transmission line, free-field and resonator methods are presented for measuring the complex permittivity and permeability of materials over the frequency range 10 kHz to 100 GHz. Measurement methods for thin and bulk solids are emphasized with limited discussion of methods for measuring gases and liquids. The advantages and disadvantages of each method are discussed. Non-destructive measurement methods as well as specialized techniques for measuring anisotropic and inhomogeneous materials are also discussed. Metrology considerations and theoretical background are presented as needed, together with literature citations.

A2-2 1420 LOW RF CHARACTERIZATION OF CONCRETE MATERIAL USING A PARALLEL-PLATE FIXTURE

Ossama A. Hazim, Wansheng Su, Sedki M. Riad, and Imad L. Al Qadi

Center for Infrastructure Assessment and Management, CIAM

Virginia Polytechnic Institute and State University

Blacksburg, Virginia 24061, USA

(Phone: +1-703-231-4463, FAX: +1-703-231-3362)

A parallel plate fixture for permittivity measurements at low RF frequencies was designed and constructed. The purpose is to characterize the dielectric properties of Portland cement concrete. The fixture consists of two horizontal steel plates with adjustable separation. Using a network analyzer, The impedance is recorded with specimens placed at the center of the fixture between the two plates. The concrete specimens used are 7.5cm x 10cm x 7.5cm blocks. Calibration for the connectors, cables, as well as the fixture itself is done using an S-parameter one-port model. For that purpose, open, short and 50-ohm calibration standanrds were developed. Using a complex capacitance model based on a parallel-plate capacitor geometry, the complex permittivity of the material under test is computed. Using this method, permittivity measurements for concrete over frequencies up to 40 MHz are possible. The method is believed to be reliable as verified by finite element field analysis as well as measurements of samples of known materials.

A2-3 1440   Large Coaxial Line Fixture for Wideband Characterization of Concrete Material

Wansheng Su, Ossama Hazim, Sedki M. Riad, and Imad L. Al Qadi
Center for Infrastructure Assessment and Management, CIAM
Virginia Polytechnic Institute and State University
Blacksburg, Virginia 24060, USA
(Phone: +1-703-231-4463, FAX: +1-703-231-3362)

A large coaxial line fixture is developed for wideband characterization of concrete material. The basic requirements for this fixture are: accommodating a concrete sample under test, providing the mechanical and electrical connections between the test fixture and measurement system, and well defined characterization performance.

The coaxial line structure was chosen based on these requirements. The size of the coaxial line is determined by the aggregate size of the concrete and frequency band of interest. Due to the nonhomogenous nature of concrete, in order to obtain an average effect of the concrete, certain amount of aggregates or sample dimensions are needed. On the other hand, the high order modes limit the upper operating frequency. To balance this contradiction, the central portion of the line is designed as 100 Ohms to reduce the size of the center conductor and accommodate more aggregates inside the sample. The tapered portions provide mechanical and electrical adaptation between the measurement instrument and the test fixture.

For the coaxial line approach, the main error source is the gap between the concrete sample and center conductor of the coax. To minimize this error at the center conductor, a dedicated center conductor piece was used while casting every concrete sample to be measured.

An HP 8510 network analyzer was used to perform the measurements. The traditional TRL calibration scheme was used to calibrate the fixture. The three calibration standards, Through, Reflection and Line, were obtained as follows. Through standard was realized by directly connecting the two tapered air sections without the sample holder section. Without the sample holder section, two open ends offer Reflection standards. The line standard is obtained by connecting the sample holder section without concrete inside.

A TDR setup was used to aid the design. Mismatches and discontinuities were measured by the instrument. The TDR information was then used to refine and modify the design during the manufacturing the fixture. This procedure greatly improved the electrical performance of the coaxial line fixture.

A2-4   BROADBAND CHARACTERIZATION OF HIGH-
1520   PERMITTIVITY MATERIALS USING LARGE
              -DIAMETER COAXIAL AIR LINE

Chriss A. Jones, John H. Grosvenor, Jr.
         and Claude M. Weil*
Electromagnetic Fields Division (813.08),
National Institute of Standards and
                            Technology,
Boulder, CO   80303

The Transmission/Reflection (T/R) method is a widely used measurement technique for characterizing the dielectric and magnetic properties of homogeneous and isotropic solid materials over broad ranges of the RF/microwave spectrum. The transmission line geometry of choice is generally the 7 mm diameter coaxial air line, owing to its very broadband coverage (DC-18 GHz), but other geometries such as the 14 mm diameter air line, as well as waveguides, are also used. Improved algorithms, based on an iterative solution, have been developed for this technique at NIST. These yield measurement accuracies of the order of +-5% for low-to-medium permittivity (ϵ_r' < 50) and medium-to-high loss materials. NIST has also organized a national intercomparison of such materials using the 7 mm coax line; major variations in the measured data submitted by participants were evident.

Applying this technique to the measurement of high-permittivity (ϵ_r' > 50) materials usually results in major inaccuracies that are caused by the inevitable presence of an air gap between sample and the coax line inner conductor. This gap always biases measured data low and must be corrected for. The use of larger-diameter coaxial lines (e.g. 76.8 mm/3.024 ins diameter) has been shown to greatly reduce air gap errors because the electric field strength across the gap is proportionally much less than is the case for say a 7 mm diameter line. The inevitable trade-off is that the operating TEM Mode bandwidth for this system is reduced down to DC-1600 MHz. However, this may be adequate for many material measurement applications.

This talk will discuss the development of a 76.8 mm diameter coaxial air line system at NIST, as well as methods of calibrating automatic network analyzers using this transmission line system. Measurement data will be presented for a high-permittivity ceramic (ϵ_r' = 275) obtained using this technique.

A2-5
1540

USE OF PARALLEL-PLATE DIELECTRIC RESONATOR FOR MATERIAL MEASUREMENTS

Richard G. Geyer
National Institute of Standards and Technology
Electromagnetic Fields Division, 813.08
325 Broadway, Boulder, CO 80303, U.S.A.

Jerzy Krupka
Instytut Mikroelektroniki i Optoelektroniki Politechniki Warszawskiej
Koszykowa 75, 00-662 Warszawa, Poland

Precise measurements of the dielectric properties of low-loss, high dielectric constant materials may be conveniently performed by a procedure known as the Hakki-Coleman or Courtney method. In this method a cylindrical dielectric resonator of the material under test is placed between two parallel metallic plates. Given the dimensions of the dynamic resonator, the resonant frequency of the $TE_{01\delta}$ mode, and the unloaded quality factor, one can accurately evaluate the relative dielectric constant and dielectric loss of the sample under test. Losses of the two parallel plates may be suitably accounted for by quality factor measurements using very low-loss check standards, such as crystalline c-axis oriented sapphire or quartz. Although the TE_{011} mode is typically employed, higher-order modes may be effectually used, subject to positive identification of each resonant mode. Introduction of a small air gap between the sample under test and either of the metallic ground planes allows the fundamental TE resonant frequency at which the sample is tested to be changed. The results of material measurements are given, for dielectric constants as large as 100 and losses as low as 3×10^{-6}.

A2-6   **DIELECTRIC SPECTROSCOPY OF PARTICULATES**
1600   Robert B. Stafford
        Institute for Telecommunications Sciences
        325 Broadway
        Boulder, CO 80303

In this report several methods for evaluating the permittivity of soil samples using measurements in the time domain are examined. Three different types of sensors are used – an open ended coaxial probe, a terminated coaxial probe and a balun driven twin lead probe. Several different methods of inverting the measured values to obtain epsilon are investigated and results from measuring dry sand, water saturated sand and saltwater saturated sand are presented.

Chairmen: Akira Ishimaru, Dept. of Electrical Engineering, Univ. of Washington, Seattle, WA 98195;
and Ezekiel Bahar, Dept. of Electrical and Center for Electro-Optics, Univ. of Nebraska,
Lincoln, NE 68588-0511

B7-1   PULSE BROADENING AND TWO-FREQUENCY MUTUAL
1400   COHERENCE FUNCTION OF THE SCATTERED WAVE FROM
            ROUGH SURFACES
            Akira Ishimaru, Lynn Ailes-Sengers, Phillip Phu and Dale Winebrenner
            Department of Electrical Engineering
            University of Washington
            Seattle, WA 98195

There has been an increasing interest and need for understanding pulse broaden-
ing and coherence bandwidth of acoustic or electromagnetic waves scattered from rough
surfaces. Examples are ocean acoustic scatter channel and SAR remote sensing of earth
surfaces. There has also been a strong interest in optical remote sensing of rough surface
characteristics utilizing the angular and frequency correlations of the scattered wave.

We present analytical expressions for the two-frequency mutual coherence func-
tion and angular correlation function of the scattered wave from rough surfaces based on
the Kirchhoff approximation.   Scattered pulse shapes are calculated as the Fourier Trans-
form of the two-frequency mutual coherence function. Millimeter wave scattering experi-
ments and Monte Carlo simulations are performed on one dimensional rough surfaces
showing good agreement with the analytical results. The theory is applicable to the range
of parameters with the rms slopes less than 0.5 and the correlation distance $l \geq \lambda$. For the
case where the rms slopes are close to one, where backscattering enhancement takes place,
the second order Kirchhoff approximation needs to be included. This will be discussed in
a separate paper.

The results show that the coherence bandwidth depends on the illumination area
as well as the incident and scattered angles and the surface characteristics. Both the ana-
lytical and experimental two-frequency mutual coherence function show that the fre-
quency correlation function is maximum at the center frequency and drops rapidly
towards zero as the frequency moves away from the center frequency. This results in a
finite coherence bandwidth. The inverse of this bandwidth is the pulse broadening. The
broadening of the scattered pulse is minimum at the specular direction due to the mini-
mum travel time and increases as the observation angle deviates from the specular region.

B7-2   TRANSITION OPERATORS AND RESOLVENT KERNELS IN
1420   RANDOM SCATTERING
        Gary S. Brown, Bradley Dept. of Electrical Engineering
        Virginia Polytechnic Institute and State University
        Blacksburg, VA 24061-0111

The early literature of wave scattring and propagation thru random media is dominated by physics-oriented jargon. This occurs because of the high interest in the so-called many body problem which involves the interaction of many scattering bodies under the mechanism which engineers usually refer to as multiple scattering. In this literature and continuing to the present, one encounters significant use of what has come to be called the transition operator. This transition operator is the mathematical operation by which one converts the incident field into the scattered field. Clearly, this operator is very convenient when trying to develop analysis techniques or even approximations which do not depend on the specific form of the operator, e.g., such as attempting to sum a number of multiple scattering effects involving two or more of the scatterers. In short, it is a most convenient operator to use in abstract manipulations.

However, when it comes down to actually defining the operator, the situation becomes a bit more complicated. There are cases where this operator has a clear and easily understood meaning. For example, when the scattering bodies have shapes which are congruent with one of the geometries in which the wave equation is separable, modal expansions can be used to form the transition operator; this is the source of the famous T-matrix. In general, however, a rapid an easily understood identification of the transition operator is not so easy.

The way engineers frequently envision scattering problems such as encountered when using the transition operator is to first calculate the current induced in or on the scattering body by a given source and then calculate the reradiation of this current to produce the scattered field. When it is the far zone scattered field that is of interest, it is sufficient to consider what amounts to the Fourier transform of the induced current. As is obvious, this incident-to-scattered field transformation is clearly a two step process and this is why it is difficult to see is as representable by a single "transition operator". That is, one must first solve the integral equation satisfied by the current and then Fourier transform this result to get the far zone scattered field. The key to relating this means of calculation to the transition operator is to recognize that if the current satisfies a Fredholm integral equation of the second kind then it can be put in the form $J = J_i + LGJ_i$ where the J_i is the known current due to the incident field and G is the resolvent kernel. Thus, if one is interested in the far zone field, the transition operator becaomes equal to the Fourier transform of the operator $(1 + LG)$, where L is the integral over the scattering body or bodies. The key then to understanding the transition operator is the resolvent kernel. This kernel satisfies its own integral equation which is well known from the theory of Fredholm integral equations. This point will be discussed in the presentation.

B7-3   WAVE PROPAGATION IN AN ANISOTROPIC RANDOM MEDIUM LAYER
1440

Saba Mudaliar
Rome Laboratory
Hanscom AFB, MA 01731

The geometry of the problem consisits of an anisotropic medium layer sandwiched between two homogeneous isotropic media. The anisotropic medium is in general biaxial and its permittivity is defined by a symmetric matrix. However its random fluctuation is defined by a scalar quantity. The principal coordinate system of the anisotropic medium can have arbitrary orientation with respect to the layer geometry. Also the correlation function is in general anisotropic.

The mean field in the random medium layer due to an arbitrary source is conveniently obtained through the mean Green's function (the fundamental solution of the problem). We first derive the Dyson equation which is the equation for the mean Green's function (MGF). The nonlinear approximation is employed to the mass operator. Because of the nonlinearlity involved the standard perturbation series approach to solve the Dyson equation leads to secular terms. Hence we use the two-variable expansion technique to ellimenate the secular terms. Thus the zeroth order solution to the problem is obtained. Here we have used the unperturbed Green's function derived by us in an earlier paper. Note that there are two characteristic waves (both extraordinary) in the anisotropic medium each with distinct propagation constants. The MGF has the same structure as that of the unperturbed Green's function. But the coefficients and the propagation constants are modified. It may be noted that the nonlinear approximation is a better approximation than the bilocal approximation and it is energetically consistent with the ladder approximation used to solve the Bethe- Salpeter equation. The MGF thus derived is not only useful in obtaining the scattered field but also is vital to derive other important physical quantities such as scattered intensity, scattering cross section, etc.

B7-4   PREDICTIONS OF THE ELLIPSOMETRIC PARAMETERS OF
1500   MULTILAYERED STRUCTURES

Robert D. Kubik and Ezekiel Bahar
Department of Electrical Engineering and Center for Electro-Optics
University of Nebraska - Lincoln
Lincoln, NE 68588-0511

Measurement of the ellipsometric parameters of multilayered media is proposed to remotely sense the dielectric properties, layer thickness, and the parameters of the two-dimensional random rough interface. The full wave approach is used here to predict the ellipsometric parameters of a three media structure (R. D. Kubik, Ph.D. Dissertation, University of Nebraska, 1993). The upper interface is a random rough surface whose height is characterized by a gamma probability density function. The second surface is assumed to be planar. Thus, field expressions are derived that account for scattering upon reflection and scattering upon transmission in a self consistent manner.

Several illustrative examples are presented. It is shown that if the random rough surface root mean square (rms) height is less than one wavelength, the time consuming commutations of multidimensional integration's can be significantly reduced. Thus using iterative techniques, the analysis can be used to predict the rough surface rms height and the medium parameters from measurements (using a personal computer) when the rms height of the rough surface is small (compared to the wavelength).
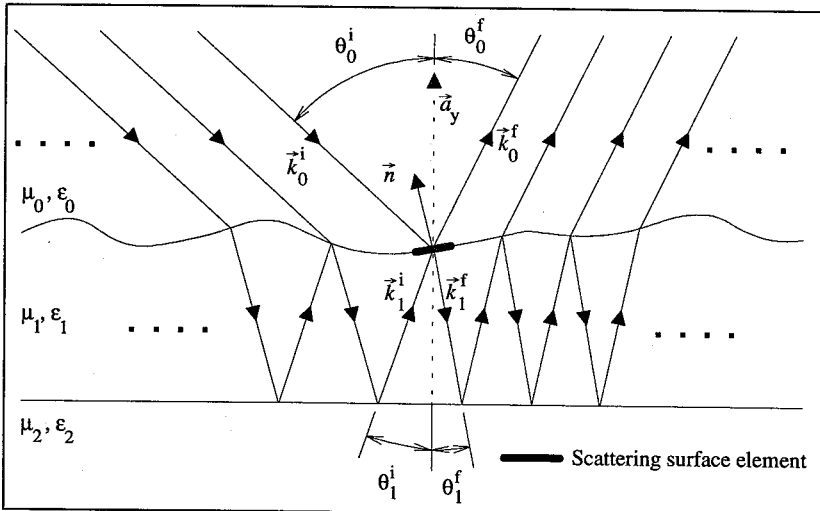
Figure 1. The multiple bounce ray interpretation of the field scattered from a differential rough surface element.

B7-5
1540

LIMITS OF VALIDITY OF PERTURBATION THEORY FOR CALCULATIONS OF THE REFLECTIVITY OF ONE-DIMENSIONAL RANDOMLY ROUGH, DIELECTRIC SURFACES

J. A. Sanchez-Gil and A. A. Maradudin
Department of Physics
and Institute for Surface and Interface Science
University of California
Irvine, CA 92717, U.S.A.
E. R. Méndez
División de Fisica Aplicada, CICESE
Apartado Postal 2732
Ensenada, Baja California, Mexico

We have calculated the reflectivity of p- and s-polarized light incident on a one-dimensional, randomly rough, dielectric surface for several angles of incidence, when the plane of incidence is normal to the generators of the surface, by second-order, small-amplitude perturbation theory, and by a second-order, self-energy perturbation theory. The wavelength of the incident light is $\lambda = 0.6328\mu m$ and the dielectric constant of the scattering medium is $\epsilon = 2.25$. The surface roughness is characterized by an rms height δ and a transverse correlation length a. From a comparison of the results of these approximate calculations with those obtained by a numerical simulation approach for each polarization of the incident light, and for each angle of incidence, curves of δ/λ as a function of a/λ are constructed below which each perturbative method is valid with an error that is smaller than 2.5%. It is found that for a given value of a/λ the reflectivity obtained by the use of self-energy perturbation theory is valid for larger values of δ/λ than is the reflectivity obtained by the use of small-amplitude perturbation theory.

B7-6
1600

THEORETICAL STUDIES OF THE SCATTERING
OF LIGHT FROM ONE-DIMENSIONAL RANDOMLY
ROUGH SURFACES BY THE USE OF LOCAL AND
NONLOCAL IMPEDANCE BOUNDARY CONDITIONS
A. A. Maradudin
Department of Physics
and Institute for Surface and Interface Science
University of California
Irvine, CA 92717, U.S.A.
E. R. Méndez
División de Física Aplicada, CICESE
Apartado Postal 2732
Ensenada, Baja California, Mexico

Local and nonlocal surface impedances of p- and s-polarized electromagnetic fields at the curved interface between vacuum and a metal, defined by the equation $x_3 = \zeta(x_1)$, when the plane of incidence is the $x_1 x_3$-plane, are derived as expansions in the ratio of the optical skin depth of the metal at the frequency of the electromagnetic field to the local radius of curvature of the surface. The conditions for the validity of a local impedance boundary condition are established. The results are used in computer simulation studies of the scattering of light in the visible and infrared regions of the optical spectrum from a large rms height, large rms slope, one-dimensional, randomly rough, metal surface. It is shown, by comparison with the results of formally exact simulations, that the use of a local impedance boundary condition, even for light in the visible region of the optical spectrum, yields accurate results with a significant saving of computer time. The use of an impedance boundary condition in calculations of the scattering of light from one-dimensional, randomly rough, dielectric surfaces is also discussed.

B7-7
1620

EXPERIMENTS ON CONICAL SCATTERING BY ONE-DIMENSIONAL RANDOMLY ROUGH METALLIC SURFACES

Rafael E. Luna* and E. R. Mendez
Division de Fisica Aplicada,
Centro de Investigacion Cientifica y de Educacion Superior
de Ensenada,
Apdo. Postal 2732, 22800 Ensenada, B.C., Mexico.

We present light scattering measurements in a conical configuration from two well characterized one-dimensional randomly rough metallic surfaces whose statistical properties approximate Gaussian random processes with Gaussian correlation functions. The scattering geometry is shown schematically in the figure. The term conical refers to the case in which the wavevector of the incident beam has a component parallel to the grooves. In this case, the scattered light describes a cone and the measurements are done on a semicircle determined by the intersection between the cone and a plane parallel to the plane.

Of the surfaces studied one has a correlation length $a=2.6\mu m$ and a standard deviation of heights $\delta=1.17\mu m$. The surface slopes are then relatively large and multiple scattering effects are expected in this case. The other surface has parameters $a=20.0\mu m$ and $\delta=1.90\mu m$ and its scattering properties are well described by theories based on the Kirchhoff approximation. The experiments, were performed at a wavelength $\lambda=0.633\mu m$. Among other things, the results obtained with the multiple scattering surface show the presence of interference effects related to enhanced backscattering.
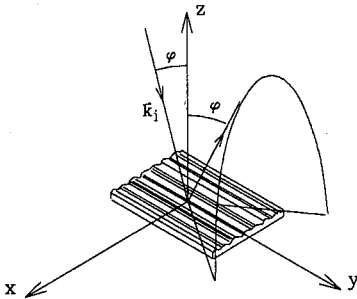
* On leave from Escuela de Ciencias Fisico-Matematicas, Universidad Autonoma de Sinaloa.

B8-1
1400

3D FDTD CHARACTERIZATION of COMPLEX MICROWAVE STRUCTURES

B. Houshmand, and T. Itoh

Department of Electrical Engineering

University of California, Los Angeles

Los Angeles, CA 90024-1594

ABSTRACT

Finite Difference Time-Domain (FDTD) algorithm is used for analyzing interconnects and other packaging configurations. While the FDTD algorithm is more tractable than the frequency domain methods for this class of problems, the computational cost can be prohibitive. In this talk various speed up techniques to reduce the computational cost are presented. Characterization of interconnects for MMIC and MIC modules is important as they are being used in the monolithic circuits. A typical interconnect is a complex three dimensional discontinuity which can be analyzed in the time domain for a range of frequency. In this talk the s-parameters for a number of complex structures are presented. Parameter dependence on the configuration variations will be discussed.

APPLICATION OF A HYBRID FDTD/FVTD METHOD TO RANDOM ROUGH SURFACE SCATTERING AND DIELECTRIC GRATING COUPLERS

J. T. Elson and C. H. Chan
Electromagnetics and Remote Sensing Laboratory
Department of Electrical Engineering, FT-10
University of Washington
Seattle, Wa 98195

The finite-difference time-domain (FDTD) method, in its most basic form, uses a "staircasing" approach to approximate scatterers. Curvilinear and conformal grid approaches have vastly improved the accuracy of the method, as they approximate scattering shapes with much greater accuracy. Recently, we developed a hybrid finite-difference time-domain (FDTD)/finite-volume time-domain (FVTD) technique to model field propagation within a waveguide, and have extended the method to treat random rough surface scattering problems. This method implements a vertex-based conformal grid as opposed to previous edge-based algorithms we have used in the past.

In this paper, we show the application of the FDTD/FVTD technique to rough surface scattering and dielectric grating problems. This method uses a rectangular FDTD grid and a conformal FVTD grid which linearly approximates the scatterer profile and extends only a few grid zones above the surface. Therefore, this dual-grid scheme has both accuracy, resulting from the use of the conformal grid, and efficiency, owing to the rectangular grid. Bilinear interpolation is used to couple information between the overlapping grids.

For the rough surface scattering problems, both tapered wave and plane wave incidence cases are considered. The scattering cross section is observed in the frequency domain as in other established numerical methods, but we can also view the results in the time domain, where the presence of backscattering enhancement, a higher order effect, is viewed as a late-time response.

The method is extended to model a dielectric grating coupler, which in this case is a dielectric film with a sinusoidally-varying top layer deposited on successive layers of dielectrics. The presence of the periodic surface causes energy traveling down the film in a traditional (modal) fashion to be coupled out of the film in discrete angles, providing an effective coupling mechanism. Experimentation with such parameters as refractive index, layer thickness, and periodicity of roughness allow for improved coupler design.

B8-3
1440
FDTD NUMERICALLY EXACT ABSORBING BOUNDARY CONDITIONS FOR THE DOMINANT MODE IN A SHIELDED WAVEGUIDE

Tian-Wei Huang and Tatsuo Itoh
Department of Electrical Engineering
University of California, Los Angeles
Los Angeles, CA 90024

A numerically exact absorbing boundary condition (ABC) is developed based on the finite-difference time-domain (FDTD) Diakoptics method. This ABC is ultra-wideband, incident-angle independent, and includes both physical and numerical dispersion. For a general field absorption, this ABC requires a matrix convolution. For a dominant mode absorption, however, the computation is reduced to a scalar convolution.

This exact ABC is especially suitable for the S-parameter calculation that assumes the dominant mode propagation. A return loss around -90 dB is obtained by this ABC over the entire Gaussian bandwidth. This exact ABC also has a simpler algorithm and a higher computational efficiency than the Engquist and Majda's first-order ABC with superabsorption. One algorithm for using this ABC to absorb the reflected wave on the excitation plane during the excitation is provided to minimize the computational volume. The advantage of using this ABC is also demonstrated by comparison with first-order and superabsorption ABC in their return loss and S-parameter calculation. For the future development, this dominant-mode exact ABC can be applied to a completely open structure, like microstrip line or coplanar waveguide.

B8-4
1500
PHASE ERROR CONTROL FOR FD-TD METHODS
OF SECOND AND FOURTH ORDER ACCURACY.

Peter G. Petropoulos,

AL/OES, Armstrong Laboratory,

Brooks AFB, TX 78235-5102.

It has recently been realized that for frequency-domain Maxwell's equations finite element methods the electrical size of the computational domain (and hence a scaled time-frequency, $k = \omega/c$) is nonlinearly related to the quantity $k\Delta = 2\pi/N_{ppw}$, where c is the speed of light in vacuum, Δ is the characteristic spatial scale of the discretization, and N_{ppw} is the points per wavelength. To maintain a constant error level with these methods N_{ppw} should increase as the domain's electrical size increases, so higher order methods should be used on electrically large problems since they require a smaller N_{ppw} for the same error level in comparison to the second order methods. In this talk we will consider the time-domain problem and look for N_{ppw} estimates that depend on how long in time one computes with the FD-TD methods, thus connecting the spatial discretization to the physical computation time. We will derive a property of Finite-Difference Time-Domain (FD-TD) methods that relates the spatial resolution of the discretized domain to total computation time for a desired phase error. The relationship applies to the Yee scheme, and to a new 2nd-order-in-time/4th-order-in-space accurate FD-TD type scheme for comparison with the standard scheme. It will be shown that for a fixed phase error level the spatial step in FD-TD methods should vary as $\Delta x \sim \frac{1}{t_c^{1/s}}$, where t_c is the total computation time, and $s(=2, \text{ or } 4)$ is the spatial order of accuracy of the scheme. Significantly, we show that _the thumb rule_ of using 10 to 20 points per wavelength to determine the spatial cell size _is not optimal_. A two-dimensional numerical experiment confirming this result for the time-domain Maxwell's equations will be presented.

B8-5
1540

STABILITY AND PHASE ERROR ANALYSIS OF FD-TD
METHODS FOR DISPERSIVE DIELECTRICS.

Peter G. Petropoulos,

AL/OES, Armstrong Laboratory,

Brooks AFB, TX 78235-5102.

The stability and phase error properties of the standard FD-TD ap-
proach are well known. In sharp contrast, little is known of the numerical
error properties of the discretizations of FD-TD extensions to dispersive
media. The new schemes are useful in studies concerning possible med-
ical effects of human exposure to pulsed electromagnetic fields. In this
talk four such extensions for modeling pulse propagation in dispersive
media of Debye or Lorentz type will be analyzed through studying the
stability and phase error properties of the coupled difference equations
corresponding to Maxwell's equations and to the equations for the dis-
persion. We will show that for good overall accuracy all schemes should
be run at their Courant stability limit, and that the timestep should
finely resolve the medium timescales. Particularly, for Debye schemes it
should be at least $\Delta t = 10^{-3}\tau$, while for Lorentz schemes it should be
$\Delta t = 10^{-2}\tau$, where τ is a typical medium relaxation time. A numer-
ical experiment will confirm this. The implication is that one usually
will have to resolve a scale that may be a hundredth or a thousandth of
that of the incident pulse. Such disparity of scales occurs often in prac-
tice where experimental data indicates that typical medium timescales
are $O(10^{-8} - 10^{-12})$ sec while the duration of pulses of large amplitude
(of interest to health and safety analysts) is of the order of hundreds
of nanoseconds. Additional attributes of the schemes will be presented.
Some new analytical results that bear on the development of numerical
methods for dispersive problems will be shown, and their ramifications
will be discussed.

RADIATION AND SCATTERING INVOLVING BIOLOGICAL TISSUE: COMPARISON BETWEEN MOM AND FDTD

J. S. Colburn, M. A. Jensen and Y. Rahmat-Samii
Department of Electrical Engineering
University of California, Los Angeles
Los Angeles, CA, 90024-1594

With the recent growth in wireless communication, there has been a renewed interest in the interaction of electromagnetic fields with biological bodies. Researchers in this arena are concerned not only with the effects of radio frequency energy on biological tissue but also with the influence of the human body on the performance of communications antennas. A detailed understanding of these effects is greatly facilitated through the use of powerful computational tools – such as the moment method (MOM) and the finite difference time domain (FDTD) approach – which are capable of predicting the electromagnetic field distribution within a biological body for different source configurations. In this paper, a comparative study of these two approaches will be provided.

Using the moment method, a volume integral equation can be solved to obtain the fields within the body for a given incident field. Once these fields are known, the scattered field can be obtained through integration of equivalent currents. This approach can be combined with a moment method solution of a thin-wire integral equation to allow determination of the coupling between the body and the radiator. The FDTD methodology uses a spatial and temporal discretization of Maxwell's differential equations to determine the time-evolution of the fields within a body subjected to electromagnetic radiation. It can be used to accurately model very complex geometries for both radiation and scattering.

Comparisons between these two numerical techniques will be made through presentation of various examples of radiation and scattering involving dielectric bodies. Because these two techniques are based on different solution methodologies, such a comparison supplies an independent check of computed results. Issues such as relative accuracy as well as computational complexity and efficiency will be addressed. Emphasis will be placed upon the performance degradation of antennas designed for handheld communications devices placed in the vicinity of a human operator and the absorption of energy within the body when subjected to antenna radiation.

B8-7
1620

A REVIEW OF THE HYBRID FINITE ELEMENT-BOUNDARY INTEGRAL FORMULATION FOR SCATTERING AND RADIATION ANALYSIS

John L. Volakis

Radiation Laboratory
Electrical Engineering and Computer Science Dept.
University of Michigan
1301 Beal Ave.
Ann Arbor, MI. 48109-2122

This presentation will review the hybrid finite element-boundary integral formulation for scattering and radiation analysis of two- and three-dimensional configurations. The formulation combines the geometrical adaptability of the finite element method(FEM) and the rigorous boundary integral (BI) method for truncating the computational domain. As is usually the case, the FEM can model rather complex inhomogeneous configurations, but for radiation and scattering problems, the FEM must be supplemented with suitable mesh truncation schemes which ensure the outgoing nature of the waves and can be enforced close to the scatterer or radiator, thus, minimizing the computational domain. The boundary integral equation is an exact truncation operator and when combined with the FEM, it leads to a partly sparse, partly full matrix system. However, even for moderately sized geometries, the fully populated boundary integral submatrix dominates the storage and computational requirements of the hybrid FEM-BI method. To alleviate these requirements, the BI equations must be judiciously enforced to obtain a block Toeplitz BI submatrix which can be efficiently stored. Moreover, when the resulting system is solved using an interactive algorithm, the FFT can be employed to execute the matrix-vector products to keep the CPU requirements to a minimum and reduce the storage of the entire system to O(N).

In this presentation we will review the implementation of the FEM-BI formulation for both two-dimensional and three-dimensional applications. First, the salient features of the method will be discussed by examining a specific two dimensional example and will then proceed with three dimensional applications to scattering and radiation. Scattering and radiation data will be presented for a variety of cavity-backed patch antenna configurations involving different types of elements (rectangular and circular patches; circular, annular and rectangular slots; planar and non-planar spirals etc.) and which show the method's accuracy and adaptability. Implementations with rectangular and tetrahedral elements will be discussed and how the latter can be interfaced with the conjugate gradient-FFT solver. Finally, we will address the performance of less accurate mesh truncation schemes involving artificial absorbers and vector absorbing boundary conditions.

B8-8
1640

HEM3D: A HYBRID FEM/BEM COMPUTER CODE FOR ANISOTROPIC MULTI-DIELECTRIC, MULTI-CONDUCTING SCATTERERS

P. Soudais
Structures Department
ONERA BP 72 92322 Chatillon Cedex, France

The coupling of local Maxwell equations and integral equations via the hybrid Finite Element Method/Boundary Element Method is a promising technique to compute scattering from complex objects. It is often argued that this allows to take benefits of both methods. These benefits are: exact boundary conditions from the integral equations and rich modelling capabilities of the local equations (several media, anisotropic media).

Several authors have developed such hybrid formulations. We have constructed a specific one that yields a symmetric matrix with positive real part (J.J. Angelini, C. Soize, P. Soudais, IEEE Trans. on. Antennas and Propagat., 41, 66-76, 1993). The system is solved by an iterative algorithm. A computer code has been built upon these developments and has been validated.

We present here validations on complex 3D objects that show the advantages of such hybrid FEM/BEM methods. The scattering by multi-dielectric and conducting objects has been computer. The external boundary of the scatterers are dielectric (coating) or partly dielectric, partly perfectly conducting. Results for anisotropic dielectric are also shown.

1700 Round Table

REMOTE SENSING OF WINDS AND PRECIPITATION
Chairman: T.E. VanZandt, NOAA R/E/AL3, Boulder, CO 80303

F5-1 **AN ALGORITHM TO DEDUCE HYDROMETEOR TYPES AND CONTENTS FROM**
1400 **MULTI-PARAMETER RADAR DATA**

Jerry M. Straka
School of Meteorology & Center for Analysis
  and Prediction of Storms, University of Oklahoma

and

Dusan S. Zrnic
National Severe Storms Laboratory
1313 Halley Circle
Norman, OK 73069

A new algorithm has been developed to automatically deduce bulk hydrometeor types and contents from polarimetric, reflectivity, dual-wavelength and Doppler radar data. The algorithm was developed to improve moisture and thermodynamic initializations in cloud / mesoscale models. Furthermore, analyses made with the algorithm may provide useful information to help understand microphysical processes in both stable and convective precipitation systems.

Using the known behaviors of the multi-parameter radar variables, hydrometeor types are first deduced. If bulk hydrometeor types are within a threshold of certainty, known relationships between appropriate multi-parameter variables and water contents of the hydrometeors are evaluated. Internal consistency checks are possible by using more than just one estimate of bulk hydrometeor type and amount from different radar parameters.

The algorithm is being tested initially with polarimetric, reflectivity, dual-wavelength and multiple-Doppler radar data from the 13 June 1984 Denver, Colorado hailstorm, which was well observed with NCAR's CP-2 and CP-4 radars. This storm produced hail as large as 9 cm in diameter, caused 1 death, 22 injuries, and $350,000,000 in damage. Some areas near Denver received large hail for up to 40 minutes. The algorithm is also being tested using data from NSSL's Cimarron radar.

F5-2
1420
USING THE 915 MHz WIND PROFILER TO CLASSIFY TROPICAL PRECIPITATING CLOUD SYSTEMS

Christopher R. Williams
University of Colorado, CIRES
CIRES Mail Box R/E/AL3
Campus Box 216
Boulder, CO 80309-0216
Kenneth S. Gage and Warner L. Ecklund
NOAA Aeronomy Laboratory
R/E/AL3
Boulder, Colorado 80303

A 915 MHz lower tropospheric wind profiler was developed by the NOAA Aeronomy Laboratory to measure the planetary boundary layer winds. Several of these profilers have been deployed in the tropics for long-term measurement in support of the Tropical Ocean Global Atmosphere (TOGA) program. This profiler measures horizontal and vertical motions from about 100 meters above the surface up to altitudes of 3 to 6 km in the tropics depending primarily on the humidity. However, in the presence of precipitating cloud systems the profiler height coverage increases substantially because the hydrometeors enhance the signal return power at the radar's wavelength of 33 cm. It is not uncommon to have measurements exceeding 10 km while deep convective clouds are directly overhead. A classification scheme using the signal-to-noise, radial velocity, and spectral width deduced from the vertically pointing radar beam has been developed which categorizes the precipitating cloud systems according to their vertical structure. This data analysis technique can discriminate between stratiform, deep convective, and low-level precipitating clouds. This profiler based technique should provide valuable ground truth for satellite methods of precipitation measurements. This classification scheme as well as some results using data from Christmas Island (2°N, 157°W) and Manus Island (2°S, 147°E) will be presented.

F5-3
1440

RETRIEVAL OF RAINDROP SIZE DISTRIBUTIONS USING TWO DOPPLER WIND PROFILERS: MODEL SENSITIVITY AND TESTING

W.B. Maguire II and S.K. Avery
University of Colorado, Boulder
CIRES, Campus Box 216
Boulder, CO 80309-0216

The behavior of precipitation is of great importance in obtaining a better understanding of heat transport estimates and global processes in the atmosphere. This paper discusses improvements in the raindrop size distribution model of Currier *et al.* (Geophys. Res. Letters, 19, 1017–1020, 1992) that utilizes two Doppler wind profilers to obtain accurate measurements of rainfall. A UHF Doppler wind profiler provides a precipitation return while a VHF Doppler wind profiler provides vertical clear-air velocities (which influence the raindrop fall speeds). Due to the unique scattering effects from rain of the two wind profilers, we expect to obtain accurate raindrop size distributions as functions of height without the necessity of *a priori* assumptions of vertical clear-air motions. Given accurate drop size distributions, we may integrate to find total water content and rain rate. The raindrop size distribution model is tested using simulated data. Sensitivity tests examine the model's ability to estimate rainfall characteristics given typical (noisy) Doppler spectra, and the model's sensitivity to atmospheric parameters. Because it is necessary to estimate pressure, temperature, raindrop temperature, and water vapor pressure at the location of the radar volume, the sensitivity tests examine the effects of errors in the estimates of these parameters. Sensitivity testing of the raindrop size distribution model with simulated data indicates model accuracy and reliability and is necessary in the interpretation of results using real data. Testing shows that the model is very capable at estimating even multiple-peaked drop size distributions from noisy UHF spectra. Sensitivity analyses of atmospheric parameters reveal that model results are quite robust, yielding good accuracy for a wide range of atmospheric parameter estimation errors.

PROGRESS ON THE USE OF WIND-PROFILING RADARS TO MEASURE SYNOPTIC AND MESOSCALE VERTICAL MOTION IN FLAT TERRAIN

J. M. Warnock[1], G. D. Nastrom[2], P. E. Johnston[1], and W. L. Ecklund[1]

1. Aeronomy Laboratory, NOAA, Boulder, Colorado
2. Dept. of Earth Sciences, St. Cloud State University, St. Cloud, Minnesota

Wind-profiling radars have an unique capability to measure the vertical motion of the air directly with excellent time resolution. Because of the importance of synoptic and mesoscale vertical velocity measurements to dynamic processes and weather forecasting, it is important to verify radar measurements at these scales. In many locations, however, the vertical motion is frequently dominated by orographic effects. To minimize these effects, the Flatland Radar Observatory (FRO) was located in very flat terrain far from mountains near Urbana-Champaign, IL. The instrumentation at FRO consists of a VHF profiling radar, a UHF profiling radar with RASS (Radio Acoustic Sounding System), a meteorological surface station, a mesoscale digital barometer network, and a radiosonde sounding system.

Unfortunately, there is no standard method to use to verify the radar vertical velocity measurements. Therefore, we make redundant measurements with different antenna beam configurations to estimate the precision of the measurements. Furthermore, to evaluate the accuracy of the measurements, we compare the co-located Flatland VHF and UHF radar measurements, compare the Flatland VHF radar with the Urbana VHF radar located 23 km to the north-east and with indirect calculations of vertical velocity made from a series of sounding balloons. Examples of these comparisons made during field campaigns with balloon soundings will be given at the meeting. We find that during the meteorological conditions studied to date, profiling radars can indeed make useful vertical velocity measurements. This capability should have a major impact on the design and siting of future radar systems and on the use of their data for meteorological research and forecasting.

F5-5   A COMPARISON OF SOME VHF WIND PROFILER VERTICAL
1540   MOTION OBSERVATIONS
W.L. Clark, G.D. Nastrom*, T.E. VanZandt, J.M. Warnock
NOAA Aeronomy Laboratory, Boulder , CO 80303
*Dept of Earth Sciences, St. Cloud State University, St. Cloud, MN 56301

The ability of VHF clear-air radar (i.e., VHF wind profilers) to profile horizontal wind to a useful precision is well accepted. Similarly,profiles of the vertical wind component for large amplitude, short period events can be treated with confidence, provided periods with heavy precipitation are avoided or scaled with special techniques. The situation with the much smaller amplitude, long period motions associated with mesoscale and larger circulation systems is less clear. It is well known, for example, that the Flatland profiler has, since its inception in 1987, observed stronger than expected long-term mean downward motion throughout the troposphere. Extensive effort has uncovered no equipmental source of error capable of explaining the observations. Further, a comparison of the available results of observations from other radars located around the world indicate that, at mid-latitude, cm/s amplitudes of yearly mean vertical motion are the rule, rather than the exception, and are in general downward in the troposphere. Comparison also suggests that there is a pattern to the structure of the observations related to spatial and temporal situations, including season, proximity to orographic features, the nature of these orographic features, and to location in temperature or tropical climes.

Some of the observed vertical motion is definitely bulk flow. At Flatland, for example, about 1 cm/s is routinely due to motion along the prevalent tilt of the local isentropic surfaces, still leaving the majority (a few cm/s) of the apparent downward motion to be explained. Under some conditions, however, this isentropically tilted flow is much larger. For example, in temperature latitudes a significant source of downward motion appears to be related to isentropic flow about the jet stream axis. This feature has been well observed and documented at the MU radar in Japan (Fukao et al., 1991, Mon. Weather Rev., 119, 1479-1489) and the SOUSY radar in Germany (Yoe et al., 1992, Mon. Weather Rev., 120, 2378-2382). This circulation influences flow well away from the jet stream, and the downward flow along an isentropic surface has been observed to transfer parcel tracers from the stratosphere to the surface during cold air outbreaks associated with. On the other hand, in the tropics the amplitude of the observed downward motion, which is usually of the order of 1 cm/s, may be more related to the motion needed to balance energy losses due to high cirrus shielding the sun (Gage et al., 1992, Geophys. Res. Lett., 19, 1827-1830).

On the other hand, reflectivity effects seem to be at least as important. For example, the role of hydrometers in distorting and hiding clear-air Doppler echoes has not yet been completely quantified, though its effects are often obvious. Similarly, anisotropic scattering, clearly present in the troposphere on occasion, could play a role, but comparisons between VHF and UHF systems, as well as VAD and dual-beam methods of observing vertical motion, argue against importance to long-term means.

Perhaps the most serious atmospheric instrumental effect, however, is a new theoretical prediction of bias presented by VanZandt and Nastrom in this conference, that results from a subtle echo reflectivity correlation with the sign and strength of vertical motions induced by passing gravity waves.

2 MHz ANTENNA ARRAY FOR WIND PROFILING

V. Jevremovic, S. Avery, B. Popovic, Z. B. Popovic
Department of Electrical and Computer Engineering
University of Colorado at Boulder, Campus Box 425
Boulder, CO 80309

The University of Colorado at Boulder has been using a 2 MHz radar at Kauai Island for observing the D region dynamic atmospheric irregularities. The radar uses Spaced Array Drift Technique to determine the velocity components and locations of these irregularities. The transmitter consists of four dipoles suspended 24.4 meters above the ground. Mounting this transmitting antenna is difficult and expensive. This paper describes a transmitter design that requires 9 meter high poles and provides the radar resolution of 3 kilometers. The effect of height and length of dipoles was modeled and optimal solution chosen. An artificial ground plane consisting of a wire mesh was designed to eliminate conductivity variation due to weather changes. A scaled 50 MHz model was built and tested, and comparisons with the design results are presented.

LEGEND

▣   9m poles

•   9m poles

78m

73m
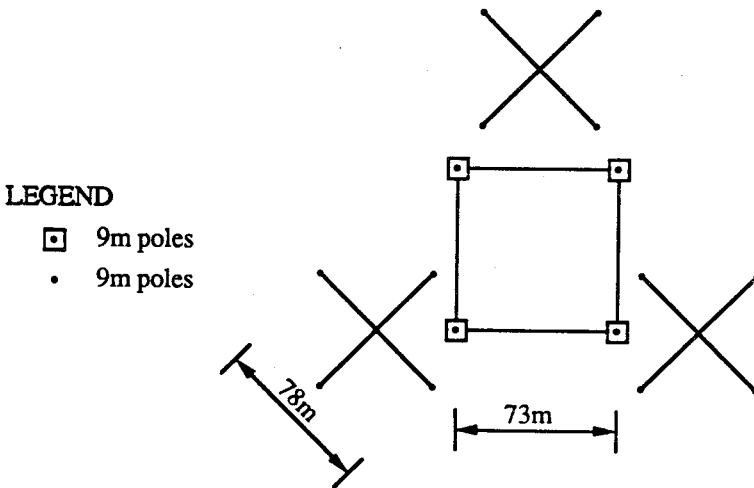
Figure 1: 2 MHz Radar Layout

F5-7   A GRAVITY-WAVE-INDUCED APPARENT MEAN VERTICAL
1620   VELOCITY SEEN BY WIND-PROFILER RADARS

T. E. VanZandt
NOAA R/E/AL3
325 Broadway
Boulder CO 80303
G. D. Nastrom
Dept. of Earth Sciences
St. Cloud State University
St. Cloud MN 56301

In the troposphere most VHF wind-profiler radars observe an apparent mean downward velocity $\overline{w}$ that is much larger than expected. At the Flatland radar, located in very flat terrain in Illinois, $\overline{w}$ is ~ - 5 cm/s, only weakly dependent on season. In this paper we show this $\overline{w}$ could arise from the correlation between the lapse rate of potential temperature and the vertical perturbation velocity of gravity waves with upward energy propagation (downward phase propagation).

Since the radar reflectivity is proportional to the square of the lapse rate, the more downward perturbation velocities will have larger reflectivities, so that the measured $\overline{w}$ will be downward even if the true $\overline{w}$ is zero. For a single gravity wave

$$\overline{w} = \frac{m}{w} \, \hat{w}^2$$

where m is the vertical wave number, ω is the wave intrinsic frequency and $\hat{w}$ is the wave amplitude. For a model spectrum of gravity waves with total energy = 10 m²/s², a power-law ω spectrum with $p = 5/3$, $f/N = 1/120$, and $N = 10^{-2}$ rad/s, and a modified-Desaubies spectrum of waves (T.E. VanZandt and D.C. Fritts, *PAGEOPH*, 130, 399-420, 1989) with $(s,t) = (1,3)$

$$\overline{w}(\text{m/s}) = 5700 \, \frac{\sigma^2 \Delta\alpha}{\lambda_{z*}}$$

where σ^2 (m²/s²) is the variance of the vertical velocity, $\Delta\alpha$ is the difference between the fractions of waves with upward and downward energy propagation, and λ_{z*} (m) is the characteristic vertical wavelength of the model spectrum.

The observed $\overline{w}$ ~ - 5 cm/s lies within the range of the model $\overline{w}$ with values of σ^2 and λ_{z*} within the observed ranges and with a reasonable choice of $\Delta\alpha$. Note that the effect is independent of the radar frequency.

F5-8
1640

VERTICAL VELOCITIES AT PLATTEVILLE, COLORADO:
AN INTERCOMPARISON OF SIMULTANEOUS
MEASUREMENTS BY THE 50 AND 404 MHZ PROFILERS
J.R. McAfee, K.S. Gage, NOAA Aeronomy Laboratory,
Boulder, CO 80303
R.G. Strauch, University of Colorado, CIRES,
Boulder, CO 80309

Even though vertical velocities are important dynamical quantities for atmospheric processes ranging from microscales through climatological time scales, direct measurements of atmospheric vertical motions are rare. In the last few years, wind profilers at several locations have been used to measure vertical motions. However, the accuracy of vertical velocities measured by wind profilers has not been fully established, and many questions already raised in various experiments have not been suitably explained. The extent to which such measurements are influenced by the scattering mechanism is one of the more important issues.

One of the few sources of information concerning the accuracies of profilers is the intercomparison between different types of profilers. This paper is concerned with such a comparison of vertical velocities as measured by the VHF (50 MHz) and UHF (404 MHz) profilers located at Platteville, Colorado during a six week period in October and November, 1991. This location (40°N, 105°W) is 40 km east of the foothills of the Rocky Mountains on relatively flat terrain at an elevation of 1.5 km.

The two profilers are similar both physically and electronically, with the most obvious difference being the wavelengths, six meters and less than a meter. This difference in wavelength leads to a difference in the scattering mechanisms for the two radars, which in turn can lead to possible differences in the measured velocities.

Initial attempts at comparing the results between the two profilers have established periods when there is excellent agreement and also some when there are substantial differences. Currently, we are attempting to find a relationship between periods of agreement and non-agreement as related to the other spectral parameters, received signal power and variance, as well as relating all parameters to local atmospheric conditions.

G/H2-1
1400

THE HAARP INSTRUMENT AS A PROBE OF NATURAL PHENOMENA IN THE GEOPHYSICAL ENVIRONMENT

K. M. Groves[1] and F. T. Djuth[2]
[1]Ionospheric Effects Division, Phillips Laboratory,
Hanscom AFB, MA 01731-3010
[2]Geospace Research Inc., 550 N. Continental Blvd.,
Suite 110, El Segundo, CA 90245

The High-Frequency Active Auroral Research Program (HAARP) entails the construction of a high-power HF facility and an incoherent scatter radar near Gakona, Alaska.   The HAARP facility will operate in the frequency range 2.8 - 10 MHz and generate a maximum effective radiated power of 1 - 3 GW. Co-located with the HF facility will be an incoherent scatter radar that will radiate at a frequency near 440 MHz. Although the incoherent scatter radar design has not been firmly established at this point, it is expected to achieve a sensitivity of 40 MWm^2K^{-1}. The planned HAARP research facility will be supported by a host of additional ground-based diagnostics. These include HF/VHF coherent backscatter radars, HF sounder, HF/VHF imaging riometer, optical imager, IR photometer/imager, LIDAR, scintillation detection system, magnetometer, and ELF/VLF/LF receivers.

Although the HAARP HF facility will be the world's premier ionospheric modification instrument, there is considerable interest in expanding the overall HAARP mission to include studies of the natural environment.   In this presentation, several possibilities for use of the HAARP instrument as a diagnostic probe of the mesosphere, ionosphere, and magnetosphere will be discussed.   More generally, our goal is to encourage the atmospheric/radio physics community to suggest research topics and scientific programs that can be addressed with the HAARP facilities. Current plans call for the development of necessary diagnostic instrumentation to accomplish this broad spectrum of research in the next few years.

G/H2-2
1420

DETERMINATION OF D-REGION HEATING AND COOLING TIME CONSTANTS USING A MODIFIED FORM OF THE CROSS-MODULATION EXPERIMENT

A. J. Ferraro
Department of Electrical Engineering and
Applied Research Laboratory
225 Electrical Engineering East
The Pennsylvania State University
University Park, PA 16802

With the advent of higher power heater facilities coming on line in the future, like HAARP, some consideration of the effect of these higher power densities upon the time constants of heating or cooling requires further study. Techniques for increasing the heated area by beam pointing to create several spots is one application of interest.

A modified form of the cross-modulation experiment is investigated with the intent to measure this power density dependence. Instead of using a vertical incidence beam for the "heater" and using an essentially co-located sensor signal, the "wanted" wave, advantage is taken of the ability of future heaters to position the beam. By pointing the beam approximately 25 degrees from the vertical and placing a vertical incidence wanted emitter and cross-modulation receiver at about 25 Km from the heater, two types of experiments are possible. The terminology of WBD and DBW is used referring to the "wanted pulsed on before the disturbing" and the "disturbing pulsed on before the wanted" respectively. The WBD can be used to measure electron density distributions of the D-region while the DBW can be used to estimate cooling time constants. Different height regions of the D-region overhead can be illuminated by tilting the beam. Calculations are shown for the feasibility to use the method for determining time constants.

In a related topic, the effect of various models for time constant heater power density dependence are studied for various modulation waveforms. The cross-modulation can give some insight upon the form of the power dependent if observable.

G/H2-3   DIAGNOSTICS FOR IONOSPHERIC MODIFICATION
1440   Suman Ganguly
            Center for Remote Sensing
            P. O. Box 9244
            McLean, VA 22102

Several diagnostics for ionospheric modification
are reviewed and compared with primary emphasis on
two most important diagnostics e. g. incoherent
scatter radar and H. F. probing. The author has
worked with both of these techniques and the
relevant issues associated with ionospheric heating
are addressed.

H. F. techniques offer some unique advantage in
terms of large S/N ratio, short time scales,
resonance with the plasma and in several other
aspects. These advantages have not been properly
exploited and we suggest the use of modern
elctronics and techniques for a superior diagnosis
of the "heated" ionosphere using H. F. probing.

G/H2-4 **VLF REMOTE SENSING OF HF HEATING**
1520   **OF THE LOWER IONOSPHERE**

T. F. Bell, U. S. Inan, M. Danielson, and S. Cummer
Space,Telecommunications and Radioscience Laboratory
Stanford University
Stanford, CA 94305-4055

The amplitude and phase of subionospherically propagating VLF signals are known to be sensitive indicators of the electron density and temperature at D-region altitudes. In this paper, we describe a new program of observations at multiple stations in Alaska, positioned to provide measurements of VLF signals propagating over long paths which lie beneath the ionospheric region heated by the HIPAS HF Heater near Fairbanks Alaska. Preliminary analysis of data from a campaign conducted in Sept.- Oct.1992 has demonstrated the feasibility of the measurement. In roughly 60% of the cases analyzed, the amplitude of the 23.4 kHz signal from the NPM transmitter in Hawaii as observed in Fort Yukon, Alaska, exhibited a measurable change in amplitude with the same ON/OFF modulation pattern as that of the HF transmissions at 2.8 MHz. In almost 70% of the cases analyzed, the same signal exhibited similar measurable changes in phase. The amplitude changes ranged from -0.2dB to +0.4dB, with the sensitivity of the measurement being approximately $\pm$ 0.02dB. The phase changes ranged from about $-4°$ to $-0.3°$, and the sensitivity of the measurement was typically about $\pm 0.4°$. The observed amplitude and phase changes are generally consistent with predictions of theoretical models. Comparison of theory and data allows an assessment of the nighttime D region density and temperature.

G/H2-5 Generation of ELF and VLF Waves in the HF Heater-modulated Polar Electrojet*
1540

S. P Kuo and Antony Y. Ho
Weber Research Institute and Department of Electrical Engineering,
Polytechnic University, Farmingdale, NY 11735

M. C. Lee
Plasma Fusion Center, MIT, Cambridge, MA 02731

By applying an amplitude modulated HF heater, the electron temperature of the electrojet is modulated accordingly. This in turn causes the modulation of the conductivity and, thus, the current of the electrojet. Emissions are then produced at the modulation frequency and its harmonics. In this generation process, it can be shown that the transient response of the electrojet plasma to the HF modulation is unstable initially, which is attributed to a positive feedback in the electron-neutral collisional heating process. However, the nonlinear effect of the inelastic collisional loss tends to quickly stabilize the instability. Thus, the nonlinear steady state spectrum of the emissions is considered to be of practical interest.

In this work, the nonlinear evolution of the ELF/VLF waves produced by two heater-modulation schemes are studied numerically. In one scheme, the HF heater is modulated by a rectangular periodic pulse. The other one uses two overlapping heater waves (beat wave scheme) having a frequency difference equal to the chosen modulation frequency. These two schemes provide two different functional forms of input heat sources to the electrojet and the governing equation of electron thermal energy. This equation together with the wave equation are solved numerically to determine the nonlinear evolutions of the generated ELF/VLF waves. The Fourier spectra of the results show that the signal quality and the generation efficiency of the second (beat wave) scheme are better than those of the first one. The field intensity of the emission at the fundamental modulation frequency is found to increase with the modulation frequency, consistent with the Tromso observations.

G/H2-6
1600

MODIFICATION OF THE *D* REGION
BY VERY-LOW-FREQUENCY TRANSMITTERS

J. V. Rodriguez, U. S. Inan, and T. F. Bell
Space, Telecommunications and Radioscience Laboratory
Stanford University
Stanford, CA 94305-4055

Heating of the nighttime *D* region by the U. S. Navy very-low-frequency (VLF) transmitters NAA (24.0 kHz, 1000 kW ERP), NSS (21.4 kHz, 265 kW ERP), and NLK (24.8 kHz, 245 kW ERP) has been observed for the first time using other VLF transmitter signals propagating in the Earth-ionosphere waveguide as probe waves. When the heating transmitter turns off and on, in the course of normal operations, the amplitude and phase of a probe wave passing near the heater sometimes shift simultaneously in response to the changing ionospheric conditions. For example, heating by NAA has been observed to increase the amplitude and retard the phase of the NSS probe wave observed at Gander, Newfoundland, by 0.7 dB and 4.9°, respectively. This is in contrast to the first observations of VLF heating of the nighttime *D* region (U. S. Inan, *Geophys. Res. Lett.*, *17*, 729-732, 1990; U. S. Inan et al., *Geophys. Res. Lett.*, *19*, 2071-2074, 1992), in which the heater was less powerful (NAU, 28.5 kHz, 100 kW ERP) and superposed-epoch analysis was required to reveal the heating signatures, the largest of which was 0.12 dB (no phase data).

Using a three-dimensional model of wave absorption and electron heating in a magnetized, weakly ionized plasma, the heated region over a VLF transmitter is predicted to be annular with a geomagnetic north-south asymmetry and a radius at the outer half-maximum of about 200 km. Larger temperature changes occur in a more tenuous nighttime *D* region, by as much as a factor of 3 to 4 over NAA. The results of this model are used with a three-dimensional model of propagation in the Earth-ionosphere waveguide (W. L. Poulsen et al., *J. Geophys. Res.*, *98*, 1705, 1993) to predict the effect of the heated region on the VLF probe wave, with results consistent with observations.

J5-1
1340

EARLY RESULTS FROM THE VLBA CORRELATOR
Jonathan D. Romney
National Radio Astronomy Observatory
Post Office Box O
Socorro, New Mexico   87801-0387

The Very Long Baseline Array (VLBA) was formally opened on 1993 August
20. A multi-purpose instrument, it is capable of continuum,
spectroscopic, astrometric/geodetic, multi-frequency, bandwidth
synthesis, polarization, and pulsar measurements --- with a variety of
bandwidths, sampling rates, quantization schemes, and multi-band
modes. Frequent joint observations are expected to combine the Array
with existing telescopes to produce global and/or extremely sensitive
arrays. The VLBA correlator was designed to support routine processing
of all observations involving the Array, in all these operating modes.

Commissioning of the VLBA correlator is nearing completion. A crucial
milestone in this process was reached recently: first scientific images
have been obtained. These and subsequent early results will be
presented. This paper will focus on reviewing the correlator's current
capabilities, and the outlook for availability of features not yet
supported.

J5-2
1400
HIGH FREQUENCY PERFORMANCE OF THE VLBA

V. Dhawan, P. Napier, C. Walker, A. Zensus
National Radio Astronomy Observatory
P.O. Box 'O', Socorro, NM 87801

All 10 VLBA antennas have been fully operational since the completion of the construction phase in Jan 1993. We discuss the following parameters of the array, with emphasis on the short wavelengths - λ 13, 7, and 3 mm:

Antenna efficiencies and system temperatures.

Pointing/tracking performance.

Opacity correction technique.

Calibration dataflow.

Interferometric phase stability.

Efficiency improvements from subreflector re-alignment.

Expected 3mm performance.

Unsolved problems.

THE VLBA AMPLITUDE AND PHASE CALIBRATION SYSTEM

D. S. Bagri and P. J. Napier
National Radio Astronomy Observatory
P O Box O, Socorro, NM 87801

The accuracy of the calibration applied to measured visibility data limits the dynamic range and fidelity achievable in a very long baseline interferometry (VLBI) image made using the data. Amplitude and phase calibrations of VLBI data have been difficult in the past due to the lack of a uniform calibration system on the various antennas used for observations. Therefore, users had to rely on self calibration techniques to calibrate the data, and the self calibration methods do not work well in cases where data have low signal to noise ratios or when images have complex brightness distributions. In such cases people had to resort to adhoc calibration methods. In the recently completed Very Long Baseline Array (VLBA) we have incorporated on each antenna (1) a broadband noise calibration system, and (2) a coherent pulse calibration system. The calibration signals are injected at the inputs of various receivers. These signals are used for measuring the system temperature, and calibrating the amplitude and phase response of the complete electronics system. An additional possible use of the accurate measurements of the sytem temperature variations is in estimating the tropospheric (propagation) phase changes for each antenna. This will allow longer coherent integrations, making imaging of weak sources possible using self calibration techniques. Further, these (calibration) signals, along with (1) a global positioning system (GPS) timing receiver at each antenna, and (2) the capability for (almost) real time fringe checking using radio sources, allow almost continuous monitoring of the system performance. The calibration systems are also very useful for quick diagnosis and trouble-shooting, resulting in improved array reliability.

In this paper we will describe the various VLBA calibration systems and present results from test observations demonstrating their applications.

J5-4   USING GEOSTATIONARY SATELLITES TO ASSESS
1440   VLBA ANTENNA PERFORMANCE
            A.J. Beasley, M.J. Kesteven
            National Radio Astronomy Observatory
            P.O. Box 'O', Socorro, NM 87801

We discuss the use of 12 & 38 GHz geostationary satellites in high S/N measurements of VLBA antenna performance. These 'pseudo-astronomical' sources can be used for optical-path alignment, real-time interferometry, and phase-referenced dish holography. We also plan to examine the long-term/seasonal effects of the wet and dry troposphere on high-frequency signal propogation at the VLBA sites.

J5-5   NEW-GENERATION VLBI DATA-ACQUISITION
1500   AND CORRELATION SYSTEM
Alan R. Whitney
MIT Haystack Observatory
Westford, MA 01886

Modern VLBI observations for both astronomy and geodesy continue to demand the utmost in sensitivity. Of the methods potentially available for increasing the sensitivity of continuum VLBI observations, increasing the recorded bandwidth is generally the most cost effective.

Over the past three years a broadly-supported program has been undertaken at Haystack Observatory to increase the sensitivity of the Mark IIIA VLBI system by more than a factor of 2. The result is an upgrade to the existing Mark IIIA data-acquisition system, dubbed Mark IV, which increases the maximum data rate to 1024 Mbits/sec, more than quadrupling the maximum data-rate of the Mark IIIA.

A new VLBI correlator, directly expandable to 32 stations at 2 Gbit/sec/station, is being designed to support the Mark IV data-acquisition system. An international collaborative effort has been mounted to support this effort, which will be applied to both VLBI and connected-element interferometers in both the U.S. and Europe.

J5-6
1540

SENSITIVITY OF A MILLIMETER VLBI ARRAY USING BASELINE
SEARCH, GLOBAL SEARCH AND BISPECTRUM

A.E.E. Rogers,
S.S. Doeleman
Haystack Observatory
Westford, MA 01886

A theoretical comparison of the detection threshold for a baseline oriented fringe search, a global station oriented fringe search and the bispectrum is made for a VLBI array in the presence of coherence limiting atmospheric phase fluctuations. Examples of fringe detections are shown for a VLBI array operating at 3 millimeter wavelength. A method for the measurement of closure phases using the optimized coherent integration of the complex fringe amplitude and subsequent coherent integration of the complex triple product (also known as the bispectrum) around a triangle of baselines is analyzed and examples of the optimization of coherent integration presented. Optimization of the determination of unbiased correlation amplitudes is also discussed.

J5-7
1600

A TEST OF WVR-BASED TROPOSPHERE DELAY
CALIBRATION USING VLBI OBSERVATIONS ON
A 20 KM BASELINE

L.P. Teitelbaum, B.L. Gary, S.J. Keihm,
M.J. Mahoney, K.A. Marsh, R.P. Linfield,
R.N. Treuhaft, S.J. Walter, J.Z. Wilcox
Jet Propulsion Laboratory
California Institute of Technology
4800 Oak Grove Drive
Pasadena, CA 91109-8099

Six sessions of S/X band Very Long Baseline Interferometry (VLBI) observations on a 20 km baseline at Goldstone, CA were conducted in April and May 1993, using 26m and 34m Deep Space Network (DSN) antennas. A number of troposphere calibration instruments were employed during these observations, including a Water Vapor Radiometer (WVR) within 50 m of each radio antenna, a Microwave Temperature Profiler at one site, radiosonde launches approximately every 6 hours at both sites, and surface meteorology at both sites.

This experiment was designed to test the error budget for WVR-based troposphere delay calibration, and to test possible refinements in path delay retrieval algorithms. A preliminary analysis of the data has shown a significant reduction in the scan-to-scan rms residual VLBI delay scatter using standard statistical retrieval algorithms for WVR line-of-sight delay estimates. Results will also be presented for model-based retrieval algorithms.

J5-8
1620

FAR SIDELOBES OF 25m RADIOASTRONOMY ANTENNAS AT λ 18cm.

V. Dhawan, B. Brundage, P. Lilie, G. Petencin,

B. Sahr, B. Clark

National Radio Astronomy Observatory

P.O. Box 'O', Socorro, NM 87801

Interference to Radio Astronomical Observations enters the receiver mainly from the far sidelobes of the antenna. The VLA and VLBA L-Bands cover approximately 1200-1800 MHz, and include many potential sources of interference, both terrestrial and in orbit.

Detailed knowledge of the sidelobes is useful to evaluate the impact of present and future RFI levels, and design into planned systems some protection for Radio Astronomy. The VLA and VLBA feeds are sufficiently different that it is useful to measure both types of 25m antennas. We discuss the measurements, the observed features and causes, and the implications for RFI from satellites.

J5-9
1640

L-BAND RFI SURVEY AT THE VLA.

B. Brundage, P. Crane[1], V. Dhawan

National Radio Astronomy Observatory

P.O. Box 'O', Socorro, NM 87801.

[1] Present Address: Interferometrics, Inc. McLean VA.

Results are presented of a long-term RFI monitoring project over 1220-1750 MHz at the VLA.

Dependence of RFI on array extent and time of day are investigated, sources are identified, and an empirical probability of interference vs. frequency is derived from the data.

Implications are discussed for the choice of default observing frequencies; for observations at non-standard frequencies; and for the impact of RFI on the VLA All-Sky Astronomical Survey of several year's duration.

Session A/J   0855-Sat.   CRO-30
SOLAR SYSTEM RADIO AND RADAR ASTRONOMY: NEW MEASUREMENT TECHNOLOGY
Chairman: Michael M. Davis, Arecibo Observatory, Arecibo, PR 00613-0995

A/J-1   COHERENT RANDOM FREQUENCY MODULATION PROPERTIES
0900   FOR OVERSPREAD PLANETARY RADAR TARGETS

Benjamin C. Flores   Raymond F. Jurgens[*]
Electrical Engineering Department Jet Propulsion Laboratory
The University of Texas at El Paso 4800 Oak Grove Drive
El Paso, Tx 79968   Pasadena, CA 91109

With the discovery of polar ice on Mercury inferred from Earth-based radar observations, there is a renewed interest in the global imaging of Mercury, Mars, and the Galilean moons. Typically, the normal delay-Doppler imaging technique is inadequate for these highly overspread targets due to adverse alias. Sulzer (Radio Science 21, 1986) demonstrated that a long binary phase code can be processed in coherent segments eliminating the alias. Recently, Hagfors and Kofman (Radio Science 26, 1991) showed that a random Gaussian modulation can also overcome the alias. However, the self noise can be a serious limitation if the number of independent averages is not large. Hagfors and Kofman also proposed a polarization modulation scheme for further reducing the self noise.

We have explored the use of random frequency modulation (FM) as a viable means to overcome the delay-Doppler aliasing of overspread targets. Our decision to attempt this technique was inspired by the recent development of digitally programmed oscillators which are capable of high tracking rates, coherent upgrade from 10^3 to 10^4 times per second, and settings of 1 μHz. These oscillators normally track the Doppler shift of the incoming signal or provide the up-link frequency shift for the transmitter to compensate for the Doppler at a receive site. The addition of a random hop capability is therefore a simple matter. We have chosen the use of 256 equally spaced frequency hop states spread over a bandwidth β. The states are selected from a linearly connected maximum length shift register that generates 8-bit words. These words determine the hop state to be transmitted at each time interval. The range resolution is controlled by the selection rate or baud rate, and the Doppler resolution is controlled by the sampling rate and the size of the Fast Fourier Transform used to extract the Doppler. The bandwidth β must be as broad as the target to cause a uniform sea of self noise. The proposed FM modulation has reduced sidelobes and a higher compression ratio relative to binary phase coding. This may permit a lower sampling rate than the binary phase technique. Figure 1 shows an estimate of the average ambiguity function obtained by processing 100 frequency hop code observations. Notice the narrow peak response at zero lag and the surrounding self noise level.
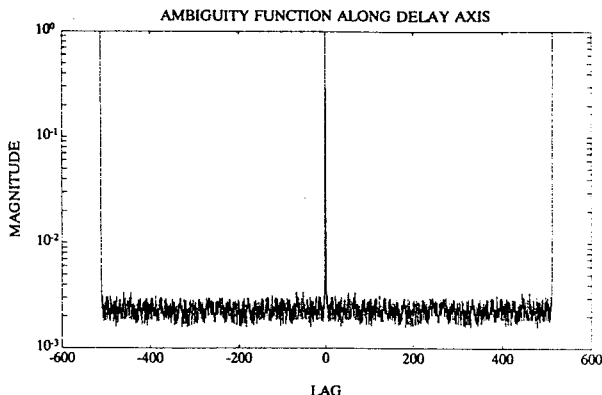
Figure 1.   Average ambiguity function of 100 random frequency hop code observations.

A/J-2   ABSOLUTE FLUX CALIBRATIONS OF VENUS AND
0920   JUPITER AT 32 GHz

Mark S. Gatti, Michael J. Klein
Jet Propulsion Laboratory
California Institute of Technology
Pasadena, Ca 91109

The microwave flux densities of Venus and Jupiter at 32 GHz have been measured using a calibration-standard radio telescope system at the Owens Valley Radio Observatory (OVRO) during April and May of 1993.   A preliminary analysis of these data suggests that the absolute accuracy of the results is of the order +/- 5% (0.2 dB). These measurements are part of a joint JPL/Caltech program to accurately calibrate a catalog of other radio sources · using the two bright planets as flux standards.

The calibration standard radio telescope at OVRO consisted of a 1.5-meter diameter offset feed cassagrainian reflector, with a dual beam Dicke radiometer. The antenna system including the radiometer feed horns were previously calibrated by the National Institute for Standards and Technology (NIST) in the near-field measurement facility.   The antenna employed dual shaping for both the main and subreflectors yielding an efficiency of 80% for each of the dual secondary beams. The two antenna feeds are aligned in the horizontal plane so that atmospheric effects are   nearly identical for each beam on the sky.

The measurements are of high accuracy due both to the NIST calibrations and frequent radiometer calibrations during the observations. The dicke radiometer consisted of a state-of-the-art cryogenically cooled high electron mobility transistor (HEMT) amplifier and a high speed circulator switch. The total system temperature provided by the radiometer/antenna combination was 75 kelvin during the time of the observations.

An independent set of measurements of the two planets and the standard calibration radio sources Virgo A (3C274) and DR 21 were made with a 34-meter diameter beam-waveguide antenna at the research and development station of NASA's Goldstone Deep Space Communication Complex. These observations were made from April through July at 33.68 GHz using a total power radiometer that was calibrated frequently during each observing session. The ratio of the Venus/Jupiter fluxes from the OVRO and Goldstone measurements was highly correlated and the absolute magnitudes of the resultant flux densities are highly accurate. The results of the Goldstone observations will be used to enhance the radio source calibration work that will be reported in the near future.

A/J-3
0940

THE PRECISION MEASUREMENT OF TIME-VARIABLE FARADAY ROTATION WITH THE VERY LARGE ARRAY

S.R. Spangler and T. Sakurai
Dept. of Physics and Astronomy
University of Iowa
Iowa City, IA 52242

In a number of radioastronomical applications such as the measurement of coronal Faraday rotation or pulsar Faraday rotation, one needs precision measurements of a time-variable polarized source. In this paper we discuss the limits to polarization position angle measurement with the Very Large Array, and the way in which these limitations may be circumvented. Linear polarization measurements of fourteen sources were made at 1465 and 1635 MHz on March 21, 1990. The sources were observed about ten times over a twelve hour period. Normal VLA polarization calibration procedures were followed, with the exception that a more sophisticated model for the ionospheric Faraday rotation was employed. The rms variations of the calibrated position angles at 18 and 20 cm varied from 2 to 5 degrees, and were in all cases greater than the variation expected from radiometer noise. We assumed that these excess variations were attributable to errors in the estimate of the ionospheric Faraday rotation and in the instrumental polarization parameters (referred to in VLA technical literature as the D factors). A simple polarimeter model was developed and a self-calibration algorithm adopted which utilized data from all suitable sources to determine the ionospheric Faraday rotation and instrumental residuals. The residual Faraday rotation was found to be ± 1.5 degrees out of a total of $\simeq 17$ degrees. The residual D factors were found to be a few percent of their total values, and showed temporal variations on a time scale of a few hours. Knowledge of these residuals allowed us to perform a second order polarization calibration. A significant improvement in the position angle stability was achieved for sources far from the sun. The rms position angle variations were reduced to under 2 degrees, and in some cases approached the theoretical radiometer noise. These techniques and procedures may be easily applied to other types of VLA polarimetric observations which require high precision or temporal stability.

A/J-4
1000

VERY LARGE ARRAY POLARIMETRIC STUDIES
OF THE CORONAL PLÁSMA

T. Sakurai and S.R. Spangler
Dept. of Physics and Astronomy
University of Iowa
Iowa City, IA 52242

We used the Very Large Array to make measurements of Faraday rotation through the solar corona on a line of sight to the extragalactic radio source 0010+005. Polarimetric observations were made at 1465 and 1635 MHz. The line of sight passed within about 9 $R_\odot$ at closest approach. The polarization data were processed with a second order polarization calibration procedure to remove uncorrected ionospheric Faraday rotation and instrumental polarization, as discussed in an accompanying paper. We measured a rotation measure of -12.6 rad/m^2 along the line of sight to this source. Use of a model for the electron density profile in the corona and lower solar wind, and a model for the solar magnetic sector structure on the day of the observations allows us to extract a value for the magnitude of the coronal magnetic field at 9 $R_\odot$ of 12.5 milliGauss. This value is comparable to, but somewhat greater than some previous estimates for this part of the corona. Our observations showed a slow change in the rotation measure during the course of the observing session, at a rate of about 1 rad/m^2/hr. Part of this change is attributable to the changing penetration of the line of sight in the corona during the session, and part to an unidentified plasma structure in the corona. We also searched for rotation measure fluctuations on hour timescales, which could be attributed to coronal Alfven waves. Only upper limits were obtained, which are comparable in magnitude, although somewhat larger than those reported from Faraday rotation measurements of the Helios spacecraft transmitter. We use our measurements to set an upper limit to the Alfven wave energy flux at the base of the corona. We will discuss a number of ways in which observations of this sort could be improved, to be able to yield more precise and sensitive measurements of waves and magnetic fields in the corona.

A/J-5
1040
TROPOSPHERIC CALIBRATION FOR THE MARS OBSERVER
GRAVITY WAVE EXPERIMENT

Steven J. Walter, John Armstrong
Jet Propulsion Laboratory, Mail Stop T-1182/3
California Institute of Technology
4800 Oak Grove Drive
Pasadena, CA 91109

In spring 1993, microwave radiometer-based tropospheric calibration was provided for the Mars Observer gravitational wave search. The Doppler shifted X-band radio signals propagating between earth and the Mars Observer satellite were precisely measured to determine path length variation that might signal passage of gravitational waves. Experimental sensitivity was restricted by competing sources of variability in signal transit time. Principally, fluctuations in solar wind and ionospheric plasma density combined with fluctuations in tropospheric refractivity determined the detection limit. Troposphere-induced path delay fluctuations are dominated by refractive changes caused by water vapor inhomogeneities blowing through the signal path. Since passive microwave remote sensing techniques are able to determine atmospheric propagation delays, radiometer-based tropospheric calibration was provided at the Deep Space Network Uranus tracking site (DSS-15). Two microwave water vapor radiometers, (WVRs) a microwave temperature profiler, (MTP) and a ground based-meteorological station were deployed to determine line-of-sight vapor content and vertical temperature profile concurrently with Mars Observer tracking measurements. This calibration system provided the capability to correct Mars Observer Doppler data for troposphere-induced path variations. We present preliminary analysis of the Doppler and WVR data sets illustrating the utility of WVRs to calibrate Doppler data. This takes an important step toward realizing the ambitious system required to support the future Ka-band Cassini satellite gravity wave tropospheric calibration system.

A/J-6
1100

KA-BAND VERNIER POINTING OF A 34-METER BEAM WAVEGUIDE ANTENNA

L. Alvarez, M. Moore and W. Veruttipong
Jet Propulsion Laboratory
Pasadena, California, 91109-8099

Since 1976, the NASA/JPL Deep Space Network (DSN) antennas have successfully employed the conical scan (conscan) angle tracking technique to track deep space satellites. This method nutates the entire tipping portion of the antenna, and therefore the microwave beam, in elevation and cross-elevation, displaced about 0.1 dB from boresight. Beam pointing error estimates are then derived from the resultant receiver output signature. The conscan technique has persevered through the DSN upgrade from S-band (2.3 GHz) to the X-band (8.4 GHz) frequency. However, as the Network moves toward Ka-band (32 GHz) communications, the 0.1 dB beamwidth scan radii now are reduced to about .0016 and 0.0009 degrees for the 34-meter and 70-meter antennas, respectively. The desire to relieve the axis servomechanisms of these stringent Ka-band scanning requirements, as well as increasing the bandwidth of the beam switching capability, has lead to investigation into alternatives (both by mechanical and RF means) to the current DSN conscan method.

In this paper, a simple approach to Ka-band vernier pointing of the 34-meter DSS 13 beam waveguide antenna at Goldstone, California is presented. The scheme is to rotate one of the reflector plates in the beam waveguide RF path in order to scan the beam. While mechanically modulating any flat plate mirror in the beam waveguide feed system can be used to conscan the overall RF antenna beam, the last flat mirror (M6) has been chosen for concept demonstration at DSS 13. To achieve a scan radius of .0016 degrees, a rotation .094 degrees is needed at M6. The rotation results in minimal gain loss due to the increased noise.   The advantages of scanning the drastically smaller mirror with less precision will be discussed. In addition to the RF predicts, the structural mechanical and control system implementations will be highlighted. Preliminary Ka-band measurements taken at DSS 13 will be presented.

Modification and Identification
of the Beam Waveguide Antenna Control System Model

Caroline Racho and Wodek Gawronski
Jet Propulsion Laboratory, California Institute of Technology
Pasadena, CA 91109

This work is the first step toward increasing the bandwidth of the NASA/JPL 34 meter beam waveguide (BWG) antenna position loop controller. A wider bandwidth of the controller allows for faster tracking rates and better pointing performance under windy conditions. To achieve this goal the antenna control system model must accurately reflect the dynamic properties of the antenna.

The position controller at the 34 meter beam waveguide antenna located at Goldstone, California does not currently employ a model-based control law. In the interest of implementing model-based control, an analytical model was developed, and an experiment was designed to gather data at the 34 meter BWG antenna. The data was used to modify the analytical model, and to identify a new antenna model using SOCIT software of NASA Langley Research Center. The empirical transfer function and the transfer function of the identified model compared in Figure 1a,b show good coincidence.
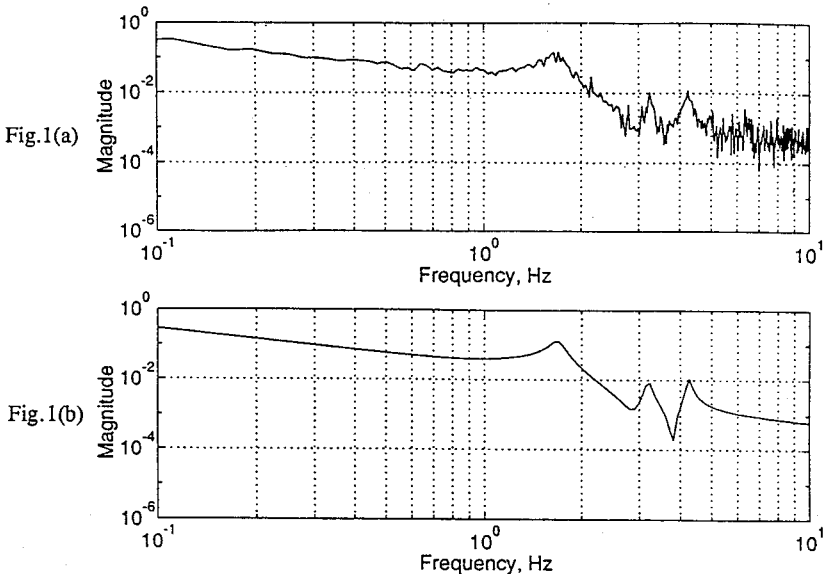
Fig.1. Transfer function of the antenna (azimuth I/O): (a) estimated from the collected data, and (b) obtained from the identified model.

A/J-8
1140
COMPENSATION OF GRAVITY INDUCED STRUCTURAL DEFORMATIONS ON A 34-METER BEAM WAVEGUIDE ANTENNA

M. Thorburn, M. Britcliffe, A. Loh,
M. Moore, & D. Strain
Jet Propulsion Laboratory
California Institute of Technology
Pasadena, California 91109-8099

The NASA Deep Space Network (DSN) is the largest and most sensitive scientific-telecommunications and radio-navigation network in the world. The DSN is made up of three Deep Space Communications Complexes and each complex consists of four Deep Space Stations (DSS). At the Goldstone complex, located in the Mojave Desert in California, a 34-meter diameter beam-waveguide (BWG) antenna, DSS-13, was constructed in 1988-1990 and has become an integral part of the advanced systems program and a test-bed for technologies being developed for the several BWG antennas scheduled to be built in the DSN in the next several years.

In the first phase of the performance calibration of DSS-13, the antenna efficiency at 32 GHz was found to depend significantly on the elevation angle, i.e. it decreased from 45% to 35% as the elevation angle changed from 45 degrees to 20 degrees. (Slobin, JPL Report D-8451). This elevation angle dependence is due to the deformation in the main reflector caused by the resulting change in the gravitational force applied to the antenna structure. Systems designed to compensate these gravitational errors have been developed at JPL in the past few years and include a variety of technologies ranging from the use of hydraulic actuators (Levy & Strain, JPL TDA Progress Report 42-114), to deformable mirrors (Galindo-Israel, Rengarajan, Veruttipong, & Imbriale, IEEE A/P 1993 Symposium Digest) to electronically phased array feeds (Vilnrotter, Rodemich, & Dolinar, IEEE T-Com, Vol. 40, No. 3). In some instances prototypes of these systems have been constructed and tested.

In this paper, the most promising mechanical designs for gravity compensation will be presented along with performance predictions and some recent measurements which can be used to make a relative comparison. The shape of the compensation surfaces are found using electromagnetic analyses. Details concerning the mechanical realization, and tolerances, of these desired shapes will be discussed. The gravity compensation systems included in this discussion will be the large scale deformation of the entire backup structure, the deformation of a mirror in the BWG, the deformation of the subreflector at the apex of the antenna, and the actuation of the panels on the main-reflector surface.

B9-1   SAMPLING CRITERIA FOR RESONANT
0900   SCATTERERS AND ANTENNAS

Arthur D. Yaghjian
Electromagnetics Directorate
RL/ERCT, Hanscom AFB, MA 01731

The sampling criteria necessary for the reconstruction of fields out-side antennas and scatterers are usually based on the hypothesis that the reactive fields are negligible more than a couple of wavelengths from the antenna/scatterer; or alternatively, on the hypothesis that the fastest angular variations a wavelength or so from the antenna/scatterer will be that of surface waves traveling at about the speed of light in free space. Both these hypotheses lead to the spherical sampling requirement of $(1+\epsilon)k_0(a+\lambda_0)$ modes and the planar sampling spacing of $.5\lambda_0/(1+\epsilon)$. In addition, the maximum total radar cross section of a scatterer is usually assumed to be approximately equal to twice the cross-sectional area of the scatterer $(2\pi a^2)$.

In this presentation we show that both these commonly assumed results have to be modified for penetrable scatterers and traveling-wave antennas that exhibit significant resonances. Specifically, the number of spherical modes and planar sampling spacing is modified to $(1+\epsilon)k(a+\lambda_0)$ and $.5\lambda/(1+\epsilon)$, respectively, where $k = 2\pi/\lambda$ is the relevant propagation constant of the penetrable scatterer or traveling-wave antenna. In addition, the maximum possible total radar cross section of the scatterer or effective area of the antenna is shown to be $2\pi a^2 k^2/k_0^2$, which is also shown to be the maximum possible extent of the significant reactive fields.

An example of this resonant scattering is given and we explain how these unusual phenomena are consistent with the theorem that scattered fields are determined by the incident fields over only the physical scatterer.

B9-2   SPECTRUM OF TWO-DIMENSIONAL SOLUTIONS IN
0920   ANTENNAS AND SCATTERING

Sembiam R. Rengarajan and Per-Simon Kildal*
Electrical and Computer Engineering Department
California State University
Northridge, CA 91328-1283
*Chalmers University of Technology
S-412 96 Gothenburg, Sweden

We present an efficient and accurate procedure to solve radiation and scattering problems for cylindrical structures with finite length sources, e.g., waveguide-fed slots with different cylindrical outer structures. This problem is formulated first in k_z spectrum by performing a Fourier transform of spatial domain fields. One then obtains a spectrum of two-dimensional solutions by solving a two-dimensional problem (with a harmonic z-variation) for each spectral value. The spatial domain fields are obtained by an inverse Fourier transform process. This process may be made very efficient by considering a suitable asymptotic model for the problem. This technique is well suited for parallel processing type computational algorithms. Applications such as slots cut in rectangular waveguides radiating into an exterior region containing baffles or other arbitrary structures, and slots for dual polarization applications will be discussed with their asymptotic models. Green's functions for some of these structures will be presented. Two-dimensional solutions in spectral domain of integral equations technique for cylindrical waveguides to obtain the mode spectrum, cut-off frequencies etc. will be reviewed briefly.

B9-3   **SCATTERING BY A GROOVE IN AN IMPEDANCE PLANE**
0940   Sunil S. Bindiganavale and John L. Volakis
       Radiation Laboratory
       Department of Electrical Engineering and Computer Science
       The University of Michigan
       Ann Arbor, MI 48109-2122

An analysis of two-dimensional scattering from a narrow groove in an impedance plane is presented. The groove is represented by an impedance surface and hence the problem reduces to that of scattering from an impedance strip in an otherwise uniform impedance plane. On the basis of this model, appropriate integral equations are constructed using a form of the impedance plane Green's functions involving rapidly convergent integrals. The integral equations are solved by introducing a single basis representation of the equivalent current on the narrow impedance insert. Both tranverse electric (TE) and transverse magnetic (TM) polarizations are treated. The resulting solution is validated by comparison with results from the standard boundary integral method (BIM) and a high frequency solution. It is found that the presented solution for narrow impedance inserts can be used in conjunction with the high frequency solution for the characterization of impedance inserts of any given width.
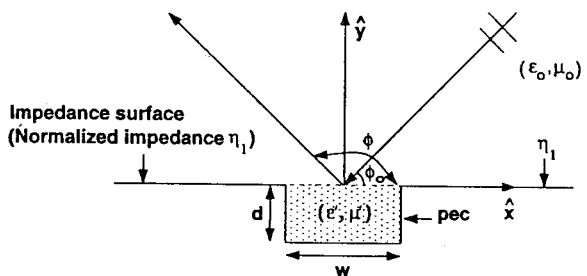
Geometry of the groove in an impedance plane.

B9-4
1020

AN ABSOLUTE STANDARD FOR VALIDATING GENERAL NUMERICAL CODES FOR SCATTERING FROM AN OBJECT COATED WITH ANISOTROPIC SURFACE IMPEDANCE

Hung-Mou Lee
Department of Electrical and Computer Engineering
Naval Postgraduate School (EC/Lh)
Monterey, CA 93943-5121

General purpose numerical codes for computing electromagnetic scattering from an object coated with anisotropic surface impedance have been developed by several groups of researchers including L.N. Medgyesi-Mitschang and J.M. Putnam [*IEEE Trans., AP-33*, 206-214, 1985] and A.H. Chang, et. al. [*IEEE Trans., AP-40*, 1992]. In order to validate such codes, it is desirable to find a model which can be constructed easily for experimental testing and is simple enough to allow accurate theoretical computation. This special theoretical solution can then be utilized to validate those general purpose numerical codes over a wide range of desirable parameters. An infinitely thin conducting tubular cylinder coated with different anisotropic impedances on its inside and outside surfaces has been chosen for this endeavor.

Formulation of the boundary value problem utilizing the sums of the inside and outside surface currents of both the electric and the magnetic types as the independent unknown variables preserves the duality symmetry of Maxwell equations. It can be deduced, without solving the complete problem, that with some particular surface impedance tensors, there will be no back-scattering for a plane wave incident along the axis of the cylinder. These special cases can serve as an absolute standard for validating any general purpose numerical codes.

Similar to the condition deduced by V.H. Weston [*IEEE Trans. AP-11*, 578-584, 1963], the determinant of the average of the inside and outside normalized impedance tensors must equal unity. The impedance tensors must be symmetric. If the impedance tensors are different, their elements must be related in a certain manner. These relations will be reported.

B9-5
1040

RADIATION AND SCATTERING BY CONDUCTING BODIES OF REVOLUTION EMBEDDED IN PLANE-STRATIFIED MATERIAL MEDIA

A. K. Abdelmageed and K. A. Michalski
Electromagnetics & Microwave Laboratory
Department of Electrical Engineering
Texas A&M University
College Station, TX 77843–3128

The mixed-potential integral equation (MPIE) originally developed for arbitrarily shaped conducting objects embedded in plane-stratified material media (Michalski and Zheng, *IEEE Trans. Antennas Propagat.*, 38, 335–344, 1990; Michalski, *J. Electro. Waves Applic.*, 7, 899–917, 1993) is specialized to the case of a body of revolution (BOR) whose axis is perpendicular to the interfaces between dissimilar layers of the medium. The BOR MPIE is then numerically solved for the surface current density by well-established method of moments procedures (Glisson and Wilton, *IEEE Trans. Antennas Propagat.*, AP–28, 593–603, 1980). Once the surface current is found, other quantities of interest, such as the radar cross-section (RCS) of the object, are readily obtained.

Sample numerical results are presented for several conducting objects of revolution near to or penetrating an interface between contiguous dielectric half-spaces. Included among the structures considered is a pillbox floating in sea water. For open vertical cylinders, comparisons are made with the results obtained from azimuthally-invariant formulations (Chang and Wait, *IEEE Trans. Antennas Propagat.*, AP–18, 182–188, 1970; Butler and Michalski, *Digest URSI National Radio Sci. Meeting*, 55, 1983; W. A. Johnson, *Radio Sci.*, 18, 1273–1281, 1983). For a pillbox scatterer, the BOR results are validated against the corresponding results obtained from a general three-dimensional computer code (Michalski and Zheng, *IEEE Trans. Antennas Propagat.*, 38, 345–352, 1990).

B9-6   TIME-FREQUENCY ANALYSIS OF BACKSCATTERED
1100   DATA FROM FINITE DIELECTRIC GRATINGS
          J. Moore and H. Ling
          Department of Electrical and Computer Engineering
          The University of Texas at Austin
          Austin, TX 78712-1084

We have recently explored several time-frequency analysis tools in the interpretation of backscattered data (H. Kim and H. Ling, IEEE Trans. Antennas Propagat., 41, 200-207, 1993) and (H. Ling, J. Moore, D. Bouche, and V. Saavedra to appear in IEEE Trans. Antennas Propagat.). Scattering mechanisms, which may not be immediately visible in the traditional time domain or the frequency domain, were found to become quite revealing in the joint time-frequency plane. The time-frequency plane allows scattering centers, target resonances, and dispersive phenomena to be simultaneously displayed and identified. They can also be correlated with target scattering physics and even extracted individually. The targets we have studied include open-ended waveguide ducts, inhomogeneous dielectric objects, and coated plates.

In this work, we investigate the scattering phenomenology in a finite, dielectric grating (shown below) using time-frequency analysis. The motivation for this structure stems from our recent work in grooved coatings for backscattering control applications (J. Moore, H. Ling, and C. S. Liang to appear in IEEE Trans. Antennas Propagat.), as well as from a continued interest among the electromagnetics community in edge effects of finite periodic structures such as frequency selective surfaces and antenna arrays. The backscattered data for a finite conductor-backed dielectric grating under H-polarized incidence are generated using a two-dimensional moment-method code. The resulting frequency spectrum of backscattered data (from 2 to 18 GHz) are then used in generating the two-dimensional time-frequency display via the short-time Fourier transform (STFT). Through the time-frequency, we are able to pinpoint the Floquet harmonics due to the incident plane wave, the Floquet harmonics due to surface waves, and the higher order diffraction mechanisms due to the edges of the grating. In addition, the Floquet harmonic due to the surface waves excited by the edges of the strip is also identified. This mechanism is unique to the finite grating.
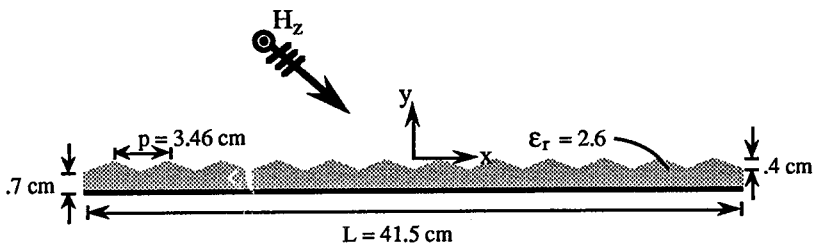
B9-7
1120

THE RESPONSE OF ANOMALOUSLY DISPERSIVE DIELECTRIC MEDIA TO ARBITRARY ELECTROMAGNETIC PULSES.

Peter G. Petropoulos,

AL/OES, Armstrong Laboratory,

Brooks AFB, TX 78235-5102.

We determine the response of a dispersive dielectric half-space to an arbitrary electromagnetic pulse by deriving and analyzing a novel single high-order partial differential equation for the Electric field. The medium properties are modeled by an arbitrary number of Debye orientational polarization mechanisms which fit experimentally determined permittivity values for a typical medium in the microwave range of frequencies. The general dependence of the response on medium and pulse properties will be described. A "skin-effect" for pulses, reminiscent of the well known effect for harmonic waves, will be shown to exist. While the field in the "skin-layer" is exponentially decaying, we will show three types of response deeper in the medium, each type realized according to whether $T_p/\tau \gg 1$, ~ 1, or $\ll 1$, where T_p is the incident pulse duration, and τ is a characteristic maximum or minimum relaxation time of the dielectric. The main disturbance will be shown to satisfy an advection-diffusion equation. After the "skin-depth," the amplitude of the response will be shown to decay as $1/\sqrt{z}$ where z is the depth, or as $1/\sqrt{t}$, where t is time, for fixed z. A consequence of this is that the electric field energy in the medium will be decaying as $1/z$ $(1/t)$, thus pulsed fields can penetrate significantly deeper than continuous waves. Also, it will be shown that in Debye media the main disturbance travels with the DC phase velocity. These results are verified by solving the full Maxwell's equations with a numerical method based on finite differences. Such results may have an impact on studies whose goal is to include short-pulse phenomena in a future update of the IEEE RF exposure standard.

SCATTERING OF PULSED RADIATION FROM AN IMPERFECTLY-CONDUCTING INFINITE PERIODIC SEA SURFACE

J. Song, A. Norman, D. Nyquist, J. Ross, P. Ilavarasan,
M. Seneski, K. Chen and E. Rothwell
Department of Electrical Engineering
Michigan State University
East Lansing, Michigan 48824

The scattering of pulsed electromagnetic radiation from an imperfectly-conducting, infinite, periodic sea surface is studied. Such scattering influences the performance of impulse radars operating in a sea-surface environment. The time-domain transient response is synthesized from frequency-domain transfer functions for the induced surface and scattered fields. The two-medium scattering problem consists of space and sea-water regions separated by a periodic sea surface and illuminated by a plane wave incident from the space region. It is assumed that the space region (1) is located above sea-surface contour C, with permittivity $\epsilon_1 = \epsilon_0$. The sea-water region (2) is located below sea-surface contour C, with complex permittivity ϵ_2. Wavenumbers in the two regions are $k_i = \omega \sqrt{\mu_0 \epsilon_i}$ for $i = 1,2$. Unit normal vectors to the interface contour C are chosen as $\hat{n}_{1,2}$, directed outward from the respective regions, such that $\hat{n}_2 = -\hat{n}_1 = \hat{n}$. A coordinate system is chosen with the z-axis normal to the sea plane, while the sea surface is uniform along y and periodic along x as $z(x) = -h\cos(2\pi x/L)$ with h the sea height and L its period.

The transverse magnetic scattering problem is of greatest interest, due to the potential absence of specular reflections at the Brewster's incidence angle. For the TM polarization, all EM fields can be expressed in terms of the generating field $\vec{H} = \hat{y} H_y(x,z) = \hat{y}\psi(x,z)$. Surface field ψ and its normal derivative satisfy the coupled integral equations (where $\vec{\rho} = \hat{x}x + \hat{z}z$ is the 2-D position vector)

$$\frac{\psi(\vec{\rho})}{2} - PV\!\int_{C_p}\left[\psi(\vec{\rho}')\frac{\partial G_1(\vec{\rho}\,|\,\vec{\rho}')}{\partial n'} - \frac{\partial\psi(\vec{\rho}')}{\partial n'}G_1(\vec{\rho}\,|\,\vec{\rho}')\right]dl' = \psi^i(\vec{\rho})$$

$$\frac{\psi(\vec{\rho})}{2} + PV\!\int_{C_p}\left[\psi(\vec{\rho}')\frac{\partial G_2(\vec{\rho}\,|\,\vec{\rho}')}{\partial n'} - \frac{\epsilon_2}{\epsilon_1}\frac{\partial\psi(\vec{\rho}')}{\partial n'}G_2(\vec{\rho}\,|\,\vec{\rho}')\right]dl' = 0$$

with periodic Green's-function kernels represented in Floquet-mode series expansions. The incident magnetic field is $\psi^i(\vec{\rho}) = H_0 e^{-j\beta x}e^{jqz}$ with $\beta = k_1\sin\theta_i$, $q = k_1\cos\theta_i$ where θ_i is the incidence angle. Notation PV implies evaluation of integrals in a principal-value sense, and C_p is the first period of the sea surface. The integral equations are solved numerically by the method of moments to obtain frequency domain spectra for the surface and scattered fields. Results are compared with those obtained from an approximate Floquet-mode-matching analysis based upon the Rayleigh approximation; agreement is found to be excellent within the regime of the latter approximation.

The frequency-domain spectra are used to construct the time-domain pulse response of the sea surface using the inverse FFT. Results are found to be significantly influenced by cutoff frequencies associated with the Floquet modes. For the backscattered field, each such mode has a lower cutoff frequency, below which it becomes evanescent in the z-direction, and an upper cutoff frequency, above which it becomes forward propagating. Extensive numerical results are obtained.

G5-1   COORDINATED RADIO, OPTICAL AND SATELLITE
0920   MEASUREMENTS OF AURORAL ELECTRODYNAMICS

E. J. Weber[1] , J.F. Vickrey[2] , and H.A. Gallagher[3]
[1] Phillips Laboratory/GPIA
Hanscom AFB MA 01731
[2] Geoscience and Engineering Center
SRI International
[3] Department of Physics
Boston College

Jurgen Buchau played a major role in investigating high latitude
ionospheric structure and dynamics through deployment of diagnostic
capabilities at several polar stations. In this paper, we report recent
results from measurements at two locations where Jurgen had been the
lead campaign scientist: dayside auroral dynamics from Ny Alesund,
Spitsbergen, and nightside electrodynamics from Sondrestrom,
Greenland. All Sky Imaging Photometer (ASIP) measurements at Ny
Alesund provide large-scale coverage of the cusp/cleft auroral
precipitation regions. Multi-wavelength images provide information at
both E- and F-region altitudes which distinguish hard and soft
precipitation regions. Overpasses of the DMSP satellites provide a
north-south snapshot of precipitating ions and electrons as well as
plasma drifts. The high temporal and spatial resolution of the ASIP
images, combined with the large coverage area, provides a means to
help differentiate between spatial and temporal structures present in the
satellite data.
The nightside measurements at Sondrestrom include data from the
Incoherent Scatter Radar (ISR), operated in a scan mode designed to
maximize resolution of the plasma flow in the vicinity of auroral arcs.
These combined measurements provide the ionospheric signature of
fields and currents associated with the arcs, and again provide the
temporal and spatial context in which to interpret the DMSP satellite
particle and plasma drift data.

G5-2 **THE DIGITAL IONOSPHERIC SOUNDING SYSTEM**
0940 **(DISS) NETWORK OF THE US AIR FORCE AIR**
WEATHER SERVICE

T.W. Bullett[1], A.E. Ronn[2], K.D. Scro[2], and J.L. Carson[3]
[1] Phillips Laboratory/GPIA, Hanscom AFB, MA 01731-3010
[2] Air Force Space Forecast Center, Falcon AFB, CO
[3] Headquarters Air Weather Service, Scott AFB, IL

Over the last twenty years, with great dedication and a comprehensive knowledge of ionosondes and the ionosphere, Jurgen Buchau was the driving force behind ionosonde development for the US Air Force. Due to his efforts, a network of twenty Digital Ionospheric Sounding Systems (DISS) of the United States Air Force Weather Service (AWS) collects real-time ionospheric data on a global scale. The Space Forecast Center (SFC) at Falcon AFB, Colorado, uses the real-time data to prepare ionospheric specifications and forecasts for communications, surveillance and navigation systems. Thirteen DISS are currently deployed, with six in the Arctic, six in the northern hemisphere mid-latitude region and one in Australia. The network is enhanced with three Digisonde 256s, the scientific version of the DISS, and the deployment of further DISS is in progress. Both systems have identical data outputs provided by the DISS autoscaling system ARTIST (Automatic Real Time Ionogram Scaler with True Height). Twenty seconds after completion of the ionogram sounding the data become available in an output buffer as IONOS and IONHT messages. The AWS Automated Weather Net (AWN) polls the network's stations and transfers the IONOS and IONHT messages to SFC for direct use by the central data processing computer.

The DISS messages, together with other data, are used to provide an estimate of the effective sunspot number, R_{eff}, as the driver for remotely operated models and to update the AWS Parameterized Real-Time Ionospheric Specification Model (PRISM). Real-time PRISM updating using DISS, DMSP satellite, and magnetic activity data is under development. DISS data are typically acquired every half hour, with the full digital ionograms recorded on tape for quality control, scientific analysis and archiving. While scientific analysis of the global and specifically the high latitude data base is conducted at the Phillips Laboratory, all data are available within approximately six months at the World Data Center A, Boulder, Colorado, which is in charge of the quality control for the autoscaled ionograms.

Continuing Jurgen Buchau's work, and in cooperation with the University of Massachusetts Lowell, it is planned to monitor ionospheric drifts with the DISS/Digisonde network and to develop a Polar Convection Monitor.

G5-3   MONITORING THE IMF WITH GROUND BASED IONOSONDES
1000

J. Buchau
Phillips Laboratory, Hanscom AFB, Massachusetts
J.L. Scali, C.G. Dozois and B.W. Reinisch
University of Massachusetts Lowell
Center for Atmospheric Research
450 Aiken Street
Lowell, Massachusetts

A Digisonde 256 at Qaanaaq, Greenland (87°N CGML) routinely measures F region drifts at 5 or 15 minute intervals. Analysis of the measured plasma flow shows its control by the IMF components Bz and By as expected by the statistical and physical models. The inverse problem is to determine the Bz and By components, or at least their signs, from the HF drift measurements. Such analysis was done for a one year observation period, and the deduced signs of Bz and By were compared with IMP8 IMF measurements. With our current analysis technique we were able to correctly deduce the IMF orientation in 65 to 70% of the time where Qaanaaq Digisonde and IMP8 data were available. A network of polar cap Digisondes could increase the reliability of the IMF deduction and would lead to the specification of the prevailing polar cap convection pattern in real time.

Jurgen Buchau died on 9 August 1993.

G5-4
1040 LARGE SCALE IONOSPHERIC STRUCTURES AND
SCINTILLATION IN THE POLAR REGION

S. Basu[1] and Sunanda Basu[2]
[1]Phillips Laboratory/GPIA, Hanscom AFB, MA 01731-3010
[2]Institute of Space Research, Boston College, MA 02159

Jurgen Buchau, to whom this session is dedicated, used his digisonde measurements to make many original contributions on ionospheric structures and their convection in the polar region. Among these, the Buchau et al., *Radio Sci, 20*, 325, 1985 paper makes a truly outstanding contribution. It showed that the patches of enhanced electron concentration observed in the winter polar cap can be explained by the convection of solar produced plasma equatorward of the cusp into the polar cap rather than by local production. The paper also suggested that the electron concentration in the central polar cap should exhibit a universal time control.

In this paper, we use the above framework to explain the UT/ seasonal variation of scintillation observed at Sondrestrom and Thule, Greenland. We find that small scale irregularities develop on large scale structures or patches with enhanced electron concentration which convect through the cusp into the polar cap and structure due to the gradient drift instability. Such structured patches cause intense scintillation of 250 MHz satellite signals. The patches of scintillation are also detected downstream at Thule due to anti-sunward plasma convection. We shall show that long term scintillation measurements at Thule can be understood on the basis of the Buchau et al., concept as extended by recent quasi-global model studies of Sojka et al (1993).

G5-5   THE EFFECTS OF MULTIHOP HF PROPAGATION ON THE
1100   PERFORMANCE OF OTH BACKSCATTER RADARS

J. Buchau[1], G. S. Sales[2], B.S. Dandekar[1], B. Weijers[3],
D. Reynolds[4], D. Anderson[1]
1. Ionospheric Physics Laboratory, Phillips Laboratory,
   Hanscom AFB, MA
2. Center for Atmospheric Research, University of Massachusetts
   Lowell, Lowell, MA
3. Rome Laboratory, Hanscom AFB, MA
4. Radex Corporation, Bedford, MA

Analysis of approximately one year's data from an operational OTH radar shows that equatorial clutter, originating in the ionosphere in regions up to 14,000 km from the radar, directly impacts the radar's performance. Radio waves propagating into these regions often involve three or more ground hops depending on the radar's azimuth and range from the magnetic equator. This interaction with nighttime equatorial irregularities are important to all OTH radar systems since all great circle paths cross the magnetic equator.

Special data processing was developed for this program that uses both the long range (to 8000 nm) wideband (6 to 28 MHz) backscatter ionograms made routinely at selected azimuths and the radar's amplitude, range and Doppler data format to measure the frequency of occurrence, range and intensity of the ionospheric clutter as a function of time and azimuth. These data indicate that intense random ionospheric irregularities associated with the nighttime equatorial activity produce Doppler spread scattered energy that increases the effective radar noise level and directly affects the performance of the radar. Using the Parametric Ionospheric Model developed at the USAF Phillips Laboratory and numerical ray tracing, the specific interaction regions for the radar signal and the ionospheric irregularities are shown and an explaination for the observed temporal and spatial behavior is proposed. Mechanisms for Doppler spreading of the clutter signal are also reviewed.

G5-6   BUBBLE FORMATION OBSERVED BY A NETWORK OF
1120   EQUATORIAL IONOSPHERIC SOUNDERS

J.A. Whalen
Geophysics Directorate, GPIA
Phillips Laboratory
Hanscom AFB, MA 01731-3010

The equatorial F layer in the western hemisphere is observed by a network of 15 ionospheric sounders spanning $\pm 30°$ DIPLAT. Recordings of foF2 provide latitudinal distributions of nmF2 at hourly intervals for a continuous period of 30 days near equinox at solar maximum.

During quiet periods spread F often occurs following sunset that precludes measurement of foF2, and is so pervasive that it is seen concurrently at stations within approximately $\pm 5°$ DIPLAT for durations of 3 to 8 hours. During such periods this spread F condition can also occur at anomaly latitudes (at $12°$ to $20°$ DIPLAT) in both hemispheres for durations of 1 or 2 hours. This spread F in the anomaly is taken to indicate that bubbles have formed at the equator and risen to altitudes where they intersect magnetic field lines passing through the F layer of the anomaly station. Such a signature yields information about where and when the bubble formed and thus permits the examination of the ionospheric conditions at the equator leading up to formation. One such condition is the that equatorial foF2 undergoes a rapid decrease prior to the onset of spread F.

INDEX

Thursday, 6 January (cont.)
1355-1515
B-4   INVERSE SCATTERING   CR2-28

1515-1700
B-5   SPECIAL SESSION ON LEAKY AND SURFACE WAVES   CR2-28

1700-1800
Commission B Business Meeting   CR2-28
Commission D Business Meeting   CR1-9
Commission G Business Meeting   CR2-6
Commission J Business Meeting   CR0-30

1955-2140
J-3   COSMIC MICROWAVE BACKGROUND   CR0-30

Friday, 7 January
0835-1200
A/D   ELECTROOPTIC DEVICE CHARACTERIZATION   CR1-9
F-4   PROPAGATION AND ENVIRONMENTAL   CR2-26
      MEASUREMENTS RELATED TO PROPAGATION
J-4   REMOTE TELESCOPE OPERATIONS   CR0-30

0855-1200
B-6   MEMORIAL SESSION HONORING PETR BECKMANN   CR2-28
E-2   SPECTRUM ISSUES FOR THE EMERGING WIRELESS SERVICES   CR1-40
G-4   LOW/HIGH LATITUDE PHENOMENA   CR1-46
G/H-1 IONOSPHERIC MODIFICATION BY HIGH POWER RADIO WAVES   CR2-6

1335-1700
J-5   VLBI AND APERTURE SYNTHESIS   CR0-30

1355-1700
A-2   MATERIAL CHARACTERIZATION   CR1-42
B-7   RANDOM MEDIA   CR1-40
B-8   SPECIAL SESION ON FINITE AND HYBRID METHODS   CR2-28
F-5   REMOTE SENSING OF WINDS AND PRECIPITATION   CR2-26
G/H-2 IONOSPHERIC MODIFICATION BY HIGH POWER RADIO WAVES   CR2-6

Saturday, 8 January
0855-1200
A/J   SOLAR SYSTEM RADIO AND RADAR ASTRONOMY:
      NEW MEASUREMENT TECHNOLOGY   CR0-30
B-9   SCATTERING II   CR2-28

0900-1200
G-5   IONOSPHERIC SOUNDING AND PROBING   CR2-6
      JURGEN BUCHAU MEMORIAL SESSION